Functional and mechanistic insights into MALT1-mediated regulation of immune homeostasis

Dissertation

der Fakultät für Biologie

der Ludwig-Maximilians-Universität München

angefertigt am

Helmholtz Zentrum München

Deutsches Forschungszentrum für Gesundheit und Umwelt

Institut für Molekulare Toxikologie und Pharmakologie

Abteilung Zelluläre Signalintegration

vorgelegt von

Carina Graß

München, den 07.11.2022

Diese Dissertation wurde angefertigt

unter der Leitung von **Prof. Dr. Daniel Krappmann**

am Helmholtz Zentrum München

Deutsches Forschungszentrum für Gesundheit und Umwelt

Institut für Molekulare Toxikologie und Pharmakologie

Abteilung Zelluläre Signalintegration

Erstgutachter/in:	Prof. Dr. Daniel Krappmann
Zweitgutachter/in:	Prof. Dr. Christof Osman
Tag der Abgabe:	07.11.2022
Tag der mündlichen Prüfung:	23.06.2023

Eidesstattliche Erklärung:

Ich versichere hiermit an Eides statt, dass meine Dissertation selbstständig und ohne unerlaubte Hilfsmittel angefertigt worden ist.
Die vorliegende Dissertation wurde weder ganz, noch teilweise bei einer anderen Prüfungskommission vorgelegt.
Ich habe noch zu keinem früheren Zeitpunkt versucht, eine Dissertation einzureichen oder an einer Doktorprüfung teilzunehmen.

München, den 07.11.2023 Carina Graß

Table of contents

List of Figures

1 Summary

Balanced regulation of T cell signaling is essential for initiating adaptive immune responses and for preventing autoimmunity. Antigenic stimulation of the T cell receptor (TCR) induces the formation of the higher-order CARD11-BCL10-MALT1 (CBM) complex, leading to NF-κB signaling and subsequent T cell activation, proliferation and differentiation into distinct T cell effector subsets. The MALT1 paracaspase has a dual function by acting as molecular scaffold and protease. Whereas MALT1 recruits the ubiquitin ligase TRAF6 via two TRAF6 binding motifs (T6BMs) to channel upstream TCR signaling to downstream IκB kinase (IKK)/NF-κB activation, MALT1 cleaves, via its paracaspase domain, several signaling mediators and post-transcriptional regulators to modulate T cell responses. The MALT1-TRAF6 interaction represents a critical control switch in balancing immune homeostasis and T cell activation. MALT1-TRAF6 binding positively regulates activation of IKK/NF-κB signaling in activated T cells, but restricts chronic CBM complex assembly and MALT1 protease activity in resting T cells to prevent cell-autonomous tonic T cell signaling and autoimmunity. As an additional layer of regulation, *MALT1* is prone to alternative splicing and the two isoforms MALT1A and MALT1B differ in their ability to interact with TRAF6. In this study, the aims were to: (1) analyze the contribution of MALT1B to immune homeostasis and activation *in vivo*, (2) to study the molecular mechanisms how TRAF6 counteracts chronic CBM complex and MALT1 activity and (3) to unravel the basic machinery for alternative splicing of the *MALT1* transcripts.

For aim 1, a mouse model was established to analyze the function of the shorter MALT1B isoform. While MALT1A contains two interfaces for binding to TRAF6, T6BM1 encoded by exon7, is excluded in MALT1B, which thus contains only the C-terminal T6BM2. We have characterized a patient-derived hypomorphic homozygous missense mutation in T6BM2 (MALT1 E806D) that selectively disrupts TRAF6 binding to the MALT1B isoform, causing a complex human immune disorder manifested by immune suppression and autoimmunity. The mutation was introduced by CRIPSR/Cas9 gene editing into the murine MALT1 orthologue to generate *Malt1* E814D (TRAF6 binding motif 2 mutant: TBM2) mice. Strikingly, selective disruption of MALT1B binding to TRAF6 causes fatal, early-onset autoinflammation in C57BL/6N mice, highly similar to mice with complete loss of MALT1-TRAF6 interaction. Expression analyses identified MALT1B as the major splice variant which dictates T cell activation and immune homeostasis. Moreover, the much milder immune pathology in the patient was attributed to the higher expression levels of MALT1A in human compared to murine immune cells which is able to compensate for the loss of TRAF6 binding in MALT1B. In aim 2, the molecular mechanisms of TRAF6-mediated restriction of CBM complex assembly and MALT1 protease function were dissected. We used structural, genetic and biochemical methods to show that BCL10 upstream of MALT1 is the molecular target of TRAF6 to counteract

MALT1 protease activity. TRAF6 E3 ligase activity initiates the attachment of linear ubiquitin chains by LUBAC (linear ubiquitin chain assembly complex) to the CARD domain of BCL10, which counteract CBM complex formation and MALT1 activity to restrict T cell activation. Hence, this negative regulatory mechanism involving ubiquitination and CBM deconstruction raises the threshold for T cell signaling or facilitates termination of prolonged T cell activation. In aim 3, in cooperation with structural biologists, cellular splicing assays were employed to unravel the basic machinery controlling alternative splicing of the *MALT1* pre-mRNA and exclusion of exon7. We demonstrated that *MALT1* exon7 inclusion depends on secondary RNA structures that sequester essential splice elements. Competitive binding of RNA binding proteins (RBPs) hnRNP U and hnRNP L to *MALT1* stem-loop RNA elements modulates the accessibility of the 5′ and 3′ splice sites flanking exon7. Whereas hnRNP U stabilizes stem-loop RNA conformations to maintain exon7 skipping, hnRNP L promotes exon7 inclusion by opening these structural elements and facilitating the recruitment of essential splice factors. These studies will be the basis for understanding how TCR signaling can affect *MALT1* splicing to modulate T cell responses. Overall, this work provides functional and mechanistic insights into how differential TRAF6 recruitment to distinct MALT1 splice variants controls T cell activation and immune homeostasis.

2 Zusammenfassung

Eine regulierte T-Zell-Signalübertragung ist entscheidend, um adaptive Immunantworten zu initiieren und Autoimmunität zu verhindern. Die Stimulation des T-Zell-Rezeptors (TZR) durch Antigene führt zur Bildung des CARD11-BCL10-MALT1 (CBM)-Komplexes, der den NF-κB-Signalweg induziert und schließlich zur Aktivierung, Proliferation und Differenzierung von naiven zu verschiedenen Effektor-T-Zellen führt. Die MALT1-Paracaspase hat eine duale Funktion und fungiert als molekulares Gerüstprotein sowie als Protease. Zum einen, rekrutiert MALT1 über zwei TRAF6-Bindemotive (T6BM) die Ubiquitin-Ligase TRAF6, um TZR-Signale zum IκB-Kinase (IKK)/NF-κB-Signalweg zu leiten. Zum anderen, spaltet MALT1 über seine Paracaspase-Domäne mehrere Signalproteine und posttranskriptionale Regulatoren und moduliert dadurch T-Zell-Immunantworten. Die MALT1-TRAF6-Interaktion ist ein entscheidender Regulationsschritt für das Gleichgewicht zwischen Immunhomöostase und T-Zell-Aktivierung. Die MALT1-TRAF6-Bindung fördert die Aktivierung des IKK/NF-κB-Signalwegs in aktivierten T-Zellen, schränkt aber eine dauerhafte CBM-Komplexbildung und MALT1-Proteaseaktivität in ruhenden T-Zellen ein, um eine zellautonome, tonische T-Zell-Signalübertragung und Autoimmunität zu verhindern. Als zusätzliche Regulierungsebene unterliegt *MALT1* alternativem Spleißen. Die beiden resultierenden Isoformen MALT1A und MALT1B unterscheiden sich in ihrer Fähigkeit, mit TRAF6 zu interagieren. Ziel dieser Studie war es, (1) den Beitrag von MALT1B zur Immunhomöostase und -aktivierung *in vivo* zu analysieren, (2) die molekularen Mechanismen zu untersuchen, wie TRAF6 der chronischen CBM-Komplexbildung und MALT1-Aktivität entgegenwirkt, und (3) den grundlegenden Mechanismus für das alternative Spleißen der *MALT1*-Transkripte zu entschlüsseln.

Um die Funktion der kürzeren MALT1B-Isoform in der ersten Fragestellung zu analysieren, wurde ein Mausmodell erstellt. Während MALT1A zwei Bindestellen für die Bindung an TRAF6 enthält, fehlt MALT1B das T6BM1, welches durch Exon7 kodiert wird, und besitzt nur das C-terminale T6BM2. Kürzlich haben wir eine hypomorphe, homozygote Missense-Mutation in T6BM2 (MALT1 E806D) in einer Patientin beschrieben. Diese Mutation verhindert selektiv die Bindung von TRAF6 an die MALT1B-Isoform und verursacht eine komplexe Immunerkrankung, welche sich durch Immundefizienz und Autoimmunität äußert. Mittels CRIPSR/Cas9-Genom-Editierung wurde die Mutation in das murine *MALT1*-Gen eingeführt, um *Malt1* E814D (TRAF6 Bindemotiv 2 mutierte: TBM2) Mäuse zu erhalten. Die selektive Störung der MALT1B-Bindung an TRAF6 in C57BL/6N-Mäusen verursacht eine tödliche, früh einsetzende Autoinflammation, die der von Mäusen mit vollständigem Verlust der MALT1-TRAF6-Interaktion sehr ähnlich ist. Expressionsanalysen identifizierten MALT1B als vorherrschende Spleißvariante, die über T-Zell-Aktivierung und Immunhomöostase bestimmt. Darüber hinaus konnte die wesentlich mildere Symptomatik der

Patientin auf eine höhere MALT1A Expression in menschlichen, im Vergleich zu murinen Immunzellen zurückgeführt werden, die den Verlust der TRAF6-Bindung an MALT1B kompensieren kann. Für die zweite Fragestellung wurden die molekularen Mechanismen der TRAF6-vermittelten Inhibierung der CBM-Komplexbildung und der MALT1-Proteasefunktion untersucht. Mittels strukturellen, genetischen und biochemischen Methoden konnte gezeigt werden, dass BCL10 das molekulare Zielprotein von TRAF6 ist, um der MALT1-Proteaseaktivität entgegenzuwirken. Die E3-Ligaseaktivität von TRAF6 initiiert das Anfügen linearer Ubiquitinketten durch den LUBAC (Linear Ubiquitin Chain Assembly Complex) an die CARD-Domäne von BCL10. Dadurch wird der Bildung des CBM-Komplexes und der Proteaseaktivität von MALT1 entgegengewirkt und schließlich eine Aktivierung von T-Zellen verhindert. Dieser negative Regulierungsmechanismus, bestehend aus Ubiquitinierung und Auflösung des CBM-Komplexes, erhöht die Schwelle für die T-Zell-Signalübertragung oder erleichtert das Beenden einer anhaltenden T-Zell-Aktivierung. Für die dritte Fragestellung wurde mit Strukturbiologen zusammengearbeitet. Mittels zellulärer Spleiß-Assays konnte der grundlegende Mechanismus entschlüsselt werden, der das alternative Spleißen der *MALT1*-prä-mRNA und den Ausschluss von Exon7 reguliert. Wir konnten zeigen, dass eine Inklusion von Exon7 von sekundären RNA-Strukturen abhängt, die wesentliche Spleiß-Elemente verbergen. Die kompetitive Bindung der RNA-Bindeproteine (RBP) hnRNP U und hnRNP L an *MALT1*-Haarnadelstrukturen reguliert die Zugänglichkeit der 5'- und 3'-Spleißstellen, die das Exon7 flankieren. Während hnRNP U die Haarnadel-Konformationen stabilisiert und den Ausschluss von Exon7 aufrechterhält, fördert hnRNP L die Inklusion von Exon7, indem es diese Strukturelemente öffnet und die Rekrutierung essenzieller Spleißfaktoren erleichtert. Die Studie bildet eine Grundlage, um zu verstehen, wie die TZR-Aktivierung das *MALT1*-Spleißen beeinflussen kann, um gezielt T-Zell-Immunantworten zu modulieren. Insgesamt liefert diese Arbeit funktionelle und mechanistische Erkenntnisse darüber, wie eine unterschiedliche TRAF6-Rekrutierung an verschiedene MALT1-Spleißvarianten die T-Zell-Aktivierung und Immunhomöostase steuert.

3 Introduction

3.1 T lymphocytes in adaptive immunity

The immune system is a cooperative network of lymphoid organs, specific immune cells, humoral factors and cytokines with the essential function to protect the host against both external and internal threats. Immunity can be divided into two general parts, the innate and adaptive (acquired) immune system, which strongly differ in speed and specificity of action (Parkin & Cohen, 2001). Innate immunity functions as a first line of defense within hours of antigen encounter, acting in a non-specific (antigen-independent) manner without immunologic memory, and is thus unable to recognize the same pathogen upon future re-infection. In contrast, the adaptive immune system is antigen-dependent and highly specific, but with delayed response time as it requires expansion of specific adaptive immune cells. The key features of acquired immunity are self-tolerance, meaning the ability to distinguish between foreign (non-self) and own (self) antigens, and the capacity for memory, which enables the host to respond to subsequent exposure of the same antigen more rapidly and effectively (Abbas et al., 2021; Warrington et al., 2011). Innate and adaptive immunity are not exclusive defense mechanisms, but rather cooperate to combat infections. Thus, impairment in either system can lead to the development of diseases, including cancer, autoimmunity and chronic infections (Warrington et al., 2011).

3.1.1 The adaptive immune system

There are two types of adaptive immunity, the humoral and cell-mediated responses, which differ in cell types and function. Antibodies and their producing cells, the B lymphocytes, mediate humoral immunity in extracellular fluids. B cells are activated by foreign antigens and undergo proliferation and differentiation into antibody-secreting plasma cells or long-lived memory B cells, which are activated upon re-exposure with a specific antigen (Abbas et al., 2021; Parkin & Cohen, 2001). However, antibodies are only capable of neutralizing extracellular microbes. Once an infection is established, T lymphocytes, the cells of cell-mediated immunity, are needed to either directly kill infected cells or help to do so by secreting cytokines (Abbas et al., 2021; Warrington et al., 2011).

B and T lymphocytes arise from bone marrow progenitor cells and mature in the bone marrow/spleen and the thymus, respectively. Both express antigen receptors (B cell receptor (BCR)/ T cell receptor (TCR)) on their surface to be able to recognize specific antigens. Antigen receptors display an extremely diverse repertoire from a limited number of genes. This is possible via gene rearrangement, where segments of antigen receptor genes are randomly recombined and nucleotide sequence variations are introduced to generate a variety of variable region-encoding exons. In the process of lymphocyte development, several positive and negative selection events

ensure that only lymphocytes with functional antigen receptors and useful specificity will mature and enter peripheral lymphoid tissues (Abbas et al., 2021). In contrast to B lymphocytes, T cells exclusively recognize antigens that are bound to surface major histocompatibility complex (MHC) molecules. Cells that capture and display antigens to T lymphocytes are called antigen-presenting cells (APCs) and include dendritic cells (DCs), macrophages and B cells. There are two main classes of MHC molecules, which differ in the type of antigen and T cell they are presenting to. MHC class I molecules sense intracellular events, such as viral and bacterial infections, to cytotoxic CD8+ T cells, and are therefore ubiquitously expressed and presented in all cell types. Thereby, misfolded or microbe-derived proteins are ubiquitinated in the cytosol and degraded into peptides by the proteasome, followed by transport to the endoplasmic reticulum (ER) and binding to nascent MHC class I molecules. Finally, peptide-MHC class I complexes are transferred via the Golgi complex to the cell surface, where they may be recognized by peptide antigen-specific CD8+ T cells. In contrast, MHC class II molecules present extracellular antigens taken up via phagocytosis to CD4+ T cells. Internalized proteins are degraded enzymatically in endosomes and lysosomes, in which they are loaded to MHC class II molecules and transported to the cell surface for presentation (Abbas et al., 2021; Vyas et al., 2008). Upon recognition of their specific antigens, CD4+ and CD8+ T cells become activated leading to cytokine secretion, proliferation, clonal expansion and differentiation of naïve T cells into effector and memory lymphocytes (Abbas et al., 2021).

3.1.2 Activation and differentiation of T lymphocytes

Mature CD4+ and CD8+ T cell clones migrate from the thymus into secondary lymphoid organs (spleen and lymph nodes) where they encounter antigens presented by APCs. Before T lymphocytes are activated by an antigen they are in a resting state and classified as naïve T cells. During the process of T cell activation, the expression of various surface molecules changes, which are involved in T cell migration and induction and regulation of T cell responses (Abbas et al., 2021). Naïve T cells are characterized by low CD44 and high CD62L expression ($T_{naïve}$: $CD44^{lo}CD62L^{hi}$). CD62 ligand or L-selectin (CD62L) facilitates T cell entrance into lymph nodes, whereas the hyaluronic acid receptor CD44 is critical for activated T cells and implicated in lymphocyte homing (Gerberick et al., 1997; Haynes et al., 1989). Upon antigenic stimulation, T cells enlarge and proliferate. Activated T cells increase their expression of CD69, CD25 and CD44, whereas CD62L expression decreases. CD69 expression retains activated T cells in lymphoid organs until they receive the signals to initiate proliferation and differentiation into effector and memory cells. In contrast, CD25 is a subunit of the interleukin-2 (IL-2) receptor and essential for binding of the correspondent growth factor inducing proliferation of the antigen-stimulated T cells. Lymphocytes differentiate into short lived effector cells, which leave secondary lymphoid organs and migrate to the site of infection to eliminate the

antigen. Other progeny of antigen-stimulated T cells differentiate into long-lived memory T cells with enhanced ability to respond to antigens, and either localize in secondary lymphoid organs (central memory T cells, T_{CM}: $CD44^{hi}CD62L^{hi}$) or in recently infected tissues (effector memory T cells, T_{EM}: $CD44^{hi}CD62L^{lo}$). Central memory T cells provide a pool of memory cells that is able to develop into effector cells upon antigenic stimulation, whereas effector memory T cells rapidly produce effector cytokines or become cytotoxic when they re-encounter an antigen (Abbas et al., 2021; Golubovskaya & Wu, 2016).

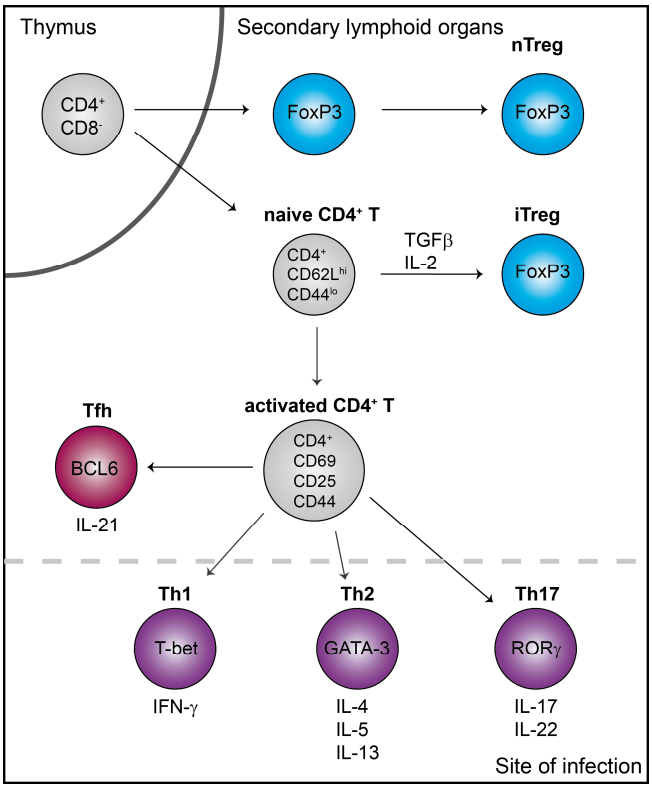

Figure 3-1: Differentiation of CD4+ T cells into distinct effector subsets and regulatory T cells.
Naïve CD4+ T cells mature in the thymus and migrate to secondary lymphoid organs, where they may get activated by an antigen. Activated lymphocytes upregulate specific surface markers and differentiate into four main subtypes of CD4+ effector T cells, which are distinguished by expression of distinct transcription factors and cytokine secretion. T helper Th1, Th2 and Th17 cells migrate to the site of infection to facilitate antigen elimination, whereas T follicular helper (Tfh) cells remain to help B cells with antibody production via T cell-dependent activation. Naïve CD4+ T cells can also differentiate into suppressive T cells, known as induced regulatory T (iTreg) cells, which are distinct from thymus derived natural Treg (nTreg) cells.

CD4+ (also called T helper (Th)) and CD8+ (also called cytotoxic) T cells are two functionally distinct T lymphocyte populations. Whereas CD8+ T cells directly kill infected host cells via delivery of cytotoxic proteins, including interferon gamma (IFNγ), granzymes and perforin, CD4+ T cells mainly function by secreting cytokines and surface molecules which activate other cells to kill microbes or help B cells with the antibody production. There are four major subsets of CD4+ effector T cells which are distinguished by cytokine expression, transcription factors and function: Th1, Th2, Th17, and T follicular helper (Tfh) cells (Abbas et al., 2021) (Figure 3-1). Th1 cells, the main population in

phagocyte-mediated host defense, are driven by T-box transcription factor (T-bet), which activates the expression of IFN-γ (Abbas et al., 2021; Szabo et al., 2000). Th2 cells promote humoral immune responses and tissue repair via the expression of GATA binding protein 3 (GATA-3) (Zheng & Flavell, 1997) and the cytokines IL-4, IL-5, and IL-13. Th17 cells are characterized by the transcription factor RAR-related orphan receptor gamma t (RORγt) (Ivanov et al., 2006) and the cytokines IL-17 and IL-22, and are responsible for recruitment of neutrophils to clear bacterial and fungal infections. Tfh cells are specialized in helping B cells with antibody production and are distinct from the other three CD4+ T cell subsets in their gene expression profile. Tfh cell differentiation is mainly driven by the transcription factor BCL6 and expression of inducible T cell costimulator (ICOS) and CXCR5 as well as IL-21 secretion (Abbas et al., 2021; Liu et al., 2013). Besides CD4+ effector T cells, there is another distinct CD4+ T cell subset, the regulatory (Treg) T cells, which suppress immune responses. They are characterized by high levels of the IL-2 receptor α chain (CD25) and the transcription factor forkhead box P3 (FoxP3). Treg cells either develop in the thymus via recognition of self-antigens (natural Treg cells (nTregs) or are generated from naïve CD4+ T cells in a TGFβ- and IL-2-dependent manner in the periphery (induced Treg cells (iTregs)) (Abbas et al., 2021; Chaplin, 2010). Treg inhibitory function is mediated by distinct mechanisms, including the production of immunosuppressive cytokines, expression of inhibitory receptors or consumption of the essential growth factor IL-2 (Abbas et al., 2021). Treg cells have a critical function in maintaining immune homeostasis and peripheral self-tolerance. Thus, disruption in Treg development or function is a primary cause of autoimmune and inflammatory diseases (Sakaguchi et al., 2008).

3.1.3 TCR signaling in immune activation

Upon T cell activation, several signal transduction pathways are induced. T cell signaling is initiated by TCR recognition of an antigen peptide loaded on an MHC molecule on the surface of an APC (Figure 3-2). Antigen ligation leads to the assembly of a supramolecular receptor cluster, consisting of a functional TCR-CD3 complex, a CD4 or CD8 receptor and an additional co-stimulatory receptor, such as CD28. CD28 associates with its ligands, for example CD80 or CD86, on APCs and provides additional signals required for productive T cell activation (Schmitz & Krappmann, 2006). TCR complex assembly induces the phosphorylation-dependent activation of the tyrosine kinase LCK, which in turn phosphorylates intracellular activating signaling motifs of the CD3-TCR complex called immunoreceptor tyrosine-based activation motifs (ITAMs). Via the recruitment of zeta chain-associated protein kinase 70 kDa (ZAP70), several scaffolding proteins, including linker for the activation of T cells (LAT) and SH2-containing leukocyte phosphoprotein 76 kDa (SLP-76), are phosphorylated, ultimately leading to the activation of phospholipase C γ (PLCγ) (Paul & Schaefer, 2013; Smith-Garvin et al., 2009). Activated PLCγ catalyzes the hydrolysis of phosphatidylinositol-4,5-

bisphosphate (PIP_2) to the second messenger molecules inositol-1,4,5-triphosphate (IP_3) and diacylglycerol (DAG), which both trigger further downstream activation of the transcription factors nuclear factor of activated T cells (NFAT), activator protein-1 (AP-1) and nuclear factor kappa B (NF-κB) (Gavali et al., 2021; Schulze-Luehrmann & Ghosh, 2006).

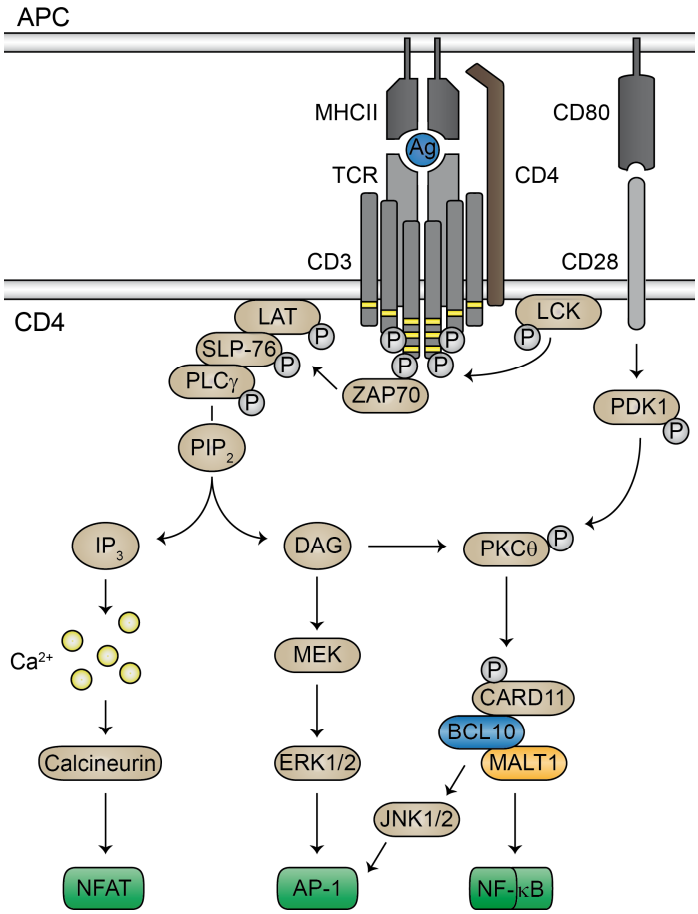

Figure 3-2: Proximal signaling events downstream of the TCR.
Signaling transduction is initiated via TCR ligation with an MHC II-antigen in the presence of CD28 co-receptor binding. Via phosphorylation of ITAMs (marked in yellow) within the TCR CD3 subunits by LCK, the tyrosine kinase ZAP70 is recruited, inducing phosphorylation of several downstream signaling mediators, ultimately leading to PLCγ-mediated hydrolysis of PIP_2 into IP_3 and DAG. IP_3 induces the activation of the transcription factor NFAT via calcium, and DAG triggers AP-1 and NF-κB signaling. DAG-dependent PKCθ activation initiates CARD11 phosphorylation and CBM complex formation, which finally leads to JNK signaling and NF-κB activation.

IP_3 triggers Ca^{2+} influx from the ER into the cytosol and subsequent activation of calcineurin, a potent signaling inducer of the NFAT transcription factor pathway. DAG induces the activation of protein kinase C (PKC) θ and mitogen-activated protein kinase kinase (MEK) signaling, resulting in extracellular signal-regulated kinase (ERK1/2) activation and AP-1 transcription factor activity. DAG-induced PKCθ activity is additionally increased via phosphorylation by protein-dependent kinase 1 (PDK-1), which is activated by co-receptor binding. PKCθ phosphorylates the scaffolding protein caspase recruitment domain family member 11 (CARD11, also termed CARMA1), which promotes the assembly of the CBM complex consisting of CARD11, B Cell CLL/Lymphoma 10 (BCL10) and

mucosa-associated lymphoid tissue protein 1 (MALT1). The CBM complex ultimately triggers downstream activation of canonical NF-κB signaling (Meininger & Krappmann, 2016; Ruland & Hartjes, 2019), as well as the c-Jun N-terminal kinase (JNK) pathway, which modulates lymphocyte proliferation as part of the AP-1 transcription factor complex (Lu et al., 2018).

3.2 The NF-κB signaling pathway

3.2.1 The transcription factor NF-κB

The NF-κB signaling pathway regulates survival, differentiation and proliferation of T cells. Thus, tight regulation of NF-κB is essential to prevent autoimmune disease or immune suppression (Meininger & Krappmann, 2016). The NF-κB transcription factor family contains the five members RelA/p65, RelB, c-Rel, p50 (NF-κB1), and p52 (NF-κB2), which form homo- or heterodimers via κB sites. NF-κB proteins contain an N-terminal Rel homology domain (RHD) mediating subunit dimerization, binding to IκB (inhibitor of NF-κB) proteins and DNA contact. However, only the Rel proteins RelA, c-Rel, and RelB possess C-terminal transactivation domains (TADs) that enable transcriptional gene regulation. The NF-κB proteins p50 and p52 are generated by processing of the precursors NF-κB1 and NF-κB2, respectively. These precursor molecules contain the RHD and several copies of ankyrin repeats, which can inhibit nuclear translocation and transcriptional activity of NF-κB dimers and thus are also classified as IκB proteins. In resting T cells, NF-κB dimers are captured in the cytosol through the association with IκBα molecules, which mask their nuclear localization signals. Upon TCR stimulation, IκBα is phosphorylated via the IκB kinase (IKK) complex consisting of the serine-threonine kinases IKKα (IKK1) and IKKβ (IKK2) and the regulatory subunit NF-κB essential modulator (NEMO/IKKγ). IκBα phosphorylation induces its ubiquitin-dependent protein degradation, which releases NF-κB dimers, allowing them to translocate into the nucleus and bind to DNA κB sites in promoters and enhancers of target genes to induce their expression (Hayden & Ghosh, 2012; Oeckinghaus & Ghosh, 2009).

3.2.2 Ubiquitination in the NF-κB signaling pathway

3.2.2.1 General principles of ubiquitination

NF-κB signaling is governed by post-translational modifications with ubiquitin, a small protein of 76 amino acids (aa), which can be covalently attached via its C-terminus to one or more lysine (K) residues of target proteins. Ubiquitination occurs in three distinct steps, known as activation, conjugation and ligation (Zinngrebe et al., 2014). In the first step, ubiquitin is activated by the ubiquitin-activating enzyme, E1, in an ATP-dependent reaction, which results in the formation of a thioester linkage between ubiquitin and the E1. In the second step, activated ubiquitin is transferred to the active-site cysteine of the ubiquitin-conjugating enzyme, E2. Finally, an E3 ubiquitin ligase

catalyzes the formation of an isopeptide bond between the C-terminal glycine of ubiquitin and a lysine residue of the target protein. Thereby, the E3 ligase, of which more than 600 exist, ensures substrate specificity (Zinngrebe et al., 2014). Ubiquitin contains seven lysine residues (K6, K11, K27, K29, K33, K48, and K63) and each of them can therefore serve as substrate leading to the assembly of ubiquitin chains. In addition, ubiquitin molecules can be linked via the amino terminal methionine (M1) resulting in the formation of M1- or linear linkages. Thus, eight distinct ubiquitin linkages can be formed in total, each of them fulfilling a different physiological function. Ubiquitin chains are either homotypic, where the same ubiquitin residue is modified during elongation, or heterotypic, if different ubiquitin residues are linked (Komander & Rape, 2012). Heterotypic chains can be classified as mixed chains, in which each ubiquitin is modified only once by another ubiquitin molecule, or as branched chains, in which each ubiquitin can be modified by two or more ubiquitin molecules (Daniel et al., 2020). Whereas some ubiquitin linkages are intensively studied, including K48- and K63-linked ubiquitin chains, the function of other linkage types is poorly understood. K48-linkage targets proteins for proteasomal degradation by the 26S proteasome (Chau et al., 1989; Pohl & Dikic, 2019), whereas K63-linked ubiquitin chains mostly have non-proteolytic roles and are involved in cell signaling events triggering protein kinase activation, DNA damage response or membrane trafficking (Chen & Sun, 2009). M1- or linear ubiquitin linkages are involved in cell signaling upon activation with different stimuli, such as TNF, IL-1β or lipopolysaccharide (LPS), and are essential for the prevention of TNF-induced cell death (Zinngrebe et al., 2014). M1-linked ubiquitin chains are catalyzed by the linear ubiquitin chain assembly complex (LUBAC), which consists of HOIL-1 (Heme-oxidized IRP2 Ub ligase-1, also termed RBCK1), HOIP (HOIL-1-interacting protein, also termed RNF31), and SHARPIN (Shank-associated RH domain-interacting protein, also termed hSIPL1) (Boisson et al., 2015; Boisson et al., 2012; Gerlach et al., 2011; Ikeda et al., 2011; Kirisako et al., 2006; Tokunaga et al., 2011). Ubiquitination is a highly dynamic and reversible protein modification. Removal of ubiquitin is mediated by deubiquitinating enzymes (DUBs), which prevent continuous activation of cellular signaling pathways and ensure the maintenance of cellular homeostasis. Similar to ubiquitin ligases, DUBs are usually specific for certain linkage types (Snyder & Silva, 2021).

3.2.2.2 Ubiquitination positively regulates NF-κB signaling

The first link of ubiquitin and NF-κB signaling was suggested by Zhijian Chen, who discovered that signal-induced phosphorylation targets IκBα for its ubiquitin-dependent degradation (Chen et al., 1995). IKKβ-mediated phosphorylation at serine residues 32 and 36 of IκBα induces the attachment of K48-linked ubiquitin chains by the specific E3 ubiquitin ligase Skp1-Cul1-F-box ligase containing the F-box protein βTrCP (SCF-βTrCP). Thereby, β-TrCP recognizes the IκBα degron, which was formed following phosphorylation, thus coupling IκBα phosphorylation to ubiquitination. Polyubiquitinated

IκBα is then selectively degraded by the 26S proteasome, freeing NF-κB dimers for translocation into the nucleus to induce target gene expression (Kanarek & Ben-Neriah, 2012). With another discovery by Chen, namely that the IKK complex itself is controlled by ubiquitination (Chen et al., 1996), the stage was set to further study the role of ubiquitination in NF-κB signaling. Since then, many polyubiquitination events of NF-κB kinases and signaling mediators were discovered. For instance, the E3 ligase TRAF6 catalyzes K63 polyubiquitination of MALT1 and the IKK subunit NEMO, and thus facilitates recruitment and activation of IKK downstream of the CBM complex (Oeckinghaus et al., 2007; Shambharkar et al., 2007; Sun et al., 2004). There were also several DUBs identified to negatively regulate TCR signaling via ubiquitin removal. A20 deubiquitinates MALT1 to prevent sustained interaction between ubiquitinated MALT1 and the IKK complex (Düwel et al., 2009). Further, CYLD detaches ubiquitin chains from TAK1 to restrict downstream NF-κB and JNK activation (Reiley et al., 2007). Thus, tight regulation of ubiquitination of critical NF-κB mediators balances NF-κB signaling and T cell activation.

3.3 CARD11-BCL10-MALT1-(CBM)-dependent NF-κB signaling

The CBM complex is a critical signaling platform that bridges TCR upstream signaling to downstream IKK/NF-κB activation (Meininger & Krappmann, 2016)(Figure 3-3). CBM complex formation is initiated by phosphorylation-dependent activation of CARD11, which binds to pre-assembled BCL10-MALT1 dimers and induces BCL10 oligomerization. Thereby, CARD11 functions as a molecular seed and triggers the formation of large filaments composed of a BCL10 core and MALT1 assembled at the periphery of the filament (David et al., 2018; Qiao et al., 2013; Schlauderer et al., 2018). Via distinct TRAF6 binding motifs (T6BMs) MALT1 recruits the E3 ubiquitin ligase TRAF6, leading to its oligomerization and activation (Meininger et al., 2016; Noels et al., 2007; Sun et al., 2004). In addition, CBM assembly activates MALT1 paracaspase function and induces the cleavage of distinct substrates, which further regulate T cell activation. Attachment of polyubiquitin chains to several NF-κB signaling mediators promotes the recruitment of the kinase complexes TAB2/3-TAK1 and the IKK complex. TAK1 activates IKKß via phosphorylation (Sun et al., 2004) which in turn induces the phosphorylation and subsequent degradation of IκBα (Meininger & Krappmann, 2016).

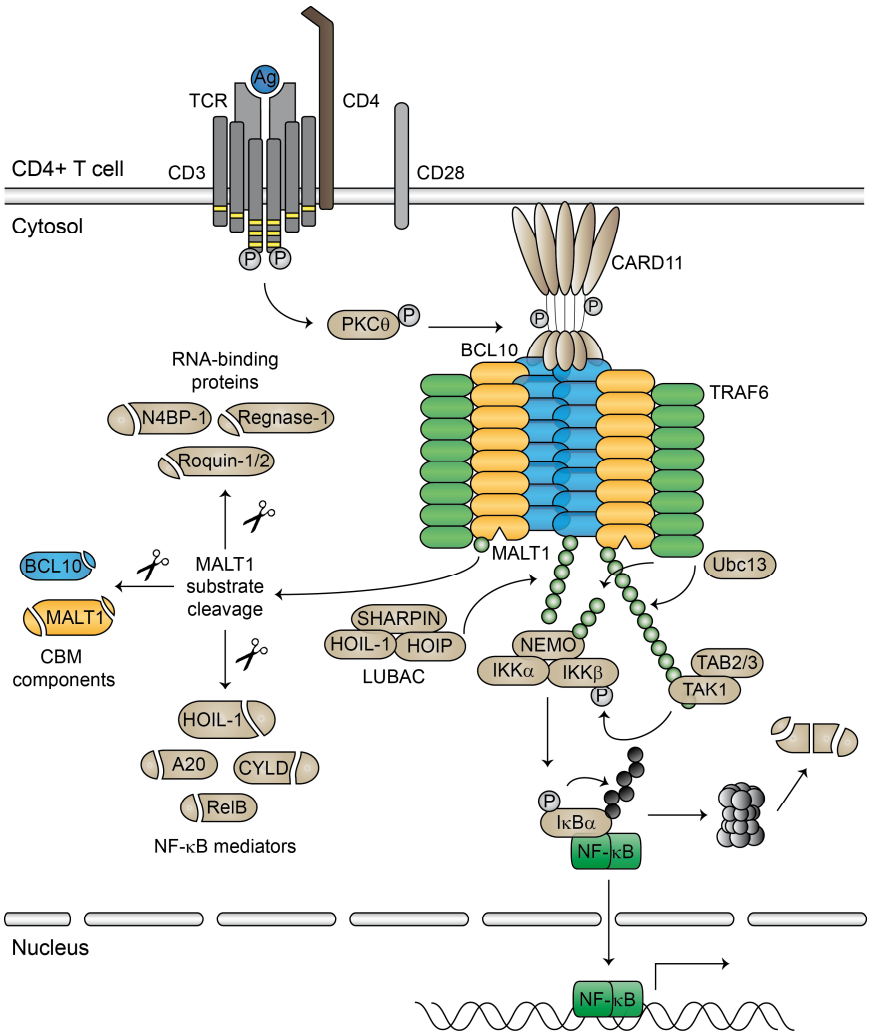

Figure 3-3: CBM complex formation bridges TCR engagement to downstream IKK/NF-κB and MALT1 paracaspase activation.

Antigen-binding to the TCR leads to PKCθ-mediated phosphorylation of CARD11. Activated CARD11 functions as a seed and triggers the formation of BCL10-MALT1 filaments. TRAF6 recruitment induces Ubc13-dependent MALT1 and NEMO K63-polyubiquitination, bringing the IKK complex and TAB2/3-TAK1 complex in close proximity. BCL10 polyubiquitination via the LUBAC is suggested to support NEMO recruitment. TAK1-mediated phosphorylation of IKKβ activates the IKK complex, which in turn phosphorylates IκBα, initiating its ubiquitin-dependent degradation via the proteasome. NF-κB dimers translocate to the nucleus and activate the expression of target genes. CBM complex formation and monoubiquitination activates MALT1 protease function leading to substrate cleavage which further modulates NF-κB signaling and T cell activation.

3.3.1 CARD11 acts as the seed for CBM complex formation

CARD11 functions as molecular seed or nucleator and initiates CBM complex formation upon TCR signaling. The ~130 kDa protein belongs to the caspase recruitment domain (CARD) family of scaffold/adaptor proteins and contains an N-terminal CARD, a coiled-coil (CC) domain and linker region, and a C-terminal membrane-associated guanylate kinase (MAGUK) domain for membrane interaction (Bedsaul et al., 2018). In resting T cells, CARD11 is kept in a closed, auto-inhibited conformation, which is mediated via interactions of the linker region with the CARD/CC domain (Jattani et al., 2016; McCully & Pomerantz, 2008). Upon T cell activation, CARD11 transitions to an

open and active conformation (Matsumoto et al., 2005; Sommer et al., 2005), allowing for recruitment and association with preassembled BCL10-MALT1 heterodimers (Li et al., 2012). Structural rearrangements are regulated by post-translational modifications, including phosphorylation and ubiquitination (Lork et al., 2019). Thereby, PKCθ catalyzes both stimulatory and inhibitory phosphorylation events in CARD11, which shape the dynamics of CBM complex assembly and subsequent NF-κB activation (Kutzner et al., 2022; Matsumoto et al., 2005; Sommer et al., 2005)

3.3.2 BCL10 filament formation induces CBM activation

BCL10 functions as the linker of CARD11 and MALT1 and is thus essential for CBM complex formation. Via CARD11 binding, BCL10 filaments channel TCR engagement to the NF-κB signaling pathway. In addition, BCL10 is essential for MALT1 protease activation and substrate cleavage, which further regulates T cell activation and function (Gehring et al., 2018). Originally, BCL10 was identified from the chromosomal translocation breakpoint t(1;14)(p22;q32) in MALT1 B cell lymphomas and was thus named B cell lymphoma/ leukemia 10 (Willis et al., 1999). Overexpression experiments showed that BCL10 both induces apoptosis and activates NF-κB (Koseki et al., 1999; Willis et al., 1999). $BCL10^{-/-}$ mice are severely immune-deficient due to defective NF-κB activation and display impairments in the development and function of various immune cell populations including Treg cells and B cell subsets (Rosenbaum et al., 2019; Ruland et al., 2001; Xue et al., 2003).

BCL10 is a ~27 kDa protein consisting of an N-terminal CARD domain and a C-terminal Ser/Thr (S/T)-rich region (Figure 3-4). Upon T cell signaling, BCL10 associates with CARD11 via heterotypic CARD-CARD interactions (Li et al., 2012) which induces aggregation and filament formation of BCL10 (Qiao et al., 2013). Cryo-electron microscopy (cryo-EM) experiments solved the architecture and assembly of BCL10 filaments and provided detailed structures of the BCL10 CARD-CARD and BCL10-MALT1 interfaces (David et al., 2018; Schlauderer et al., 2018). *In vitro*, BCL10 assembles into helical filaments with left-handed symmetry and three to four BCL10 molecules per helical turn. There are three types of homotypic CARD-CARD interactions between the BCL10 filaments which induce BCL10 oligomerization. Type I and type II interactions are inter-strand contacts between BCL10 subunits in adjacent helical turns, whereas the type III interface exhibits intra-strand interactions in the helical-strand direction (David et al., 2018; Schlauderer et al., 2018). BCL10 residues R42 in interface I and R36 in interface II were shown to be essential for CARD11 recruitment and subsequent MALT1 protease and NF-κB activation. BCL10 filaments are decorated with MALT1 molecules, which protrude into the periphery and orchestrate binding of additional NF-κB mediators. The MALT1 death domain (DD) interacts with the C-terminal part of the BCL10-CARD domain and forms a BCL10-MALT1 interaction surface, which is stabilized by a tight network of several salt bridges (Schlauderer

et al., 2018). TRAF6 cooperatively decorates BCL10-MALT1 filaments via binding to MALT1, resulting in the assembly of higher-order CBM filaments (David et al., 2018). Taken together, concomitant BCL10 oligomerization, as well as BCL10 binding to CARD11 and MALT1, are crucial for the formation of a functional CBM complex and downstream NF-κB signaling.

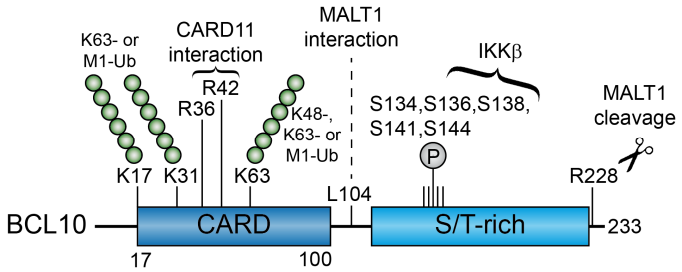

Figure 3-4: Molecular structure and post-translational modifications of BCL10.
BCL10 contains an N-terminal CARD-domain and a serine/threonine-rich region at the C-terminus. Amino acid residues, which are critical for protein interactions, MALT1-mediated cleavage, or function as acceptor sites for ubiquitination or phosphorylation are highlighted. Abbreviations: CARD, caspase recruitment domain; S/T-rich, Serine/Threonine-rich; R, Arginine; S, Serine; K, Lysine.

BCL10 is regulated by a variety of post-translational modifications and processes, including phosphorylation, ubiquitination, degradation and C-terminal cleavage by the MALT1 protease (Gehring et al., 2018; Lork et al., 2019) (Figure 3-4). Calmodulin kinase II (CaMKII) and GSK3β are supposed to phosphorylate BCL10 and thereby augment downstream NF-κB activation (Abd-Ellah et al., 2018; Oruganti et al., 2011). In contrast, IKKß-mediated phosphorylation at serines 134, 136, 138, 141, and 144 in the C-terminus of BCL10 was reported to counteract CBM signaling and to function as a negative feedback mechanism (Wegener et al., 2006). Besides phosphorylation, BCL10 is modified by polyubiquitin chains, which have been associated with triggering downstream NF-κB signaling, BCL10 degradation and CBM destruction (Gehring et al., 2018). Lysines 17, 31 and 63 in the BCL10 CARD were suggested to serve as direct conjugation sites of K63- and M1-linked polyubiquitin chains, which thereby promote the recruitment of the IKK regulatory subunit NEMO to BCL10 and trigger downstream IKK/NF-κB signaling (Wu & Ashwell, 2008; Yang et al., 2016). HOIP, the catalytically active subunit of the LUBAC, was reported to mediate M1-linked BCL10 polyubiquitination at these sites upon antigen receptor stimulation and in aggressively growing lymphoma cells that are addicted to chronic antigen receptor signaling (Satpathy et al., 2015; Yang et al., 2014; Yang et al., 2016). Furthermore, conjugation of K48- or K63-linked polyubiquitin chains on lysines 31 and 63 may induce BCL10 removal via proteasomal degradation and p62/Sequestosome-1-dependent autophagy (Paul et al., 2012; Scharschmidt et al., 2004; Wu & Ashwell, 2008). Inducible BCL10 ubiquitination relies on the presence of MALT1 and CARD11, indicating that ubiquitin conjugation takes place within the assembled CBM complex (Wu & Ashwell,

2008; Yang et al., 2016). Further, BCL10 is regulated via MALT1 cleavage at arginine 228, removing the last five amino acids from the C-terminus of BCL10 after T cell stimulation. So far, the physiological relevance of BCL10 cleavage is unknown, but it is implicated in integrin-dependent adhesion of T cells to fibronectin and may thus be crucial for efficient contact between T cells and APCs (Rebeaud et al., 2008).

3.3.3 MALT1 scaffolding and protease drive downstream CBM signaling

MALT1 was first identified as a fusion protein with the inhibitor of apoptosis 2 (API2; also known as cIAP2) as a consequence of chromosomal translocation in MALT lymphoma (Dierlamm et al., 1999). The API2-MALT1 fusion protein is a potent activator of canonical and non-canonical NF-κB signaling. The API2 moiety mimics TNF receptor signaling and efficiently activates the canonical NF-κB machinery at least in part via MALT1 moiety-dependent TRAF6 recruitment. Additionally, API2-MALT1 has constitutive proteolytic activity, which induces cleavage of NF-κB-inducing-kinase (NIK) resulting in chronic activation of the alternative NF-κB pathway and apoptosis resistance (Rosebeck et al., 2016). MALT1 is a ~92 kDa protein containing an N-terminal death domain (DD), three immunoglobulin-like (Ig) domains and a paracaspase (caspase-like) domain. Its dual role as scaffold and protease is unique in CBM-dependent NF-κB signaling. MALT1 scaffolding relies on BCL10 binding for CBM complex assembly (Schlauderer et al., 2018), and on TRAF6 binding motifs (T6BMs) for TRAF6 interaction (Kutukculer et al., 2021; Meininger et al., 2016; Noels et al., 2007; Sun et al., 2004). The paracaspase domain with the active site cysteine-464 confers proteolytic activity and mediates cleavage of distinct substrates in response to TCR stimulation (Coornaert et al., 2008; Rebeaud et al., 2008; Yu et al., 2011).

3.3.4 The physiological role of MALT1 paracaspase and scaffolding

To study the *in vivo* functions of MALT1 with respect to both its scaffolding and protease activities, various MALT1 mouse models have been generated. MALT1-deficient mice, which lack both scaffolding and protease function, are severally immune deficient, in line with the immunosuppressive phenotype of CARD11 and BCL10 KO mice (Egawa et al., 2003; Ruefli-Brasse et al., 2003; Ruland et al., 2001; Ruland et al., 2003) (Figure 3-5). MALT1 deficiency severely impairs activation, proliferation and survival of T and B cells upon antigen encounter. Even though overall lymphocyte numbers are normal, differentiation into specific lymphocyte subsets is defective. Similar to all CBM components, MALT1 is required for the development of Treg, Tfh and Th17 cells (Brüstle et al., 2017; Brüstle et al., 2012). Furthermore, MALT1 deficiency impairs the generation of marginal zone B (MZB) cells and peritoneal B1 B cells, as well as germinal center formation and

plasma cell differentiation (Ruefli-Brasse et al., 2003; Ruland et al., 2003). Overall, both molecular functions of MALT1 are essential for the development of a functional immune system.

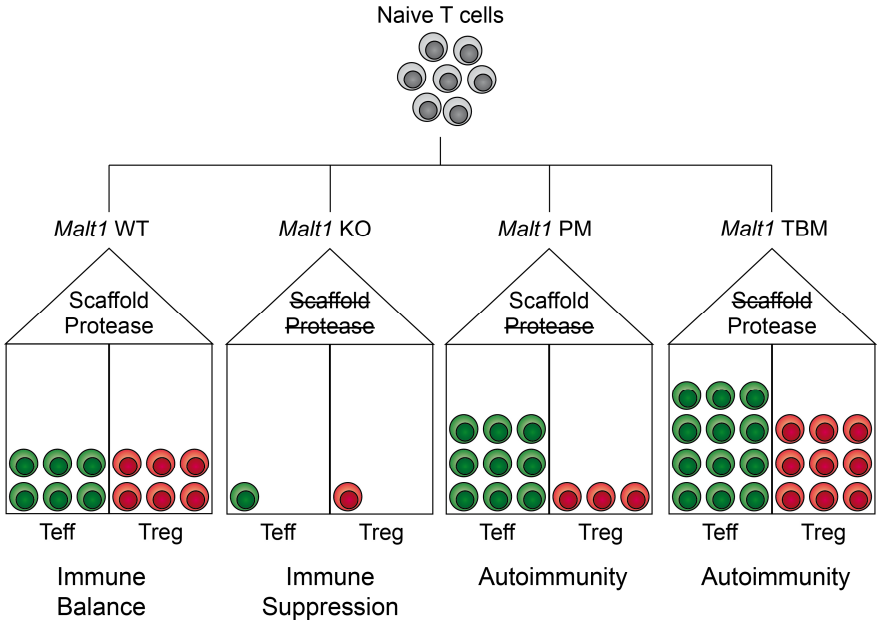

Figure 3-5: Overview of murine *Malt1* models.
Malt1 WT mice with intact scaffolding and protease function have balanced effector (Teff) and regulatory (Treg) T cell populations resulting in balanced immune responses. Loss of both MALT1 functions in *Malt1* KO mice leads to a strong reduction of Teff and Treg cells and causes immune deficiency. *Malt1* paracaspase mutant (PM) mice lack protease activity but have intact scaffolding function. Due to the requirement of MALT1 protease activity for Treg development, PM mice are impaired in Treg cell number and function leading to Increased Teff cell activity and autoimmunity. Mice with intact MALT1 protease but lacking TRAF6 binding motifs (*Malt1* TBM) show increased Teff and Treg cell populations. Even though Treg cells are functional, Teff are able to escape their suppressive function.

To investigate the physiological role of each MALT1 function individually, *Malt1* paracaspase mutant (PM) and *Malt1* TRAF6-binding mutant (TBM) mice were generated. Surprisingly, both murine models develop an autoimmune phenotype, but the cellular and molecular mechanisms of immune activation are very distinct (Bornancin et al., 2015; Gewies et al., 2014; Jaworski et al., 2014; O'Neill et al., 2021) (Figure 3-5). *Malt1* PM mice lack paracaspase activity due to mutation of the active site cysteine-472 but retain scaffolding function. Conditional T cell-specific or complete inactivation of MALT1 protease function causes weight loss and the development of neurological impairments and ataxia, which could be attributed to pathological changes in the cerebellar cortex (Demeyer et al., 2019; Gewies et al., 2014). Immune phenotyping revealed loss of FoxP3+ Treg cells resulting in expansion of conventional effector (Teff) T cells. In addition, marginal and peritoneal B1 B cell populations were severely reduced, indicating that Treg and innate-like B cell development relies on MALT1 protease activity. However, NF-κB signaling and lymphocyte activation were only mildly affected, showing that NF-κB activation is largely independent of MALT1 protease activity (Bornancin et al., 2015; Gewies et al., 2014; Jaworski et al., 2014). Thus, the catalytic activity of MALT1 is critical for cell fate decisions and immune homeostasis.

Impairment of MALT1 scaffolding in *Malt1* TBM mice revealed an unexpected dual role of the MALT1-TRAF6 interaction, whereupon TRAF6 acts as both a positive and negative regulator for maintaining immune homeostasis (O'Neill et al., 2021). MALT1-TRAF6 interaction is mediated via T6BMs within MALT1 and *in vitro* data showed that TRAF6 recruitment is essential for downstream NF-κB signaling (Meininger et al., 2016; Noels et al., 2007; Sun et al., 2004). Conditional T cell-specific loss of TRAF6 in so called *Traf6*-ΔT mice causes multi-organ inflammation due to spontaneous activation of conventional Teff cells which escape Treg cell suppression (King et al., 2006). However, it was unclear how TRAF6 renders T cells susceptible to regulation and if TRAF6 recruitment to MALT1 is relevant for the immune pathology caused by TRAF6 deletion in T cells. Therefore, *Malt1* TBM mice were generated in which both T6BMs are mutated. TBM mice develop a fatal inflammatory disease caused by spontaneous lymphocyte activation (O'Neill et al., 2021). The immune disorder is T cell driven, but not caused by absent or dysfunctional Treg cells, similar to *Traf6*-ΔT mice, which is in sharp contrast to autoimmunity driven by loss of Treg cells in *Malt1* PM mice (Bornancin et al., 2015; Demeyer et al., 2019; Gewies et al., 2014; Jaworski et al., 2014; King et al., 2006; O'Neill et al., 2021). CD4+ T cells from *Malt1* TBM-T and *Traf6*-ΔT mice fail to induce NF-κB activation upon TCR stimulation, confirming that MALT1-dependent recruitment of TRAF6 is essential for NF-κB signaling downstream of the CBM complex (O'Neill et al., 2021). However, cells display spontaneous MALT1 protease activity in the absence of stimulation, suggesting that TRAF6 acts as negative regulator of MALT1 paracaspase function. Deregulated MALT1 protease activation was identified as the primary driver of the immune pathology, because inactivation of MALT1 paracaspase using CRISPR-Cas9 gene editing in zygotes of *Malt1* TBM mice completely reverted the autoimmune phenotype. Further, treatment of *Traf6*-ΔT mice with a MALT1 inhibitor was able to ameliorate uncontrolled immune activation caused by loss of TRAF6 (O'Neill et al., 2021). In fact, mice with destruction of both MALT1 functions phenotypically copy *Malt1* KO mice and show the same developmental defects in Treg and B cell compartments (O'Neill et al., 2021; Ruefli-Brasse et al., 2003; Ruland et al., 2003). Taken together, disruption of MALT1-TRAF6 binding leads to a loss-of-function in NF-κB signaling but a gain-of-function of MALT1 protease activity. Thus, this interaction functions at the same time as a positive regulator of immune activation and as a negative regulator of MALT1 activity for maintenance of immune homeostasis (O'Neill et al., 2021).

3.3.4.1 MALT1 scaffolding function is modulated via expression of two distinct splicing isoforms

MALT1-TRAF6 binding is modulated by alternative splicing of *Malt1*, which mediates the inclusion and exclusion of exon7 (Meininger et al., 2016). Whereas the MALT1A splicing variant contains the 33-nucleotide (nt)-long exon7, this section is missing in MALT1B. Exon7 encodes an additional T6BM between the Ig2 and the paracaspase domain of MALT1, and thus MALT1A contains two T6BMs

(T6BM1 and T6BM2), whereas MALT1B only has the very C-terminal T6BM2 (Figure 3-6). Of note, an additional, third T6BM between the paracaspase domain and Ig3 domain of MALT1 was suggested based on sequence similarity (Noels et al., 2007; Sun et al., 2004), but mutation of this site does not interfere with TRAF6 binding (Meininger et al., 2016). Whereas naïve CD4+ T cells express almost exclusively the shorter MALT1B isoform, TCR engagement induces alternative exon7 splicing and MALT1A upregulation. Exon7 inclusion in MALT1A therefore augments MALT1 scaffolding function and enhances TRAF6 recruitment to the CBM complex upon antigen stimulation. As a result, stronger NF-κB signaling is induced which is critical for optimal T cell activation (Meininger et al., 2016).

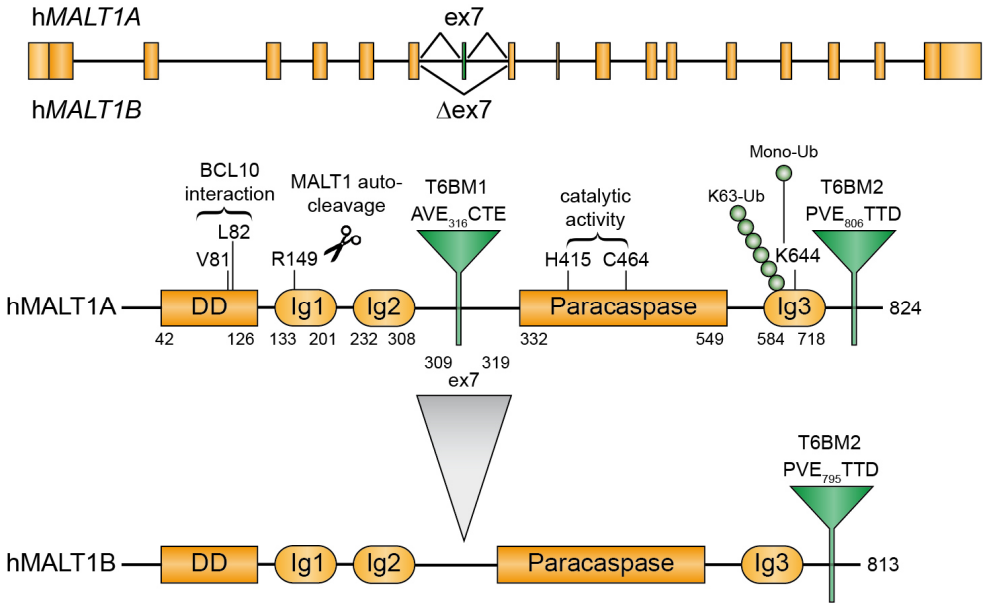

Figure 3-6: Scheme of h*MALT1* gene and molecular structure of the splicing isoforms MALT1A and MALT1B.
MALT1 exon7 is alternatively spliced leading to the expression of the two conserved isoforms MALT1A and MALT1B. MALT1A includes the 11 amino acid long exon7 which encodes an additional T6BM. Both isoforms contain an N-terminal death domain, three immunoglobulin-like domains, a paracaspase domain and the very C-terminal T6BM2. Amino acid residues, which are critical for protein interactions, catalytic activity, MALT1 auto-cleavage, or function as ubiquitin acceptor sites for ubiquitination are highlighted. Abbreviations: DD, death domain; Ig, immunoglobulin-like; T6BM, TRAF6 binding motif; C, Cysteine; R, Arginine; P, Proline; E, Glutamic acid; K, Lysine; V, Valine; T, Threonine; D, Aspartic acid; L, Leucine.

TRAF6 belongs to the tumor necrosis factor receptor–associated factor (TRAF) protein family, which function as key signaling molecules in various signaling pathways. TRAF6 contains an N-terminal RING and zinc finger 1 domain, which confer ubiquitin ligase activity (Ha et al., 2009), and a C-terminal TRAF domain mediating binding to adaptor proteins (Ye et al., 2002). Together with the E2 conjugating Ubc13/Uev1A complex, TRAF6 catalyzes non-degradative K63-linked polyubiquitination of various substrates (Deng et al., 2000; Shi & Sun, 2018). Upon TCR engagement, TRAF6 ubiquitinates MALT1 and thus facilitates recruitment of the IKK complex and subsequent NF-κB activation (Oeckinghaus et al., 2007). Additionally, TRAF6 mediates polyubiquitination of NEMO, the

regulatory subunit of the IKK complex, which induces IKK activation (Deng et al., 2000; Shambharkar et al., 2007; Sun et al., 2004). In addition to the TCR, TRAF6 functions downstream of Toll-like receptors (TLRs) and the IL-1R and is essential for NF-κB and MAPK signaling in various immune and non-immune cells (Dainichi et al., 2019).

3.3.4.2 MALT1 paracaspase activity mediates cleavage of distinct substrates

MALT1 paracaspase domain is structurally homologous to mammalian caspases and is therefore categorized as a caspase-like protease or paracaspase (Hulpiau et al., 2016; Uren et al., 2000). However, whereas caspases recognize aspartate at the P1 position to cleave substrates, MALT1 specifically cleaves substrates after arginine (Hachmann et al., 2012). MALT1 proteolytic activity relies on dimerization and formation of a catalytic dyad between C464 and H415 upon substrate binding (Uren et al., 2000; Wiesmann et al., 2012; Yu et al., 2011). In the absence of a substrate, MALT1 is kept in an inactive state, which is mediated through the auto-inhibitory function of the C-terminal Ig3 domain. Activation of MALT1 protease is initiated by dimerization, followed by substrate binding which induces conformational rearrangements and releases the paracaspase domain from auto-inhibition (Wiesmann et al., 2012). Further requirements for the proteolytic activity of MALT1 are CBM complex assembly and monoubiquitination at lysine 644 within the Ig3 domain (Pelzer et al., 2013; Qiao et al., 2013).

Several substrates have been identified that are cleaved by MALT1 upon TCR activation. MALT1 substrates can be divided into three distinct groups depending on their cellular functions and activities: Group 1 comprises regulators of NF-κB and MAPK signaling, including A20, HOIL-1, cylindromatosis (CYLD) and RelB (Coornaert et al., 2008; Elton et al., 2016; Hailfinger et al., 2011; Klein et al., 2015; Staal et al., 2011); group 2 are factors controlling RNA metabolism, such as the RNA-binding proteins (RBPs) Regnase-1, Roquin-1/2 and N4BP-1 (Jeltsch et al., 2014; Uehata et al., 2013; Yamasoba et al., 2019); and the group 3 consists of the CBM components BCL10 and MALT1, which are also prone to MALT1 cleavage (Baens et al., 2014; Ginster et al., 2017; Rebeaud et al., 2008). Recently, a combinatorial approach using bioinformatic substrate predictions and a co-expression screen identified seven new MALT1 substrates, including TRAF family member associated NF-κB activator (TANK), TAK1 binding protein 3 (TAB3), caspase-10 (CASP10), zinc finger CCCH domain-containing protein 12D (ZC3H12D), zinc finger CCCH domain-containing protein 12B (ZC3H12B), immunoglobulin-like domain containing receptor 2 (ILDR2), and ciliogenesis associated kinase1 (CILK1)(Bell et al., 2022). However, the physiological relevance of MALT1-mediated cleavage of these new substrates has to still be discovered.

The group 1 MALT1 substrates A20 and CYLD are both deubiquitinases which negatively regulate NF-κB and JNK signaling. A20 catalyzes the cleavage of K63 ubiquitin chains on MALT1, TRAF6 and NEMO (Coornaert et al., 2008; Düwel et al., 2009), and CYLD removes K63 ubiquitin chains from TAK-1, TRAF6 and NEMO (Reiley et al., 2007; Sun, 2010; Yoshida et al., 2005). MALT1-dependent cleavage of both deubiquitinases inactivates the proteins and thereby promotes NF-κB and JNK-signaling (Coornaert et al., 2008; Staal et al., 2011). MALT1 induced degradation of RelB increases canonical NF-κB signaling via the elimination of transcriptionally inactive RelB-RelA and RelB-c-Rel dimers (Hailfinger et al., 2011). Thus, proteolysis of A20, CYLD and RelB fine-tunes and prolongs NF-κB and JNK signaling. In contrast, cleavage of HOIL-1 serves as a negative feedback mechanism to dampen NF-κB activation. HOIL-1 is part of the LUBAC, which catalyzes the attachment of linear ubiquitin chains to several signaling proteins. Thus, HOIL-1 cleavage indirectly downregulates NF-κB activation via the reduction of M1-linked ubiquitin chains, which serve as critical signaling scaffolds (Klein et al., 2015). Furthermore, the HOIL-1 C-terminal cleavage fragment was suggested to function as negative regulator by inhibiting the catalytic activity of the LUBAC (Elton et al., 2016). Taken together, MALT1-mediated cleavage of positive and negative NF-κB regulators is able to balance the strength of signaling responses. Even though, MALT1 protease function does not directly impact initial TCR-induced NF-κB and JNK activation (Düwel et al., 2009; Jaworski et al., 2014), it may influence T cell signaling and fate decisions upon long term activation.

The group 2 MALT1 substrates Regnase-1 and Roquin-1/2 degrade distinct subsets of mRNA transcripts by binding to a common stem-loop element within their 3‘ untranslated regions (Jeltsch et al., 2014; Mino et al., 2015; Uehata et al., 2013). Targets that are negatively regulated by Regnase-1 and Roquin-1/2 encode inflammatory cytokines and chemokines (IL-6, TNF, IL-1β and CXCL1), immune regulatory surface receptors (CTLA4, ICOS and OX40) and intracellular signaling molecules (IκBNS and IκBζ) (Jeltsch et al., 2014; Uehata et al., 2013; Vogel et al., 2013). Through MALT1-mediated cleavage, these target mRNAs are stabilized, resulting in spontaneous T cell activation, inflammation and autoimmunity (Jeltsch et al., 2014; Uehata et al., 2013; Yu et al., 2007). Recently, the RBP NEDD4-binding protein 1 (N4BP-1) was identified as a MALT1 substrate. N4BP-1 is a negative regulator of the human immunodeficiency virus type-1 (HIV-1) and MALT1-mediated cleavage was suggested to facilitate the reactivation of latent HIV-1 proviruses (Yamasoba et al., 2019). Overall, MALT1-mediated cleavage of RBPs contributes to optimal T cell activation by modulating post-transcriptional gene regulation.

The third group of MALT1 substrates comprises MALT1 itself and its constitutive binding partner BCL10. Removal of the last five amino acids from the C-terminus of BCL10 contributes to cell

adhesion but is dispensable for expression of NF-κB target genes (Rebeaud et al., 2008). MALT1 auto-cleavage between its DD and Ig1 domain after arginine 149 does not affect its proteolytic activity but is required for the expression of the NF-κB target genes IL-2 and CSF2 (Baens et al., 2014). Prevention of auto-cleavage impairs Treg cell function (Baens et al., 2018), but the cleaved fragment is hardly detectable in an endogenous setting. In addition to R149, R781 was suggested as target site for MALT1 auto-proteolysis (Ginster et al., 2017). The overall significance of MALT1 auto-cleavage and BCL10 cleavage and how these events contribute to cellular responses is incompletely understood (Meininger & Krappmann, 2016).

3.3.4.3 Alternative *MALT1* splicing

3.3.4.3.1 General mechanisms of alternative splicing

Alternative splicing of pre-mRNA is a critical mechanism for post-transcriptional gene regulation, providing significant expansion of the functional proteome of eukaryotic organisms (Lee & Rio, 2015). Thereby, protein-coding exons are joined in different combinations, which lead to the generation of multiple protein isoforms from one single pre-mRNA. Splicing is carried out by a macromolecular ribonucleoprotein complex, the spliceosome, which consists of five small nuclear ribonucleoprotein particles (snRNPs) and several auxiliary factors. It recognizes pre-mRNA sequences positioned at the exon-intron boundaries, including the 5' splice site (5' SS), the 3' splice site (3' SS), branch point sequences (BPS) and the poly-pyrimidine tract (Py-tract) (Wahl et al., 2009). Exons are targeted for splicing by binding of snRNPs to splice sites, which is primarily mediated through base-pairing interactions between the snRNPs and the splice-site sequences. Since most mammalian splice sites only weakly base-pair with the snRNAs, auxiliary sequence elements are essential to modulate snRNP-substrate interactions. These *cis*-regulatory elements are located within exons or introns and either promote or suppress exon inclusion via exonic and intronic splicing enhancers (ESEs, ISEs,) or exonic and intronic splicing silencers (ESSs, ISSs) (Martinez & Lynch, 2013). Exonic elements predominantly interact with two ubiquitous families of *trans*-acting factors. Whereas serine-/arginine-rich (SR) proteins mainly enhance alternative exon inclusion, heterogeneous nuclear ribonucleoproteins (hnRNPs) primarily counteract them. However, both factors can also regulate the opposite process, meaning that SR proteins function as splicing suppressors and hnRNP proteins as enhancers (Taylor & Sobczak, 2020). Through site-specific binding via RNA recognition motifs (RRMs), SR and hnRNP proteins direct their influence on pre-mRNA splicing. In case of hnRNPs, RGG boxes (repeats of Arg-Gly-Gly tripeptides) and glycine-rich, acidic or proline-rich domains promote protein-protein interactions that ultimately mediate splicing decisions (Busch & Hertel, 2012). hnRNPs suppress splicing via different mechanisms, including repressing spliceosomal assembly through multimerization along exons (Zhu et al., 2001), preventing the recruitment of snRNPs

(House & Lynch, 2006; Tange et al., 2001) or by looping out entire exons (Martinez-Contreras et al., 2006). Besides *cis*-acting sequence motifs in the pre-mRNA and *trans*-acting RBPs, the pre-mRNA structure itself is suggested to contribute to alternative splicing regulation (Taylor & Sobczak, 2020). Co- or post-transcriptional RNA folding into distinct secondary and tertiary structures is mainly determined by the composition of the RNA linear sequence and the high propensity of RNA bases and the backbone to interact with each other. mRNAs can form either single-stranded (ssRNA) or double-stranded (dsRNA) structures attained through intermolecular forces (hydrogen bonds and Van der Waals´ forces) and hydrophobic effects. Basic RNA secondary structural motifs include stem-loop structures, bulges, internal and hairpin loops, and multi-stem junctions (Taylor & Sobczak, 2020). These secondary structures impact splicing regulation via different mechanisms. For example, stem-loop structures can appropriate cis-regulatory RNA motifs, making them inaccessible for the spliceosome or essential trans-acting RBPs (Warf & Berglund, 2010). In turn, binding of proteins can modulate pre-mRNA structures and thereby influence the accessibility of splice sites (Lee et al., 2018; Warf & Berglund, 2010). It is also suggested that secondary structural motifs bring splice sites in sufficient spatial proximity to initiate splicing and bypass the requirement of RBPs for early spliceosome assembly (Lin et al., 2016). However, the molecular mechanisms of how RPB binding to pre-mRNA structures modulates exon inclusion and exclusion are still poorly understood.

3.3.4.3.2 hnRNP U and hnRNP L modulate *MALT1* alternative splicing

The two alternative splice isoforms of MALT1 only differ in the inclusion (MALT1A) and exclusion (MALT1B) of exon7 (Figure 3-6). Isoform expression, exon/intron boundaries and amino-acid sequences of exon7 are highly evolutionary conserved across mammals, indicating biological relevance of controlled isoform expression (Meininger et al., 2016). It was previously shown that the RBPs hnRNP U and hnRNP L exert opposing roles on *MALT1* exon7 inclusion and exclusion (Meininger et al., 2016). Whereas hnRNP U negatively regulates MALT1A protein levels, hnRNP L promotes exon7 inclusion and MALT1A expression. Knockdown of hnRNP U enhances TCR-induced MALT1A upregulation and optimal T cell activation. Initial experiments suggested that enhancer and silencer regions in the vicinity of exon7 control alternative *MALT1* splicing (Meininger et al., 2016). However, the underlying molecular mechanism of *MALT1* splicing regulation by hnRNP U and hnRNP L have remained elusive.

3.3.4.4 Human immune disorder associated with selective disruption of MALT1B scaffolding

Recently, a 19-year-old woman from Turkey with a complex primary immune disorder was described (Kutukculer et al., 2021). The patient shows signs of immune deficiency, such as chronic ear and bronchial infections, and symptoms of autoimmunity including skin psoriasis, dermatitis,

lymphadenopathies, and the presence of autoantibodies. Next-generation sequencing (NGS) identified a single homozygous missense mutation, c.2418G>C, in the second T6BM within exon17 of the *MALT1* gene. The mutation leads to a Glu806Asp (E806D) and a Glu795D (E795D) exchange in MALT1A and MALT1B protein, respectively (Figure 3-7). Analyses revealed that the alteration is hypomorphic and only affects TRAF6 binding to the MALT1B isoform, which lacks exon7 and the additional T6BM1, whereas MALT1A-TRAF6 interaction is still intact, albeit to a reduced extent (Kutukculer et al., 2021). Due to the dual role of TRAF6, the conserved E795D mutation in MALT1B disrupts NF-κB signaling but also induces constitutive MALT1B protease activation (Kutukculer et al., 2021; O'Neill et al., 2021). The patient-derived E-to-D exchange has a comparable effect as the E-to-A mutations in *Malt1* TBM mice, even though it represents a conservative amino acid replacement (Kutukculer et al., 2021; O'Neill et al., 2021). However, in *Malt1* TBM mice both T6BMs are disrupted, whereas in the patient only T6BM2 is mutated, raising the question why selective destruction of MALT1B causes such a severe immune pathology in the patient.

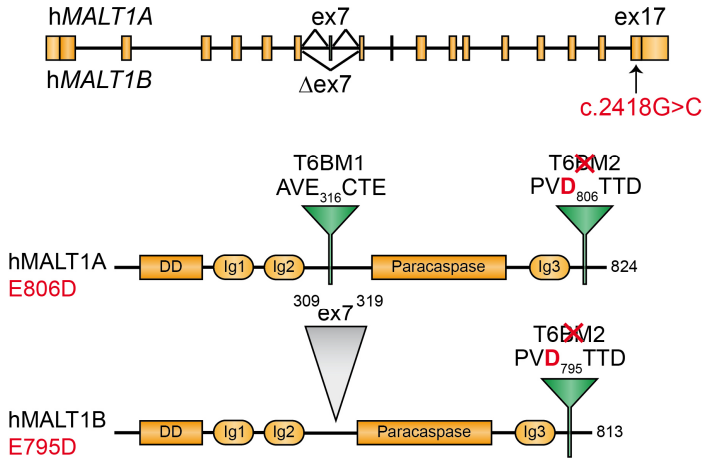

Figure 3-7: A patient-derived hypomorphic MALT1 mutation selectively disrupts MALT1B-TRAF6 interaction.
The c.2418G>C missense mutation is located in exon17 of *MALT1* and leads to Glu806Asp (E806D) substitution in MALT1A and Glu795Asp (E795D) in MALT1B. The exchange occurs within the C-terminal TRAF6 binding motif 2 (T6BM2) and selectively affects MALT1B, which lacks exon7 and T6BM1.

3.4 Aims of the study

The MALT1-TRAF6 interaction is a critical control switch in balancing immune homeostasis and T cell activation. As a negative regulator, TRAF6 restricts MALT1 protease activity in resting T cells, but positively mediates TCR-induced NF-κB signaling (O'Neill et al., 2021). The significance of this dual role becomes even more apparent through the human immune disorder caused by selective disruption of TRAF6 binding to the shorter MALT1B isoform which leads to both immune suppression and autoimmunity (Kutukculer et al., 2021). Since the *Malt1* TBM mouse model develops a drastic immune phenotype with early lethality, it is not suitable to study the development and progression of the human immune pathology. Further, both MALT1 isoforms are mutated in *Malt1* TBM mice which does not allow for the study of the biological relevance of both MALT1 splicing variants. Therefore, one focus of the work was to introduce the homologous human germline missense mutation c.>2418G>C into murine blastocysts, leading to a mouse strain that ubiquitously expresses the MALT1 E814D disease variant. This *Malt1* TBM2 (TRAF6 binding mutant 2) mouse with selective destruction of TRAF6-MALT1B interaction represents the first murine model with a patient-derived MALT1 mutation. The aim was to describe in detail the phenotype of the *Malt1* TBM2 mice, which suffer from an early onset fatal autoinflammatory disease. Via blood and serum analysis, the cause of the early lethality could be correlated to strong anemia in the mice. Further, we aimed to investigate the cell-intrinsic effect of defective MALT1B on TCR-induced NF-κB signaling and MALT1 protease activity.

Chronic MALT1 substrate cleavage in *Malt1* TBM2 mice prompted us to investigate the molecular mechanism, how TRAF6 restricts MALT1 protease activity in resting T cells. Since previous experiments demonstrated that constitutive MALT1 proteolytic activity requires a functional T cell receptor and assembly of the CBM complex (O'Neill et al., 2021), we hypothesized that TRAF6 prevents tonic TCR signaling to MALT1. However, neither a distinct target of TRAF6 nor the mechanism for negative regulation has been solved. In a combinatorial approach using structural data of BCL10-MALT1 filaments and biochemical studies, it was investigated in how far TRAF6- and LUBAC-mediated ubiquitination could be involved in negative regulation of the CBM complex to prevent spontaneous MALT1 protease function and overshooting immune responses. BCL10 was identified as the putative target for the negative regulatory effect of MALT1-TRAF6 interaction, which is enhanced and facilitated by LUBAC activity. Our work was able to uncover a new ubiquitin-dependent process that either raises the threshold for T cell signaling or helps to terminate T cell activation post-induction.

The drastic phenotype of *Malt1* TBM2 mice provoked us to analyze how alternative *Malt1* splicing regulates the severity of the autoimmune inflammation. Therefore, we determined the expression levels of both MALT1 isoforms in different human and murine cell types to better understand the phenotypical differences between the human patient and the murine TBM2 model. Further, we investigated in how far the presence of WT MALT1 in heterozygous *Malt1* TBM2 mice is able to prevent autoimmune inflammation and analyzed the effect of functional MALT1A protein on constitutive MALT1B protease activity. Since faithful control of MALT1 isoform expression can impact immune balance, as highlighted by the patient and the *Malt1* TBM2 mouse model, we were highly interested in the regulation of alternative *Malt1* splicing. Our collaboration partner at the Institute of Structural Biology of Helmholtz Munich solved the secondary structure of *MALT1* pre-mRNA. By using these structural data and cellular assays, we aimed to unravel the mechanisms of splice site selection and propose a model, in which differential binding of the RBPs hnRNP U and hnRNP L modulates *MALT1* pre-mRNA structure and accessibility of exon7 splice sites. We provide an intriguing new model for how positive and negative acting splice factors control exon inclusion or exclusion through modulation of pre-mRNA secondary structure.

4 Results

4.1 The MALT1 isoform B dictates T cell activation and immune homeostasis

4.1.1 Mouse model for patient-derived missense mutation in *Malt1* T6BM2

Combined mutation of both TRAF6 binding motifs (T6BMs) in MALT1 leads to a fatal auto-inflammation in mice (O'Neill et al., 2021). Selective disruption of the second T6BM (T6BM2) causes a complex immune disorder with clinical features of primary immune deficiency and autoimmunity (Kutukculer et al., 2021). To study the effect of exclusive impairment of T6BM2 and thus MALT1B-TRAF6 interaction *in vivo*, the patient-derived *MALT1* c.2418G>C missense mutation was introduced into the *Malt1* gene of C57BL/6N zygotes using CRISPR-Cas9 editing combined with homology directed repair (HDR). A single-guide RNA (sgRNA) targeting *Malt1* exon17 was introduced together with Cas9 protein and a DNA repair template containing the Glu/Asp (E/D) replacement in T6BM2 for targeted destruction of MALT1B-TRAF6 protein interaction. Additional silent mutations were inserted to enable genotyping of offspring mice using T6BM2 wildtype- and mutation-specific primers or restriction digestion via the artificial AlwI cleavage site proximal to T6BM2 (Figure 4-1A and B).

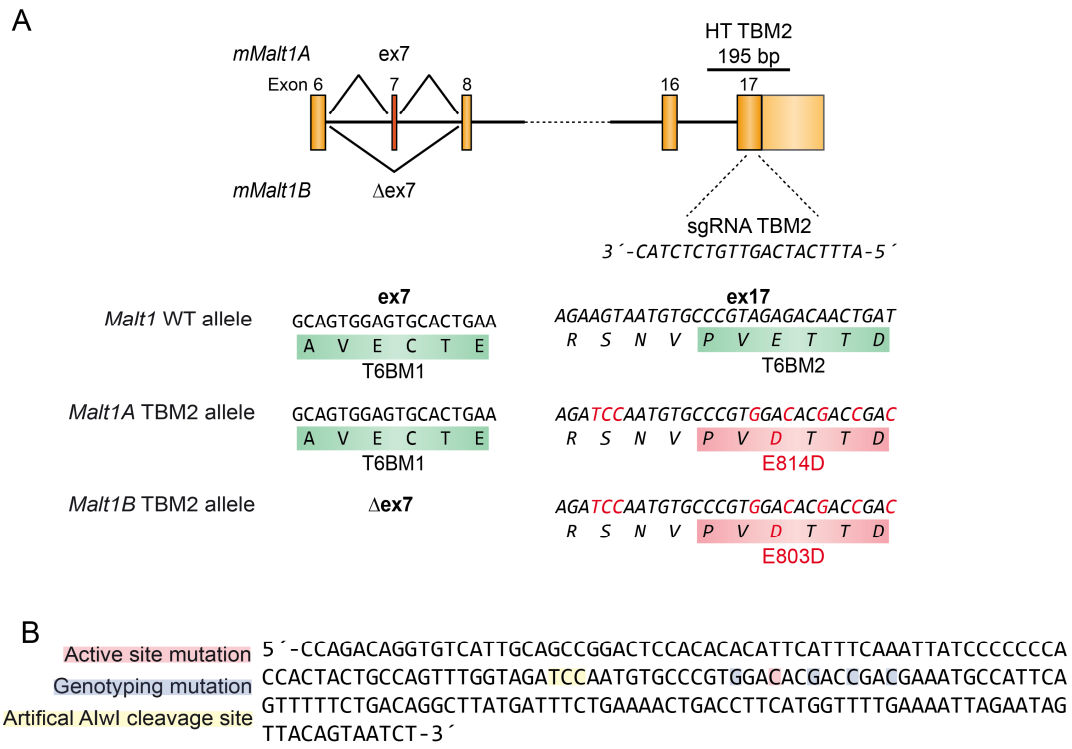

Figure 4-1: CRISPR-Cas9 targeting strategy for insertion of the patient-derived *Malt1* T6BM2 mutation.
A) Schematic representation of the murine *Malt1* genomic locus with exon-intron structure. Below, wildtype and mutated DNA and amino acid sequences of MALT1A and MALT1B (ΔEx7) are depicted. The sequence of the single guide (sg) RNA targeting T6BM2 in exon17 is shown above.
B) Sequence of the homology directed repair (HDR) template showing the patient-derived E-to-D mutation in T6BM2 (red), insertion of additional silent mutations (blue) and artificial AlwI cleavage site (yellow) for screening.

The workflow for targeting T6BM2 is depicted in Figure 4-2. Briefly, zygotes isolated from pregnant C57BL/6N mice were electroporated with active ribonucleoprotein complexes to induce a double strand break (DSB) in close proximity to T6BM2 in *Malt1* Exon17 followed by HDR. CRISPR-Cas9-edited zygotes were transferred into carrier females and chimeric offspring mice were analyzed for desired T6BM2 mutation.

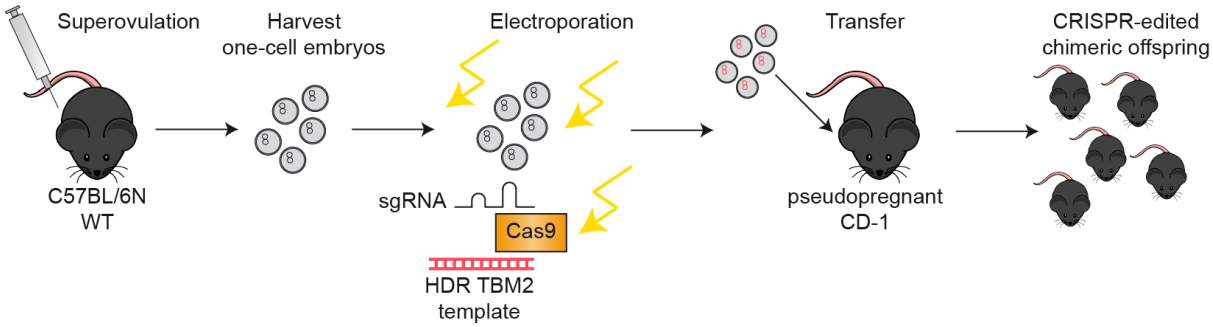

Figure 4-2: Generation of *Malt1* TBM2 mice.
Zygotes from superovulated C57BL/6N females were electroporated with active ribonucleoprotein complex consisting of sgRNA targeting *Malt1* T6BM2, Cas9 protein and HDR template containing the patient mutation. Manipulated zygotes were transferred into pseudopregnant CD-1 mice to generate chimeric offspring with the desired MALT1 T6BM2 mutation. Zygote electroporation was performed by Florian Giesert, Institute for Developmental Genetics, Helmholtz Zentrum München, Neuherberg.

Surprisingly, three chimeric offspring mice had to be euthanized at the age of 33 days due to severe skin eczema and dermatitis on scalp and ears (Figure 4-3A). Necropsy revealed enlarged lymph nodes but normal spleens compared to healthy littermates (Figure 4-3B). Sequencing of genomic DNA identified these mice as homozygous carriers of the targeted E-to-D missense mutation in MALT1 T6BM2 (Figure 4-3C). Basic immune phenotyping showed a drastic decrease in splenic B220+ B cells which did not significantly affect relative numbers of CD3+ T cells (Figure 4-3D-F) or CD4+ and CD8+ T cell ratios (data not shown). To analyze activation of T cells, we performed a co-staining of CD4+ and CD8+ T cells with the cell-surface markers CD44 and CD62L to identify activated effector memory (T_{EM}) T cells. In both, CD4+ and CD8+ T cells, percentages of $CD44^{hi}CD62L^{lo}$ T_{EM} cells were increased, indicating immune activation in homozygous *Malt1* TBM2 chimeras (Figure 4-3G-J).

Subsequent genomic sequencing identified several mice which were heterozygous for MALT1 T6BM2 mutation. However, the majority had to be sacrificed due to onset of dermatitis on ears and tail between 7 and 18 weeks of age, before they produced offspring. Ultimately, one heterozygous male (Mouse ID: 80014037) did mate with a wildtype C57BL/6N female and thus constituted the $Malt1^{TBM2/+}$ founder mouse, before it was also euthanized due to dermatitis. Taken together, expression of one allele with *Malt1* T6BM2 mutation appears to be sufficient to disrupt immune balance in chimeric mice. However, we can not exclude that the second *Malt1* allele was affected by additional mutations leading to disruption of the *Malt1* gene locus.

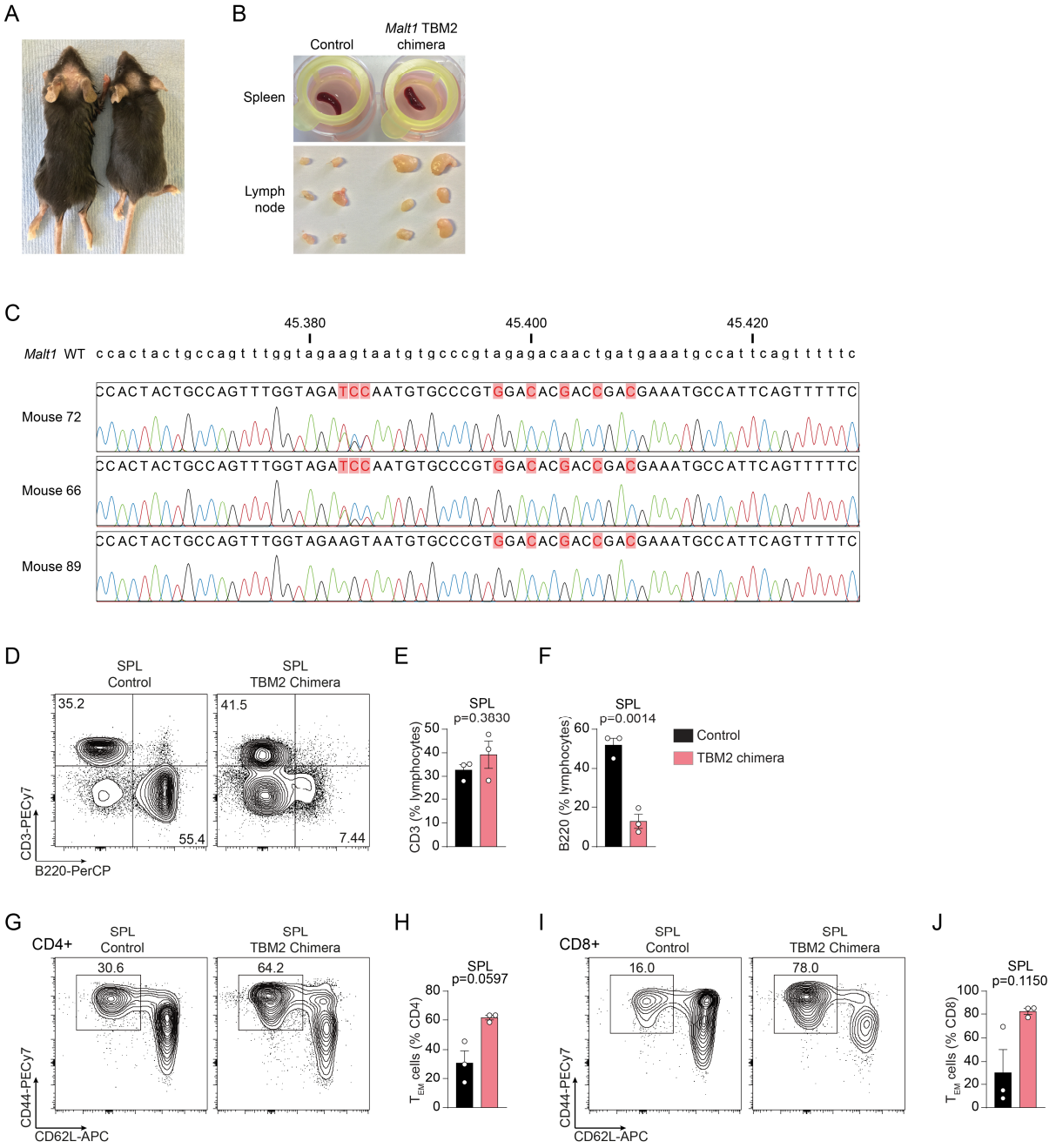

Figure 4-3: Chimeric mice with homozygous *Malt1* T6BM2 mutation.

A) Chimeric offspring with severe skin eczema and dermatitis on scalp and ears.

B) Representative image showing spleen and lymph nodes of chimeric mice.

C) Sequencing results of genomic DNA isolated from chimeric offspring. Mice 72, 66 and 89 were homozygous carriers of the targeted *Malt1* T6BM2 mutation. WT sequence is shown in the top, mutated nucleotide residues are highlighted in red.

D-F) Flow cytometry analysis of CD3+ T and B220+ B cells in spleen (SPL) of homozygous chimeric offspring and littermate controls.

G-J) Flow cytometry analysis of CD4+ and CD8+ naïve T cells ($T_{naïve}$: $CD44^{lo}$ $CD62L^{hi}$), central memory T cells (T_{CM}: $CD44^{hi}$ $CD62L^{hi}$) and effector memory T cells (T_{EM}: $CD44^{hi}$ $CD62L^{lo}$) in spleen of homozygous chimeric offspring and littermate controls.

A-J) Mice were analyzed at the age of 33 days. Wildtype littermates (black) were compared to chimeric mice identified as homozygous carrier of *Malt1* T6BM2 mutation (red). Each dot represents one mouse, and bars show means ± SEM. P-values were calculated with unpaired Student´s t-test with Welch´s correlation.

Heterozygous *Malt1*$^{TBM2/+}$ offspring mice from the founder were intercrossed to obtain homozygous *Malt1*$^{TBM2/TBM2}$ (*Malt1* TBM2) mice. *Malt1*$^{+/+}$, *Malt1*$^{TBM2/+}$ and *Malt1*$^{TBM2/TBM2}$ genotypes were distinguished via differential polymerase chain reaction (PCR) using *Malt1* wild-type- (WT) and TBM2-specific primers (Figure 4-4A and B). Furthermore, correct genome editing was verified by genomic DNA sequencing using tissue from ear punches (Figure 4-4C). Western blot analysis indicated slightly lower MALT1 protein expression in lysates of total splenocytes from *Malt1*$^{TBM2/+}$ and *Malt1*$^{TBM2/TBM2}$ compared to *Malt1*$^{+/+}$ (Figure 4-4D).

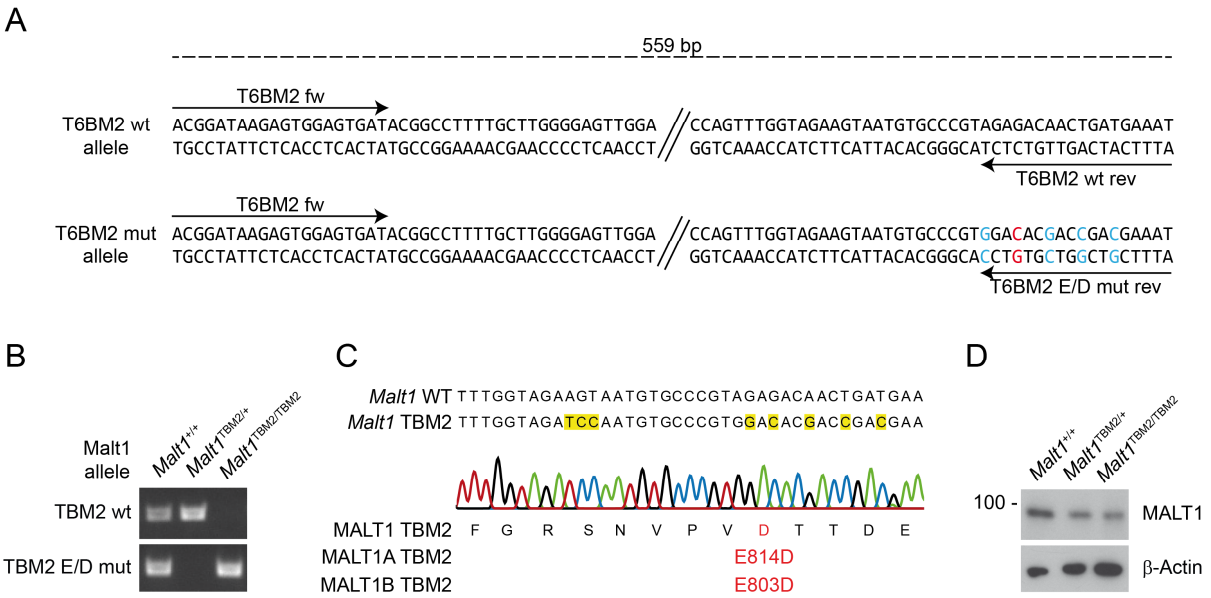

Figure 4-4: Verification of *Malt1* TBM2 genotypes.

A) Genotyping strategy for differential PCR of *Malt1* WT and TBM2 alleles. Primers are indicated with arrows. Functional E-to-D point mutation is highlighted in red, additional silent mutations in blue.

B) Representative genotyping of *Malt1* TBM2 mice with *Malt1*$^{+/+}$, *Malt1*$^{TBM2/+}$ and *Malt1*$^{TBM2/TBM2}$ genotypes.

C) Sequencing of genomic DNA from a *Malt1*$^{TBM2/TBM2}$ mouse with targeted mutations indicated in yellow.

D) Analysis of MALT1 protein expression by Western Blot in lysates of total splenocytes from *Malt1*$^{+/+}$, *Malt1*$^{TBM2/+}$ and *Malt1*$^{TBM2/TBM2}$ mice. β-Actin served as loading control.

4.1.2 Selective destruction of MALT1 T6BM2 causes fatal auto-immune activation

Malt1 TBM2 mice were born at Mendelian ratios and developed normally until 2 weeks of age. Thereafter, *Malt1*$^{TBM2/TBM2}$ stopped thriving and displayed a significant weight loss compared to unaffected *Malt1*$^{+/+}$ and *Malt1*$^{TBM2/+}$ control mice at the age of 17-20 days (Figure 4-5A) requiring euthanasia at a median age of 18 days (Figure 4-5B). To exclude confounding effects of severe inflammation in moribund mice, subsequent analyses were done at the age of 12-14 days before any signs of severe burden were visible. Necropsy at this age revealed lymphadenopathy and splenomegaly in *Malt1*$^{TBM2/TBM2}$ mice (Figure 4-5C-E). Additional signs of inflammation were represented by partially elevated INF-γ serum cytokine levels and high TNF-α and anti-dsDNA autoantibodies (Figure 4-5F-H). This auto-immune phenotype was persistent through five

generations of backcross to C57BL/6N, indicating that the observed effects are specific to the introduced MALT1 T6BM2 mutation.

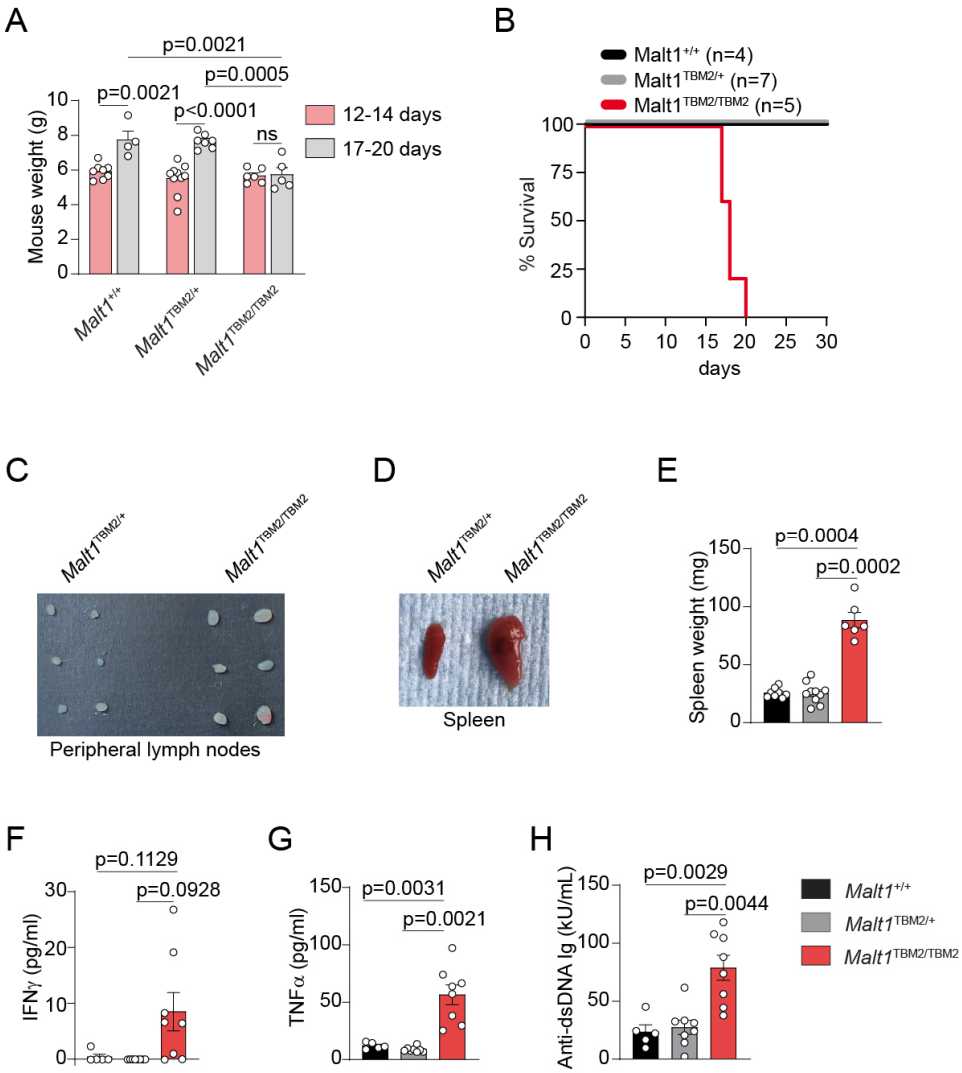

Figure 4-5: Survival and phenotypic signs of inflammation in *Malt1* TBM2 mice.

A) Mouse weight of *Malt1*$^{+/+}$, *Malt1*$^{TBM2/+}$ and *Malt1*$^{TBM2/TBM2}$ mice at days 12-14 and 17-20 after birth.

B) Survival curve of *Malt1*$^{+/+}$, *Malt1*$^{TBM2/+}$ and *Malt1*$^{TBM2/TBM2}$ mice. *Malt1*$^{TBM2/TBM2}$ mice showed a median survival of 18 days. Statistics for survival were calculated using a log-rank test.

C) Representative image of peripheral lymph nodes from *Malt1*$^{TBM2/+}$ and *Malt1*$^{TBM2/TBM2}$ mice at the age of 13 days.

D) Representative image of spleens from *Malt1*$^{TBM2/+}$ and *Malt1*$^{TBM2/TBM2}$ mice at the age of 12 days.

E) Spleen weight of *Malt1*$^{+/+}$ (black), *Malt1*$^{TBM2/+}$ (grey) and *Malt1*$^{TBM2/TBM2}$ mice (red) at the age of 12-14 days.

F-G) Blood serum levels of INF-γ (F), TNF-α (G), and anti-dsDNA autoantibodies (H) in *Malt1*$^{+/+}$, *Malt1*$^{TBM2/+}$ and *Malt1*$^{TBM2/TBM2}$ mice at the age of 12-14 days.

A, E-H) Each dot represents one mouse. All bars show the means ± SEM, and P values were calculated by two-way ANOVA combined with Sidak's multiple comparisons test (A) or by one-way ANOVA with Brown-Forsythe and Welch ANOVA test (E-H).

4.1.3 Drastic loss of B cells and lymphocyte activation in *Malt1* TBM2 mice

To analyze relative numbers and activation of B and T lymphocyte populations, immune phenotyping via flow cytometry was performed (Figure 4-6). Homozygous *Malt1* TBM2 mice showed drastically decreased percentages of B220+ B cells in spleen and to a lesser extent in lymph nodes with a relative reduction of CD3+ T cells in the spleen (Figure 4-6A-C). Splenic CD4+ and CD8+ percentages were normal, whereas lymph nodes displayed only mild changes in CD4+ and CD8+ ratios which did not affect relative CD3+ T cell numbers (Figure 4-6D-F). Analysis of thymic T cell populations revealed a slight increase in double negative (DN) and CD8+ T cells combined with fewer double positive (DP) T lymphocytes in *Malt1* TBM2 mice (Figure 4-6G and H). Taken together, *Malt1*$^{TBM2/TBM2}$ mice showed a drastic loss of B cells and aberrations in T lymphocyte populations in all tested lymphatic organs, which seemed not to be caused by a developmental defect in the thymus.

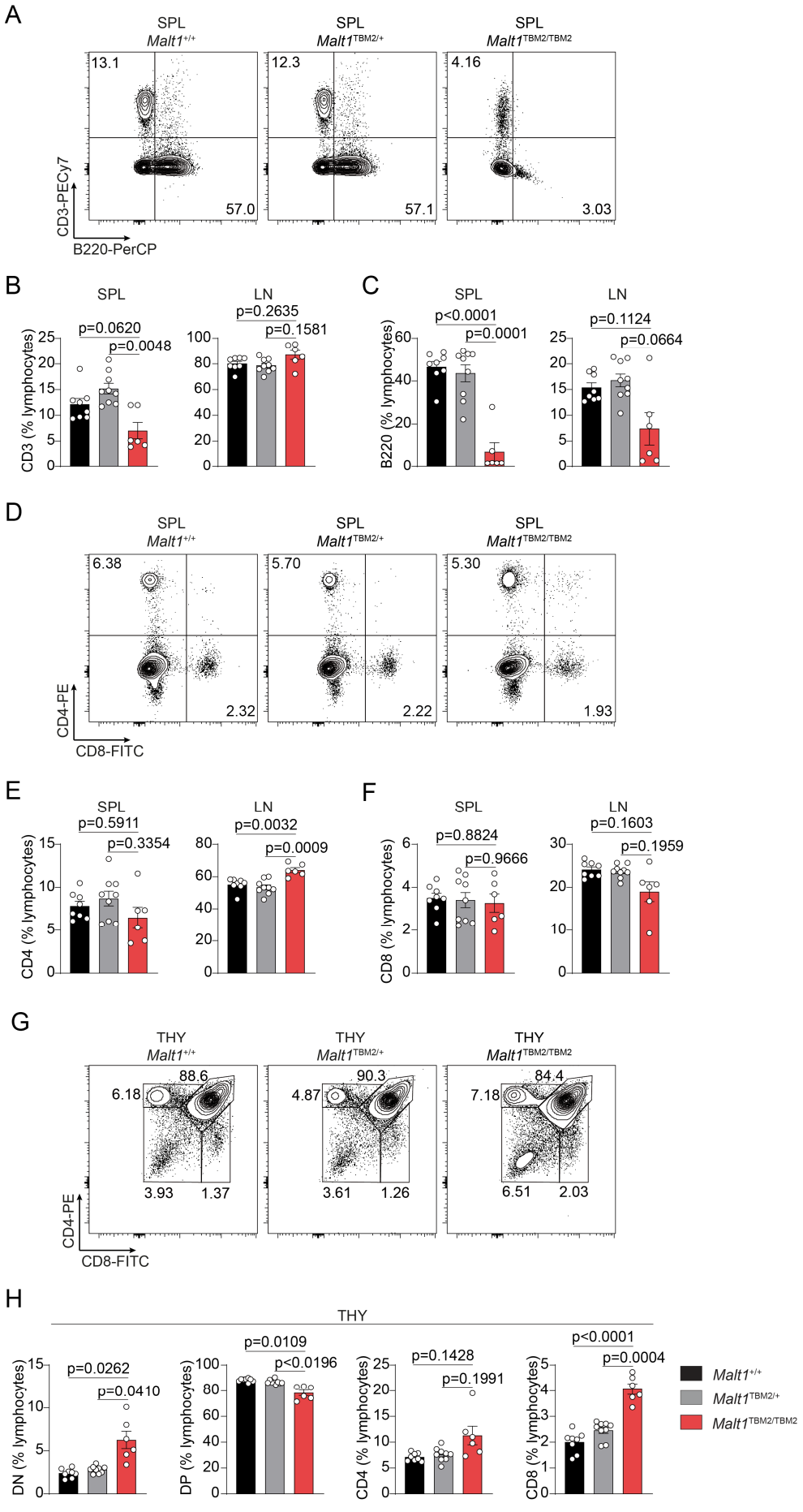
A
SPL
Malt1+/+
SPL
Malt1TBM2/+
SPL
Malt1TBM2/TBM2
13.1
57.0
12.3
57.1
4.16
3.03
CD3-PECy7
B220-PerCP
B
SPL
LN
p=0.0620
p=0.0048
p=0.2635
p=0.1581
CD3 (% lymphocytes)
C
SPL
LN
p<0.0001
p=0.0001
p=0.1124
p=0.0664
B220 (% lymphocytes)
D
SPL
Malt1+/+
SPL
Malt1TBM2/+
SPL
Malt1TBM2/TBM2
6.38
2.32
5.70
2.22
5.30
1.93
CD4-PE
CD8-FITC
E
SPL
LN
p=0.5911
p=0.3354
p=0.0032
p=0.0009
CD4 (% lymphocytes)
F
SPL
LN
p=0.8824
p=0.9666
p=0.1603
p=0.1959
CD8 (% lymphocytes)
G
THY
Malt1+/+
THY
Malt1TBM2/+
THY
Malt1TBM2/TBM2
88.6
6.18
3.93
1.37
90.3
4.87
3.61
1.26
84.4
7.18
6.51
2.03
CD4-PE
CD8-FITC
H
THY
p=0.0262
p=0.0410
p=0.0109
p<0.0196
p=0.1428
p=0.1991
p<0.0001
p=0.0004
DN (% lymphocytes)
DP (% lymphocytes)
CD4 (% lymphocytes)
CD8 (% lymphocytes)
Malt1+/+
Malt1TBM2/+
Malt1TBM2/TBM2

Figure 4-6: T and B lymphocyte populations in lymphoid organs of *Malt1* TBM2 mice.
A-C) Flow cytometry analysis of CD3+ T and B220+ B cells in spleen (SPL) and lymph nodes (LN) of *Malt1*$^{+/+}$, *Malt1*$^{TBM2/+}$ and *Malt1*$^{TBM2/TBM2}$ mice.
D-F) Flow cytometry analysis of CD4+ and CD8+ T cells in spleen and lymph nodes of *Malt1*$^{+/+}$, *Malt1*$^{TBM2/+}$ and *Malt1*$^{TBM2/TBM2}$ mice.
G, H) Flow cytometry analysis of CD4+ and CD8+, as well as CD4 CD8 double negative (DN) and double positive (DP) T cells in thymus of *Malt1*$^{+/+}$, *Malt1*$^{TBM2/+}$ and *Malt1*$^{TBM2/TBM2}$ mice.
A-H) Mice were analyzed at the age of 12-14 days after birth. Unaffected *Malt1*$^{+/+}$ (black) and *Malt1*$^{TBM2/+}$ (grey) littermates were used as control and compared to *Malt1*$^{TBM2/TBM2}$ mice (red). Each dot represents one mouse. All bars show means ± SEM, and p-values were calculated by one-way ANOVA with Brown-Forsythe and Welch ANOVA test.

To investigate the cause of inflammation in *Malt1*$^{TBM2/TBM2}$ mice, detailed immune phenotyping was performed. There was a massive increase in both CD4+ and CD8+ T_{EM} cells in spleen and lymph nodes of TBM2 mice, indicating strong immune activation. Upregulation of T_{EM} cells led to a strong relative decrease in CD4+ and CD8+ naïve ($T_{Naïve}$: $CD44^{lo}CD62L^{hi}$) and central memory (T_{CM}: $CD44^{hi}CD62L^{hi}$) T cells (Figure 4-7A-F). In addition, CD69, an early activation marker expressed on immune cells, was highly upregulated in CD3+ T cells derived from spleen and lymph nodes (Figure 4-7G, H). Thus, destruction of MALT1 T6BM2 induces strong T cell activation resulting in an increase in T_{EM} cells.

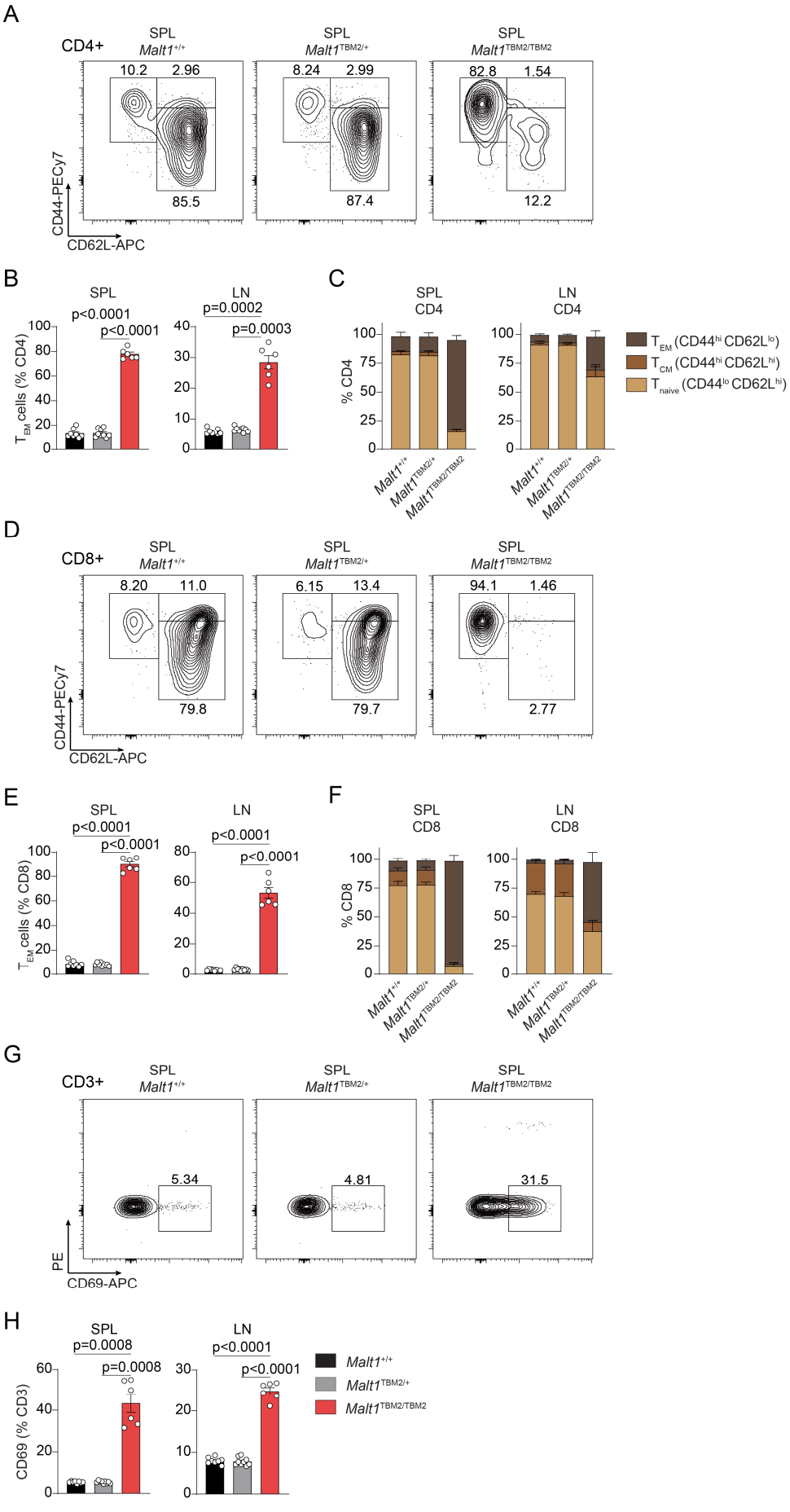
A
CD4+
SPL
Malt1+/+
SPL
Malt1TBM2/+
SPL
Malt1TBM2/TBM2
10.2
2.96
85.5
8.24
2.99
87.4
82.8
1.54
12.2
CD44-PECy7
CD62L-APC
B
SPL
LN
p<0.0001
p<0.0001
p=0.0002
p=0.0003
TEM cells (% CD4)
C
SPL CD4
LN CD4
% CD4
TEM (CD44hi CD62Llo)
TCM (CD44hi CD62Lhi)
Tnaive (CD44lo CD62Lhi)
Malt1+/+
Malt1TBM2/+
Malt1TBM2/TBM2
D
CD8+
8.20
11.0
79.8
6.15
13.4
79.7
94.1
1.46
2.77
E
TEM cells (% CD8)
F
SPL CD8
LN CD8
% CD8
G
CD3+
5.34
4.81
31.5
PE
CD69-APC
H
CD69 (% CD3)

Figure 4-7: Activation status of T lymphocytes in *Malt1* TBM2 mice.

A-C) Flow cytometry analysis of CD4+ naïve ($T_{naïve}$: $CD44^{lo}$ $CD62L^{hi}$), central memory (T_{CM}: $CD44^{hi}$ $CD62L^{hi}$) and effector memory T cells (T_{EM}: $CD44^{hi}$ $CD62L^{lo}$) in spleen (SPL) and lymph nodes (LN) of *Malt1*$^{+/+}$, *Malt1*$^{TBM2/+}$ and *Malt1*$^{TBM2/TBM2}$ mice.

D-F) Flow cytometry analysis of CD8+ $T_{naïve}$, T_{CM} and T_{EM} cells in spleen and lymph nodes of *Malt1*$^{+/+}$, *Malt1*$^{TBM2/+}$ and *Malt1*$^{TBM2/TBM2}$ mice.

G, H) Flow cytometry analysis of CD3+ CD69+ T cells in spleen and lymph nodes of *Malt1*$^{+/+}$, *Malt1*$^{TBM2/+}$ and *Malt1*$^{TBM2/TBM2}$ mice.

A-H) Mice were analyzed at the age of 12-14 days after birth. Unaffected *Malt1*$^{+/+}$ (black) and *Malt1*$^{TBM2/+}$ (grey) littermates were used as control and compared to *Malt1*$^{TBM2/TBM2}$ mice (red). Each dot represents one mouse. All bars show means ± SEM, and p-values were calculated by one-way ANOVA with Brown-Forsythe and Welch ANOVA test.

We also analyzed the phenotypic changes on B cell activation markers, regardless of the strong reduction of their relative numbers in TBM2 mice. Similar to T lymphocytes, B220+ B cells from *Malt1*$^{TBM2/TBM2}$ mice displayed high expression levels of CD69 compared to *Malt1*$^{+/+}$ and *Malt1*$^{TBM2/+}$ control mice (Figure 4-8A, B). Furthermore, CD86, a co-stimulatory surface molecule, was high in homozygous TMB2 mice (Figure 4-8C, D). Taken together, selective disruption of MALT1B-TRAF6 protein interaction induces a spontaneous activation of both T and B cells to a similar extent as complete loss of MALT1-TRAF6 binding in *Malt1* TBM mice (O'Neill et al., 2021).

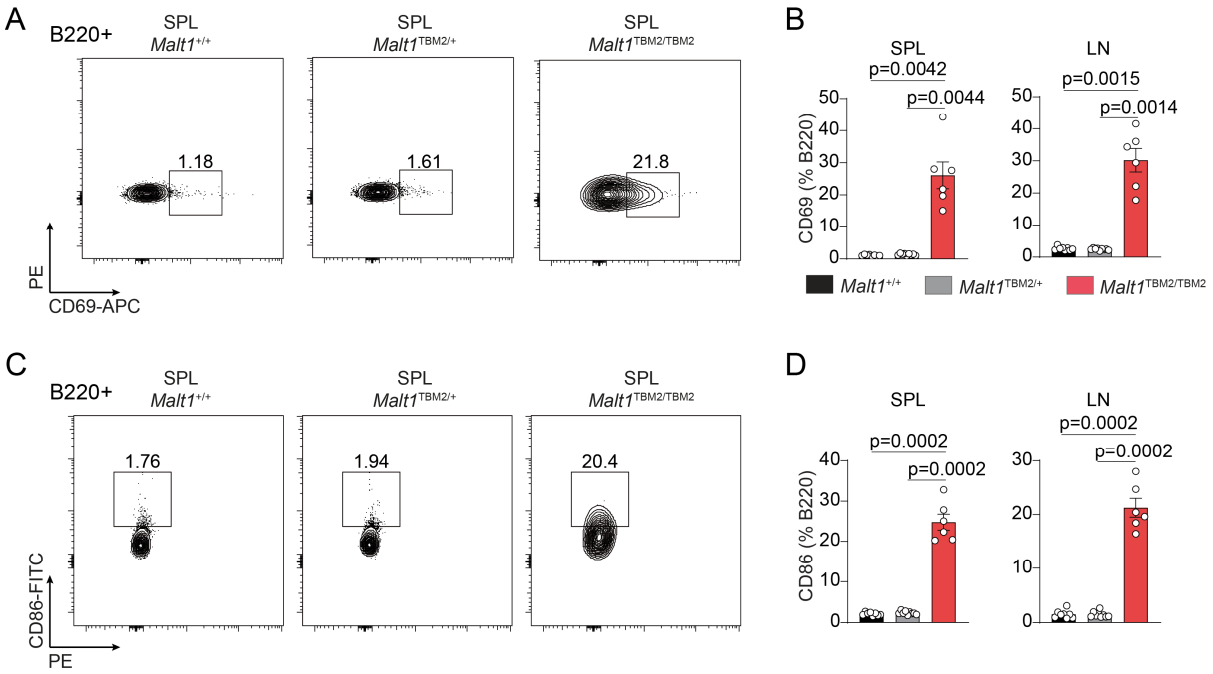

Figure 4-8: Activation status of B lymphocytes in *Malt1* TBM2 mice.

A, B) Flow cytometry analysis of B220+ CD69+ B cells in spleen (SPL) and lymph nodes (LN) of *Malt1*$^{+/+}$, *Malt1*$^{TBM2/+}$ and *Malt1*$^{TBM2/TBM2}$ mice.

C, D) Flow cytometry analysis of B220+ CD86+ B cells in spleen and lymph nodes of *Malt1*$^{+/+}$, *Malt1*$^{TBM2/+}$ and *Malt1*$^{TBM2/TBM2}$ mice.

A-D) Mice were analyzed at the age of 12-14 days after birth. Unaffected *Malt1*$^{+/+}$ (black) and *Malt1*$^{TBM2/+}$ (grey) littermates were used as control and compared to *Malt1*$^{TBM2/TBM2}$ mice (red). Each dot represents one mouse. All bars show means ± SEM, and p-values were calculated by one-way ANOVA with Brown-Forsythe and Welch ANOVA test.

4.1.4 *Malt1* TBM2 mice display elevated Treg numbers and function

Regulatory T (Treg) cells are crucial for maintaining peripheral tolerance and preventing autoimmunity by suppression of conventional (Tconv) T cells (Vignali et al., 2008). Several studies have shown that MALT1 protease function is essential for the development of functional Treg cells. Mice carrying the C472A mutation in the paracaspase domain (*Malt1* paracaspase mutant (PM) mice) develop an autoimmune phenotype due to the loss of suppressive Treg cell number and function (Bornancin et al., 2015; Gewies et al., 2014; Jaworski et al., 2014; Rosenbaum et al., 2019). In contrast, CD4+FoxP3+ Treg cells derived from spleen, lymph nodes and thymus of *Malt1*$^{TBM2/TBM2}$ mice were present and even slightly increased compared with heterozygous and wildtype controls (Figure 4-9A and B). In addition, relative numbers of CD44^{hi}CD62L^{lo} CD4+ effector (e)Treg cells of homozygous *Malt1* TBM2 mice and to a lesser extent of heterozygous littermates were elevated (Figure 4-9C). *Malt1* TBM2 eTregs expressed equal levels of the suppression marker CTLA-4, but higher levels of Ox40 and PD-1 indicating that eTregs are functional (Figure 4-9D). Thus, selective disruption of MALT1B-TRAF6 binding is able to induce a spontaneous activation of Tconv cells which is not due to loss of Treg cell number or function.

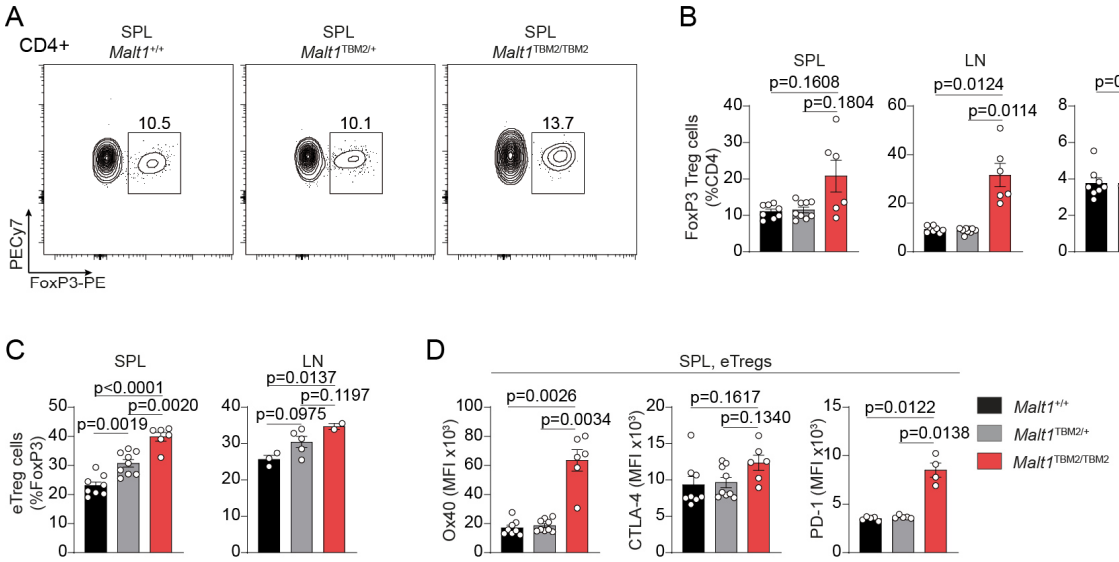

Figure 4-9: Immune phenotyping of regulatory T cells in *Malt1* TBM2 mice.

A, B) Flow cytometry analysis of CD4+ FoxP3+ regulatory T (Treg) cells in spleen (SPL), lymph nodes (LN) and thymus (THY) of *Malt1*$^{+/+}$, *Malt1*$^{TBM2/+}$ and *Malt1*$^{TBM2/TBM2}$ mice.

C) Flow cytometry analysis of CD4+ FoxP3+ CD44^{hi} CD62L^{lo} effector Tregs (eTreg) in spleen and lymph nodes of *Malt1*$^{+/+}$, *Malt1*$^{TBM2/+}$ and *Malt1*$^{TBM2/TBM2}$ mice.

D) Flow cytometry analysis of Ox40, CTLA-4 and PD-1 expression on eTregs in spleen of *Malt1*$^{+/+}$, *Malt1*$^{TBM2/+}$ and *Malt1*$^{TBM2/TBM2}$ mice. Graphs show Median Fluorescence Intensity (MFI).

A-D) Mice were analyzed at the age of 12-14 days after birth. *Malt1*$^{+/+}$ (black) and *Malt1*$^{TBM2/+}$ (grey) littermates were used as control and compared to *Malt1*$^{TBM2/TBM2}$ mice (red). Each dot represents one mouse. All bars show means ± SEM, and p-values were calculated by one-way ANOVA with Brown-Forsythe and Welch ANOVA test.

4.1.5 *Malt1* TBM2 mice die due to severe liver damage and anemia

During analysis of *Malt1* TBM2 mice, we consistently observed thin, colorless blood, and isolated femur bones seemed to lack red bone marrow and appeared transparent (Figure 4-10A). Therefore, we performed a blood count and analyzed clinical parameters of blood serum at the age of 12 – 14 days before mice showed signs of severe disease. Whereas leukocyte levels were normal or slightly elevated, erythrocytes as well as hemoglobin and hematocrit levels were reduced, indicating an incipient anemia in *Malt1*$^{TBM2/TBM2}$ mice (Figure 4-10B-E). Analysis of aspartate aminotransferase (AST) and glutamate dehydrogenase (GLDH) revealed that serum levels are increased in *Malt1* TBM2 mice (Figure 4-10F and G). Both enzymes are mainly found in the liver and an increase in blood serum indicates damaged or necrotic hepatocytes. Thus, massive inflammation in *Malt1* TBM2 induces severe liver damage, resulting in a fatal anemic phenotype due to insufficient oxygen supply.

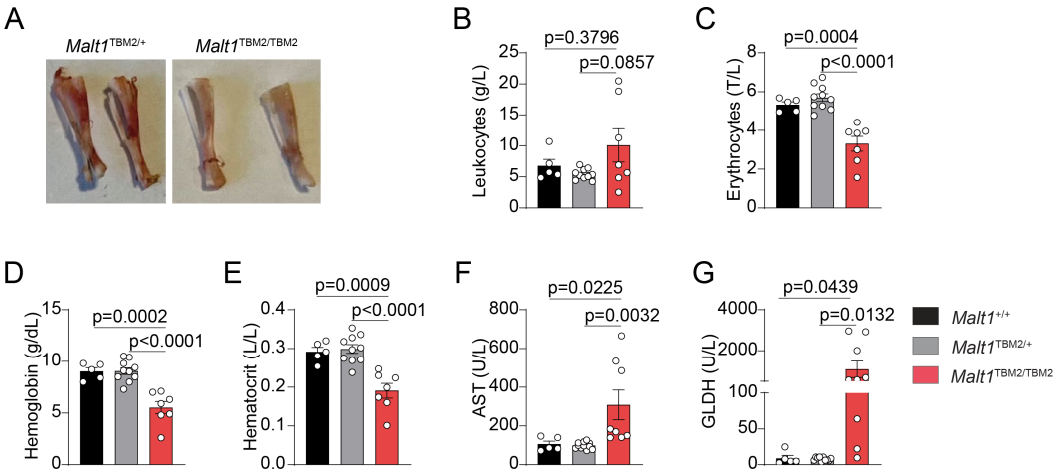

Figure 4-10: Blood and serum analysis of *Malt1* TBM2 mice.
A) Representative image of the femur bone isolated from *Malt1*$^{TBM2/+}$ and *Malt1*$^{TBM2/TBM2}$ mice.
B-E) Analysis of leukocytes (B), erythrocytes (C), hemoglobin (D) and hematocrit (E) in whole blood of *Malt1*$^{+/+}$, *Malt1*$^{TBM2/+}$ and *Malt1*$^{TBM2/TBM2}$ mice.
F-G) Analysis of aspartate aminotransferase (AST; F) and glutamate dehydrogenase (GLDH; G) in sera of *Malt1*$^{+/+}$, *Malt1*$^{TBM2/+}$ and *Malt1*$^{TBM2/TBM2}$ mice.
A-J) Mice were analyzed at the age of 12-14 days after birth. Unaffected *Malt1*$^{+/+}$ (black) and *Malt1*$^{TBM2/+}$ (grey) littermates were used as control and compared to *Malt1*$^{TBM2/TBM2}$ mice (red). Each dot represents one mouse. All bars show means ± SEM, and p-values were calculated by one-way ANOVA.

4.1.6 Selective loss of MALT1B-TRAF6 protein interaction impairs NF-κB signaling

MALT1-TRAF6 binding is crucial for CBM-dependent downstream NF-κB signaling in T cells (Meininger et al., 2016; O'Neill et al., 2021). Due to defective MALT1-TRAF6 binding and NF-κB activation in primarily MALT1B E795D-expressing T cells, the immune response of the patient with homozygous MALT1 c.2418G>C transversion is severely compromised. In line with this, the patient suffers from symptoms of immune deficiency manifested by chronic ear and bronchial infections (Kutukculer et al., 2021). To study NF-κB signaling in *Malt1* TBM2 mice on single cell level, we checked IκBα protein expression in splenic CD4+ T and CD19+ B cells using flow cytometry (Figure 4-11A). In general, *Malt1*$^{TBM2/TBM2}$ mice expressed higher IκBα protein levels in unstimulated cells of both lymphocyte populations, suggesting that basal IκBα degradation may be impaired leading to protein accumulation (Figure 4-11B and D). To induce NF-κB activation, total splenocytes were stimulated with either αCD3/CD28 for TCR activation or PMA/Ionomycin (P/I) for TCR-independent activation of PKC upstream of the CBM complex. IκBα degradation was analyzed by comparing median fluorescence intensity (MFI) values of stimulated to unstimulated cells. Whereas CD4+ and CD19+ lymphocytes of *Malt1*$^{+/+}$ and *Malt1*$^{TBM2/+}$ mice displayed reduced IκBα expression upon stimulation, cells of *Malt1*$^{TBM2/TBM2}$ were strongly impaired in IκBα degradation (Figure 4-11A-E). Furthermore, we assessed NF-κB signaling in a second approach using Western Blot of lysates from total splenocytes. Induction of IκBα phosphorylation and degradation as well as p65 phosphorylation was absent in *Malt1* TBM2 mice upon P/I stimulation (Figure 4-11F). Thus, MALT1B-TRAF6 protein interaction dictates downstream NF-κB activation in mice.

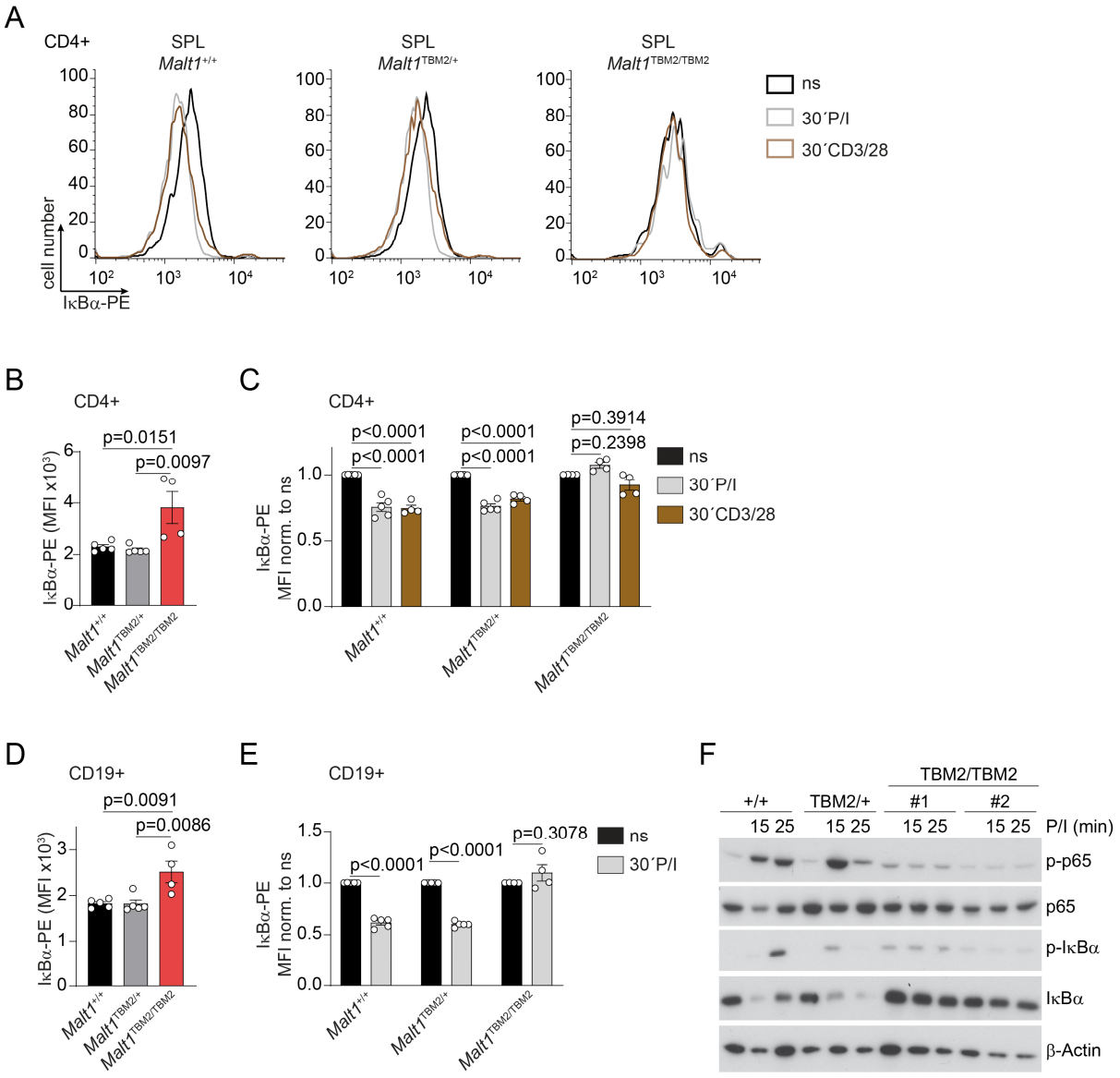

Figure 4-11: NF-κB activation in *Malt1* TBM2 mice.

A-C) Flow cytometry analysis of IκBα degradation in unstimulated (ns), PMA/Ionomycin (P/I) and CD3/CD28 stimulated CD4+ T cells from spleen (SPL) of *Malt1*$^{+/+}$, *Malt1*$^{TBM2/+}$ and *Malt1*$^{TBM2/TBM2}$ mice shown as Mean Fluorescence Intensity (MFI) (B) and MFI normalized to ns cells (C).

D-E) Flow cytometry analysis of IκBα degradation in CD19+ B cells from spleen of *Malt1*$^{+/+}$, *Malt1*$^{TBM2/+}$ and *Malt1*$^{TBM2/TBM2}$ mice shown as Mean Fluorescence Intensity (MFI) (D) and MFI normalized to ns cells (E).

F) Western blot analysis in lysates of total splenocytes from *Malt1*$^{+/+}$, *Malt1*$^{TBM2/+}$ and *Malt1*$^{TBM2/TBM2}$ mice after P/I stimulation. The onset of NF-κB signaling was determined by IκBα phosphorylation/degradation and p65 phosphorylation. β-Actin served as loading control.

A-E) Mice were analyzed at the age of 12-14 days after birth. Unaffected *Malt1*$^{+/+}$ and *Malt1*$^{TBM2/+}$ littermates were used as control and compared to *Malt1*$^{TBM2/TBM2}$ mice. Each dot represents one mouse. All bars show means ± SEM, and p-values were calculated by one-way ANOVA with Brown-Forsythe and Welch ANOVA test (B and D) or by two-way ANOVA combined with Sidak's multiple comparisons test (C and E).

4.1.7 Constitutive MALT1B paracaspase activity induces upregulation of T cell activators

The autoimmune phenotype of TBM mice could be attributed to deregulated MALT1 protease activity. In resting T cells, TRAF6 functions as molecular brake and suppresses low, steady-state MALT1 substrate cleavage (O'Neill et al., 2021). In line with this, splenocytes of *Malt1* TBM2 mice showed constitutive cleavage of the MALT1 substrates CYLD, HOIL-1 and N4BP-1 in unstimulated conditions, indicating that selective destruction of MALT1B-TRAF6 protein interaction is sufficient to activate MALT1 paracaspase (Figure 4-12A). Deregulated MALT1 protease activity leads to a partial inactivation of the RNA binding proteins (RBPs) and MALT1 substrates Regnase-1 and Roquin-1/2 (O'Neill et al., 2021). Both are essential regulators of pro-inflammatory mRNAs and maintain peripheral tolerance (Essig et al., 2017; Jeltsch et al., 2014; Vogel et al., 2013). Therefore, we tested expression of the Regnase-1 and Roquin-1/2 target genes NFκBID/IκBNS and ICOS. *Malt1*$^{TBM2/TBM2}$ mice showed high expression of both targets in CD4+ and CD8+ T cells compared to control mice, indicating constitutive cleavage of Regnase-1 and Roquin-1/2 which results in loss of post-transcriptional regulation of their target genes (Figure 4-12B-D). Taken together, *Malt1* TBM2 mice confirm that TRAF6 functions as a negative regulator of MALT1 protease activity in resting T cells and prevents spontaneous immune activation.

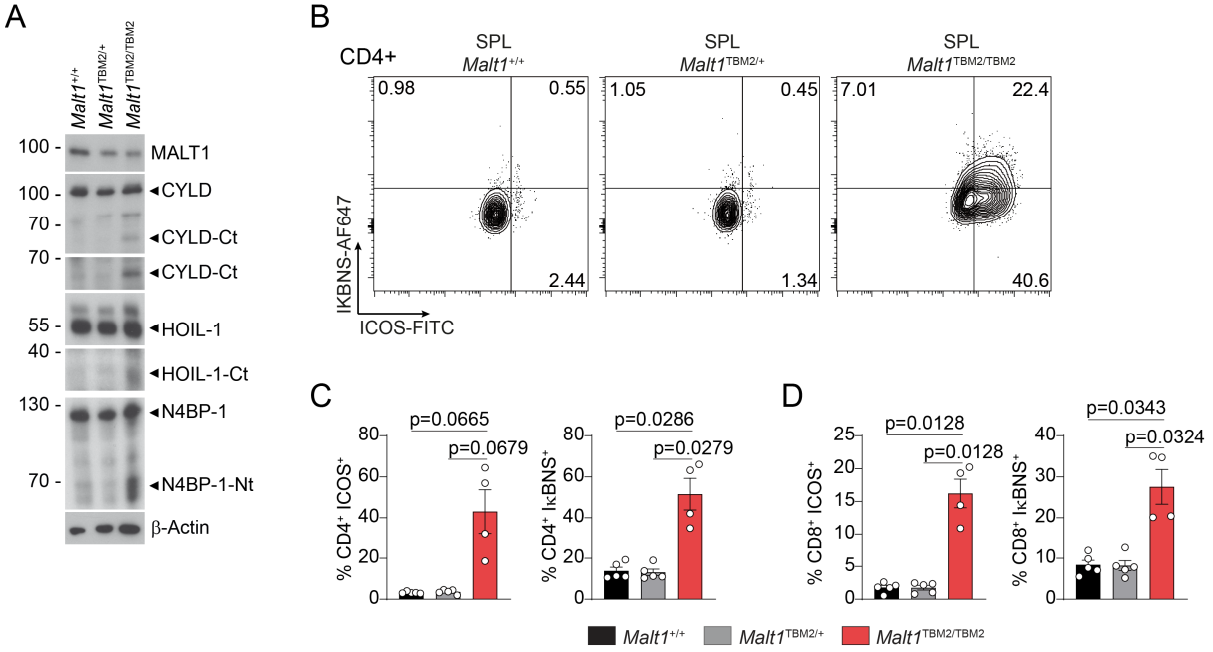

Figure 4-12: Constitutive MALT1 substrate cleavage in *Malt1* TBM2 mice.

A) Western blot analysis of MALT1 substrate cleavage in lysates of splenocytes from *Malt1*$^{+/+}$, *Malt1*$^{TBM2/+}$ and *Malt1*$^{TBM2/TBM2}$ mice. Ct: C-terminal cleavage fragment. Nt: N-terminal cleavage fragment.

B) Representative plots of CD4+ IκBNS+ ICOS+ T cells in spleen (SPL) of *Malt1*$^{+/+}$, *Malt1*$^{TBM2/+}$ and *Malt1*$^{TBM2/TBM2}$ mice.

C, D) Flow cytometry analysis of CD4+ ICOS+ and CD4+ IκBNS+ (D) or CD8+ ICOS+ and CD8+ IκBNS+ (E) T cells in spleen. Mice were analyzed at the age of 12-14 days after birth. Unaffected *Malt1*$^{+/+}$ (black) and *Malt1*$^{TBM2/+}$ (grey) littermates were used as control and compared to *Malt1*$^{TBM2/TBM2}$ mice (red). Each dot represents one mouse. All bars show means ± SEM, and p-values were calculated by one-way ANOVA with Brown-Forsythe and Welch ANOVA test.

4.2 TRAF6/ LUBAC-dependent BCL10 ubiquitination counteracts MALT1 protease

So far, the molecular mechanism of how TRAF6 restricts MALT1 protease activity in resting T cells has not been solved. Experiments in Jurkat T cells demonstrated that constitutive and TCR-induced MALT1 protease activity have the same requirements. On the side of MALT1, K644 monoubiquitination, dimerization of the paracaspase domain and BCL10 association are essential, whereas for TRAF6, E3 ligase activity and oligomerization are critical. Furthermore, a functional TCR complex and the CBM components CARD11 and BCL10 are required (O'Neill et al., 2021). We hypothesized that either CARD11 or BCL10 are the direct targets of negative regulation of MALT1 protease activity by TRAF6. Since TCR engagement induces modification of BCL10 with polyubiquitin chains (Hu et al., 2006a; Paul et al., 2012; Satpathy et al., 2015; Scharschmidt et al., 2004; Wu & Ashwell, 2008; Yang et al., 2016), we decided to further investigate, whether TRAF6 is involved in BCL10 ubiquitination and if this might be implicated in TRAF6-mediated restriction of MALT1 protease activity.

4.2.1 TRAF6 and LUBAC regulate ubiquitination of the BCL10 CARD

BCL10 polyubiquitination was suggested to trigger initial NF-κB activation but also terminate signaling via ubiquitin-mediated BCL10 degradation and subsequent CBM complex disassembly (Hu et al., 2006a; Paul et al., 2012; Satpathy et al., 2015; Scharschmidt et al., 2004; Wu & Ashwell, 2008; Yang et al., 2016). P/I stimulation leads to the attachment of polyubiquitin chains to BCL10 in Jurkat T cells, as evident from the high molecular weight smear in BCL10 precipitates (Figure 4-13A). Staining with the ubiquitin antibody P4D1, which detects mono- and polyubiquitin, verified the high molecular weight band for immunoprecipitated BCL10. Using an anti-linear ubiquitin linkage-specific antibody further showed that BCL10 is at least in part modified with linear ubiquitin chains. CARD11- and MALT1-deficient Jurkat T cells were strongly impaired in BCL10 polyubiquitination, indicating that both proteins are essential for ubiquitin attachment to BCL10 (Figure 4-13A). Next, we wanted to test whether the absence of TRAF6 impacts BCL10 polyubiquitination and compare the effect to LUBAC KO Jurkat T cells. LUBAC catalyzes linear ubiquitination and was previously suggested to mediate attachment of linear polyubiquitin chains to BCL10 CARD (Wu & Ashwell, 2008). The LUBAC components HOIP and HOIL-1 are indeed essential for P/I-induced BCL10 polyubiquitination. However, TRAF6 deficiency also prevented detection of ubiquitinated BCL10 (Figure 4-13B). Taken together, our experiments show that CBM complex formation as well as the E3 ligases LUBAC and TRAF6 are required for BCL10 polyubiquitination.

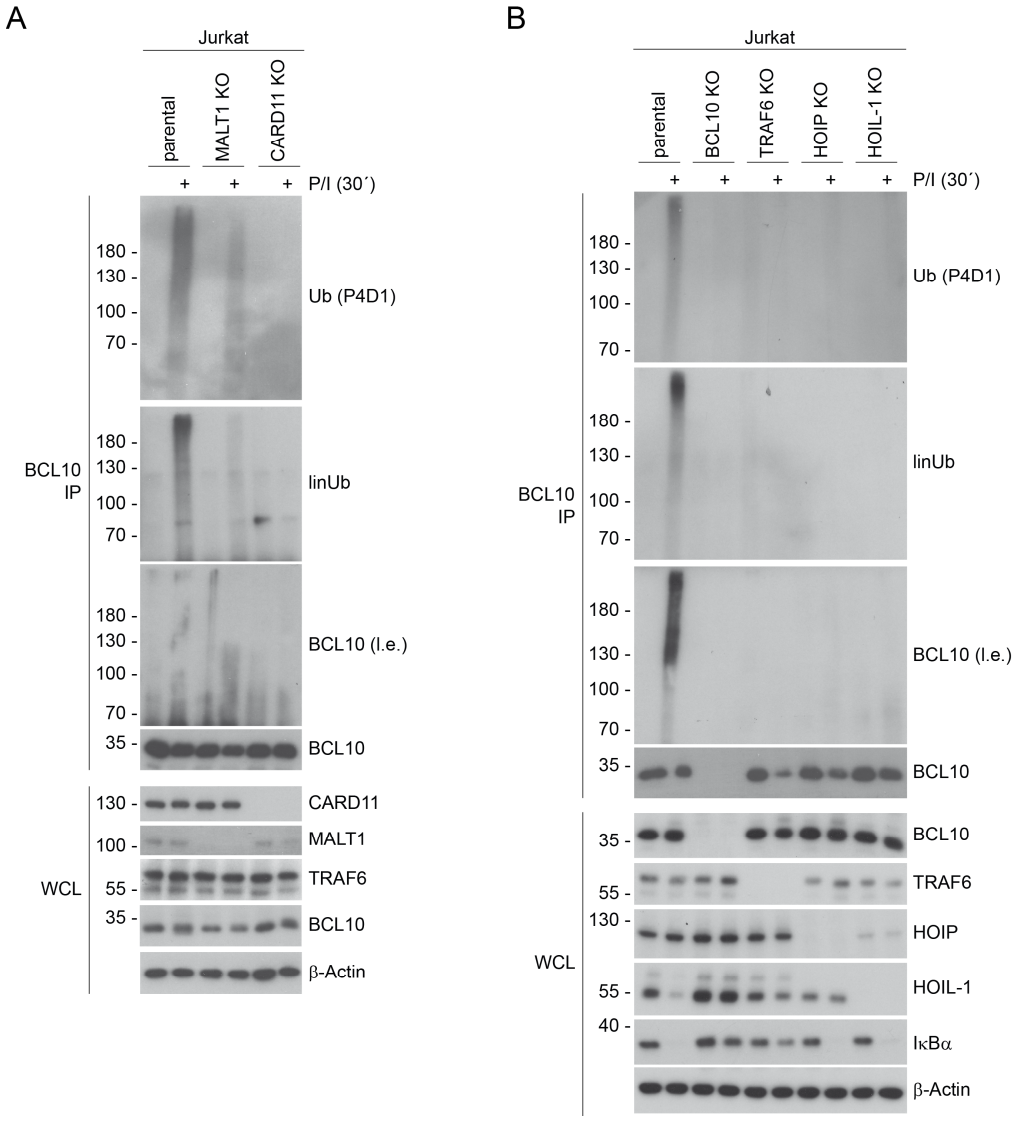

Figure 4-13: Analysis of P/I-induced BCL10 polyubiquitination in various KO Jurkat T cells.
A, B) Western blot analysis of BCL10 polyubiquitination in parental, MALT1 or CARD11 KO (A) or BCL10, TRAF6, HOIP or HOIL-1 KO (B) Jurkat T cells. Cells were stimulated with P/I and lysates were immunoprecipitated (IP) under denaturing conditions with anti-BCL10 antibody. IP: immunoprecipitation. WCL: whole cell lysate. l.e.: longer exposure.

Since TRAF6 is known to mediate K63-linked polyubiquitination, but LUBAC catalyzes M1-linked polyubiquitination, we decided to analyze the linkage specificity of BCL10 polyubiquitin chains. Therefore we incubated BCL10 precipitates with the recombinant deubiquitinases OTULIN and AMSH-LP. OTULIN is a linear ubiquitin-specific deubiquitinase which specifically hydrolyzes linear polyubiquitin chains (Keusekotten et al., 2013; Rivkin et al., 2013). In line with this, recombinant OTULIN exclusively cleaved M1-linked tetra-ubiquitin (Ub_4) but not K63-linked Ub_4 (Figure 4-14A, top). In contrast, AMSH-LP specifically hydrolyzes K63-linked ubiquitin chains (Komander et al., 2009), as evident from the detection of tri-, di- and mono-ubiquitin solely in the presence of K63-linked Ub_4 (Figure 4-14A, bottom). OTULIN drastically reduced BCL10 polyubiquitination, whereas AMSH-LP was less efficient, indicating that BCL10 is mainly M1-linked polyubiquitinated and to a

lesser extent K63-linked ubiquitinated (Figure 4-14B). Taken together, the combined action of LUBAC and TRAF6 catalyze BCL10 polyubiquitination, resulting in mixed ubiquitin chains with mainly linear linkage.

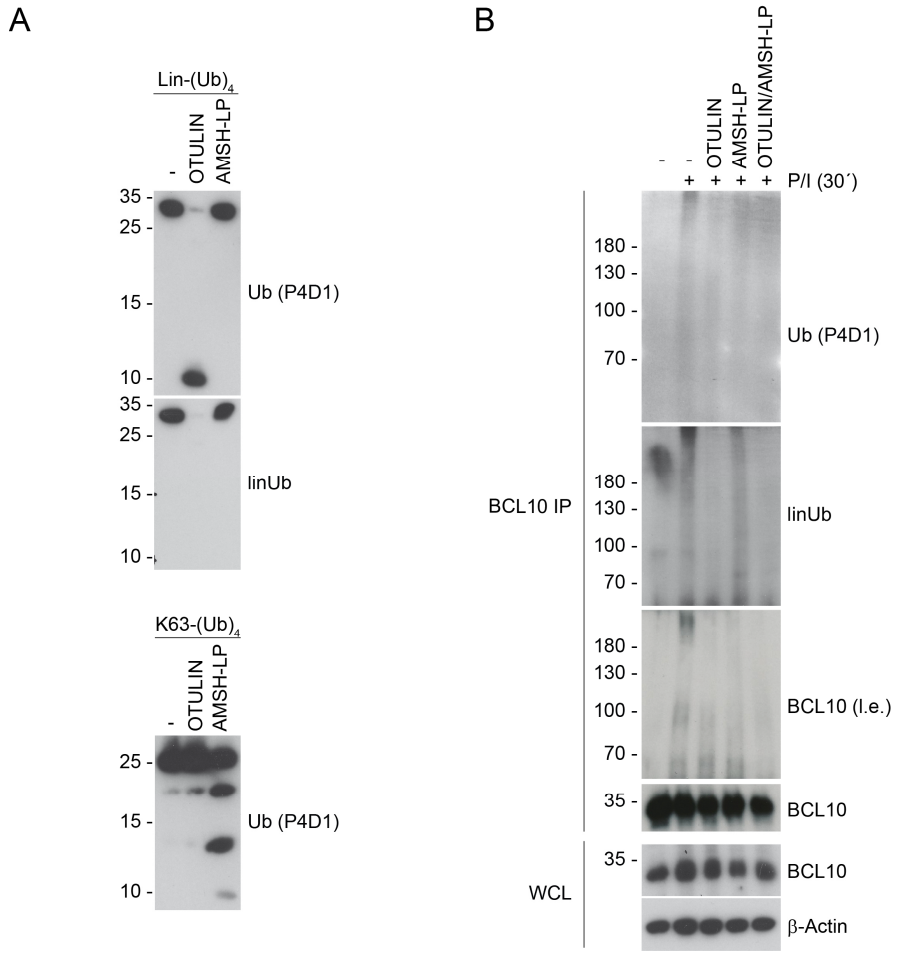

Figure 4-14: K63- and M1-linked mixed ubiquitin chains are attached to BCL10.

A) In vitro cleavage assay of linear (M1-) tetra-ubiquitin (top) or K63-linked tetra-ubiquitin (bottom) with OTULIN and AMSH-LP. Recombinant proteins were incubated with respective deubiquitinases for 60 min at 30°C. Ubiquitin chains were analyzed by Western blot.

B) Linkage analysis of Ub chains attached to BCL10 upon P/I stimulation. Jurkat T cells were stimulated with P/I and lysates were immunoprecipitated (IP) under denaturing conditions with anti-BCL10 antibody, following treatment with OTULIN, AMSH-LP or both deubiquitinases for 60 min at 30°C. Ub chains were analyzed by Western blot. IP: immunoprecipitation. WCL: whole cell lysate. I.e.: longer exposure.

4.2.2 HOIL-1 deficiency mildly affects CBM-mediated NF-κB signaling

Conjugation of M1- and K63-linked polyubiquitin chains to BCL10 was suggested to promote recruitment of the IKK complex and subsequent downstream NF-κB activation (Wu & Ashwell, 2008; Yang et al., 2016). Thus, we wanted to verify whether a functional LUBAC is essential for CBM-induced NF-κB signaling. Whereas TRAF6 deficiency strongly impaired IκBα degradation upon P/I stimulation, HOIL-1 and HOIP KO did not affect degradation of IκBα (Figure 4-13B). To study the importance of the LUBAC in NF-κB activation, we analyzed several Jurkat HOIL-1 KO clones. HOIL-1 deficiency downregulated protein expression of HOIP and SHARPIN and thus destabilized the LUBAC (Figure 4-15A). To assess NF-κB activation, we transduced an NF-κB-EGFP reporter, consisting of EGFP under the control of six NF-κB binding sites, into parental and HOIL-1 KO Jurkat T cells and determined the median fluorescence intensity (MFI) via flow cytometry (Figure 4-15B, C). In contrast to previous findings, we did not observe that HOIL-1 deficiency significantly impaired NF-κB-EGFP expression upon P/I stimulation. TCR engagement via CD3/CD28 stimulation resulted in a mild reduction of NF-κB activation in the two HOIL-1 KO clones. In contrast, TNF-α-induced NF-κB signaling was defective in both HOIL-1 KO clones. Next we performed a biochemical analysis and tested the effect of HOIL-1 deficiency on NF-κB and mitogen-activated protein kinase (MAPK) signaling, as well as MALT1 protease activation downstream of the CBM complex. P/I stimulation induced strong IκBα phosphorylation and degradation and p65 phosphorylation in parental Jurkat T cells. All three tested HOIL-1 KO clones displayed less p-p65 and p-IκBα, but showed no impairment in IκBα degradation. Activation of MALT1 protease function was comparable between WT and HOIL-1-deficient Jurkat T cells as evident from cleavage of MALT1 substrates CYLD, Regnase-1 and N4BP-1. In addition, phosphorylation of c-Jun N-terminal kinase (JNK) and extracellular signal-regulated kinase (ERK) was unaffected by HOIL-1 deficiency (Figure 4-15D). CD3/CD28 stimulation of HOIL-1 KO Jurkat T cells revealed a mild impairment in IκBα phosphorylation and degradation as well as p65 phosphorylation, but no effect on MALT1 protease activation (Figure 4-15E). Taken together, the LUBAC subunit HOIL-1 is crucial for TNF-mediated NF-κB signaling but plays a minor role in triggering CBM-dependent NF-κB activation and is dispensable for MALT1 paracaspase function. Similar results were obtained in HOIP-deficient Jurkat T cells (data by Franziska Ober, unpublished). In striking contrast to these essential LUBAC subunits, the E3 ubiquitin ligase TRAF6 is crucial for TCR-induced NF-κB signaling (O'Neill et al., 2021).

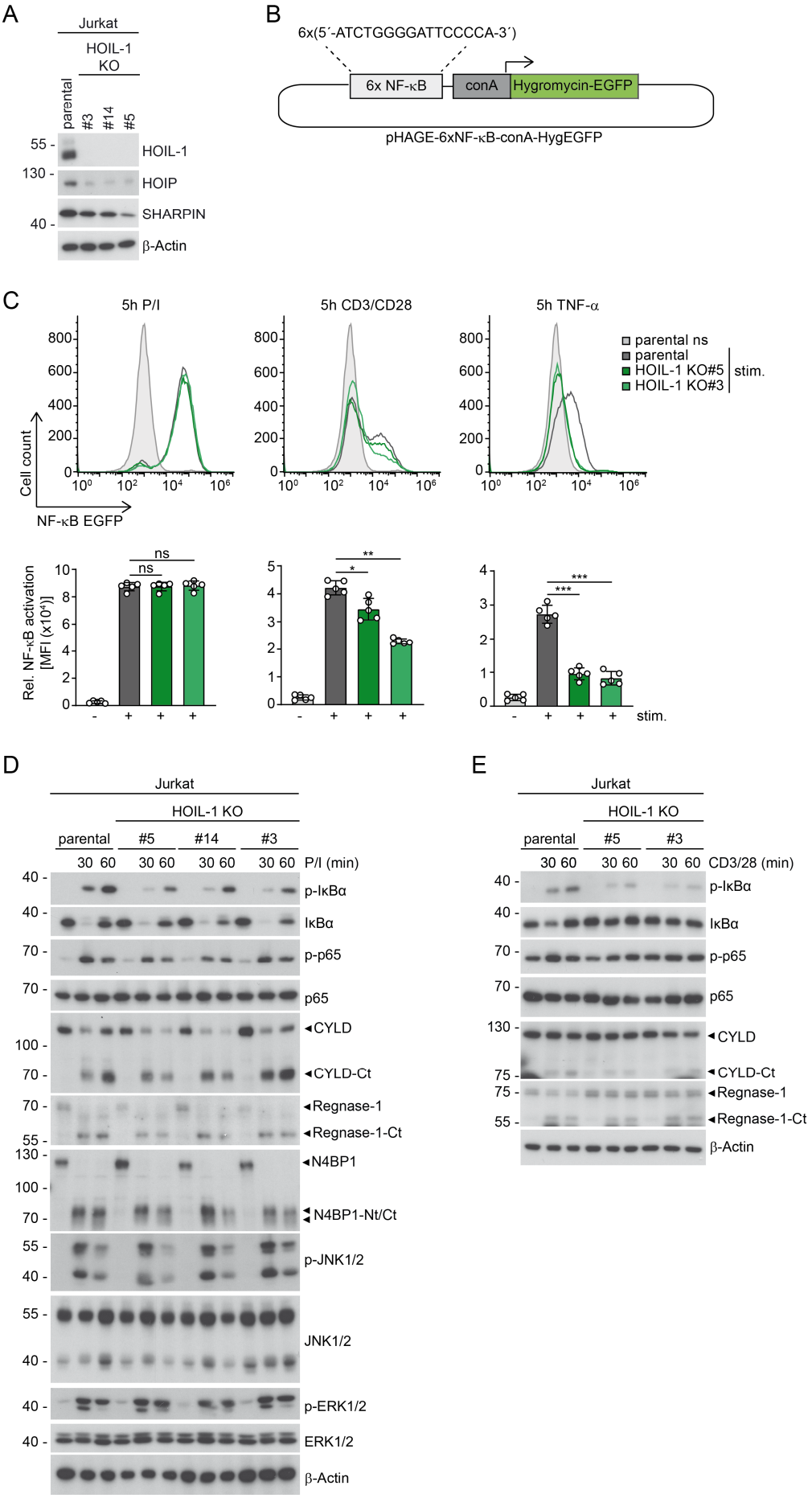
A
Jurkat
HOIL-1 KO
parental
#3
#14
#5
55 -
130 -
40 -
HOIL-1
HOIP
SHARPIN
β-Actin
B
6x(5´-ATCTGGGGATTCCCCA-3´)
6x NF-κB
conA
Hygromycin-EGFP
pHAGE-6xNF-κB-conA-HygEGFP
C
5h P/I
5h CD3/CD28
5h TNF-α
parental ns
parental
HOIL-1 KO#5
HOIL-1 KO#3
stim.
Cell count
NF-κB EGFP
Rel. NF-κB activation [MFI (x10⁴)]
ns
**
*
***
stim.
D
Jurkat
HOIL-1 KO
parental
#5
#14
#3
30 60
P/I (min)
p-IκBα
IκBα
p-p65
p65
CYLD
CYLD-Ct
Regnase-1
Regnase-1-Ct
N4BP1
N4BP1-Nt/Ct
p-JNK1/2
JNK1/2
p-ERK1/2
ERK1/2
β-Actin
E
Jurkat
HOIL-1 KO
parental
#5
#3
30 60
CD3/28 (min)
p-IκBα
IκBα
p-p65
p65
CYLD
CYLD-Ct
Regnase-1
Regnase-1-Ct
β-Actin

Figure 4-15: NF-κB signaling in HOIL-1-deficient Jurkat T cells.
A) Western blot analysis of HOIL-1 KO Jurkat T cell clones. Protein expression of HOIL-1, HOIP and SHARPIN were assessed.
B) Schematic representation of pHAGE-6xNF-κB-conA-HygEGFP reporter plasmid. Six NF-κB binding sites are fused to the minimal chicken conalbumin (conA) promoter, which controls the expression of a hygromycin-EGFP fusion gene.
C) Flow cytometry analysis of NF-κB reporter activation in parental and HOIL-1 KO Jurkat T cells. Cells were stimulated with P/I, CD3/28 or TNFα for 5h and NF-κB activation was assessed via EGFP expression. Depicted are median fluorescence intensity (MFI) values. Bars show means ± SEM (n=5), and p-values were calculated by unpaired Student's t test. *$p < 0.05$, **$p < 0.01$, ***$p < 0.001$; ns, not significant.
D, E) Western Blot analysis of NF-κB signaling and MALT1 protease activation upon P/I (D) and CD3/28 (E) stimulation in parental and HOIL-1 KO Jurkat T cells. The onset of NF-κB signaling was determined by IκBα phosphorylation/degradation and p65 phosphorylation, MALT1 paracaspase activity was assessed by cleavage of CYLD, Regnase-1 and N4BP-1. Ct: C-terminal cleavage fragment. Nt: N-terminal cleavage fragment. β-Actin served as loading control.

4.2.3 Potential BCL10 ubiquitin acceptor sites are essential for NF-κB and MALT1 paracaspase activation

Since TRAF6, but not LUBAC, positively regulated CBM-dependent NF-κB signaling, but both E3 ligases were critical for BCL10 polyubiquitination, we wanted to check if ubiquitin attachment to BCL10 itself is essential for activation of NF-κB signaling and MALT1 paracaspase. Lysine (K) residues 17, 31 and 63 in the BCL10 CARD have been suggested to serve as direct conjugation sites for M1-, K63- and K48-linked ubiquitin chains (Paul et al., 2012; Wu & Ashwell, 2008; Yang et al., 2016). We assessed the role of these putative ubiquitin acceptor sites for NF-κB activation by introducing respective BCL10 K-to-R variants into BCL10 KO NF-κB-EGFP reporter Jurkat T cells. Lentiviral infection resulted in equal transduction of Jurkat T cells as indicated by co-expressed human ΔCD2 surface marker (Figure 4-16A). BCL10 WT and K31R/K63R were expressed at endogenous levels, whereas K17R and the triple mutant K17R/K31R/K63R had lower expression, indicating that mutating lysine 17 may destabilize BCL10 (Figure 4-16B). P/I stimulation in mock-transduced cells failed to induce NF-κB activation but reconstitution with BCL10 WT rescued defective signaling caused by BCL10 deficiency. However, mutation of putative ubiquitination sites K17R and K31R/K63R severely impaired expression of the NF-κB-EGFP reporter with the triple mutant K17R/K31R/K63R showing the strongest effect (Figure 4-16C). Quantification of EGFP positive cells revealed a significant decrease in NF-κB activation for all three mutants (Figure 4-16C, bottom) as described previously (Wu & Ashwell, 2008; Yang et al., 2016). In contrast, stimulation with TNFα induced NF-κB activation in cells expressing either WT or mutant BCL10, indicating that CBM-independent NF-κB signaling was still functional.

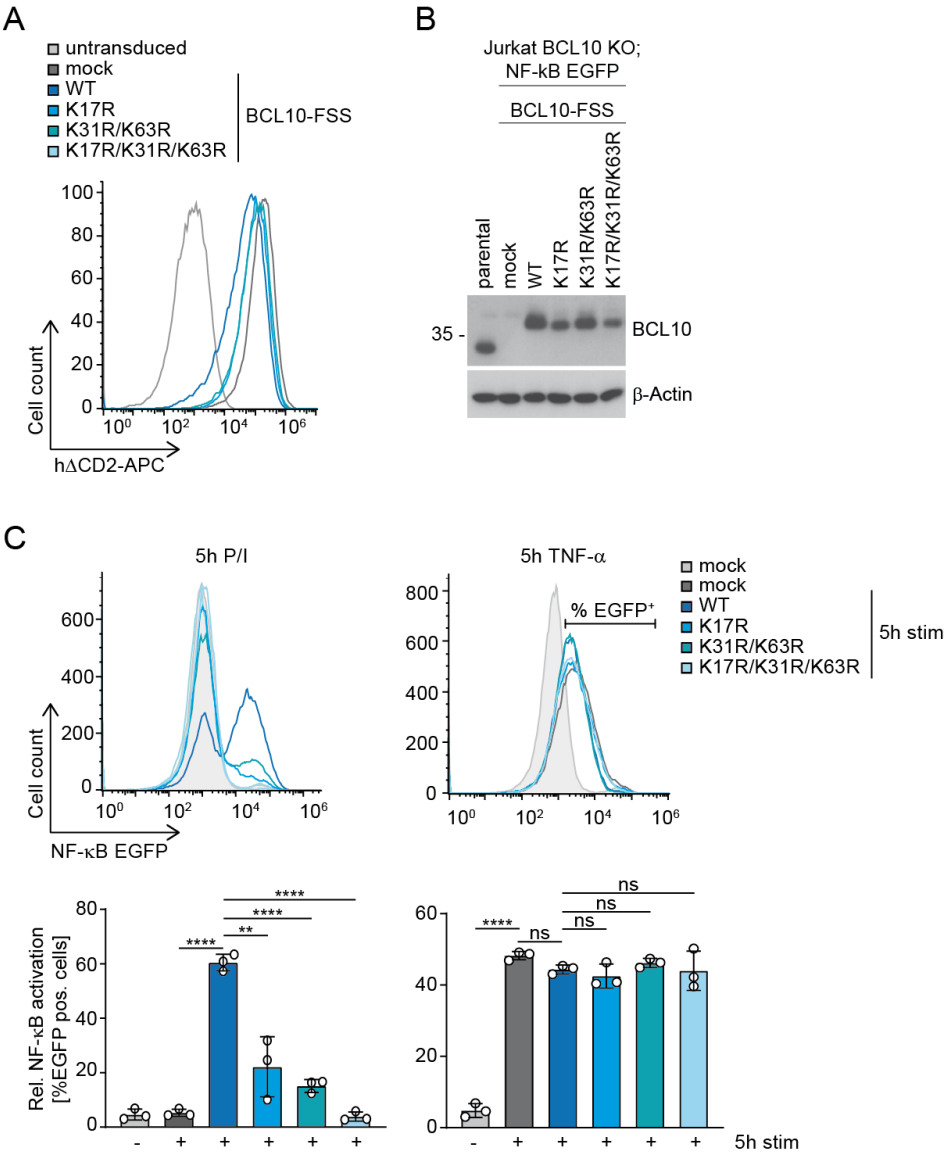

Figure 4-16: NF-κB activation in BCL10 KO Jurkat T cells reconstituted with BCL10 K-to-R mutants.

A) Transduction efficiency was determined by co-expression of the cell surface marker ΔCD2 by flow cytometry. Untransduced BCL10-deficient Jurkat T cells were used as control (light grey) and compared to mock (dark grey), BCL10 WT (dark blue), BCL10 K17R (light blue), BCL10 K31R/K63R (turquoise) and BCL10 K17R/K31R/K63R (light turquoise) reconstituted cells.

B) Protein expression of reconstituted FSS-tagged BCL10 constructs was assessed by Western blot. β-Actin served as loading control.

C) Flow cytometry analysis of NF-κB-EGFP reporter activation in reconstituted BCL10 KO Jurkat T cells. Cells were stimulated with P/I or TNFα for 5h and NF-κB activation was assessed via EGFP expression. Depicted are percentages of EGFP positive cells. Bars show means ± SEM (n=3), and p-values were calculated by unpaired Student's t test. *p < 0.05, **p < 0.01, ***p < 0.001 and ****p < 0.0001; ns, not significant.

Next, we tested whether mutation of respective lysine residues indeed prevents BCL10 polyubiquitination. We stimulated reconstituted cells with P/I and performed a Strep-pulldown under denaturing conditions to enrich polyubiquitinated BCL10. Reconstitution with WT protein induced BCL10 polyubiquitination, whereas all three K-to-R mutants failed to do so (Figure 4-17A). Furthermore, biochemical analysis confirmed previous results from the NF-κB-EGFP reporter assay.

All BCL10 mutants were severely impaired in phosphorylation of p65 and IκBα degradation and displayed reduced cleavage of MALT1 substrates HOIL-1, CYLD and BCL10 itself (Figure 4-17B). Taken together, the predicted ubiquitin acceptor lysines are indeed essential for BCL10 polyubiquitination, CBM dependent NF-κB signaling and MALT1 protease activation.

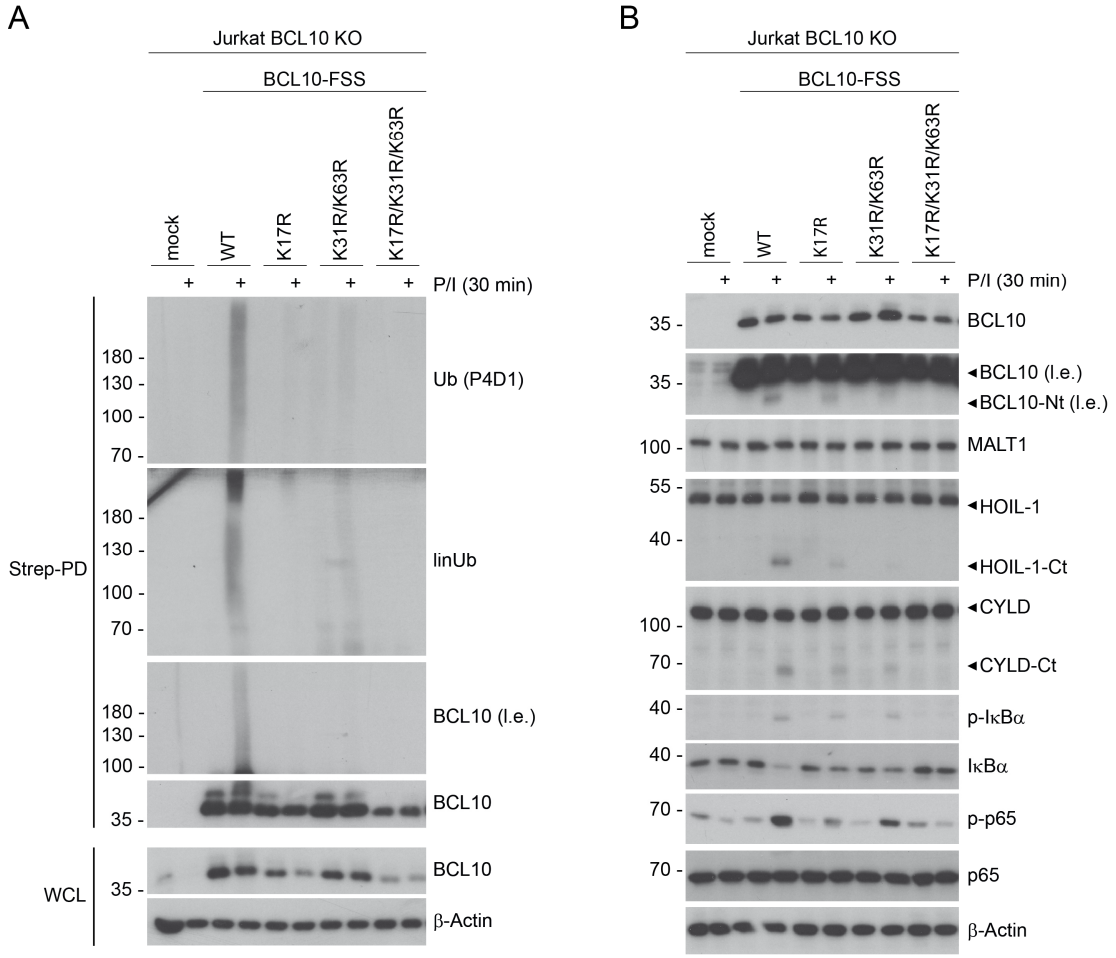

Figure 4-17: BCL10 K-to-R mutants interfere with BCL10 polyubiquitination and downstream NF-κB and MALT1 protease activation.

A) Western blot analysis of BCL10 polyubiquitination in reconstituted BCL10 KO Jurkat T cells. Cells were stimulated with P/I and FSS-tagged BCL10 was enriched via Strep-pulldown (PD) under denaturing conditions.

B) Western Blot analysis of NF-κB signaling and MALT1 protease activation upon P/I stimulation in reconstituted BCL10 KO Jurkat T cells. The onset of NF-κB signaling was determined by IκBα phosphorylation/degradation and p65 phosphorylation, MALT1 paracaspase activity was assessed by cleavage of HOIL-1, CYLD and BCL10. Ct: C-terminal cleavage fragment. Nt: N-terminal cleavage fragment. l.e.: longer exposure. WCL: whole cell lysate. β-Actin served as loading control.

4.2.4 Lysines 17, 31 and 63 are buried in BCL10-MALT1 or BCL10-BCL10 interfaces

As mentioned previously, BCL10 polyubiquitination relies on the presence of CARD11 and MALT1, suggesting that ubiquitin conjugation occurs within the assembled CBM complex (Figure 4-13A) (Wu & Ashwell, 2008; Yang et al., 2016). Recently, the cryo-electron microscopy (cyro-EM) structure of

the BCL10-CARD and BCL10-MALT1 filaments was solved revealing that an extensive network of interactions is involved in CBM complex formation (David et al., 2018; Schlauderer et al., 2018). BCL10 filaments form a left-handed helix via homotypic CARD-CARD interactions. Three CARD interfaces were identified: interfaces I and II are inter-strand connectors between BCL10 subunits in adjacent helical turns, such as in BCL10 B1-A2 (type I) or A1-A2 (type II), whereas interface III represents intra-strand connections such as in A1-B1 (Figure 4-18A). The CARD domain of BCL10 contains 13 lysine residues in total, of which K17, K31 and K63 were suggested to be direct ubiquitin conjugation sites (Wu & Ashwell, 2008; Yang et al., 2016).

We closely examined the accessibility of all BCL10 lysines in the BCL10 CARD helical structure (Figure 4-18B). Lysines 44, 45, 67, 77, 90, 98, 105, 110 and 115 are located in the outer α-helices and protrude away from BCL10, suggesting that they may be accessible for ubiquitin attachment. In contrast, lysines 17, 18, 31 and 63 are positioned in the center of BCL10 α-helices pointing towards the BCL10 CARD core. Thus, these lysine residues are less accessible for post-translational modifications, at least in the context of an assembled CBM signalosome. The putative ubiquitin acceptor sites K31 and K63 are part of CARD interface I and II interactions, providing direct electrostatic connections to the neighboring α-helices (Figure 4-18C, top) and may be critical for filament stability. Due to densely packed BCL10 filaments, it is very unlikely that K31 and K63 are accessible for E3 ligases to attach polyubiquitin chains at these sites. Molecular modeling can be used to calculate possible positions of K-to-R mutants at respective BCL10 residues. We predict that the energetically preferred positions of arginine rotamers at position 31 and 63 prevent the formation of salt bridges between K31 and Q73 as well as K63 and E35 (Figure 4-18C, bottom). However, these electrostatic connections may be critical for BCL10 oligomerization and thus CBM complex formation. Besides K31 and K63, K17 has been suggested to serve as direct ubiquitin conjugation site (Yang et al., 2016). K17 is located within the BCL10-MALT1 interface and points from the BCL10 α1-helix towards the α4-helix of the MALT1 death domain (DD) (Figure 4-18D, E). It is not clear if lysine 17 makes direct contacts with MALT1, but polyubiquitination at this side is very likely to interfere with BCL10-MALT1 conjugation. Taken together, structural data of BCL10 filaments and molecular modeling results clearly indicate that neither of the suggested lysine residues is accessible for polyubiquitination. K31 and K63 are buried in BCL10-BCL10 interfaces and K17 is crucial for BCL10-MALT1 association. Thus, attachment of ubiquitin at these sites most likely interferes with CBM complex formation.

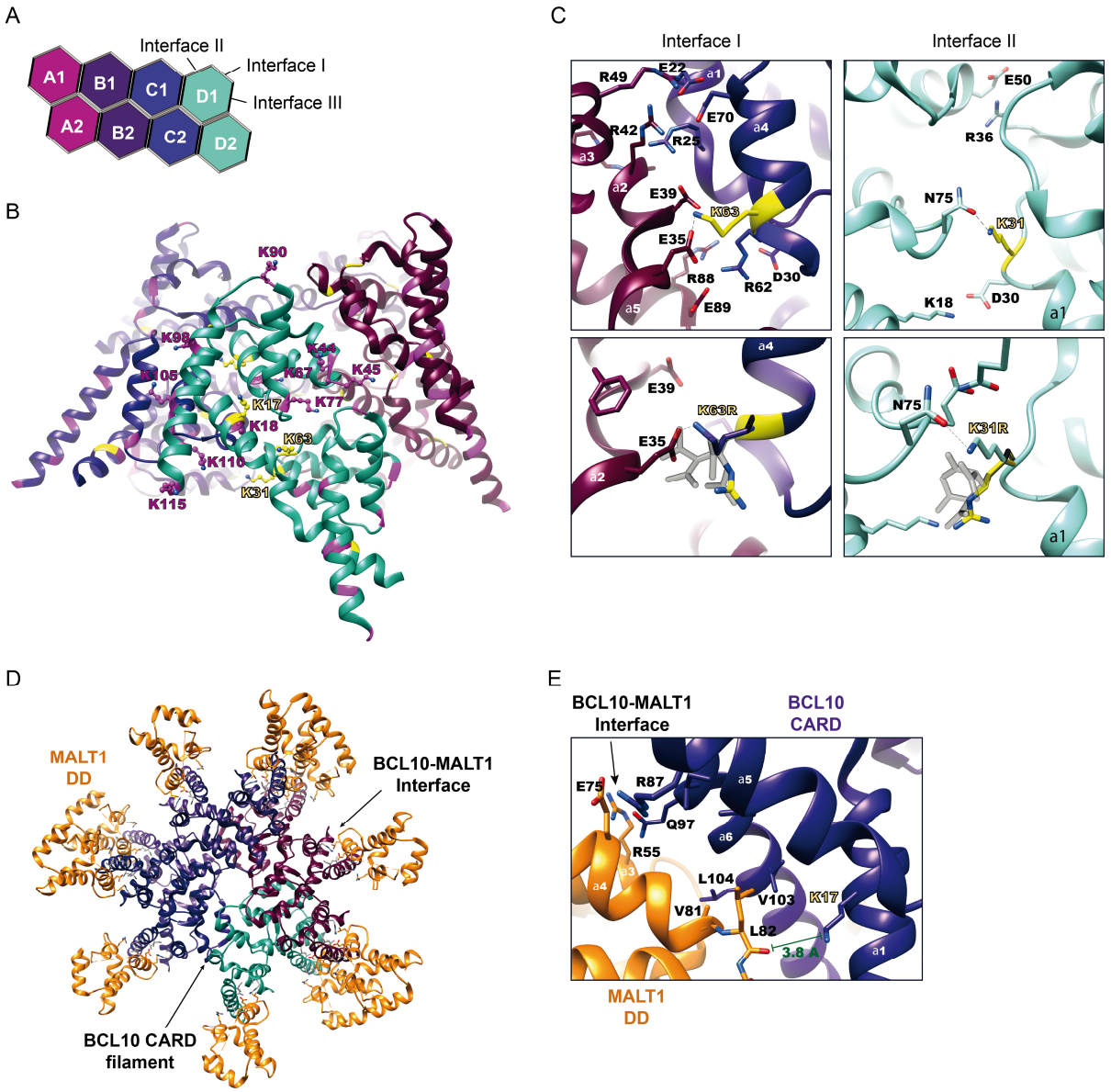

Figure 4-18: Localization of putative ubiquitin acceptor sites in BCL10.

A) Schematic representation of the BCL10 helical assembly. Each BCL10 is depicted as a hexagon with the three CARD interfaces indicated accordingly.

B) Side view of the cryo-EM BCL10 protein model as suggested in Schlauderer et al., 2018. Lysines of BCL10 are highlighted in purple, putative ubiquitin acceptor lysines are labeled yellow.

C) Detailed view of BCL10 interfaces I (left, top) and II (right, top). Interacting residues are shown in stick representation. Lysines 31 and 63 are highlighted in yellow. The bottom shows molecular modelling of respective K-to-R mutants with potential positions in light grey and the most energetically preferred position in yellow.

D) Top view of one repeat of the BCL10-MALT1 holo-complex as suggested in Schlauderer et al., 2018. MALT1 death domain (DD) is depicted in orange. BCL10 CARD-CARD interactions and BCL10-MALT1 interface are indicated with an arrow, respectively.

E) Detailed view of the BCL10-MALT1 interface. Lysine 17 is highlighted in yellow.

Cryo-EM structure (PDB ID 6GK2) and molecular modelling of K-to-R mutants was provided and edited by Katja Lammens, Gene Center LMU, München.

4.2.5 K31 and K63 mediate BCL10 oligomerization and K17 BCL10-MALT1 association

Our structural studies indicated that the exchange of lysine to arginine at positions 31 and 63 may interfere with homotypic CARD-CARD interactions. To analyze biochemically whether these residues are of structural importance, we co-transfected HA-tagged BCL10 WT and Flag-tagged BCL10 WT or K31R/K63R into HEK293 cells and performed a Flag-IP. Flag-BCL10 WT co-precipitated with HA-BCL10, whereas K31R/K63R failed to do so (Figure 4-19A). As a control, the previously reported BCL10-BCL10 interaction mutant R42E (Schlauderer et al., 2018) was used, which also interfered with CARD-CARD interaction. This demonstrates that mutation of K31 and K63 indeed abolishes BCL10 self-oligomerization. Since K17 lies within the BCL10-MALT1 interface, we assessed BCL10-MALT1 binding in HEK293 cells. While WT Flag-tagged BCL10 associated with HA-MALT1, co-precipitation of K17R or K17R/K31R/K63R with MALT1 was disrupted to a similar extent as the L104R mutant, which was previously described (Figure 4-19B)(Schlauderer et al., 2018).

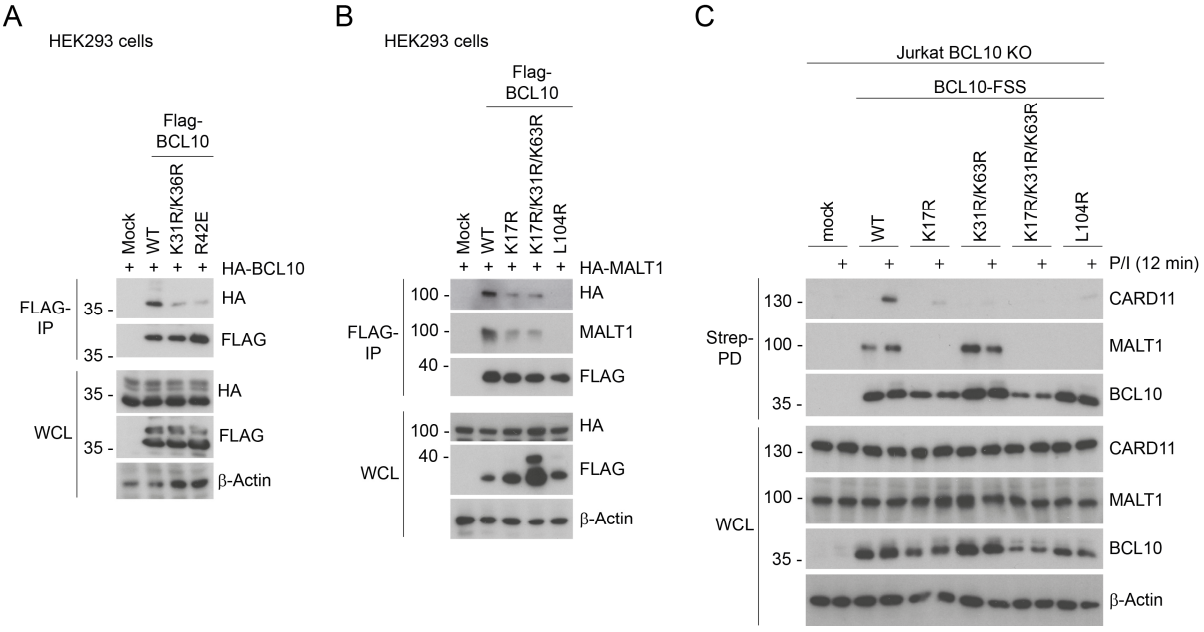

Figure 4-19: Functional analysis of BCL10 K-to-R mutants.

A) HEK293 cells were co-transfected with Flag-tagged BCL10 WT and mutant variants and HA-tagged BCL10 WT as indicated. Co-IP was carried out using anti-Flag antibody and analyzed by western blot for co-precipitation.

B) HEK293 cells were co-transfected with Flag-tagged BCL10 WT and mutants and HA-tagged MALT1 as indicated. Co-IP was carried out using anti-Flag antibody and analyzed by western blot for co-precipitation.

C) CBM-complex formation in BCL10 KO Jurkat T cells reconstituted with FSS-tagged WT or indicated BCL10 mutants. Cells were stimulated with P/I, lysates were subjected to Strep-pulldown and analyzed for CARD11 and MALT1 co-precipitation. IP: immunoprecipitation. PD: pulldown. WCL: whole cell lysate.

Finally, we tested respective BCL10 K-to-R mutants for MALT1 and inducible CARD11 association in reconstituted BCL10 KO Jurkat T cells via Strep-pulldown of BCL10. WT BCL10 constantly associated with MALT1 and bound to CARD11 upon P/I stimulation (Figure 4-19C). K17R failed to associate with MALT1 and was hindered in inducible CARD11 binding, similar to the L104R mutation. This is in line

with the observation that BCL10-MALT1 interaction is critical for the recruitment of BCL10 to CARD11 (Schlauderer et al., 2018). Loss of CARD-CARD interaction in the K31R/K63R mutant interfered with inducible CARD11 association without affecting constitutive MALT1 binding to BCL10. As expected, the triple mutant was defective in both MALT1 and CARD11 interaction (Figure 4-19C). Taken together, the functional analysis of BCL10 K-to-R mutants is in line with the cryo-EM structure of BCL10 CARD-CARD and BCL10-MALT1 filaments. Putative ubiquitin acceptor lysines 31 and 63 are essential for BCL10 self-oligomerization, whereas K17 is indispensable for BCL10-MALT1 association.

4.2.6 MALT1-TRAF6 interaction and TRAF6 activity are essential for BCL10 polyubiquitination

Since we demonstrated that defective NF-κB signaling in BCL10 K-to-R mutants is caused by disrupted CBM-complex formation (Figure 4-19C), attachment of ubiquitin chains to the lysine residues 17, 31 and 63 most likely counteract CBM complex assembly and NF-κB signaling. Thus, loss of BCL10 polyubiquitination (Figure 4-17A) seems to be a secondary effect rather than the cause of defective signaling. Furthermore, we showed that polyubiquitination of BCL10 depends on TRAF6 (Figure 4-13B), and since TRAF6 recruitment to the CBM complex is MALT1-dependent, we analyzed whether MALT1-TRAF6 interaction is critical for BCL10 polyubiquitination. Indeed, mutation of both T6BMs in MALT1A severely interfered with ubiquitin association to BCL10 (Figure 4-20A). Next, we tested reconstituted TRAF6 KO Jurkat T cells, because we speculated that TRAF6 itself catalyzes BCL10 polyubiquitination. Whereas TRAF6 WT induced BCL10 polyubiquitination, the TRAF6 E3 ligase activity-defective mutant C70A failed to do so, confirming our hypothesis. In addition, TRAF6 self-oligomerization was critical for the attachment of ubiquitin chains to BCL10, as evident from the absence of modified, high molecular weight BCL10 in TRAF6 R88A/F118A reconstituted cells(Figure 4-20B). Taken together, BCL10 polyubiquitination depends on MALT1-TRAF6 interaction, as well as TRAF6 catalytic activity and self-oligomerization.

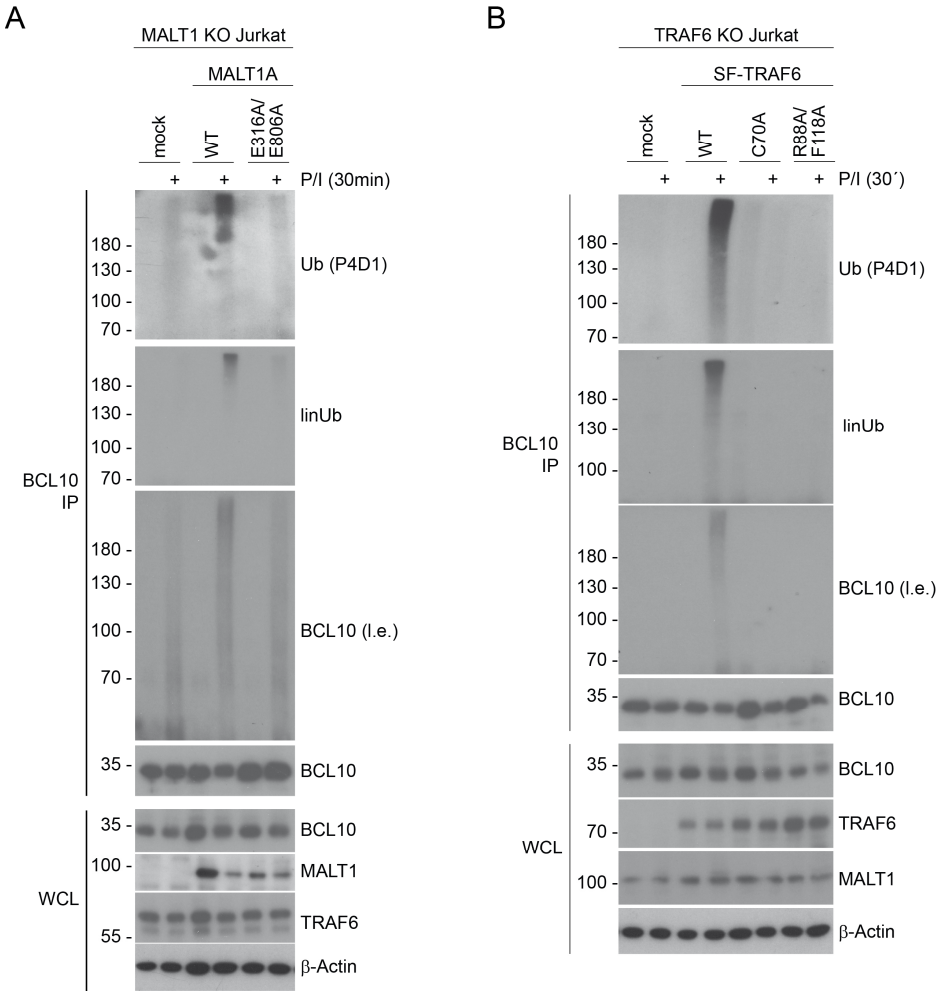

Figure 4-20: TRAF6-mediated BCL10 polyubiquitination depends on MALT1 T6BMs and TRAF6 E3 ligase activity.
A) Western blot analysis of BCL10 polyubiquitination in MALT1 KO Jurkat T cells reconstituted with mock, MALT1A WT and MALT1A E316A/E806A.
B) Western blot analysis of BCL10 polyubiquitination in TRAF6 KO Jurkat T cells reconstituted with mock, TRAF6 WT, E3 ligase-defective C70A and oligomerization mutant R88A/F118A.
A, B) Cells were stimulated with P/I and lysates were immunoprecipitated under denaturing conditions with anti-BCL10 antibody. IP: immunoprecipitation. WCL: whole cell lysate. l.e.: longer exposure.

4.2.7 LUBAC is essential for constitutive MALT1 protease activity in TRAF6 deficient Jurkat T cells

Our previous experiments demonstrated that P/I-induced BCL10 polyubiquitination and TRAF6-mediated restriction of MALT1 paracaspase activity rely on the same mechanisms (Figure 4-20) (O'Neill et al., 2021). We speculated that TRAF6-mediated BCL10 polyubiquitination at K17, K31 and K63 may also occur in unstimulated cells to prevent constitutive CBM complex formation and thus spontaneous MALT1 protease activation. However, our current biochemical tools are not sensitive enough to directly demonstrate MALT1-TRAF6 association, CBM complex formation, or BCL10 ubiquitination in the absence of a T cell stimulus. Ubiquitin linkage analysis revealed that BCL10 is attached to both linear and K63-linked ubiquitin chains upon P/I stimulation, and thus BCL10 modification is dependent upon the LUBAC components HOIP and HOIL-1, as well as TRAF6. If the

same linkage specificities of P/I-induced polyubiquitin chains apply for constant ubiquitin chains of BCL10 in resting T cells, TRAF6 and the LUBAC may cooperate to ubiquitinate BCL10 preventing chronic CBM-complex assembly and MALT1 protease activity. Thus, similar to TRAF6 loss, absence of LUBAC may also induce constitutive MALT1 paracaspase activation in unstimulated cells. To test this hypothesis, we analyzed cleavage of distinct MALT1 substrates in HOIP and HOIL-1 KO Jurkat T cells without stimulation (Figure 4-21A).

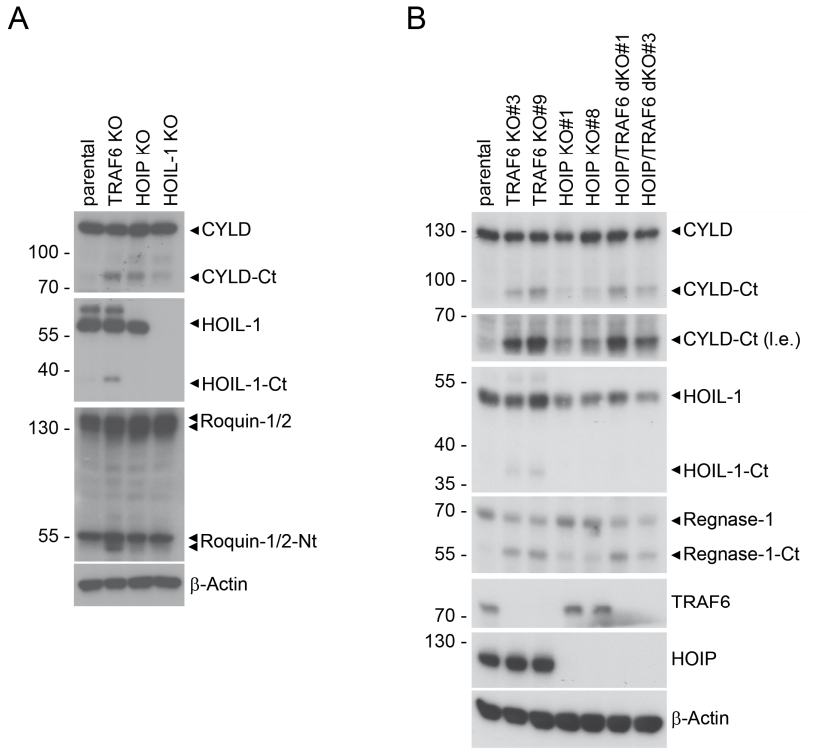

Figure 4-21: Constitutive MALT1 protease activity upon TRAF6 and HOIP deficiency.
A, B) Analysis of MALT1 protease activity in indicated single KO (sKO) and HOIP/TRAF6 double KO (dKO) Jurkat T cell clones. Cells were incubated with and without P/I and substrate cleavage was analyzed via Western blot. Ct: C-terminal fragment. Nt: N-terminal fragment. I.e.: longer exposure.

HOIP-deficient cells displayed augmented CYLD cleavage comparable to TRAF6 KO cells. Loss of HOIL-1 also induced chronic CYLD cleavage in the absence of a T cell stimulus, but the amount of the C-terminal CYLD cleavage fragment was reduced. Chronic HOIL-1 cleavage was present in TRAF6 KO but not in HOIP KO cells, since loss of HOIP destabilizes LUBAC and downregulates HOIL-1 and SHARPIN (Boisson et al., 2015). Both HOIP and HOIL-1 KO Jurkat T cells showed constitutive Roquin-1/2 cleavage, but not as strongly as TRAF6-deficient cells. Thus HOIP, the catalytic subunit of the LUBAC, and to a lesser extent HOIL-1, seems to restrict chronic MALT1 paracaspase activity. To verify this, we checked MALT1 substrate cleavage in two distinct HOIP and TRAF6 single KO (sKO) clones, and two HOIP/TRAF6 double-KO (dKO) clones. Constitutive cleavage of CYLD and Regnase-1 was present in all analyzed sKO and dKO clones, with the strongest detection of C-terminal cleavage

fragments in TRAF6 sKO and HOIP/TRAF6 dKO Jurkat T cells (Figure 4-21B). Full length HOIL-1 was again destabilized in the absence of HOIP or upon combined loss of HOIP and TRAF6. Taken together, our data indicate that the combined action of TRAF6 and the LUBAC prevent spontaneous MALT1 paracaspase activation in resting T cells. Since the negative regulatory effect of TRAF6 on MALT1 proteolytic activity was stronger compared to HOIP and HOIL-1, it might be possible that TRAF6 is the dominant factor and LUBAC functions as an auxiliary factor to amplify TRAF6 mediated restriction of MALT1 paracaspase activity via linear ubiquitination of BCL10.

4.3 Alternative *MALT1* splicing controls severity of auto-immune inflammation

TRAF6 and LUBAC cooperatively restrict MALT1 paracaspase activity and thus prevent T cell activation and autoimmunity in resting T cells. The strength of the MALT1-TRAF6 interaction is fine-tuned by alternative splicing of *MALT1*. Inclusion of exon7 in MALT1A provides an additional T6BM, resulting in enhanced MALT1-TRAF6 interaction and stronger downstream NF-κB activation (Kutukculer et al., 2021; Meininger et al., 2016). Thus, we expected that *Malt1* TBM2 mice would develop a less severe inflammatory phenotype than *Malt1* TBM mice, since the patient-derived missense mutation in TBM2 mice solely impairs TRAF6 interaction with MALT1B, whereas TRAF6 binding of both MALT1 isoforms is disrupted in *Malt1* TBM mice (O'Neill et al., 2021). Phenotypic severity of *Malt1*$^{TBM2/TBM2}$ mice and the human patient were also distinct, raising questions regarding how alternative *MALT1* splicing is generally regulated and how relative MALT1A/MALT1B expression levels affect the severity of the phenotype.

4.3.1 Predominant expression of *Malt1B* mRNA in immune cells of C57BL/6N mice

We decided to perform a detailed expression analysis of *Malt1A* and *Malt1B* in murine tissue and immune cells. To investigate inclusion or exclusion of exon7 on the mRNA level, we used primers which flank exon7 and enable simultaneous *Malt1A/B* amplification (Meininger et al., 2016). RT-PCR analysis revealed the exclusive expression of the shorter *Malt1B* isoform in spleen, lymph nodes and thymus. In contrast to the lymphoid organs, both splicing variants were expressed in liver, lung and ear tissue (Figure 4-22A). To make quantitative comparisons of *Malt1A/B* expression, we performed qPCR with exon-spanning primers that selectively amplify either *Malt1A* or *Malt1B* (Meininger et al., 2016) and used the standard curve method for absolute quantification of mRNA transcript numbers per 100 ng mRNA. Lymphoid tissue expressed less than 5,000 *Malt1A* mRNA transcripts, whereas murine liver, lung and ear displayed up to 10 fold higher *Malt1A* transcript numbers. Absolute *Malt1B* mRNA levels were in general higher than *Malt1A* in all tested tissues (Figure 4-22B). Calculation of *Malt1A*/*Malt1B* ratios confirmed that in lymphoid organs, *Malt1A* is scarcely expressed (Figure 4-22C). Next, we isolated primary peripheral blood mononuclear cells (PBMCs) from human and murine whole blood and purified RNA to directly compare the two species. *Malt1A*

mRNA was not amplified in murine PBMCs but displayed week expression levels in human PBMCs, indicating that there is indeed a difference in MALT1 isoforms ratios between human and mouse (Figure 4-22D). To reveal expression differences in distinct immune cell types, we analyzed *Malt1A/B* expression in various lymphocyte subsets. We FACS sorted B220+ B cells, CD4+ or CD8+ $T_{naïve}$ and activated CD4+ CD8+ T_{EM} cells from C57BL/6N wildtype mice and performed PCR with simultaneous amplification of both isoforms. *Malt1A* mRNA was not detected in any of the analyzed lymphocyte populations (Figure 4-22E). Finally, we analyzed *Malt1A/B* expression in *Malt1* TBM2 mice to check if genomic editing impacted the ratio of *Malt1* isoforms. However, splenocytes solely contained the shorter *Malt1B* isoform and no *Malt1A*, regardless of the genotype (Figure 4-22F). Taken together, our expression analyses showed that *Malt1* isoform ratios vary between human and mouse, as well as between distinct murine tissues. Strikingly, murine immune cells expressed barely any *Malt1A*, which mediates a more robust TRAF6 interaction due to the additional T6BM in exon7.

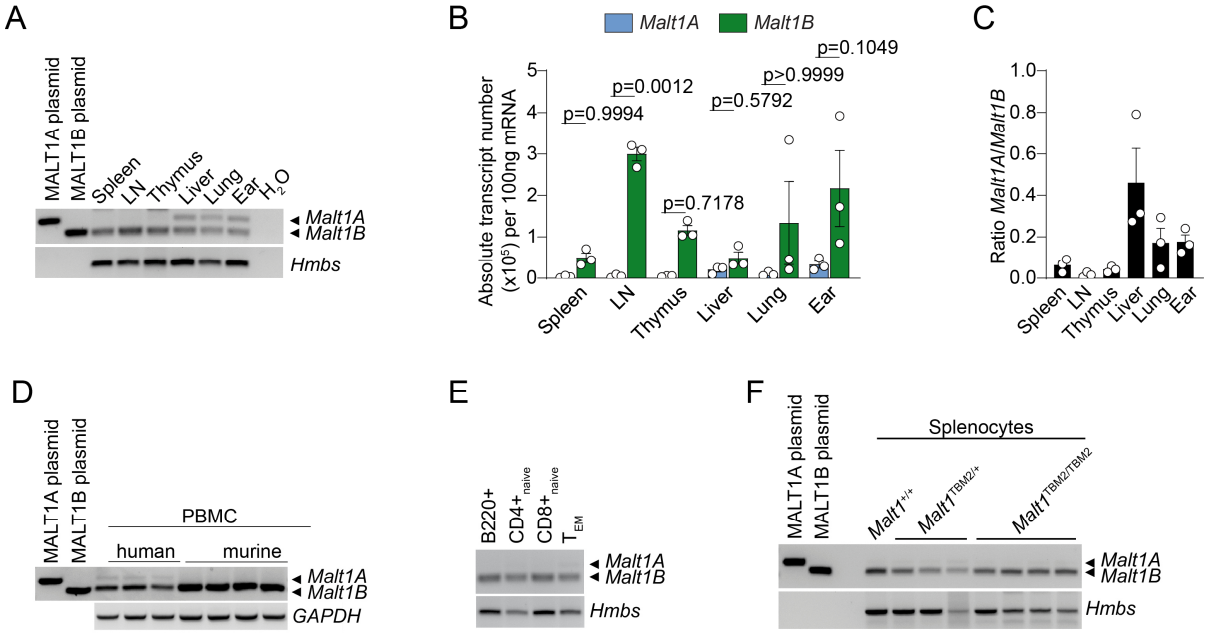

Figure 4-22: Analysis of *Malt1A/B* mRNA expression.

A) PCR analysis of *Malt1A* and *Malt1B* mRNA expression in different organs and tissues of wildtype C57BL/6N mice. Primers flank *Malt1* exon7 (ex6–ex9/10) and enable simultaneous amplification of both isoforms. MALT1A and MALT1B plasmids were used for discrimination of *Malt1A* and *Malt1B* mRNA. *Hmbs* transcript levels served as internal control.

B, C) qPCR analysis of absolute *Malt1A* (blue) and *Malt1B* (green) mRNA transcript numbers (B) or relative *Malt1A*/*Malt1B* ratios (C) in different organs and tissues of wildtype C57BL/6N mice.

D) PCR analysis of *Malt1A* and *Malt1B* mRNA expression in human and murine peripheral blood mononuclear cells (PBMCs). PBMCs from three individual human donors and four *Malt1*$^{+/+}$ mice are depicted. Primers amplify human and murine *MALT1A* and *MALT1B* mRNA.

E) PCR analysis of *Malt1A* and *Malt1B* mRNA expression in B220+ B cells, CD4+ or CD8+ naïve (T_{naive}: CD44^{lo}CD62L^{hi}) and CD4+ CD8+ effector memory (T_{EM}: CD44^{hi}CD62L^{lo}) T cells in spleen of a wildtype C57BL/6N mouse.

F) PCR analysis of *Malt1A* and *Malt1B* mRNA expression in splenocytes of *Malt1*$^{+/+}$, *Malt1*$^{TBM2/+}$ and *Malt1*$^{TBM2/TBM2}$ mice.

B, C) Each dot represents one mouse. All bars show means ± SEM, and p-values were calculated by two-way ANOVA with Tukey´s multiple comparisons test.

4.3.2 C57BL/6N T lymphocytes do not express MALT1A protein

In addition to studying *Malt1A/B* expression on mRNA level, we also wanted to analyze MALT1A/B protein levels in murine cells. Therefore, we generated a MALT1A-specific antibody (clone 4A7) which was generated against exon7 of MALT1A. Validation of the antibody was performed with CD4+ T cell lysates derived from mice with exclusive expression of MALT1A (*Malt1* IsoA mice) protein (generated by Andreas Gewies). The MALT1A antibody 4A7 specifically recognized MALT1A protein in IsoA mice, but did not detect a specific band in *Malt1*$^{-/-}$ mice. *Malt1*$^{+/+}$ mice did not show a MALT1A specific band in CD4+ T cells (Figure 4-23A). The 4A7 antibody is functional in intracellular staining and induced a fluorescence signal shift in flow cytometric analysis in CD4+ T cells from *Malt1*$^{A/A}$ mice, but not from *Malt1*$^{-/-}$, *Malt1*$^{+/+}$ or *Malt1*$^{B/B}$ mice, which exclusively express MALT1B (*Malt1* IsoB mice were generated by Andreas Gewies) (Figure 4-23B). We used the MALT1A-specific antibody to analyze MALT1A protein levels in CD4+ and CD8+ total, naïve (CD62L^{hi}CD44^{lo}) or effector memory (CD62L^{lo}CD44^{hi}) T cells. Whereas MALT1A protein was detected in all T cell subsets of *Malt1*$^{A/A}$ mice, no notable protein amounts were measured in WT mice in comparison to *Malt1*$^{-/-}$ or *Malt1*$^{B/B}$ negative controls. Thus, lymphocytes from C57BL/6N mice do not express MALT1A protein in neither naïve nor effector T cells.

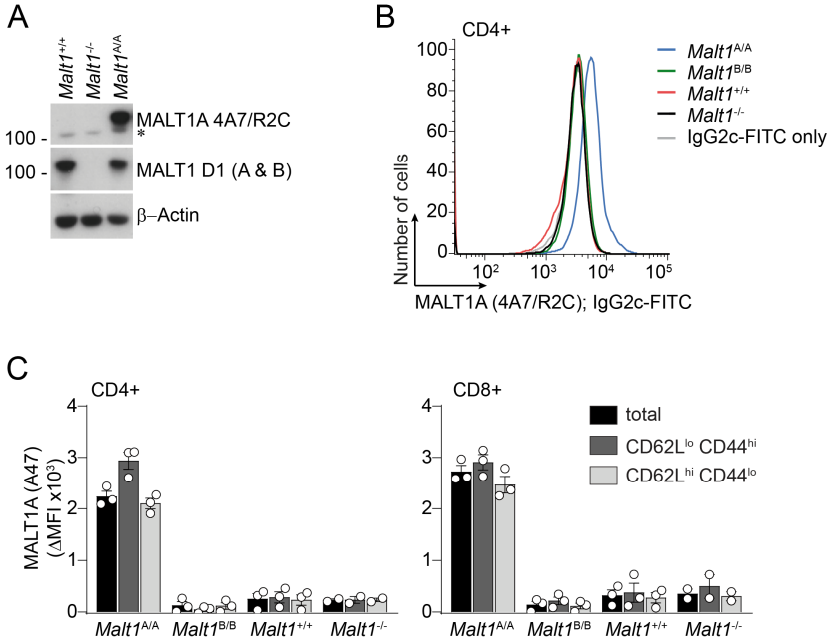

Figure 4-23: Analysis of MALT1A protein levels in T lymphocyte subsets of C57BL/6N mice.

A) Western blot analysis of total MALT1 and MALT1A protein expression in lysates of CD4+ T cells from *Malt1*$^{+/+}$, *Malt1*$^{-/-}$ and *Malt1*$^{A/A}$ mice. Antibody clone 4A7 specifically detects MALT1A, D1 detects total MALT1. Asterisk indicates unspecific antibody binding, β-Actin served as loading control.

B) Flow cytometry analysis of MALT1A protein expression in CD4+ T cells from spleen of *Malt1*$^{+/+}$, *Malt1*$^{-/-}$, *Malt1*$^{A/A}$, and *Malt1*$^{B/B}$ mice.

C) Flow cytometry analysis of MALT1A protein expression in CD4+ (left) total (black), naïve (T_{naive}: CD44^{lo}CD62L^{hi}; light grey) and effector memory (T_{EM}; CD44^{hi}CD62L^{lo}; dark grey) T cells or respective CD8+ (right) T cell subsets in spleen of *Malt1*$^{A/A}$, *Malt1*$^{B/B}$, *Malt1*$^{+/+}$ and *Malt1*$^{-/-}$ mice. Delta MFI (MALT1 4A7 staining minus IgG2c-FITC secondary only staining) is shown. Each dot represents one mouse. All bars show means ± SEM.

4.3.3 Mouse strains differently regulate alternative *Malt1* splicing

It has been previously shown that proximal TCR signaling induces *Malt1A* upregulation in murine CD4+ T cells (Meininger et al., 2016). In contrast to our study, CD4+ T cells were isolated from BALB/c mice. Since we could demonstrate that there are inter-species differences in *MALT1A* expression, we analyzed four different mouse strains to test if there are also inter-strain differences in murine lines. All four mouse strains expressed barely any *Malt1A* mRNA in unstimulated CD4+ T cells (Figure 4-24A-C). However, upon TCR stimulation CD-1, 129S2/Sv and BALB/c mice upregulated *Malt1A* expression levels, whereas C57BL/6N mice failed to do so (Figure 4-24A, B). Absolute quantification of *Malt1A* transcript numbers via qPCR confirmed that there are no significant differences in constitutive alternative splicing between BALB/c and C57BL/6N. However, *Malt1A* mRNA expression was induced by ~ 25-fold upon CD3 stimulation in BALB/c but there was no upregulation in C57BL/6N mice (Figure 4-24C). In contrast, induction of *Malt1B* expression was detected in both mouse lines, but only by a factor of ~ 5 (Figure 4-24D). Thus, C57BL/6N is the only tested mouse strain which fails to induce alternative splicing of *Malt1* exon7 upon TCR engagement.

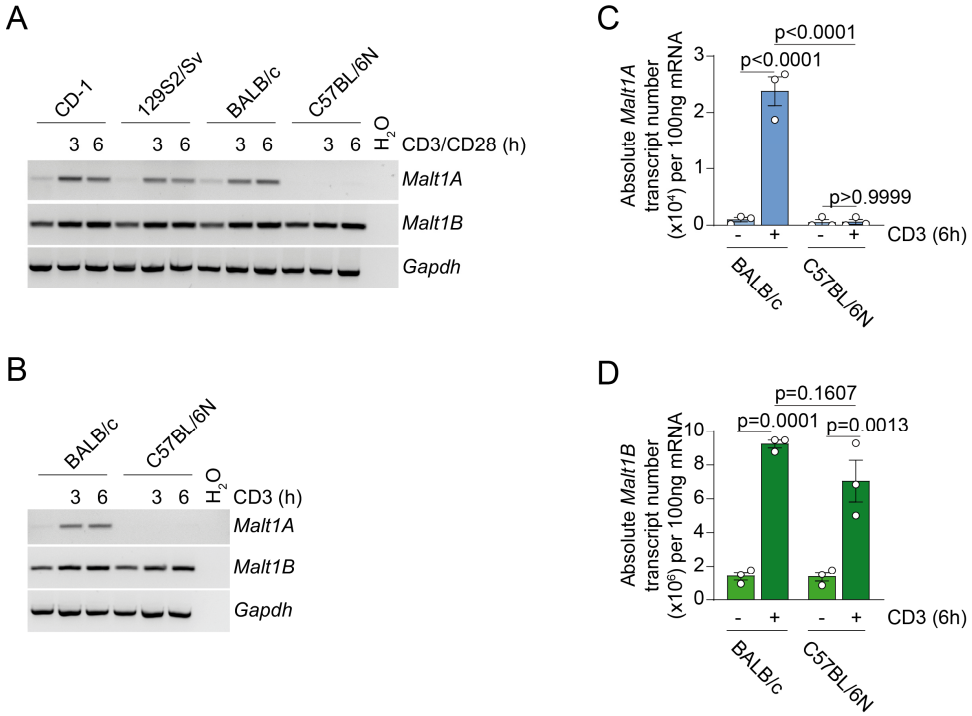

Figure 4-24: C57BL6/N mice fail to upregulate *Malt1A*.
A, B) PCR analysis of *Malt1A* and *Malt1B* mRNA expression in CD4+ T cells isolated from spleen of indicated mouse strains upon CD3/CD28 (A) or CD3 only stimulation (B). *Malt1A* and *Malt1B* isoform-specific primers were used. *Gapdh* transcript levels served as internal control.
C, D) qPCR analysis of absolute *Malt1A* (C) and *Malt1B* (D) mRNA transcript numbers (per 100 ng mRNA) in CD4+ T cells from BALB/c and C57BL/6N mice upon CD3 stimulation. Each dot represents one mouse. All bars show means ± SEM, and p-values were calculated by two-way ANOVA with Tukey´s multiple comparisons test.

Elevated expression of MALT1A could potentially attenuate the severe autoimmune phenotype of *Malt1* TBM2 mice, because MALT1A is resistant to the effects of the T6BM2 mutation (Kutukculer et

al., 2021; Meininger et al., 2016; O'Neill et al., 2021). Therefore, we set up inter-strain breedings between C57BL/6N *Malt1*$^{TBM2/+}$ and BALB/c WT mice to check if the BALB/c background has an effect on *Malt1A* expression. We also backcrossed C57BL/6N *Malt1*$^{TBM/+}$ mice, in which both T6BMs are mutated and thus TRAF6 binding to MALT1A and MALT1B is disrupted, to BALB/c. Respective *Malt1*$^{+/+}$ offspring mice from the first BALB/c backcross generation were sacrificed and analyzed for *Malt1A* induction upon TCR stimulation. Since *Malt1A* upregulation can be also detected in total splenocytes (Figure 4-25A), we used these in place of purified T cells to save material and costs. Surprisingly, all analyzed *Malt1*$^{+/+}$ offspring from the first BALB/c backcross generation of TBM and TBM2 could induce *Malt1A* expression upon CD3/CD28 stimulation (Figure 4-25B). This result indicates that inclusion of *Malt1* exon7 is regulated by potentially one or several dominant factors which were genetically inherited to the first BALB/c backcross generation.

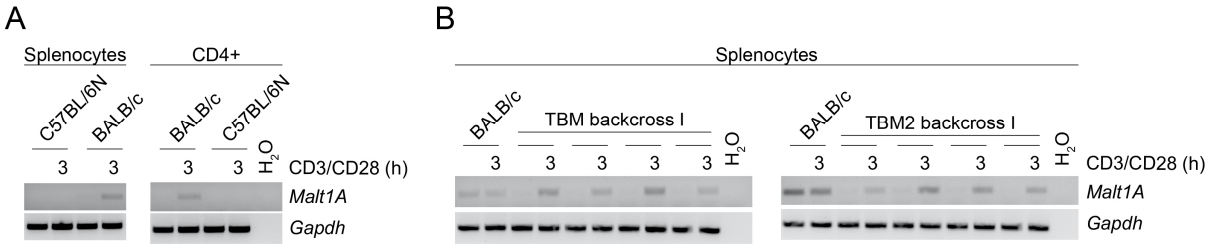

Figure 4-25: First *Malt1* TBM and TBM2 backcross generation to BALB/c.

A) PCR analysis of *Malt1A* upregulation in total splenocytes or CD4+ purified T cells from BALB/c and C57BL/6N mice upon CD3/CD28 stimulation.

B) PCR analysis of *Malt1A* upregulation in total splenocytes of the first *Malt1* TBM and TBM2 backcross generation to BALB/c upon CD3/28 stimulation.

A, B) *Malt1A* and *Malt1B* isoform-specific primers were used. *Gapdh* transcript levels served as internal control.

4.3.4 *Malt1A* expression levels in TBM2 keratinocytes are sufficient to counteract constitutive MALT1 protease activation

One symptom of the patient with the homozygous MALT1 E-to-D mutation in T6BM2 is psoriasis on the hands and feet (Kutukculer et al., 2021). Psoriasis is an inflammatory disease of the skin which is linked to gain-of-function-mutations in CARD14 (also known as CARMA2), the CARD11 homologue in keratinocytes of the epidermis (Ruland & Hartjes, 2019). CARD14 mutations lead to constitutive CBM complex formation and downstream NF-κB and MALT1 protease activation (Zotti et al., 2018). Therefore, we wanted to compare *MALT1A* and *MALT1B* expression levels in human and murine keratinocytes. We detected almost exclusively *MALT1A* mRNA in human and mRNA of both isoforms in murine primary keratinocytes (Figure 4-26A). It has been previously demonstrated that MALT1A WT neutralizes constitutive substrate cleavage by MALT1B E795D in a dominant negative manner in reconstituted Jurkat T cells (O'Neill et al., 2021). To prove that this is also the case in primary murine cells, we isolated keratinocytes from the skin of neonatal C67BL/6N *Malt1* TBM and TBM2 mice. In contrast to splenocytes, keratinocytes expressed *Malt1A* mRNA, despite slight differences in

expression levels between TBM and TBM2 litters (Figure 4-26B). As expected, *Malt1*$^{TBM/TBM}$ keratinocytes showed constitutive cleavage of CYLD and HOIL-1, and MALT1 protease was even activated in heterozygous *Malt1*$^{TBM/+}$ mice. However, MALT1 substrate cleavage was absent in keratinocytes of *Malt1*$^{TBM2/TBM2}$ mice (Figure 4-26C). Thus, our data suggest that chronic MALT1B E803D paracaspase activity can be counteracted by functional MALT1A E814D due to the presence of the additional T6BM1 in exon7 of MALT1A protein.

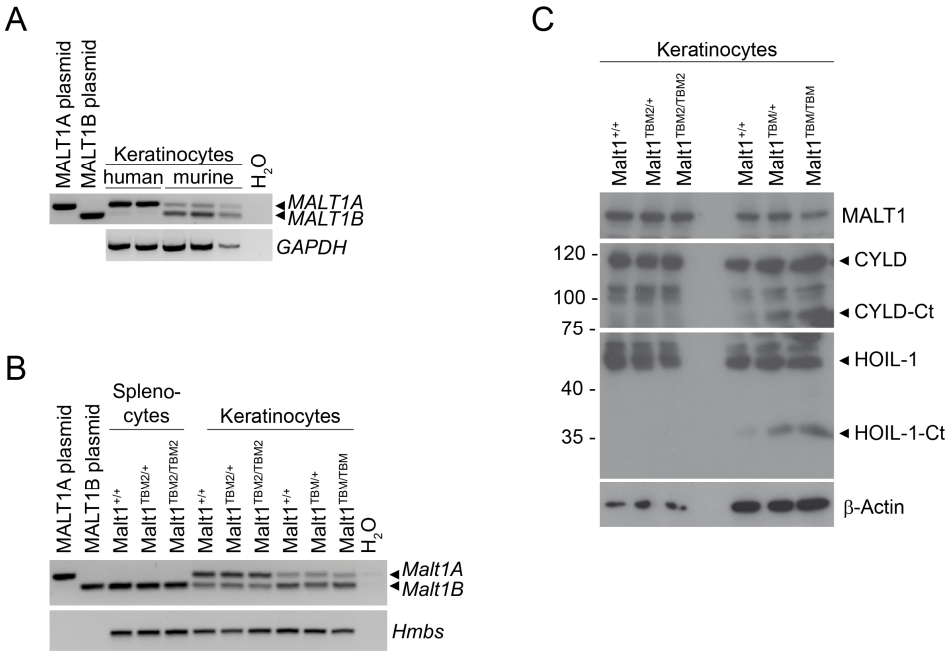

Figure 4-26: Balanced MALT1 protease activity in *Malt1* TBM2 keratinocytes.
A) PCR analysis of *MALT1A* and *MALT1B* mRNA expression in human and murine keratinocytes. Primary keratinocytes from two individual human donors and three mice are depicted. Primers flank *Malt1* exon7 (ex6–ex9/10) and enable simultaneous amplification of human and murine *MALT1A/B*. MALT1A and MALT1B plasmids were used for discrimination of both isoforms. *GAPDH* transcript levels served as internal control.
B) PCR analysis of *Malt1A* and *Malt1B* mRNA expression in splenocytes (left) or keratinocytes (right) from *Malt1* TBM2 and TBM mice.
C) Western blot analysis of MALT1 substrate cleavage in lysates of keratinocytes from *Malt1* TBM2 and TBM mice. Ct: C-terminal cleavage fragment. β-Actin served as loading control. Respective controls were littermates.

4.3.5 Delayed auto-immune phenotype in heterozygous *Malt1*$^{TBM2/+}$ mice

The severity of the immune phenotype caused by defective MALT1B strongly differs between human and mouse due to differential MALT1A expression levels. PBMCs from the patient expressed both *MALT1* isoforms (Kutukculer et al., 2021), whereas lymphocytes of C57BL/6N mice do not express *Malt1A* transcripts (Figure 4-22G). Thus, we were interested in heterozygous *Malt1*$^{TBM2/+}$ mice, which contain one functional *Malt1* WT and one defective TBM2 allele and thus may reflect the human phenotype more precisely. We analyzed *Malt1*$^{TBM2/+}$ mice at 12 month of age at which time we could not observe obvious signs of burden. However, heterozygous *Malt1*$^{TBM2/+}$ mice displayed slightly reduced body weights, and upon necropsy a mild splenomegaly (Figure 4-27A, B). Similar to the

human patient, autoantibodies were increased in the blood serum of *Malt1*$^{TBM2/+}$ mice (Figure 4-27C) (Kutukculer et al., 2021) and some heterozygous mice displayed elevated TNFα levels (Figure 4-27D). As observed in young *Malt1*$^{TBM2/TBM2}$ mice, the expression of the activation marker CD69 on T and B lymphocytes was upregulated and an accumulation of CD4+ and CD8+ T_{EM} cells was determined in *Malt1*$^{TBM2/+}$ mice (Figure 4-27E-H). Relative numbers of CD4+FoxP3+ Treg cells and CD44^{hi}CD62L^{lo} CD4+ eTregs were increased and expression of CTLA-4 and Ox40 on eTregs was equivalent or modestly higher (Figure 4-27I-L). Taken together, old heterozygous *Malt1* TBM2 mice develop autoimmunity, but with a milder and delayed onset due to the presence of one *Malt1* WT allele. Thus, our results indicate that the single *Malt1* TBM2 allele may act in a dominant manner.

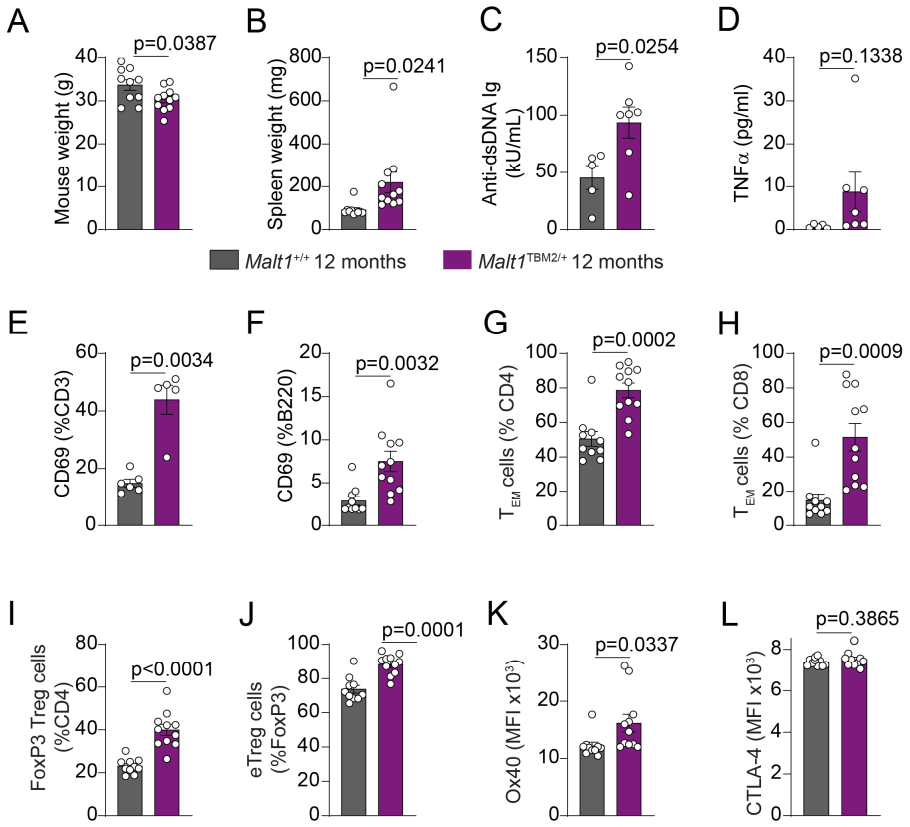

Figure 4-27: Immune phenotyping of *Malt1* TBM2 heterozygous mice at 12 months of age.

A, B) Mouse (A) and spleen weight (B) in *Malt1*$^{TBM2/+}$ and *Malt1*$^{+/+}$ mice.

C, D) Blood serum levels of anti-dsDNA autoantibodies (C) and TNFα (D) in *Malt1*$^{TBM2/+}$ and *Malt1*$^{+/+}$ mice.

E, F) Flow cytometry analysis of CD3+ CD69+ (E) and B220+ CD69+ (F) in spleen of *Malt1*$^{TBM2/+}$ and *Malt1*$^{+/+}$ mice.

G, H) Flow cytometry analysis of CD4+ (G) and CD8+ (H) effector memory T cells (T_{EM}: CD44^{hi} CD62L^{lo}) in spleen of *Malt1*$^{TBM2/+}$ and *Malt1*$^{+/+}$ mice.

I, J) Flow cytometry analysis of CD4+ FoxP3+ regulatory (Treg) T cells (I) and CD4+ FoxP3+ CD44^{hi} CD62L^{lo} effector Tregs (eTreg; J) in spleen of *Malt1*$^{TBM2/+}$ and *Malt1*$^{+/+}$ mice.

K, L) Flow cytometry analysis of Ox40 (K) and CTLA-4 (L) on eTregs in spleen of *Malt1*$^{TBM2/+}$ and *Malt1*$^{+/+}$ mice. Graphs show Median Fluorescence Intensity (MFI).

A-J) Mice were analyzed at the age of 12 months after birth. Unaffected *Malt1*$^{+/+}$ (grey) littermates were used as control and compared to *Malt1*$^{TBM2/+}$ mice (purple). Each dot represents one mouse. All bars show means ± SEM, and p-values were calculated by unpaired Student´s t test with Welch correction.

4.3.6 Modulation of pre-mRNA structure by hnRNP proteins regulates alternative splicing of MALT1

Our expression analysis revealed that *MALT1A/B* mRNA levels differ between species. In addition, we could demonstrate that notable amounts of functional MALT1A protein can counteract chronic MALT1B E803D protease activity (Figure 4-26) and that the presence of a WT *Malt1* allele delays the autoinflammatory phenotype (Figure 4-27). The fatal autoimmunity of *Malt1*$^{TBM2/TBM2}$ mice forms a striking contrast to the extenuated phenotype of the human patient and raised the question, how alternative exon7 splicing is controlled. In cooperation with Dr. Alisha Jones (Institute of Structural Biology, Helmholtz Zentrum München, Neuherberg) we aimed to elucidate the mechanism of *MALT1* splicing regulation.

4.3.6.1 Antagonistic effects of hnRNP U and hnRNP L on alternative *MALT1* exon7 splicing

It was previously demonstrated that the two RNA-binding proteins (RBPs) hnRNP U and hnRNP L exert opposing effects on *MALT1* exon7 inclusion and exclusion. Downregulation of hnRNP U enhances MALT1A expression and triggers a more robust T cell activation (Meininger et al., 2016). However, alternative splicing of MALT1 is not T cell-specific, as evident from variable *MALT1A*/*B* mRNA transcript ratios and MALT1A protein levels in human cell lines (Figure 4-28A). *MALT1A* and *MALT1B* are expressed at equivalent levels in Jurkat T cells, but HeLa, U2OS and HEK293 cells display higher *MALT1A* expression levels. Knockdown (KD) of hnRNP U induces MALT1A transcript and protein levels, whereas KD of hnRNP L downregulates MALT1A transcript and protein levels (Figure 4-28B). hnRNP L and it´s paralog hnRNP L-like (hnRNP LL) can serve overlapping functions (Rossbach et al., 2009; Shankarling & Lynch, 2013; Smith et al., 2013), and hnRNP LL was identified as critical regulator of T cell activation and differentiation (Oberdoerffer et al., 2008; Topp et al., 2008; Wu et al., 2008). However, downregulation of hnRNP LL did not affect *MALT1A*/*B* expression levels in the analyzed human cell lines (Figure 4-28B-E). Taken together, there is a cell-independent mechanism of alternative *MALT1* splicing regulation, in which hnRNP U suppresses and hnRNP L enhances *MALT1* exon7 inclusion.

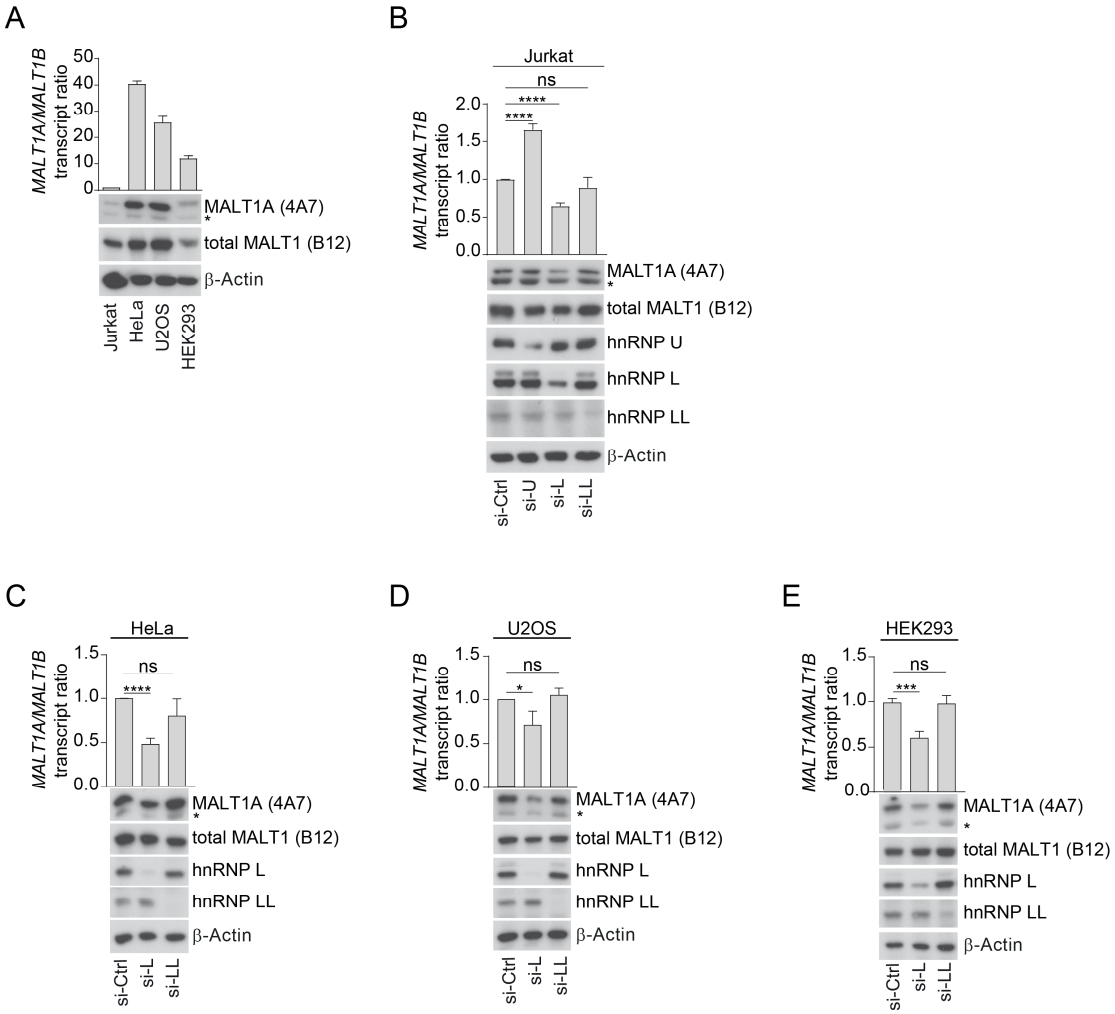

Figure 4-28: hnRNP U induces and hnRNP L counteracts MALT1A expression in human cell lines.
A) Analysis of *MALT1A*/*B* mRNA transcript ratios and MALT1A protein levels in indicated human cell lines.
B-E) Analysis of *MALT1A*/*B* mRNA transcript ratios and MALT1A protein levels upon siRNA knockdown (KD) of hnRNP U (si-U), hnRNP L (si-L) and hnRNP LL (si-LL) in Jurkat (B), HeLa (C), U2OS (D) and HEK293 (E) cells.
A-E) *MALT1A*/*B* transcript ratios were determined via qPCR using *MALT1A* and *MALT1B* isoform-specific primers. Protein levels were analyzed by Western blot. MALT1 antibody 4A7 exclusively detects MALT1 isoform A, B12 detects total MALT1. β-Actin served as loading control. Data are representative for three independent experiments. Bars show means ± SEM (n=3), and p-values were calculated by unpaired Student's t test. *p < 0.05, **p < 0.01, ***p < 0.001 and ****p < 0.0001; ns, not significant.

For further analyses, we used *MALT1* minigenes, which contain exon7 and adjacent intronic sequences of variable length (M1: ~200 and M2: ~500 additional nucleotides) cloned between constitutive exon3 and exon7 of the transmembrane phosphatase CD45 (Meininger et al., 2016) (Figure 4-29A). Minigenes can be used for structural analysis or in *in vitro* assays to study the binding of potential RBPs. Additionally, they can be introduced into cells allowing for simple and rapid quantification of splicing decisions and the identification of critical cis-acting intronic and exonic sequences. We transfected *MALT1* minigenes into Jurkat T cells and analyzed exon7 splicing via PCR using the two vector backbone primers (Figure 4-29A). Introduction of the longer M2 minigene resulted in 50:50 ratio of exon7 inclusion and exclusion, whereas the shorter M1 construct almost

completely skipped exon7. Downregulation of hnRNP U induced *MALT1* exon7 inclusion, whereas KD of hnRNP L reduced exon7 inclusion for both minigenes, respectively. In line with previous results, KD of hnRNP LL did not influence exon7 inclusion and exclusion (Figure 4-29B). Thus, minigene assays recapitulated the antagonistic regulation of *MALT1* exon7 splicing by hnRNP U and hnRNP L and revealed that regulatory sequences within and/or in proximity to exon7 control alternative exon7 splicing. Next, we performed electrophoretic mobility shift assays (EMSAs) to test whether hnRNP U and hnRNP L bind to M1 minigene. Both hnRNP proteins directly interact with M1 pre-mRNA with similar nanomolar affinities as evident from dissociation constants (K_ds) of 23.0 ± 0.5 for hnRNP U and 19.0 ± 0.2 nM for hnRNP L (Figure 4-29C). Calculation of the Hill-coefficient N (hnRNP U: N=4.7; hnRNP L: N=4.6) for binding of both proteins to M1 pre-mRNA indicated the presence of several binding sites for each protein. Because hnRNP U and hnRNP L show antagonistic effects on *MALT1* exon7 inclusion, it is likely that the two proteins do not bind *MALT1* pre-mRNA simultaneously. In line, competition EMSAs showed that increasing concentrations of free hnRNP L are able to displace preformed hnRNP U–M1 RNA complexes and vice versa (Figure 4-29D). The exchange in RBP-RNA complexes occurred at approximately 1:1 stoichiometry of both RBPs, which is in accordance with the comparable affinities of hnRNP U and hnRNP L for the M1 pre-mRNA. Since we did not observe supershifted RBP-RNA complexes, both hnRNP proteins seem to bind *MALT1* RNA separately. Taken together, hnRNP U and hnRNP L individually associate to several regulatory sequences around *MALT1* exon7 and may even compete for binding to similar regions to regulate *MALT1* splicing.

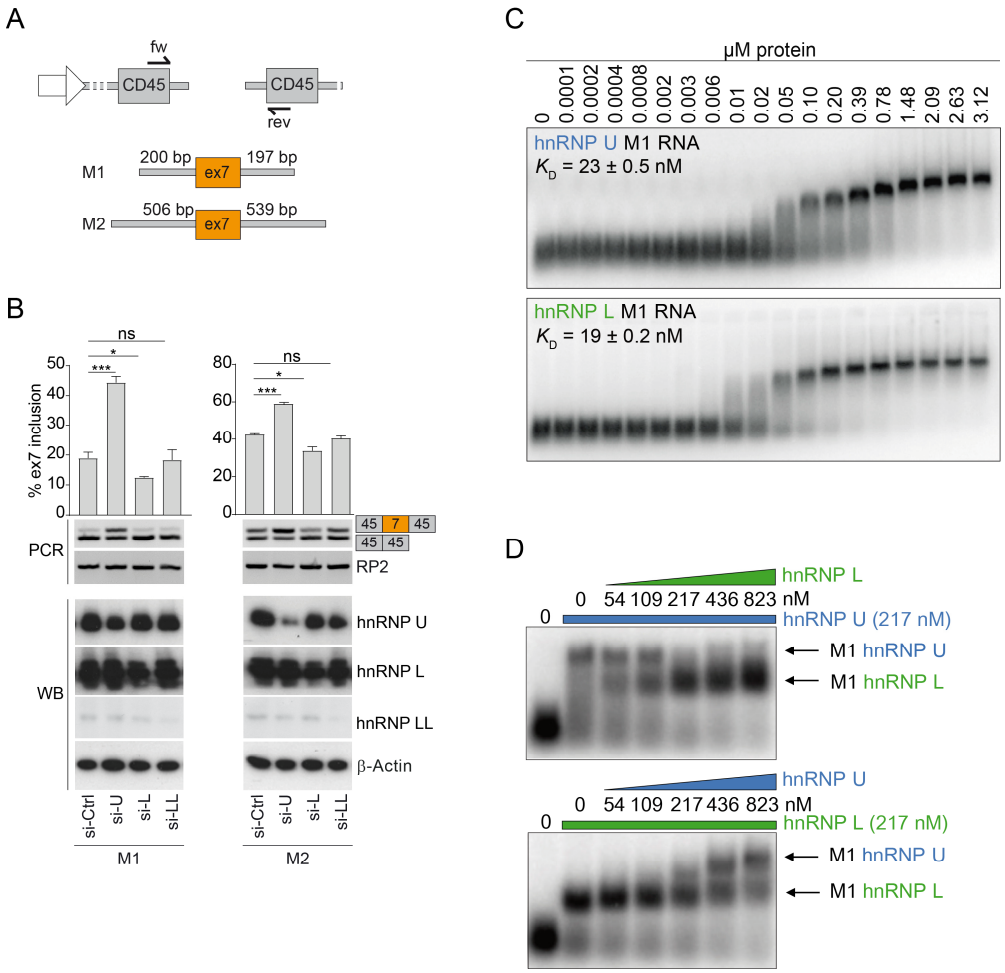

Figure 4-29: *MALT1* minigenes recapitulate antagonistic effects of hnRNP proteins on *MALT1* alternative splicing.
A) *MALT1* exon7-spanning minigenes M1 and M2. *MALT1* pre-mRNA comprising exon7 and flanking intronic sequences were cloned into a *CD45* exon3/exon7-containing plasmid. *CD45* forward (fw) and *CD45* reverse (rev) primers were used for splicing analysis.
B) *MALT1* minigene assays upon siRNA knockdown of hnRNP U (si-U), hnRNP L (si-L) and hnRNP LL (si-LL). Minigenes were introduced into siRNA transfected Jurkat T cells and analyzed for exon7 inclusion and exclusion by PCR using *CD45*-specific primers. Data are representative for three independent experiments. Bars show means ± SEM (n=3), and p-values were calculated by unpaired Student's t test. *p < 0.05, **p < 0.01, ***p < 0.001 and ****p < 0.0001; ns, not significant.
C) Binding of hnRNP U and hnRNP L to *MALT1* minigene M1 analyzed by EMSA.
D) Competitive binding of hnRNP U and hnRNP L to *MALT1* minigene M1.
C and D) EMSA assays were performed by Dr. Alisha Jones at the Institute of Structural Biology, Helmholtz Zentrum München, Neuherberg.

4.3.6.2 The RGG/G-rich region of hnRNP U and the four RRMs of hnRNP L are responsible for controlling *MALT1* splicing

Knockdown experiments showed that hnRNP U and hnRNP L expression levels influence alternative splicing of *MALT1*. Thus, we wanted to identify the regions of both RBPs necessary for controlling alternative exon7 splicing and RNA binding of *MALT1*. hnRNP U contains an N-terminal SAP domain for DNA binding, a SPRY domain mediating protein-protein interactions and RGG/G-rich region at the C-terminus for RNA-binding (Kiledjian & Dreyfuss, 1992; Ye et al., 2015) (Figure 4-30A). hnRNP L consists of a G-rich and a P-rich domain, both essential for protein-protein interactions (Busch &

Hertel, 2012) and four RNA recognition motifs (RRMs) that bind to CA repeats or CA-rich elements within mRNAs (Figure 4-30C) (Zhang et al., 2013). We overexpressed either full length (FL) or various truncated constructs of hnRNP U and hnRNP L in Jurkat T cells and analyzed the effect of distinct protein regions on exon7 inclusion and exclusion. Overexpression of FL hnRNP U reduced exon7 inclusion of *MALT1* minigene M2 (Figure 4-30B). However, the C-terminal RGG/G-rich region alone was able to reduce exon7 inclusion even more drastically than FL hnRNP U, whereas deletion of RGG/G-rich domain displayed only minor effects on exon7 inclusion. In line with this, the RGG/G-rich region and RGG domain alone bound with low nanomolar affinity to the M1 pre-mRNA (data not shown). Thus, the RGG/G-rich region of hnRNP U is sufficient to enable RNA binding and repression of MALT1 exon7 splicing. Overexpression of FL hnRNP L increased exon7 inclusion of minigenes M1 and M2. However, no effect on exon7 splicing could be observed for RRM1/2 or RRM3/4 on both minigenes, respectively (Figure 4-30D). Thus, all four RRMs of hnRNP L are required for regulation of alternative *MALT1* splicing in cells.

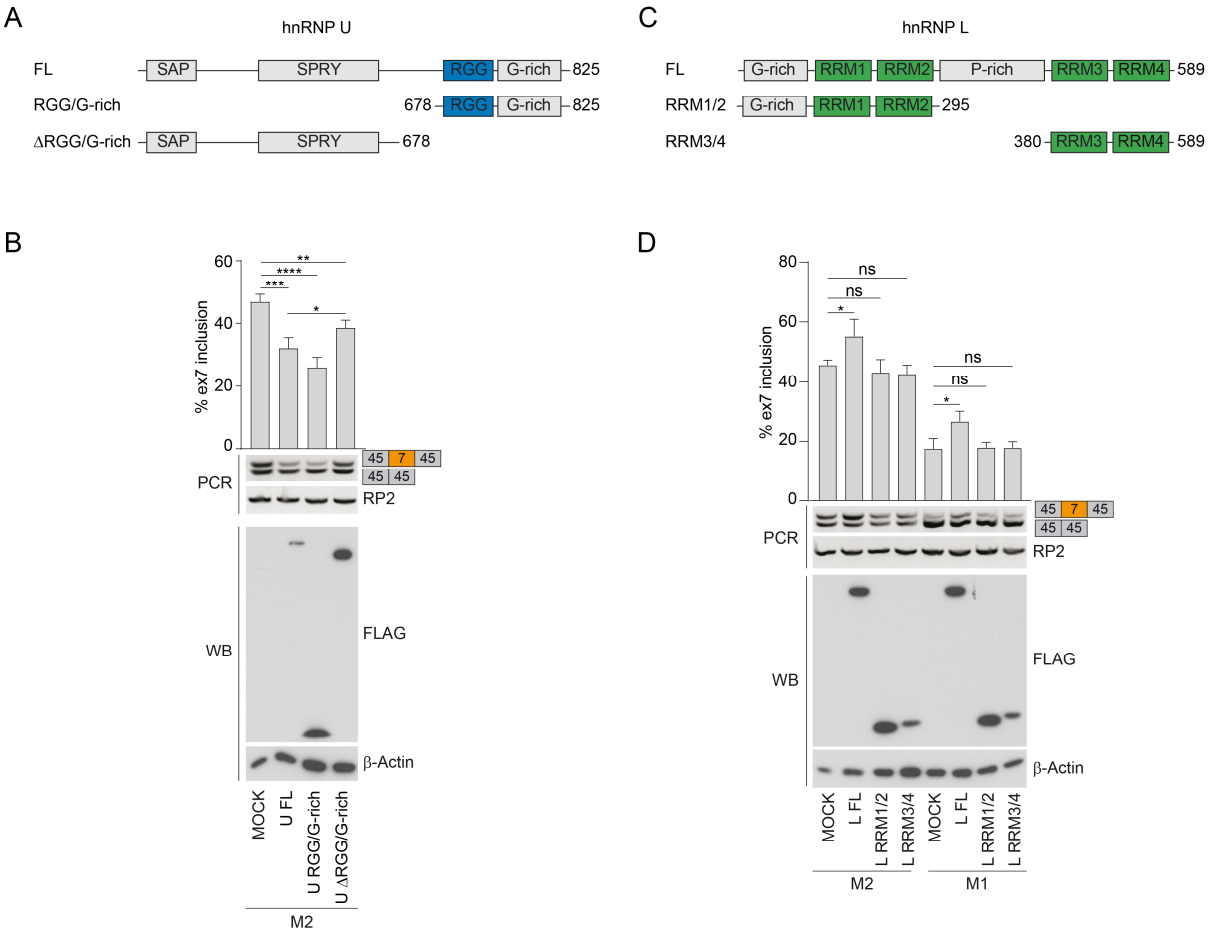

Figure 4-30: Identification of hnRNP U and hnRNP L domains regulating *MALT1* splicing.
A) Schematics of full length (FL) and truncated hnRNP U constructs.
B) *MALT1* minigene assay upon overexpression of mock, hnRNP U full length (FL), RGG/G-rich and ΔRGG/G-rich. Minigene M2 and indicated hnRNP U constructs were transfected into Jurkat cells and analyzed for exon7 inclusion and exclusion by PCR using *CD45*-specific primers.
C) Schematics of full length (FL) and truncated hnRNP L constructs.
D) *MALT1* Minigene assays upon overexpression of mock, hnRNP L full length (FL), RRM1/2 and RRM3/4. Minigene M2 (left) or M1 (right) and indicated hnRNP L constructs were transfected into Jurkat cells and analyzed for exon7 inclusion and exclusion by PCR using *CD45*-specific primers.
B, D) Data are representative for three (B, D) independent experiments. Bars show means ± SEM (n=3), and p-values were calculated by unpaired Student's t test. *p < 0.05, **p < 0.01, ***p < 0.001 and ****p < 0.0001; ns, not significant.

4.3.6.3 Secondary structure of *MALT1* pre-mRNA determines alternative splicing

Alternative splicing is regulated via cis-acting sequence motifs in the pre-mRNA which are recognized by trans-acting RBPs (Fu & Ares, 2014; Nilsen & Graveley, 2010). However, the secondary structure of pre-mRNAs has also been suggested to contribute to splicing regulation (McManus & Graveley, 2011). Therefore, we performed SHAPE (selective 2'-hydroxyl acylation analyzed by primer extension) chemical probing to map the structure of *MALT1* M1 pre-mRNA at single nucleotide resolution. SHAPE analysis revealed that *MALT1* M1 pre-mRNA is well structured and consists of two main domains (Figure 4-31A). Domain 1 contains the first ~ 150 nucleotides (nt) which form three stem-loop (SL) RNA structures (SL1 to SL3), whereas domain 2 comprises the remaining ~ 250 nt and consists of four stem-loops (SL4 to SL7). SL4 harbors the poly-pyrimidine tract (Py-tract) of the 3' splice site of the preceding intron and the first 11 nt of the alternatively spliced exon7. Exon7 extends into SL5 which forms a hammerhead-like RNA structure with SL6. The 5´ splice site of exon7 is located in SL5. Thus, the secondary structure of M1 pre-mRNA shields the regulatory splice elements flanking exon7 from the splicing apparatus, suggesting that it may be directly involved in splicing regulation. We noticed that SL2, SL4, SL5 and SL6 contain complementary GU- and CA-containing RNA sequences in the two strands that base pair in the RNA helical stem (Figure 4-31B). For example, exon7 contains CA- rich sequences which base pair with the GU-rich sequences around the Py-tract in SL4 or the 5´ splice site in SL5. Since it has been suggested that GU-rich sequences are recognized by hnRNP U, and CA-rich sequences by hnRNP L (Hui et al., 2005; Smith et al., 2013), our data indicate that *MALT1* pre-mRNA binding by hnRNP U and hnRNP L may directly regulate the accessibility of the spliceosome.

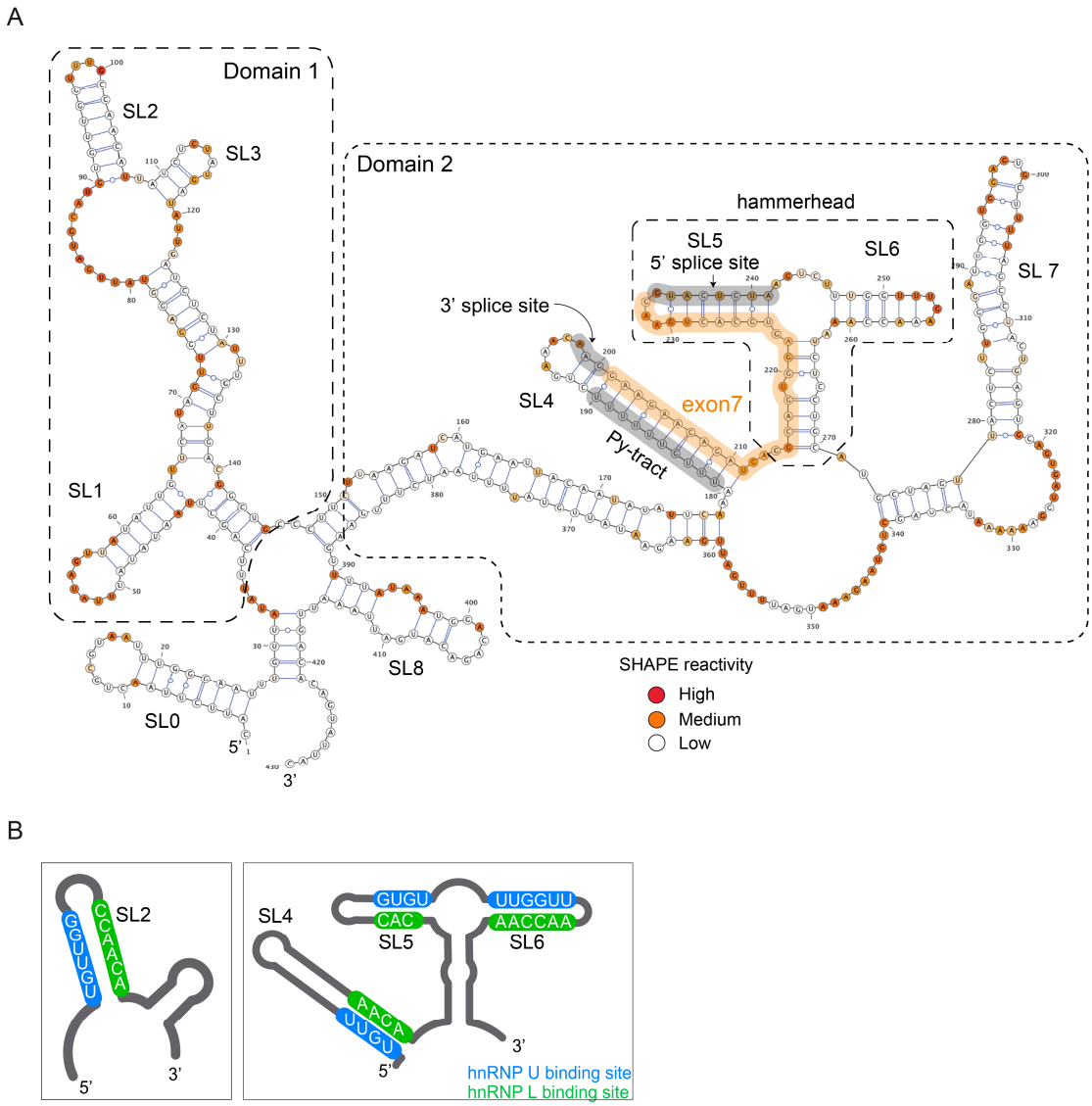

Figure 4-31: Identification of cis-regulatory motifs and RBP binding sites regulating *MALT1* splicing.
A) SHAPE-derived secondary structure of the *MALT1* minigene M1 RNA. Domains 1 and 2 are outlined, with stem loops and splice sites highlighted. Nonreactive, semireactive, and highly reactive nucleotides are colored white, orange, and red, respectively. Stem loop (SL), poly-pyrimidine tract (Py-tract).
B) Binding sites for hnRNP U (blue) and hnRNP L (green) across the *MALT1* minigene M1.
A and B) SHAPE was performed by Dr. Alisha Jones at the Institute of Structural Biology, Helmholtz Zentrum München, Neuherberg.

To investigate the functional importance of the RNA primary sequence and the secondary structure for *MALT1* exon7 splicing, we designed two minigene variants that selectively disrupt the structure of the M1 pre-mRNA without affecting essential splice signals (Figure 4-32A). In variant 1, *MALT1* exon7 was replaced with exon9, which also consists of 33 nt. Exon swapping induced conformational changes and sequestered the flanking Py-tract and 5' splice site sequences in secondary structures making them inaccessible for the splicing apparatus (Figure 4-32B). In line, inclusion of exon9 was completely abolished and splicing regulation upon hnRNP U and L KD was lost (Figure 4-32D).

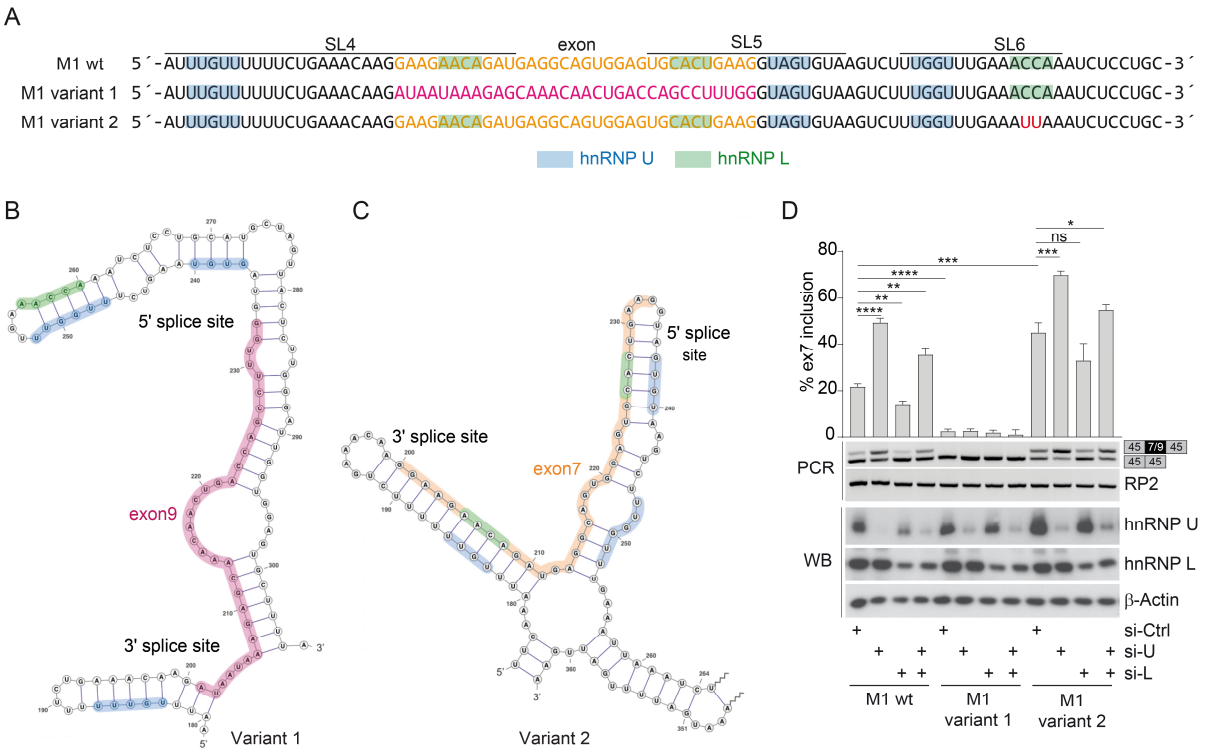

Figure 4-32: *MALT1* minigene variants highlight importance of secondary structure of *MALT1* pre-mRNA.

A) Primary sequences of *MALT1* minigene M1 and two variants. In variant 1, exon7 was replaced by exon9 (colored pink), in variant 2, two nucleotides in stem loop (SL) 6 were altered (colored red). Binding sites of hnRNP U (blue) and hnRNP L (green) are highlighted.

B, C) SHAPE-derived secondary structure of variant 1 and variant 2 of *MALT1* minigene M1 RNAs, zoomed in to the region that harbors the 5' and 3' splice sites flanking exon7.

D) *MALT1* minigene assays with M1 WT, variant 1 and variant 2 upon siRNA knockdown of hnRNP U (si-U), hnRNP L (si-L) or combined. Minigenes were introduced into siRNA transfected Jurkat cells and analyzed for exon7 inclusion and exclusion by PCR using *CD45*-specific primers. Data are representative for three independent experiments. Bars show means ± SEM (n=3), and p-values were calculated by unpaired Student's t test. *p < 0.05, **p < 0.01, ***p < 0.001 and ****p < 0.0001; ns, not significant.

B and C) SHAPE was performed by Dr. Alisha Jones at the Institute of Structural Biology, Helmholtz Zentrum München, Neuherberg.

Our SHAPE data predict, that the exon7 encoded hnRNP L binding motifs which base pair with the Py-tract and the former SL5 in the WT M1 minigene, are missing in M1 variant 1. Thus, sequestration of the Py-tract and 5' splice sites by exon9 with combined absence of hnRNP L binding motifs prevents access for the splicing machinery and subsequent inclusion of exon9. In variant 2, we altered two nucleotides in the SL6 stem of M1 pre-mRNA. SHAPE probing revealed that SL6, as well as the SL5/SL6 hammerhead structure were destructed (Figure 4-32C). In addition, we observed extended base pairing of the former SL6 with exon7 and more distant regions in the pre-mRNA. However, conformational changes did not affect the sequestration of the Py-tract in SL4 and of the 5' splice site in SL5. Minigene assays with M1 variant 2 demonstrated significantly enhanced inclusion of exon7 compared to M1 wild-type pre-mRNA (Figure 4-32D). Inclusion of exon7 was still regulated by hnRNP U and hnRNP L knockdown, suggesting that the RBP binding motifs were not

affected. Taken together, the secondary structure of *MALT1* pre-mRNA and in particular SL4 and SL5 contribute to the splicing regulation by shielding the 3´ and 5´ splice sites from hnRNP U and hnRNP L binding. Thus, alternative exon7 splicing is regulated by a combination of secondary structural elements and competitive binding of two antagonistic RBPs.

5 Discussion

NF-κB signaling plays an essential role in activation, proliferation, and differentiation of T lymphocytes in adaptive immunity. The CBM complex, consisting of CARD11, BCL10 and MALT1, is a central signaling platform which bridges TCR engagement to downstream NF-κB activation. MALT1 contributes to the CBM scaffold and at the same time acts as a protease that cleaves distinct substrates to further modulate T cell activation. Via two TRAF6-binding motifs (T6BMs), MALT1 recruits the E3 ligase TRAF6 to the CBM complex. Whereas the physiological function of MALT1 paracaspase activity has been intensively studied over the past years (Bornancin et al., 2015; Demeyer et al., 2019; Gewies et al., 2014; Jaworski et al., 2014; Rosenbaum et al., 2022), we are just beginning to understand the relevance of MALT1-TRAF6 scaffolding in adaptive immunity. TRAF6 has a unique dual role in balancing T cell activation and immune homeostasis. On the one hand, TCR-induced TRAF6 recruitment via MALT1 T6BMs triggers the attachment of K63-linked polyubiquitin chains to MALT1, which provide a docking surface for the IκB kinase (IKK) complex, yielding NF-κB activation (Meininger et al., 2016; Oeckinghaus et al., 2007). On the other hand, TRAF6 restricts constitutive MALT1 protease activity in resting T cells and thus spontaneous T cell activation and autoimmunity (O'Neill et al., 2021). MALT1 scaffolding function can be fine-tuned by alternative splicing, which affects the number of encoded T6BMs. MALT1A contains T6BM1 within exon7 and T6BM2 within exon17, whereas MALT1B only expresses the C-terminal T6BM2. In consequence, TRAF6-binding by MALT1A and subsequent NF-κB activation was shown to be more robust compared to MALT1B (Meininger et al., 2016). Of note, a single missense mutation in T6BM2 of MALT1 causes a complex human immune disorder (Kutukculer et al., 2021), prompting us to more closely investigate the functional and mechanistic role of MALT1-mediated control of immune homeostasis.

5.1 Selective destruction of the MALT1B isoform is sufficient to disrupt immune homeostasis

The homozygous *MALT1* c.2418G>C transversion was identified in a 19-year-old Turkish woman. This single missense mutation disrupts MALT1 T6BM2, preventing TRAF6 from binding to the shorter MALT1B isoform, whereas MALT1A can still bind to TRAF6 via T6BM1, albeit to a reduced extent (Kutukculer et al., 2021; Meininger et al., 2016). The patient´s immune pathology is manifested by a combination of immune suppression and autoimmunity (Kutukculer et al., 2021). It was unclear, why the patient developed such an immune disorder, considering that the longer MALT1A isoform would be expected to remain functional and could compensate for defective MALT1B. We therefore generated a mutant mouse line as a disease model, by introducing the patient derived T6BM2

mutation into the murine *Malt1* gene. On protein sequence level, this mutation corresponds to E814D in MALT1A and E803D in MALT1B. We expected *Malt1* TRAF6-binding mutant 2 (TBM2) mice to develop a less severe phenotype compared to *Malt1* TBM mice, in which both MALT1 isoforms are defective in TRAF6 binding (O'Neill et al., 2021). However, to our surprise *Malt1*$^{TBM2/TBM2}$ mice displayed massive, early onset autoimmunity just as *Malt1*$^{TBM/TBM}$ mice did. The inflammatory phenotype of TBM2 is characterized by splenomegaly, dramatically increased effector T (Teff) cells, and low survival. We demonstrate that selective destruction of the MALT1B isoform is sufficient to impair TCR-induced NF-κB signaling and induce chronic MALT1 protease activation, which was previously identified to drive cell-autonomous T cell activation (O'Neill et al., 2021). Overall, selective impairment of MALT1B or combined destruction of both MALT1 isoforms in C57BL/6N mice causes a highly similar, fatal autoimmune phenotype. In striking contrast, the human immune pathology is less severe and displays signs of both immune deficiency and autoimmunity, indicating that there may be biological differences between species.

The complex immune disorder of the patient can be explained by relative MALT1A expression levels, the stoichiometry of CBM complex assembly and the dual role of MALT1-TRAF6 interaction. During tonic T cell signaling in the absence of a strong antigenic stimulus, MALT1-TRAF6 interaction counteracts low-level CBM complex formation and thus prevents chronic MALT1 protease activity (Figure 5-1, top left). In contrast, in response to strong antigenic TCR signaling, an active CBM complex is assembled (Figure 5-1, top right). CARD11 functions as a seed and induces the formation of filaments with a BCL10 core, MALT1 assembled at the periphery of the filaments and TRAF6 further decorating the filaments by binding to MALT1 (David et al., 2018; Qiao et al., 2013; Schlauderer et al., 2018). Thereby, both BCL10-MALT1 and MALT1-TRAF6 interact in a 1:1 stoichiometry (David et al., 2018; Schlauderer et al., 2018). CBM assembly activates MALT1 protease function and induces the cleavage of various substrates, further modulating NF-κB signaling (e.g. A20 and CYLD) or post-transcriptional RNA metabolism (e.g. Regnase-1 and Roquin-1/2). TRAF6 triggers downstream IKK/NF-κB activation, resulting in NF-κB target gene expression and T cell activation (Meininger & Krappmann, 2016; Ruland & Hartjes, 2019). In the patient, MALT1B-TRAF6 interaction is disrupted via the T6BM2 mutation (Kutukculer et al., 2021). MALT1B is the predominant isoform in human blood CD4+ T cells, with approximately 5-fold higher expression than MALT1A (Meininger et al., 2016), meaning that even in the absence of a strong antigen, low level of CBM complex is able to assemble leading to constitutive MALT1 protease activity and substrate cleavage (Figure 5-1, bottom left).

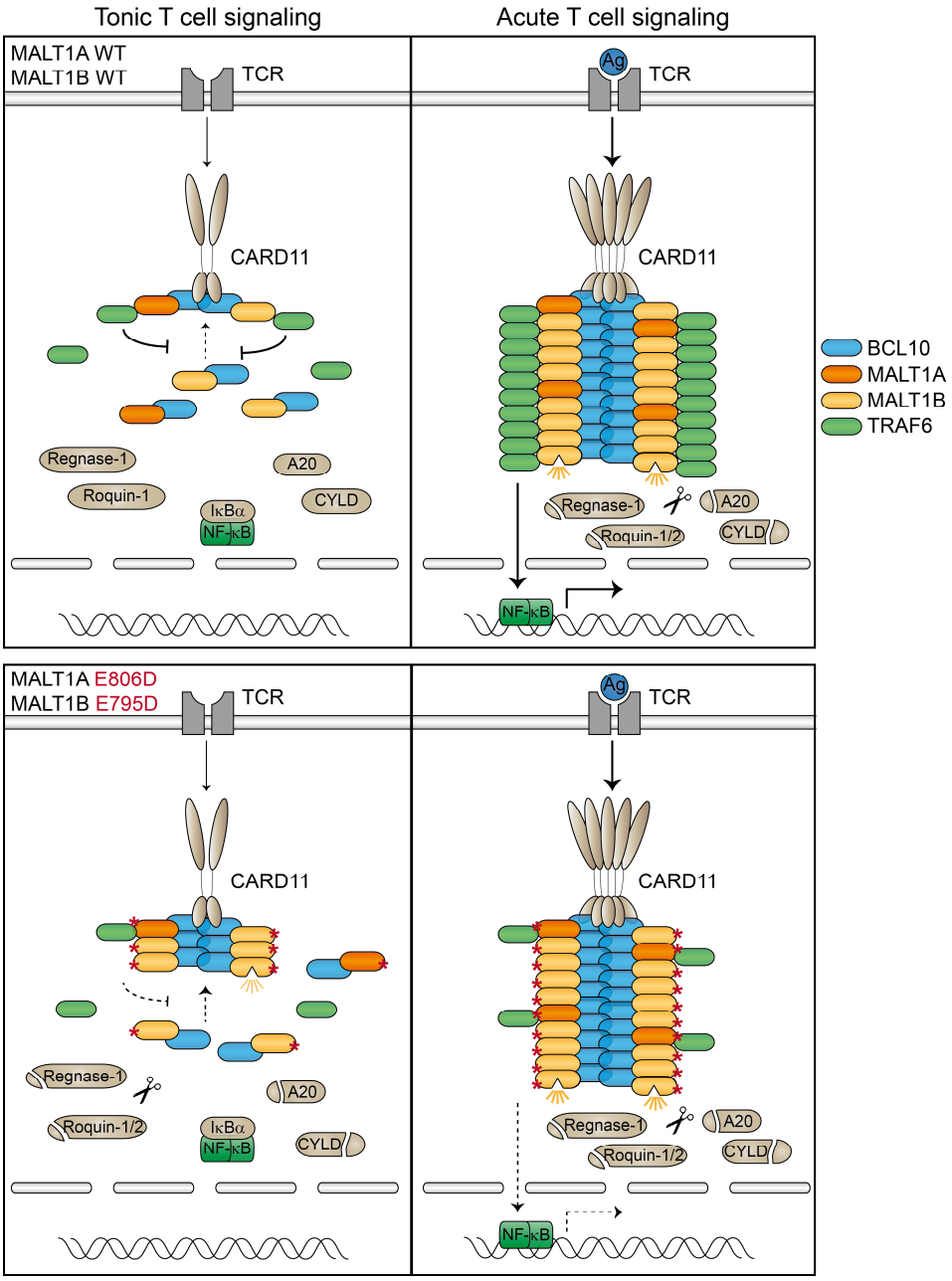

Figure 5-1: Defective MALT1B E795D disrupts immune balance in the human patient.
Top, left: In healthy individuals, both MALT1 splice isoforms interact with TRAF6 and prevent low level (tonic) CBM complex assembly and chronic MALT1 protease activity in the absence of a strong antigenic stimulus. Top, right: Upon strong antigenic TCR stimulation, a functional CBM complex assembles, consisting of CARD11 as seed and stoichiometric BCL10-MALT1 filaments decorated with TRAF6. TRAF6 facilitates downstream NF-κB signaling and active MALT1 protease cleaves distinct substrates including NF-κB mediators (A20, CYLD) and post-transcriptional regulators (Regnase-1, Roquin-1/2). Bottom, left: Selective impairment of MALT1B-TRAF6 binding due to the *MALT1* c.2418G>C mutation disrupts the immune balance in the human patient. In resting T cells, functional MALT1A E806D is not sufficient to prevent CBM complex assembly, leading to deregulated MALT1 protease activity and chronic substrate cleavage. Bottom, right: In response to acute T cell signaling, insufficient TRAF6-MALT1A E806D binding impairs NF-κB signaling, causing immune deficiency.

Low expression of mutant, but functional, MALT1A E806D in the patient may be able to counteract chronic MALT1B proteolytic activity at least to some extent. In line with this, co-expression of MALT1A WT and pathogenic MALT1B E795D in Jurkat T cells showed that chronic MALT1B protease

activity decreases upon increasing MALT1A protein levels, but substrate cleavage is only absent at a 1:1 ratio of both splicing variants (O'Neill et al., 2021). Deregulated MALT1 substrate cleavage drives abnormal T cell activation (O'Neill et al., 2021), which in the patient leads to autoimmunity manifested by dermatitis, psoriasis and presence of autoantibodies (Kutukculer et al., 2021). However, upon strong TCR signaling the patient fails to induce a proper immune response (Figure 5-1, bottom right). Antigenic stimulation is able to induce CBM complex assembly, composed of predominantly TRAF6-binding-incompetent MALT1B E795D with few functional MALT1A E806D molecules integrated in filaments, meaning that TRAF6 is insufficiently recruited to the signaling platform. Thus, NF-κB activation is severely impaired in the patient, causing immune suppression manifested by recurrent ear and bronchial infections (Kutukculer et al., 2021).

Since the phenotype of *Malt1* TBM2 mice is more severe than the human immune disorder, we assumed that the relative expression levels of MALT1A might play a role. We therefore performed an expression analysis in murine and human immune cells to dissect differences in the abundance of of MALT1A. Whereas low *MALT1A* mRNA levels were detected in primary human peripheral blood mononuclear cells (PBMCs), *Malt1A* mRNA expression was below the detection limit in murine PBMCs. In line with this observation, PBMCs isolated from the blood of the patient expressed transcripts for both isoforms (Kutukculer et al., 2021), whereas splenocytes from *Malt1* TBM2 mice exclusively contained the shorter *Malt1B* isoform. Detailed analysis of different lymphocyte subsets of C57BL/6N mice confirmed that *Malt1A* is undetectable in both naïve and effector T cells. Thus, differences in severity of the immune phenotype between human and mouse may arise from relative MALT1A expression levels (Figure 5-2). The patient expresses low levels of MALT1A E806D, which may partially restrict spontaneous CBM assembly and chronic MALT1B E795D protease activity, leading to moderate autoimmunity when compared to the mouse model. In contrast, C57BL/6N *Malt1*$^{TBM2/TBM2}$ mice exclusively contain defective MALT1B E803D. Thus, CBM complex formation in resting T cells is not counteracted and constitutive MALT1B E803D paracaspase activity is completely unrestrained resulting in the fatal autoinflammatory disease similar to *Malt1*$^{TBM/TBM}$ mice. Due the drastic early onset immune phenotype in *Malt1* TBM2 mice, signs of immune deficiency caused by defective NF-κB activation do not develop in TBM2 mice, whereas they are present in the slower progressing immune pathology of the human patient. Taken together, because MALT1B is the dominant isoform which dictates T cell activation and immune homeostasis, selective destruction of MALT1B is sufficient to cause autoimmunity and compromised immune responses. However, comparing the distinct pathology in human and C57BL/6N TBM2 mice revealed that the relative expression levels of MALT1 isoforms determine the onset and severity of disease. Therefore, the number of intact MALT1-TRAF6 interactions seems to be most critical.

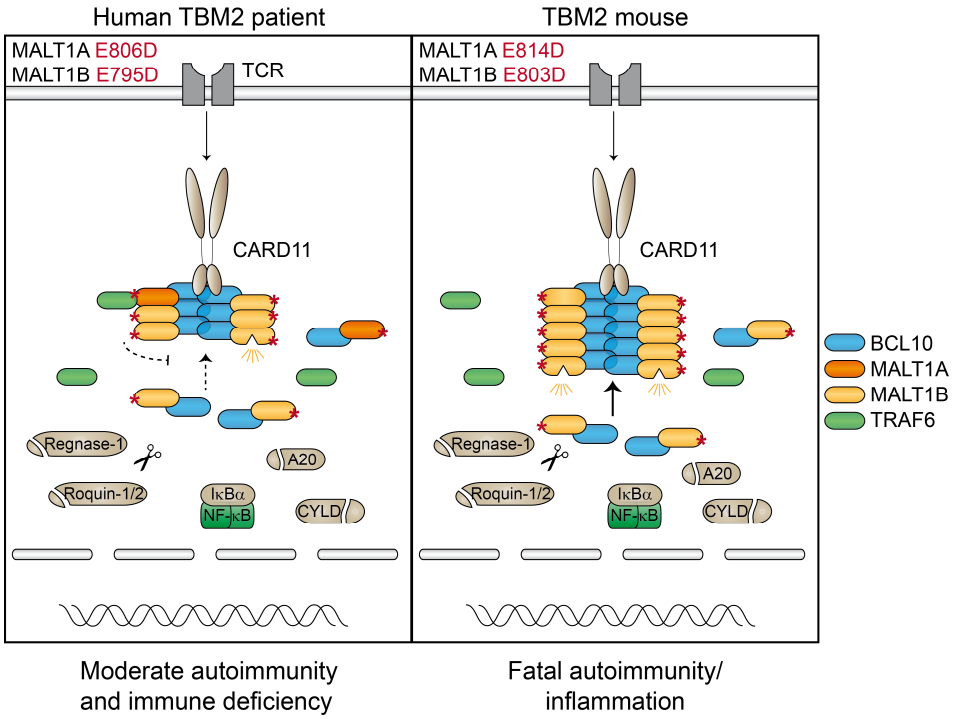

Figure 5-2: Comparison of tonic T cell signaling between the human TBM2 patient and TBM2 mice.
Low expression levels of mutated but functional MALT1A E806D partially restrains spontaneous CBM complex formation and chronic MALT1B E795D protease activity, yielding only moderate autoimmunity in the human patient. In *Malt1* TBM2 mice, complete absence of MALT1A leads to CBM assembly and fully deregulated MALT1B E803D protease activity resulting in fatal, early onset autoinflammation.

Studying disease development and progression in the human patient is not possible since the immune pathology is already manifested. Unfortunately, neither do homozygous *Malt1*$^{TBM2/TBM2}$ mice, due to early onset autoinflammation and low survival. Therefore, we followed up with heterozygous *Malt1*$^{TBM2/+}$ mice and did a final analysis at 12 months of age, at which time we could not observe obvious signs of burden. Immune phenotyping revealed high expression of the activation marker CD69 in CD3+ T cells and enhanced Teff cell populations. Similarly to the human patient, autoantibodies were increased in TBM2 mouse blood sera, aguing for an ongoing, low-level autoinflammation. Hence, heterozygous expression of T6BM2 mutation in Malt1$^{TBM2/+}$ mice is sufficient for development of late-onset autoimmunity. Overall, Malt1$^{TBM2/+}$ mice reflect the human phenotype more closely and may be more suitable to study the progression of the human immune disorder. Since presence of WT MALT1 protein is able to counteract constitutive MALT1B protease activity (O'Neill et al., 2021), deregulated catalytic activity seems to be kept to a minimum in young heterozygous mice. Over time, immune cells with dysregulated immune signaling accumulate due to chronic low-level MALT1 protease activation and eventually induce autoimmunity. In line with this, heterozygous *Malt1* TBM mice showed no differences in CD4+ and CD8+ T_{EM} cells at 3 months of age, but increased levels at 6 months and even more pronounced at 12 months of age (O'Neill et al., 2021). Thus, heterozygous TBM2 mice highlight once more that the protein level of defective

MALT1B, or conversely the number of existing MALT1A-TRAF6 protein interactions, seems to be the critical switch between immune balance and pathology. Of note, the MALT1 T6BM2 loss-of-function mutation of the patient was inherited from her parents, who are first-degree cousins and both heterozygous for the mutation. However, there is no report of obvious clinical symptoms of the parents (Kutukculer et al., 2021), indicating that heterozygous expression of the MALT1 T6BM2 mutation may not be sufficient to cause a severe immune disease in humans.

Spontaneous activation of conventional (Tconv) T cells represents a key characteristic of the autoimmune phenotype of *Malt1* TBM and TBM2 mice. Both models display a massive increase in CD4+ and CD8+ effector memory (T_{EM}) T cells (O'Neill et al., 2021). *Malt1* paracaspase mutant (PM) mice, which lack proteolytic activity due to mutation of cysteine-472, also develop autoimmunity, but the phenotype is driven by a distinct mechanism. In *Malt1* PM mice immune activation is caused by loss of Treg cell numbers and function, and thus loss of suppressive control over Teff cells (Bornancin et al., 2015; Demeyer et al., 2019; Gewies et al., 2014; Jaworski et al., 2014; Rosenbaum et al., 2019). In striking contrast, Treg cell numbers of TBM and TBM2 mice are increased and display unchanged or higher expression of the suppression markers Ox-40 and CTL4A compared to control mice (O'Neill et al., 2021). *In vitro* assays demonstrated that Treg cells defective in MALT1-TRAF6 interaction are still able to suppress proliferation of CD4+ T cells, indicating that they retain their suppressive function (O'Neill et al., 2021). Importantly, loss of MALT1-TRAF6 binding exclusively in Treg cells of *Malt1* TBM-Treg mice (*Malt1*$^{TBM/flox}$;*FoxP3-Cre*$^{Cre+}$) did not induce immune activation (O'Neill et al., 2021). Thus, even though Treg cells are present and functional in TBM and TBM2 mice, Teff cells escape their suppressive activity, resulting in loss of peripheral tolerance and autoinflammation.

Chronic MALT1 substrate cleavage is sufficient to trigger autoimmunity in *Malt1* TBM mice even in the absence of TCR-induced NF-κB signaling (O'Neill et al., 2021). It has been suggested that partial inactivation of the post-transcriptional regulators Regnase-1 and Roquin-1/2 via continuous MALT1 cleavage mainly drives aberrant immune activation of Tconv cells (O'Neill et al., 2021). Regnase-1 and Roquin-1/2 are crucial for maintaining peripheral tolerance by regulating the mRNAs of various genes, including *Rel* (c-Rel), *Tnfrsf4* (Ox40), *Icos*, *Nfκbid* (IκBNS), and *Nfκbiz* (IκBζ) (Jeltsch et al., 2014; Matsushita et al., 2009; Uehata et al., 2013; Vinuesa et al., 2005; Vogel et al., 2013). Loss-of-function mutations or ablation of these essential regulators leads to the development of autoimmune disease similar to the TBM phenotype, characterized by splenomegaly, high serum levels of cytokines and autoantibodies, cell-autonomous T cell activation and low survival (Matsushita et al., 2009; Uehata et al., 2013; Vogel et al., 2013). In line with previous data from mice

with conditional T cell-specific destruction of the TRAF6 interaction interface on MALT1 (*Malt1* TBM-T), ICOS and IκBNS are upregulated in CD4+ and CD8+ T cells from *Malt1* TBM2 mice. Currently, we are breeding a new mouse line, which expresses the MALT1 TBM mutations together with a Roquin-1 non-cleavable mutant. We speculate that absence of Roquin-1 cleavage is sufficient to at least partially ameliorate the drastic inflammatory phenotype of TBM mice and extend median survival.

5.2 Severe anemia correlates with early death in *Malt1* TBM2 mice

The drastic autoimmune phenotype of homozygous *Malt1* TBM2 mice leads to a median survival of only 18 days. To investigate the cause of early death, we conducted blood and serum analyses. Strikingly, serum parameters of typical liver enzymes, including aspartate aminotransferase (AST) and glutamate dehydrogenase (GLDH), were already drastically increased in several *Malt1*$^{TBM2/TBM2}$ mice at the age of 12 – 14 days. These specific biomarkers are present in the cytoplasm of hepatocytes and are released into the circulation upon cell damage. Thus, we speculated that autoimmune inflammation upon loss of MALT1B-TRAF6 binding may cause liver damage in TBM2 mice. We further detected low erythrocyte, hemoglobin and hematocrit levels in the blood of *Malt1*$^{TBM2/TBM2}$ mice indicating an incipient anemia. Histological analyses of moribund *Malt1*$^{TBM/TBM}$ mice showed massive infiltration of inflammatory cells in various organs including the liver (O'Neill et al., 2021). Thus, we rationalize that *Malt1*$^{TBM2/TBM2}$ mice develop a similar multi-organ inflammation leading to liver damage. As a consequence of an acute liver failure, anemia most likely causes the death of TBM2 mice due to insufficient oxygen supply. Decreased levels of erythrocytes might be caused by defective development of hematopoietic stem and progenitor cells (HSPCs) or by impairment in erythropoiesis due to an inflammatory environment in the bone marrow. To further address these questions, bone marrow cells of *Malt1*$^{TBM2/TBM2}$ mice should be analyzed more closely.

5.3 TRAF6 and LUBAC cooperate in BCL10 ubiquitination to restrict CBM complex formation

Both *Malt1* TBM and TBM2 mouse models clearly demonstrated that TRAF6 functions as a negative regulator of MALT1 protease activity in resting T cells. Previous experiments in Jurkat T cells could decipher some requirements for this restrictive role. TRAF6 acts upstream of MALT1, because BCL10 and CARD11 binding as well as a functional TCR are required for constitutive MALT1 protease activation in the absence of TRAF6 (O'Neill et al., 2021). However, the exact mechanism of regulation has not been solved so far. Thus, we hypothesized that TRAF6 counteracts homeostatic TCR signaling and low level of CBM complex assembly in resting T cells. BCL10 was identified as target for the negative regulatory effect of MALT1-TRAF6 interaction. We show here, that TRAF6 and LUBAC cooperatively polyubiquitinate BCL10, thereby counteracting CBM complex formation. Based on the

obtained results from structural data and biochemical studies, we propose the model shown in Figure 5-3.

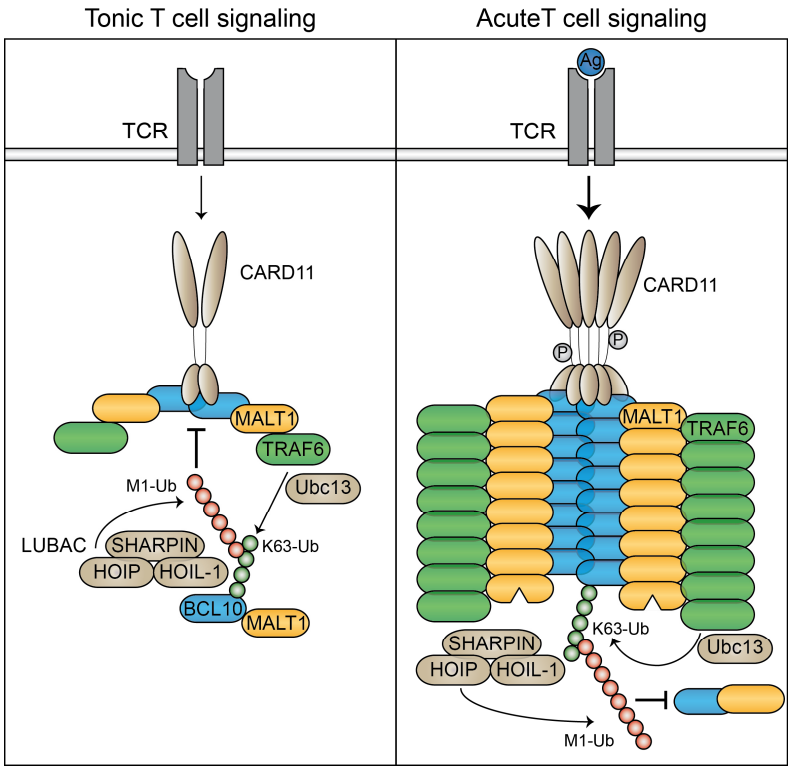

Figure 5-3: Putative model for restriction of CBM complex-mediated MALT1 protease activation.
In the absence of an antigenic stimulus, TRAF6, in cooperation with Ubc13, catalyzes K63-ubiquitination of BCL10. K63-linked ubiquitin chains induce the recruitment of LUBAC, consisting of the catalytic active subunit HOIP, HOIL-1 and SHARPIN. LUBAC amplifies BCL10 ubiquitination by attaching linear M1-ubiquitin chains to the preexisting K63-chains. This prevents chronic CBM complex formation and MALT1 protease activation. Upon prolonged TCR-induced NF-κB signaling, the same mechanism helps to terminate continuous CBM complex elongation, preventing overshooting immune responses.

In the absence of a strong antigenic stimulus, MALT1-BCL10 heterodimers constitutively associate with TRAF6 via T6BMs in MALT1. TRAF6 catalyzes low level K63 polyubiquitination of BCL10, which induces the recruitment and binding of LUBAC. In turn, LUBAC amplifies BCL10 ubiquitination via the attachment of additional linear ubiquitin chains. Resulting K63-M1-heterotypic ubiquitin chains prevent spontaneous CBM complex assembly and MALT1 protease activation by counteracting BCL10 oligomerization and BCL10-MALT1 association. Thus, TRAF6 acts as dominant negative regulatory factor and LUBAC is a critical auxiliary factor amplifying initial TRAF6-mediated BCL10 polyubiquitination. This ubiquitin-dependent mechanism for restriction of constitutive MALT1 paracaspase activity may also facilitate the termination of prolonged TCR-induced NF-κB signaling. Cooperative TRAF6- and LUBAC-dependent ubiquitination of BCL10 at the distal end of BCL10 oligomers could inhibit further BCL10 oligomerization and extension of CBM complex assembly. Thus, the identified regulatory mechanism either raises the threshold for T cell signaling or helps to terminate T cell activation post-induction.

BCL10 polyubiquitination in response to T cell activation was previously reported to promote initial NF-κB signaling (Wu & Ashwell, 2008; Yang et al., 2016) and terminate prolonged signal transduction by targeting BCL10 for degradation (Hu et al., 2006a; Hu et al., 2006b; Paul et al., 2012; Scharschmidt et al., 2004). Attachment of K48- and K63-linked ubiquitin chains to BCL10 lysine residues K31 and K63 (Paul et al., 2012; Wu & Ashwell, 2008) as well as linear ubiquitination at K17, K31 and K63 by LUBAC (Yang et al., 2016) were described. Our results confirm that the LUBAC subunits HOIP and HOIL-1 are critical for P/I-induced BCL10 polyubiquitination. However, in striking contrast to previous literature (Dubois et al., 2014; Oikawa et al., 2020; Yang et al., 2016), we find that neither HOIL-1 nor HOIP (unpublished data by Franziska Ober) are required for CBM-dependent NF-κB signaling and for MALT1 paracaspase activation. We assessed NF-κB signaling in HOIL-1 and HOIP knockout (KO) Jurkat T cells generated by CRISPR/Cas9 technology, either by using a stably expressing NF-κB-EGFP reporter gene or by biochemical analysis in western blot. We demonstrate that, in the absence of HOIL-1 or HOIP, CBM-dependent NF-κB signaling is slightly downregulated but still functional. Previous studies determined NF-κB activation in a less clean genetic setting upon siRNA mediated knockdown (KD) of LUBAC components and/or via transient NF-κB luciferase reporter (Dubois et al., 2014; Yang et al., 2016). Therefore, different results might be not surprising due to less stringent and reliable methods. In any case, in neither study was NF-κB signaling completely inhibited upon LUBAC deficiency, arguing that a functional LUBAC is rather negligible for TCR-induced NF-κB signaling. However, generation and analysis of SHARPIN-deficient Jurkat T cells will be needed to strengthen our argument.

We further demonstrate that P/I-induced BCL10 ubiquitination in Jurkat T cells depends on TRAF6. Linkage analysis of ubiquitinated BCL10 confirmed that BCL10 is partially modified with K63-linked ubiquitin chains. However, the assay also revealed that primarily linear ubiquitin chains are attached to BCL10 upon TCR signaling. In line with our data, it was previously suggested that, upon BCR signaling, BCL10 is modified by linear and K63-linked ubiquitin chains and that both TRAF6 and LUBAC are required (Satpathy et al., 2015). These findings are consistent with reports showing that K63-polyubiquitin chains function as substrates for LUBAC recruitment. For instance, K63-polyubiquitination is a prerequisite for LUBAC-mediated linear ubiquitination in Toll-like receptor (TLR)/interleukin-1 receptor (IL-1R)-induced canonical NF-κB signaling (Emmerich et al., 2013). HOIP, the catalytic subunit of LUBAC, selectively binds to K63-polyubiquitin chains and catalyzes the formation of M1-ubiquitin chains in response to IL-1, resulting in so called K63/M1-polyubiquitin hybrids. These heterotypic ubiquitin chains permit the co-recruitment of the kinase complexes TAB2/3-TAK1 and the IKK and facilitate NF-κB activation (Cohen & Strickson, 2017; Emmerich et al., 2013). Furthermore, upon TNF signaling, LUBAC is recruited to TNFR1 complex I via recognition of

cellular inhibitor of apoptosis proteins 1 and 2 (cIAP1/2)-catalyzed K63 ubiquitin chains (Fujita et al., 2014; Shimizu et al., 2016). Thus, K63/M1-linked BCL10 hybrids may be generated by initial TRAF6-mediated K63-linked ubiquitination, which induces the recruitment of LUBAC and subsequent M1-ubiquitination of BCL10.

Whereas HOIL-1 and HOIP are rather dispensable for CBM-mediated NF-κB activation, TRAF6 is absolutely critical (O'Neill et al., 2021). Hence, we investigated the role of putative BCL10 ubiquitin acceptor sites. In line with prior studies, K17, K31 and K63 are required for CBM-dependent activation of NF-κB signaling and MALT1 protease, as well as BCL10 polyubiquitination (Paul et al., 2012; Wu & Ashwell, 2008; Yang et al., 2016). Because BCL10 ubiquitination relies on the presence of CARD11 and MALT1, it was previously rationalized that the modification occurs within the assembled CBM complex (Wu & Ashwell, 2008; Yang et al., 2016). In striking contrast, we show on the basis of structural cryo-EM data and functional analyses that ubiquitination at these sites is not possible in an assembled complex. Lysine 17 is required for BCL10-MALT1 association and CARD11 binding, whereas K31 and K63 are critical for BCL10 self-oligomerization and CARD11 recruitment. Thus, lysine to arginine exchange at respective residues was sufficient to destroy CBM complex formation. Previous studies of CBM assembly were either performed in the presence of endogenous BCL10 (Wu & Ashwell, 2008) or upon overexpression in HEK293T cells (Yang et al., 2016). Instead, we used stable BCL10 K-to-R reconstituted BCL10 KO Jurkat T cells and analyzed CBM formation under physiological conditions to exclude the influence of endogenous WT protein or overexpression effects. Our data clearly demonstrate that K17, K31 and K63 are required for CBM complex formation. HOIP, the catalytic active subunit of LUBAC, was previously shown to interact with the assembled CBM complex and the IKK complex following antigen receptor engagement (Dubois et al., 2014). Since CBM complex formation is disrupted in BCL10 K31R/K63R or K17R-expressing cells, it is likely that recruitment of LUBAC or other ubiquitin ligases to BCL10 is not possible, leading to reduced BCL10 polyubiquitination at distinct sites rather as a secondary effect. Indeed, CARD11 was shown to promote TCR-induced linear ubiquitination of BCL10 by directly binding and co-recruiting HOIP (Yang et al., 2016). Loss of CARD11-BCL10 interaction by K-to-R substitution at respective BCL10 residues therefore should prevent M1-linked ubiquitination of BCL10. Thus, mutation of K17, K31 and K63 does not interfere with polyubiquitination of BCL10 per se, but rather impairs downstream interactions between CBM complex and putative E3 ubiquitin ligases mediating polyubiquitin attachment at distinct lysine residues of BCL10. Conversely, defective NF-κB signaling is not caused by loss of BCL10 polyubiquitination as previously suggested (Wu & Ashwell, 2008; Yang et al., 2016), but rather is a consequence due to disrupted CBM assembly.

In addition to promoting TCR-induced NF-κB activation, BCL10 ubiquitination was reported to terminate prolonged signaling by inducing BCL10 degradation and subsequent CBM complex disassembly (Hu et al., 2006a; Hu et al., 2006b; Paul et al., 2012; Scharschmidt et al., 2004). Both, lysosomal (Paul et al., 2012; Scharschmidt et al., 2004) and proteasomal BCL10 degradation (Lobry et al., 2007) have been suggested, but efficient removal of the higher-order BCL10 filaments can most likely only be achieved by selective autophagy and delivery to lysosomal vesicles (Gehring et al., 2018). TRAF6/LUBAC-dependent BCL10 poly-ubiquitination may act as negative regulatory feedback mechanism which facilitates the termination of T cell activation post-induction by blocking further oligomerization of BCL10 filaments and thus CBM complex extension. However, it is unclear if a BCL10 CARD interface at the distal end of BCL10 filaments is accessible for E3 ubiquitin ligases to catalyze ubiquitination. Since our data suggest that polyubiquitinated BCL10 is not part of the assembled CBM complex, it may also be possible that free BCL10-MALT1 heterodimers are ubiquitinated upon prolonged TCR signaling which therefore cannot be used for the extension and maintenance of BCL10 filaments.

We further suggest that restriction of CBM complex formation via LUBAC- and TRAF6-mediated BCL10 polyubiquitination occurs in the absence of an antigenic stimulus. By inhibiting low-level CBM complex assembly in resting T cells, BCL10 polyubiquitination may counteract chronic MALT1 paracaspase activity and thus spontaneous T cell activation. Our biochemical studies revealed that the same requirements apply for TCR-induced BCL10 polyubiquitination and TRAF6-mediated restriction of MALT1 paracaspase activity. MALT1-TRAF6 binding via T6BMs, TRAF6 E3 ligase activity and self-oligomerization are essential for both processes (O'Neill et al., 2021). We provide strong evidence that in addition to TRAF6, a functional LUBAC is critical for regulating MALT1 proteolytic activity under steady-state conditions. Unstimulated Jurkat T cells display constitutive MALT1 substrate cleavage in the absence of TRAF6, as well as upon loss of LUBAC subunits HOIL-1 and HOIP. Since substrate cleavage was less pronounced in HOIP and HOIL-1 KO Jurkat T cells, we suggest, that TRAF6 acts as decisive factor and LUBAC as critical amplifier for BCL10 polyubiquitination. LUBAC may attach linear ubiquitin chains either directly to TRAF6-catalyzed K63-ubiquitin chains leading to heterotypic chains or at a different acceptor site resulting in distinct homotypic chains. Further, heterotypic ubiquitin chains could be either branched (as shown in our suggested model in Figure 5-3) or mixed, consisting of alternating K63- and M1 ubiquitin linkages. Unfortunately, we were not able to determine the type of BCL10 ubiquitin chains in this study. However, formation of branched or mixed K63/M1 ubiquitin chains at BCL10 could be especially beneficial because they could be more resistant to deubiquitination. It was previously shown that the K63-chain specific DUB A20 has reduced activity for K63/M1 hybrids, compared with homotypic K63 chains (Wang et al., 2020; Wertz

et al., 2015). Thus, generation of heterotypic BCL10 ubiquitin chains may further strengthen the negative regulatory effect. We can only hypothesize that the same linkage specificities apply for P/I-induced and chronic BCL10 ubiquitin chains. Tonic MALT1 protease activation relies on the same molecular mechanisms as acute MALT1 activation, such as CARD11 and BCL10 binding, MALT1 mono-ubiquitination and MALT1 dimerization (O'Neill et al., 2021) lending strong support that low level TRAF6/LUBAC-mediated ubiquitination of BCL10 counteracts MALT1 activity. However, with the current methods we are unable to detect this low level of ubiquitin chains attached to BCL10 in the absence of a stimulus, which represents an experimental limitation to verify this hypothesis.

5.4 Relative MALT1A expression levels define the severity of defective MALT1B-TRAF6 interaction

Our MALT1 isoform expression analysis provided strong evidence that the fatal autoimmune phenotype of TBM2 mice with C57BL/6N background is most likely caused by the absence of functional MALT1A in immune cells. C57BL/6N mice also fail to upregulate *Malt1A* mRNA levels upon TCR engagement, whereas CD4+ T cells from BALB/c mice show a roughly 25-fold induction of *Malt1A* expression in response to CD3 stimulation. Crossings of C57BL/6N *Malt1* TBM or TBM2 mice with BALB/c WT mice resulted in hybrid mice heterozygous for respective T6BM mutations. All analyzed offspring mice upregulated *Malt1A* expression upon T cell stimulation, indicating that inclusion of *Malt1* exon7 is regulated by presumably one or more dominant factor(s) present in BALB/c, CD-1 and 129S2/Sv mice but lacking in C57BL/6N. We speculate that presence of functional MALT1A may attenuate the severe autoimmune phenotype of *Malt1* TBM2 mice, and we are currently testing this hypothesis by further backcrossing *Malt1* TBM and TBM2 mice to the BALB/c background. By comparing BALB/c background mice with complete loss of MALT1-TRAF6 interaction (*Malt1*$^{TBM/TBM}$) or selective MALT1B-TRAF6 destruction (*Malt1*$^{TBM2/TBM2}$), it will be possible to directly analyze the effect of functional MALT1A on disease development and severity. Previously, it was shown that immunization of BALB/c mice with sheep erythrocytes results in *Malt1A* upregulation, specifically in activated effector cells but not in naïve CD4+ T cells (Meininger et al., 2016). We assume that spontaneous T cell activation caused by deregulated MALT1 protease activity may also increase *Malt1A* E814D expression. Presence of partially functional MALT1A E814D protein might then lead to a delayed and less severe phenotype of BALB/c TBM2 mice, whereas BALB/c TBM mice should still develop drastic immune inflammation with very early onset because in the TBM model MALT1A is also defective in TRAF6 binding and unable to compensate for deregulated MALT1B. With this approach, we attempt to generate a mouse model which may more closely reflect the human phenotype, allowing for better study of the development and progression of the immune disorder.

As a result of overshooting immune responses, the patient identified with the homozygous MALT1 T6BM2 mutation suffers from psoriasis, a chronic autoinflammatory skin disease (Kutukculer et al., 2021). Psoriasis is characterized by well-demarcated red, scaly plaques on the affected areas of the skin (Van Nuffel et al., 2017). The pathogenesis of psoriasis has not yet been completely elucidated, but it is generally believed to arise from pathological interplay between hyperproliferating keratinocytes and infiltrating effector cells from the innate and adaptive immune system (Lowes et al., 2014; Van Nuffel et al., 2017). In recent years, gain-of-function-mutations in CARD14, the CARD11 homologue expressed in keratinocytes, have been repeatedly linked to psoriasis susceptibility (Ammar et al., 2013; Ammar et al., 2016; Jordan et al., 2012a; Jordan et al., 2012b). Expression of psoriasis-associated CARD14 variants leads to constitutive assembly of the CARD14-BCL10-MALT1 signaling complex and activation of MALT1 paracaspase activity (Howes et al., 2016; Kurgyis et al., 2021; Mellett et al., 2018). In striking contrast to C57BL/6N lymphocytes, primary C57BL/6N keratinocytes express notable amounts of the longer MALT1A isoform. Thus, keratinocytes isolated from *Malt1* TBM and TBM2 mice can be used to study the effect of functional MALT1A on chronic MALT1B E803D proteolytic activity. We demonstrated that expression of MALT1A prevents chronic MALT1B E803 protease activity in keratinocytes of TBM2 mice. Consistent with a previous study, we show that MALT1A is the major isoform expressed in human keratinocytes (Israël et al., 2018). Since functional MALT1A is able to neutralize constitutive substrate cleavage by MALT1B E803D in a dominant-negative manner (O'Neill et al., 2021), we propose that MALT1 protease activity is not deregulated in keratinocytes of the patient and that chronic MALT1 paracaspase function is not the primary cause of psoriasis. In line with this, conditional T cell-specific expression of MALT1 T6BMs mutations (*Malt1* TBM-T) leads to the development of skin eczema and epidermal inflammation (O'Neill et al., 2021). Thus, inflammatory skin lesions of the patient might be driven by skin-resident T cells rather than by a keratinocyte-intrinsic mechanism. In psoriasis, lymphocyte-derived cytokines such as IL-17, IL-22, or IFNγ can stimulate keratinocytes, which in turn amplify inflammation by recruiting more lymphocytes via chemokine synthesis. In addition, cytokines can directly induce keratinocyte activation, leading to keratinocyte hyperplasia (Lowes et al., 2014). Generation of a conditional mouse model with MALT1 T6BM1 and T6BM2 mutations expressed only in keratinocytes would be interesting to study the keratinocyte-intrinsic role of MALT1-TRAF6 interaction and chronic MALT1 protease activity in inflammatory skin disorders.

5.5 hnRNP U and hnRNP L regulate *MALT1* alternative splicing by antagonistic modulation of pre-mRNA structure

The complex immune disorder of the patient highlighted the importance of faithful control of MALT1 isoform expression and prompted us to investigate the regulation of alternative *MALT1* splicing. In

cooperation with Dr. Alisha Jones and Prof. Michael Sattler (Institute of Structural Biology, Helmholtz Zentrum München), we uncovered the mechanism of *MALT1* exon7 inclusion and exclusion, which is modulated via an interplay between RNA structure and the two counteracting RNA binding proteins (RBPs) hnRNP U and hnRNP L. Heterogeneous nuclear ribonucleoproteins (hnRNPs) are often involved in splicing regulation of early stages of spliceosome assembly by binding to cis-regulatory elements within exons and introns of pre-mRNA transcripts (Busch & Hertel, 2012). As demonstrated here for alternative *MALT1* splicing, hnRNP U and hnRNP L exert antagonistic effects on inclusion and exclusion of exon7, with hnRNP U suppressing and hnRNP L enhancing exon7 inclusion and MALT1A upregulation. Both RBPs directly interact with regulatory sequences within and in close proximity to exon7. SHAPE (selective 2'-hydroxyl acylation analyzed by primer extension) chemical probing on a *MALT1* minigene revealed that exon7 and essential pre-mRNA sequences, including the poly-pyrimidine tract (Py-tract) of the 3' splice site and the 5' splice site, are sequestered in stem-loop (SL) structures. These structural elements consist of several complementary GU- and CA-containing RNA sequences, which have been suggested as binding sites for hnRNP U and hnRNP L, respectively (Hui et al., 2005; Smith et al., 2013). Via structural and functional analyzes of two *MALT1* minigene variants, we demonstrate that the SL structures are critical for regulation of exon7 splicing because they shield the 3´ and 5´ splice sites from hnRNP U and hnRNP L binding. Our data show that hnRNP U mediates its repressive effect on *MALT1* exon7 splicing via its RGG domain by preserving double-stranded SL structures (Jones et al., 2022). It has been previously reported that hnRNP U binds to other structured RNAs, such as the lncRNA *Xist* (Chu et al., 2015; Hasegawa et al., 2010), and our data suggest that the RGG domain of hnRNP U generally stabilizes less rigid RNA structures, which are highly dynamic and switch between structured and unstructured conformations. Single-stranded conformations of *MALT1* pre-mRNA can be recognized and bound by hnRNP L via its tandem RNA recognition motif (RRM) domains. Binding of hnRNP L to SL5, which contains the 5´ splice site of exon7, destabilizes the SL structure rendering the 5´ splice site accessible for the spliceosome apparatus. All four RRMs of hnRNP L are required to promote *MALT1* exon7 inclusion, suggesting that every RRM domain binds one CA motifs within *MALT1* pre-mRNA and brings these regions in spatial proximity. Overall, the antagonistic functions of hnRNP U and hnRNP L are based on their distinct binding preferences to structured and single-stranded mRNA regions, respectively. Our data suggest that *MALT1* pre-mRNA exists in a constantly shifting equilibrium of double- and single-stranded conformations. It is possible that during the shift a ternary complex is formed consisting of hnRNP U, hnRNP L and *MALT1* mRNA. However, since we were not able to detect such ternary complexes in our *in vitro* experiments, they may be rather transient due to strong competition between hnRNP U and L for binding to *MALT1* mRNA.

hnRNP L binding to single-stranded *MALT1* pre-mRNA induces exon7 inclusion and MALT1A upregulation, posing the question how hnRNP L initiates the splicing process. In the early phase of spliceosome assembly, U1 snRNP binds to the 5´ splice site, whereas U2AF2 recognizes the Py-tract in the 3´splice site of pre-mRNA introns (Wahl et al., 2009). Since these essential cis-acting sequence elements are sequestered in double stranded SL structures of *MALT1* pre-mRNA, the RRM1,2 tandem domains of U2AF2 are not able to bind full length *MALT1* pre-mRNA or the structured SL4 RNA at reasonable protein concentrations (Jones et al., 2022). However, the presence of hnRNP L leads to a partial unwinding of SL4 RNA and induces U2AF2 binding to the Py-tract, whereas U2AF2 is unable to destabilize the SL4 structure on its own (Jones et al., 2022). Thus, by binding to CA-rich regions within exon7 of the *MALT1* pre-mRNA, hnRNP L destabilizes SL4 which induces the recruitment of U2AF2 and initiates spliceosome assembly.

We propose the following model for alternative *MALT1* exon7 splicing upon T cell activation (Figure 5-4). In resting T cells, intronic sequences flanking *MALT1* exon7 are sequestered in stem-loop RNA structures. Essential splice signals, including the Py-tract of the 3´splice site and the 5´splice site, are base-paired and inaccessible for U1 snRNP and U2AF2, which are required for early spliceosome assembly at the 5´ and 3´ splice sites. hnRNP U binding stabilizes the RNA stem-loop conformations and retains splice signals inaccessible in the secondary structure, resulting in exon7 exclusion and predominant expression of the shorter isoform MALT1B. Upon T cell activation, hnRNP U is replaced by hnRNP L, which destabilizes the structured RNA elements and facilitates recruitment of spliceosome factors. U1 snRNP and U2AF2 can bind to splice sites and induce exon7 inclusion, resulting in the upregulation of MALT1A expression. Thus, alternative exon7 splicing is regulated through the antagonistic modulation of *MALT1* pre-mRNA structure by binding of the two counteracting RBPs hnRNP U and hnRNP L.

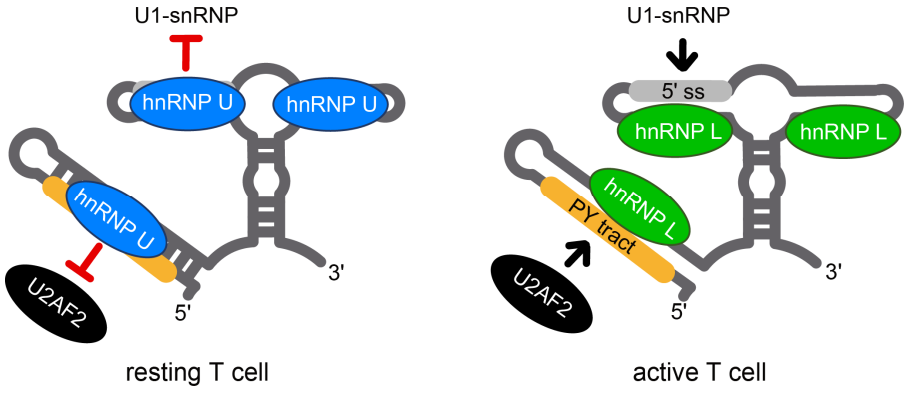

Figure 5-4: Proposed mechanism of hnRNP U- and hnRNP L-mediated splicing regulation of *MALT1* exon7 in T cells.
In resting T cells, exon7 inclusion, and thus MALT1A expression, is repressed by hnRNP U binding which stabilizes *MALT1* mRNA secondary structures, sequestering essential binding sites for U1 snRNP and U2AF2 splicing factors. Upon T cell activation, binding of hnRNP L destabilizes *MALT1* mRNA and facilitates recruitment of spliceosome factors, leading to exon7 inclusion and MALT1A upregulation. Figure from Jones et al., 2022.

So far, it is not known how TCR signaling and subsequent T cell activation communicate with the splicing machinery to induce MALT1A expression. It was shown that TCR stimulation not only upregulates both hnRNP U and hnRNP L at the RNA level, but also other splice factors which may additionally fine-tune alternative *MALT1* splicing (Meininger et al., 2016). Further, we do not know why there are differences in MALT1 isoform expression between human and mouse and even between different mouse strains. Both MALT1 splicing isoforms are highly conserved in mammals, pointing towards a functional relevance of preserving the expression of both variants (Meininger et al., 2016). Functional destruction of the shorter MALT1B isoform in *Malt1* TBM2 mice is sufficient to disrupt immune homeostasis and cause a fatal autoimmune phenotype, suggesting that MALT1B is the dominant isoform. Our lab also generated mouse lines which exclusively express either MALT1A (*Malt1* IsoA mice) or MALT1B (*Malt1* IsoB mice) (Andreas Gewies, unpublished data). Since MALT1A mediates stronger TRAF6 binding and downstream NF-κB signaling (Meininger et al., 2016), we would have expected that exclusive presence of MALT1A in IsoA mice may lead to enhanced immune cell activation in the steady state or even autoimmunity. However, IsoA mice are healthy and display no severe alterations in immune cell numbers, except for a slight reduction in peripheral Treg cells (Andreas Gewies, unpublished data). *Malt1* IsoB mice exclusively contain the shorter MALT1B splicing variant and in principle resemble C57BL/6N WT mice according to our expression analysis. In line, immune cell numbers are normal and IsoB mice are healthy up to one year of age (Andreas Gewies, unpublished data). Thus, data from MALT1 isoform-specific mouse models rather indicate that there is no distinct physiological role of each individual splicing variant in immune cell regulation, at least under the controlled housing conditions of the mouse facility. It cannot be excluded that there may be an impact of *Malt1* isoform expression during immune responses to specific microbes or during distinct disease conditions. For instance, it is known that immune responses in C57BL/6 mice are mainly mediated by Th1 effector cells, whereas BALB/c mice are more prone towards Th2 immune responses (Gorham et al., 1996; Yagi et al., 2006). We could show that C57BL/6N mice fail to enhance MALT1A expression upon TCR stimulation, but it is possible that MALT1A upregulation is specific to the type and strength of the immune response.

5.6 Conclusion and outlook

With this study, we provide both functional and mechanistic insights into MALT1-dependent regulation of immune homeostasis. It was previously known that MALT1 scaffolding function and its interaction with TRAF6 via distinct T6BMs is required for T cell activation and maintenance of immune homeostasis. *MALT1* is expressed in two distinct splicing isoforms, but so far it has not been adressed how critical both MALT1 variants are for immune regulation. In order to study a human immune disorder caused by a *MALT1* mutation that completely disrupts the TRAF6-MALT1B

interaction, we generated the *Malt1* TBM2 mouse line. In line with the drastic, early onset inflammatory disease in *Malt1* TBM2 mice, we provide evidence that MALT1B is the dominant isoform which dictates T cell activation and immune homeostasis in C57BL/6N mice. Selective disruption of MALT1B-TRAF6 binding is sufficient to induce chronic MALT1 protease activation and concommitant autoimmunity in the human patient and *Malt1* TBM2 mice. We found evidence that chronic MALT1 protease activation may deregulate immune homeostasis via partial inactivation of post-transcriptional regulators critical for T cell activation. Of note, loss of MALT1B-TRAF6 binding simultaneously impairs TCR-mediated NF-κB signaling, leading to the development of immune deficiency symptomes in the patient. Thus, the MALT1B-TRAF6 protein interaction is essential for a balanced immune activation and peripheral tolerance in both human and mouse. We show that the more drastic phenotype of *Malt1* TBM2 mice is caused by exclusive expression of defective MALT1B E803D, whereas expression of MALT1A E806D, with residual TRAF6 binding capacity, may be responsible for the milder immune pathology in the human patient. The *Malt1* TBM2 mouse model helped to describe the complex symptoms of the human patient but was not suitable for studying the progression of the disorder due to the early onset of disease. Therefore, we are currently backcrossing the TBM2 mutation into the BALB/c genetic background in order to study TBM2-mediated immune dysregulation in a murine system in which MALT1A isoform expression is induced comparable to the human situation. We expect that the TBM2 BALB/c mouse will be a more appropriate disease model to study the development of the humane disease in more detail. We hypothesize that MALT1A E814D expression might ameliorate or delay the TBM2-mediated immune pathology.

So far, we mainly studied the role of MALT1-TRAF6 binding in T cells, but the protein interaction might be also ciritical for other immune cells, including B cells, dendritic cells and macrophages. Since MALT1 and TRAF6 are ubiquitously expressed proteins, analysing the physiological role of their association in non immune cells such as keratinocytes might be interesting as well. For instance, it is known that MALT1 protease function is activated upon NF-κB signaling in keratinocytes and deregulated MALT1 protease activity may be involved in the development of inflammatory skin disorders. Therefore, additional Cre-recombinase-dependent mouse models will be needed to study cell-type intrinsic roles of MALT1 scaffolding function.

In addition to the functional characterization of MALT1B-TRAF6 interaction in immune regulation, we analyzed the molecular mechanisms involved in how TRAF6 restricts MALT1 protease activity in the absence of a strong antigenic stimulus. We were able to show that TRAF6- and LUBAC-mediated polyubiquitination of BCL10 counteracts low-level cell autonomous TCR signaling by inhibiting

spontaneous CBM complex formation and thus MALT1 protease activation. Based on structural and biochemical data, we provide strong evidence that attachment of K63- and M1-linked ubiquitin chains to BCL10 lysine residues K17, K31 and K63 disrupts BCL10 oligomerisation and BCL10-MALT1 association. Therefore, TRAF6 is the dominant negative regulatory factor that initates BCL10 polyubiquitination and LUBAC functions as critical amplifer that extents K63 chains via the attachment of linear chains. The proposed upiquitin-dependent mechanism might also facilitate the termination of prolonged TCR-induced NF-κB signaling by inhibiting further BCL10 oligomerization and CBM complex elongation. Thus, this work uncovers a new ubiquitin-mediated process that either raises the threshold for T cell signaling or helps to terminate T cell activation post-induction. In future work, it will be important to better charaterize the exact lysine acceptor sites on BCL10 and the specific linkage-types of heterotypic BCL10 polyubiquitin chains. Ubiquitin acceptor sites can be mapped via trypsin-digestion of the ubiquitinated target protein and subsequent mass spectrometry (MS) analysis of diglycine (diGly)-containing isopeptides (Kim et al., 2011; Wagner et al., 2011). In order to determine branched points of polyubiquitin chains, a combination of *in vitro* limited proteolysis and mass spectrometry can be used (Crowe et al., 2017; Valkevich et al., 2014). Alternatively, dual-color pulse-chase ubiquitination assays allow to trace ubiquitin chain priming and extension via labeling ubiquitin with fluorescence probes (Scott & Schulman, 2019).

Finally, we characterized the underlying mechanism of alternative *MALT1* splicing regulation. *MALT1* splicing depends on RNA secondary stem-loop elements sequestering the essential splice sites of the alternatively spliced exon7, and competitive binding of the RBPs hnRNP U and hnRNP L, which modulate these structural elements. While hnRNP U binding stabilizes RNA stem-loop conformations that maintain exon7 skipping, hnRNP L disrupts these secondary structures and facilitates the recruitment of the critical splicing factor U2AF2. Thus, hnRNP L induces exon7 inclusion and MALT1A upregulation leading to optimal T cell activation. Our data provide an intriguing new model for the control of splice site selection by differential RBP binding and modulation of pre-mRNA structure. In future work it will important to unravel the link between TCR signaling and induction of alternative *MALT1* splicing and to identify the potential monogenetic factor which allows for MALT1A upregulation in BALB/c, but seems to be missing in C57BL/6N mice. By unterstanding these mechanisms, we may be able to regulate immune responses or restore immune homeostasis in cases like the human TBM2 patient by manipulating *MALT1* splicing.

6 Materials

6.1 Instruments and equipment

Instrument/equipment	Source
Agarose gel chambers	NeoLab, Heidelberg
Autoclave – VX-95	Systec, Linden
Bacterial culture flasks/tubes	Schott, Zwiesel; BD, Heidelberg
BD FACS Aria III	BD, Heidelberg
Cell culture flasks/plates	BD, Heidelberg; Nunc, Wiesbaden
Cell scraper	Sarstedt, Newton, USA
Cell strainer (100 µm)	NeoLab, Heidelberg
Cell viability analyzer - ViCell-XR	Beckman Coulter, Krefeld
Centrifuge Beckman Avanti J-26 XP	Beckman Coulter, Krefeld
Centrifuges - 5810R, 5417R, 5471C, 5804	Eppendorf, Hamburg
Chemiluminescence ECL films	GE Healthcare, Freiburg
CO_2 incubators	Binder, Tuttlingen
Cryo tubes	Greiner Bio-One, Frickenhausen
Developer - Optimax	Protec, Oberstenfeld
Electroporation cuvettes - Gene Pulser	Bio-Rad, München
Electroporator - Gene Pulser Xcell System	Bio-Rad, München
Eppendorf tubes	Eppendorf, Hamburg
FACS Attune Acoustic Focusing Cytometer	Thermo Fisher Scientific, Waltham, USA
FACSCanto II flow cytometer	BD, Heidelberg
Flow cytometry tubes	BD, Heidelberg
Falcon tubes	BD, Heidelberg
Filter pipette tips- TipOne	StarLab, Hamburg
Freezers and Fridges	Liebherr, Ochsenhausen
Gel Documentation System - Intas Gel iX Imager	Intas, Göttingen
Heat blocks	Techne, Burlington, USA
Ice machine – Scotsman AF20	Scotsman Ice Systems, Vernon Hills, USA
Incubator shaker – I 26	New Brunswick Scientific, Hamburg
Incubators	Sartorius, Göttingen; Heraeus, Hanau
LightCycler480	Roche, Mannheim
LightCycler plates 96 well	4titude, Berlin
MACS columns	Miltenyi Biotec, Bergisch Gladbach
MACS magnetic rack	Miltenyi Biotec, Bergisch Gladbach
Magnetic stirrer	NeoLab, Heidelberg
Microfuge Tube Polyallomer	Beckman Coulter, Krefeld
Micro scales, scale	Kern & Sohn, Balingen
Microtiter plate (U- or V-shape), 96-well	Greiner Bio-One, Frickenhausen
Microscopes	Leica, Wetzlar
Microwave	SHARP, Hamburg
Mouse ear punch	Fine Science Tools, Heidelberg
Petri dishes	Greiner Bio-One, Frickenhausen
pH meter - inoLab pH7110	WTW, Weilheim
Pipette tips	Eppendorf, Hamburg
Pipettes - Reference	Eppendorf, Hamburg
Pipetting aid - accu-jet pro	Brand, Wertheim
Power supplies - EV202, EV243	Consort, Turnhout, Belgium

Precision scale – New Classic MS	Mettler Toledo, Gießen
Rotator – Intelli-Mixer	NeoLab, Heidelberg
SDS-PAGE gel chambers	Roth, Karlsruhe
Serological pipettes - Cellstar	Greiner Bio-One, Frickenhausen
Shaker - Polymax 1040	Heidolph Instruments, Schwabach
Spectral photometer – Biophotometer	Eppendorf, Hamburg
Syringes – 1 mL	Wagner & Munz, München
Thermocycler – Mastercycler gradient	Eppendorf, Hamburg
Thermomixer comfort	Eppendorf, Hamburg
Ultracentrifuge – Optima MAX	Beckman Coulter, Krefeld
Ultra-pure water system – Milli-Q Plus	Merck Millipore, Darmstadt
Ultrasonic Device – UP200S	Hielscher Ultrasonics GmbH, Teltow
UV-Vis Spectrophotometer – NanoDrop 2000	Thermo Fisher Scientific, Waltham, USA
Vortexer	Heidolph Instruments, Schwabach
Western blotting detection – Amersham Hyperfilm TM ECL	GE Healthcare, München
Western blotting transfer – PVDF-membrane, 0.45 µm	Merck Millipore, Darmstadt
Western blotting transfer - Semi-dry blotter	Peqlab, Erlangen
Western blotting transfer – Whatman paper	Roth, Karlsruhe

6.2 Chemicals

6.2.1 General Chemicals

Chemical	Source
Acrylamide/Bisacrylamide	Roth, Karlsruhe
Agarose	Biozym, Hessisch Oldendorf
Ampicillin	Roth, Karlsruhe
Atufect transfection reagent	Silence Therapeutics, Berlin
ß-Glycerophosphate	Sigma-Aldrich, Taufkirchen
Bovine serum albumin (BSA)	Sigma-Aldrich, Taufkirchen
Calcium chloride ($CaCl_2$)	Roth, Karlsruhe
cOmplete Tablets, Mini, EDTA-free	Roche, Mannheim
Dimethyl sulfoxide (DMSO)	Roth, Karlsruhe
Dispase II	Sigma-Aldrich, Taufkirchen
Dithiothreitol (DTT)	Sigma-Aldrich, Taufkirchen
DNA 1kb plus ladder	Thermo Fisher Scientific, Waltham, USA
dNTP-Mix	Thermo Fisher Scientific, Waltham, USA
DPBS (w/o $MgCl_2$ and $CaCl_2$)	Thermo Fisher Scientific, Waltham, USA
Ethanol (EtOH, p. a.)	Merck, Darmstadt
Ethidium bromide (EtBr)	Roth, Karlsruhe
Ethylenediaminetetraacetic acid (EDTA)	Roth, Karlsruhe
Gel Loading Dye, Purple (6x)	NEB, Frankfurt
Glycerol	Roth, Karlsruhe
Glycine	Roth, Karlsruhe
HEPES	Roth, Karlsruhe
Isopropyl alcohol (p.a.)	Merck, Darmstadt
Isopropyl _-D-1-thiogalactopyranoside (IPTG)	Thermo Fisher Scientific, Waltham, USA
LB-Agar (Luria/Miller)	Roth, Karlsruhe

LB-Medium (Luria/Miller)	Roth, Karlsruhe
Lipofectamine RNAiMAX	Thermo Fisher Scientific, Waltham, USA
Lymphoprep	Stemcell Technologies, Köln
Methanol (MeOH, p.a.)	Merck, Darmstadt
Milk powder	Roth, Karlsruhe
Nonidet P40 substitute (NP-40)	Sigma-Aldrich, Taufkirchen
PageRuler Prestained Protein Ladder	Thermo Fisher Scientific, Waltham, USA
Pierce High Capacity Streptavidin Agarose	Thermo Fisher Scientific, Waltham, USA
Polybrene	Sigma-Aldrich, Taufkirchen
Phorbol 12-myristate 13-acetate (PMA)	Merck, Darmstadt
Potassium chloride (KCl)	Roth, Karlsruhe
Protein G Sepharose (PGS) 4B	Thermo Fisher Scientific, Waltham, USA
Roti-Load 1 – 4x SDS sample buffer	Roth, Karlsruhe
Roti-Phenol/Chloroform/Isoamylalcohol	Roth, Karlsruhe
Saponin	Roth, Karlsruhe
S.O.C. Medium	Thermo Fisher Scientific, Waltham, USA
Sodium chloride (NaCl)	Roth, Karlsruhe
Sodium dodecyl sulfate (SDS)	Roth, Karlsruhe
SDS – Solution 20% pure	PanReac AppliChem, Darmstadt
Sodium fluoride	Sigma-Aldrich, Taufkirchen
Sodium hydrogen phosphate (Na2HPO4)	Roth, Karlsruhe
Sodium vanadate	Roth, Karlsruhe
Strep-Tactin Sepharose	IBA, Göttingen
TAE buffer (50x)	Omnilab, Bremen
Tetramethylethylenediamine (TEMED)	Roth, Karlsruhe
Tris(hydroxymethyl)-aminomethan (Tris)	Roth, Karlsruhe
TritonX-100	Roth, Karlsruhe
TRIzol reagent	Thermo Fisher Scientific, Waltham, USA
Trypan blue	Thermo Fisher Scientific, Waltham, USA
Tween-20	Roth, Karlsruhe
Western blotting detection (ECL substrate) 20x LumiGlo and 20x Peroxide	Cell Signaling Technology, Frankfurt
X-tremeGENE HP Transfection Reagent	Roche, Mannheim
β-Glycerophosphate	Sigma-Aldrich, Taufkirchen

6.2.2 Cell culture media and supplements

Medium/Supplement	Source
Attachment Factor Protein (1X)	Thermo Fisher Scientific, Waltham, USA
DMEM (Dulbecco's modified eagle medium)	Thermo Fisher Scientific, Waltham, USA
EpiLife CF Kit	Thermo Fisher Scientific, Waltham, USA
EpiLife Defined Growth Supplement	Thermo Fisher Scientific, Waltham, USA
Fetal calf serum (FCS)	Thermo Fisher Scientific, Waltham, USA
Keratinocyte (KC) Growth Medium 2 Kit	PromoCell, Heidelberg
ß-Mercaptoethanol	Roth, Karlsruhe
Opti-MEM reduced serum media	Thermo Fisher Scientific, Waltham, USA
Penicillin-Streptomycin (10,000 U/ml)	Thermo Fisher Scientific, Waltham, USA
RPMI (Roswell Park Memorial Institute) 1640	Thermo Fisher Scientific, Waltham, USA
TrypLE Express Enzyme (1X), no phenol red	Thermo Fisher Scientific, Waltham, USA

Trypsin (0.05%)/EDTA	Thermo Fisher Scientific, Waltham, USA

6.3 Stimulants

Stimulant	Source
Ionomycin	Merck, Darmstadt
Phorbol 12-myristate 13-acetate (PMA)	Merck, Darmstadt
Human recombinant TNF-α	Biomol, Hamburg

6.4 Buffers and Solutions

Buffer/solution	Composition
2x HBS (HEPES buffered saline)	50 mM HEPES (pH 7), 280 mM NaCl, 1.5 mM Na2HPO4
4x Stacking gel buffer	0.5 M Tris (pH 6.8)
5x Separation gel buffer	1.88 M Tris (pH 8.8)
Annealing buffer	10 mM Tris (pH 8), 50 mM NaCl, 1 mM EDTA
Blocking solution (WB)	5% (w/v) milk powder in PBS-T
Blotting buffer	25 mM Tris (pH 8.3), 192 mM Glycine, 20% (v/v) MeOH
Co-IP buffer	150 mM NaCl, 25 mM HEPES (pH 7.5), 0.2% (v/v) NP-40, 1 mM glycerol, 1 mM DTT, cOmplete protease inhibitors, 10 mM NaF, 8 mM β-glycerophosphate, 300 µM sodium vanadate
DUB reaction buffer (10x)	500 mM NaCl, 25 mM Tris (pH 7.5), 10 mM DTT
DUB dilution buffer	150 mM NaCl, 25 mM Tris (pH 7.5), 10 mM DTT
FACS buffer	3% (v/v) FCS in PBS
LB agar	40 g/l
LB medium	25 g/l
PBS (phosphate buffered saline)	137 mM NaCl, 2.7 mM KCl, 10 mM Na2HPO4, 1.7 mM KH2PO4
PBS-T	0.1% (v/v) Tween-20 in PBS
RIPA buffer	250 mM NaCl, 1% (v/v) Triton-X, 0.5% (w/v) sodium deoxycholate, 0.1% (w/v) SDS, 10 mM Tris (pH 7.4), 1 mM DTT, cOmplete protease inhibitors, 10 mM NaF, 8 mM _-glycerophosphate, 300 µM sodium vanadate
SDS Electrophoresis buffer (1x)	25 mM Tris (pH 8.8), 192 mM Glycine, 0.1% (w/v) SDS
Separation gel	375 mM Tris (pH 8.8), 7.5-15% (v/v) Acrylamide, 0.1% (w/v) SDS, 0.1% (w/v) APS, 0.1% (v/v) TEMED
Stacking gel	125 mM Tris (pH 6.8), 3% (v/v) Acrylamide, 0.1% (w/v) SDS, 0.1% (w/v) APS, 0.1% (v/v) TEMED

Stripping buffer	0.2 M glycine, 0.1% (w/v) SDS, 1% (v/v) Tween-20, pH 2.2
Saponin buffer	0.5% saponin (w/v), 1% BSA (w/v), PBS
PBMC buffer 1	0.1% BSA (w/v), 2mN EDTA (pH 7.4), PBS

6.5 Mouse Strains

Strain	Description	Source
BALB/c	BALB/c	Charles River Laboratories, Sulzbach, Germany
C57BL/6N	C57BL/6N	Charles River Laboratories, Sulzbach, Germany
Malt1 TBM	Generated and descripted in O´Neill et al., 2021	Laboratory of Daniel Krappmann in collaboration with Ronald Naumann (Transgenic Core, MPI-CBG Dresden)
Malt1 TBM2	C57BL/6N zygotes electroporated with Cas9 protein, CRISPR guide, and HDR template by Florian Giesert, HMGU	Laboratory of Daniel Krappmann in collaboration with Florian Giesert and Wolfgang Wurst (IDG, Helmholtz München)
Malt1 IsoA	Deletion of *Malt*1 intron6 via CRISPR/Cas9-mediated homologous recombination in murine R1/E ES cells and subsequent injection of a validated ES cell clone into early mouse embryos for the generation of chimeric mice and germline transmission	Laboratory of Daniel Krappmann in collaboration with Ronald Naumann (Transgenic Core, MPI-CBG Dresden)
Malt1 IsoB	Deletion of *Malt1* exon7 by direct CRISPR/Cas9 injection into C57BL/6N zygotes	Laboratory of Daniel Krappmann in collaboration with Florian Giesert and Wolfgang Wurst (IDG, Helmholtz München)
C57BL/6 *Malt1* KO	MALT1t$^{m1a(EUCOMM)Hmgu}$, ES cell clone HEPD0671_C08)	Laboratory of Daniel Krappmann
CD-1 IGS	Crl:CD1(ICR) (022)	Charles River Laboratories, Sulzbach, Germany
129S2/SvPasCr	129S2/SvPasCr (287)	Charles River Laboratories, Sulzbach, Germany

6.6 Eukaryotic cell lines

Cell line	Information	Source
HEK293 cells	human embryonic kidney cell line containing Adenovirus 5 DNA	DSMZ RRID: CVCL_0045

HEK293T cells	HEK293 cells containing SV40 large T-antigen	Laboratory of Michelle Vincendeau (Helmholtz Zentrum München)
HeLa	Human epithelial cell line, derived from cervical carcinoma	Laboratory of Michelle Vincendeau (Helmholtz Zentrum München)
U2OS	human osteosarcoma cell line	Laboratory of Kamyar Hadian (Helmholtz Zentrum München)
Jurkat T cells	human T cell line, derived from acute T cell leukemia patient	Laboratory of Lienhard Schmitz (University of Giessen)
BCL10$^{-/-}$ Jurkat T cells	human T cell line, exon1 was deleted by CRISPR/Cas9 (generated by Simon Widmann)	Laboratory of Daniel Krappmann
CARD11$^{-/-}$ Jurkat T cells	human T cell line, exon3 was deleted by CRISPR/Cas9 (generated by Simone Woods)	Laboratory of Daniel Krappmann
HOIL-1$^{-/-}$ Jurkat T cells	human T cell line, exon1 was deleted by CRISPR/Cas9 (generated by Hongli Yin)	Laboratory of Daniel Krappmann
HOIP$^{-/-}$ Jurkat T cells	Human T cell line, exon1 was targeted by CRISPR/Cas9 (generated by Aurelia Stangl)	Laboratory of Daniel Krappmann
MALT1$^{-/-}$ Jurkat T cells	human T cell line, exon2 was deleted by CRISPR/Cas9 (generated by Torben Gehring)	Laboratory of Daniel Krappmann
TRAF6$^{-/-}$ Jurkat T cells	human T cell line, exon1 and 2 were targeted by CRISPR/Cas9 (generated by Thomas Seeholzer)	Laboratory of Daniel Krappmann

6.7 *Escherichia coli* (*E. coli*) strains

Strain [Source]	Information
One Shot TOP10 Chemically Competent *E. coli*	F$^-$ *mcr*A *Δ*(*mrr-hsd*RMS-*mcr*BC) Φ80*lac*ZΔM15 Δ*lac*X74 *rec*A1 *ara*D139 Δ(*ara-leu*)*7697 gal*U *gal*K *rps*L(Str^R) *end*A1 *nup*G
One Shot Stbl3 Chemically Competent *E. coli*	F$^-$ mcrB mrr hsdS20 (r_B^-, m_B^-) recA13 supE44 ara-14 galK2 lacY1 proA2 rpsL20 (Str^R) xyl-5 λ$^-$ leu mtl-1

6.8 Kits

Kit	Source
CD4 T cell isolation kit (mouse)	Miltenyi Biotec, Bergisch Gladbach
eFluor 780 Live/Dead stain	Thermo Fisher Scientific, Waltham, USA
Fixation/Permeabilization Kit	Thermo Fisher Scientific, Waltham, USA
InviTrap Spin Universal RNA Mini Kit	Stratec, Birkenfeld

LightCycler 480 SYBR Green I Mastermix	Roche, Mannheim
Mouse anti-dsDNA Ig's (Total A+G+M) Elisa kit	Alpha Diagnostic International, San Antonio, USA
Mouse enhanced sensitivity master buffer for flex set	BD, Heidelberg
Mouse IFNγ enhanced sensitivity flex set CBA kit	BD, Heidelberg
Mouse TNFα enhanced sensitivity flex set CBA kit	BD, Heidelberg
NucleoSpin Gel and PCR Clean-up Kit	Macherey-Nagel, Düren
NucleoSpin Plasmid Mini Kit	Macherey-Nagel, Düren
Perm/Fix buffer	Thermo Fisher Scientific, Waltham, USA
Plasmid Maxi Kit	Qiagen, Hilden
Phire Tissue Direct PCR Master Mix	Thermo Fisher Scientific, Waltham, USA
Red blood cell (RBC) lysis buffer (10x)	Miltenyi Biotec, Bergisch Gladbach
RNeasy Mini Kit	Qiagen, Hilden
Verso cDNA-Synthese-Kit	Thermo Fisher Scientific, Waltham, USA

6.9 Enzymes

Name	Source
Herculase II DNA Polymerase	Agilent Technologies, Waldbronn
Rapid DNA Ligation Kit	Roche, Mannheim
T4 DNA Ligase	NEB, Frankfurt
Restriction enzymes and buffers	NEB, Frankfurt
Taq DNA Polymerase	NEB, Frankfurt

6.10 Recombinant proteins

Recombinant protein	Source	Identifier
rhGST-AMSH-LP	R&D Systems, Minneapolis, MN, USA	Cat#E-551-050
rhFAM105B/OTULIN	R&D Systems, Minneapolis, MN, USA	Cat#E-558-050
rhUb4 WT Chains (K63-linked)	R&D Systems, Minneapolis, MN, USA	Cat#UC-310B-025
rhLinear Ub4 WT (M1-linked)	R&D Systems, Minneapolis, MN, USA	Cat#UC-710B-025

6.11 Plasmids and Oligonucleotides

6.11.1 Plasmids

Vector	Information
pEF Flag	Modified pEF4 backbone (Scharschmidt et al., 2004); 3xFlag-tag
pEF Flag-BCL10 WT	N-terminal 3xFlag-tag, BamHI/NotI (Schlauderer et al., 2018)
pEF Flag-BCL10 K17R	BCL10 with point mutation K17R; N-terminal 3xFlag-tag, BamHI/NotI

pEF Flag-BCL10 K31R/K63R	BCL10 with two point mutations K31R and K63R; N-terminal 3xFlag-tag, BamHI/NotI
pEF Flag-BCL10 K17R/K31R/K63R	BCL10 with three point mutations K17R, K31R and K63R; N-terminal 3xFlag-tag, BamHI/NotI
pEF Flag-BCL10 R42E	BCL10 with point mutation R42E; N-terminal 3xFlag-tag, BamHI/NotI (Schlauderer et al., 2018)
pEF Flag-BCL10 L104R	BCL10 with point mutation L104R; N-terminal 3xFlag-tag, BamHI/NotI (Schlauderer et al., 2018)
pEF HA	Modified pEF4 backbone; HA-tag
pEF HA-BCL10 WT	N-terminal HA-tag, BamHI/NotI (Schlauderer et al., 2018)
pEF HA-MALT1 WT	N-terminal HA-tag, BamHI/NotI (Schlauderer et al., 2018)
pEF FLAG-hnRNP L	N-terminal 3xFlag-tag, BamHI/NotI (cloned by Isabel Meininger)
pEF FLAG-hnRNP L RRM1/2	hnRNP L cDNA 1-295; N-terminal 3xFlag-tag, BamHI/NotI
pEF FLAG-hnRNP L RRM3/4	hnRNP L cDNA 380-589; N-terminal 3xFlag-tag, BamHI/NotI
pEF FLAG-hnRNP U	N-terminal 3xFlag-tag, BamHI/NotI (cloned by Isabel Meininger)
pEF FLAG-hnRNP U RGG/G-rich	hnRNP U cDNA 678-825; N-terminal 3xFlag-tag, BamHI/NotI (cloned by Isabel Meininger)
pEF FLAG-hnRNP U ΔRGG/G-rich	hnRNP U cDNA 1-678; N-terminal 3xFlag-tag, BamHI/NotI
pcAT7-CDMS2 (with spacer for sequences)	Minigene vector with constitutive exon3 and exon7 of the CD45 gene (Motta-Mena et al., 2010). Obtained from Prof. Dr. Florian Heyd.
Minigene pcAT7 M1	Minigene vector with genomic *MALT1* region (intron6 200 bp-exon7-intron7 197 bp) (Meininger et al., 2016)
Minigene pcAT7 M2	Minigene vector with genomic *MALT1* region (intron6 506 bp-exon7-intron7 539 bp) (Meininger et al., 2016)
Minigene pcAT7 M1 Variant 1	Minigene vector with genomic *MALT1* region (intron6 200 bp-exon9-intron7 197 bp); BglII/BglII
Minigene pcAT7 M1 Variant 2	Minigene vector with genomic *MALT1* region (intron6 200 bp-exon7-intron7 197 bp) with intron7 C25A/C26A mutation; BglII/BglII
pSpCas9(BB)-2A-GFP (px458)	Gift from Feng Zhang (Addgene#48138); For the generation of KO cell lines. Cas9 from *S. pyogenes* with 2A-EGFP, and cloning backbone for sgRNA
pX458_T6BM2_sgRNA	pX458 containing T6BM2 sgRNA (O´Neill et al., 2021)
pHAGE-hΔCD2-T2A-SSF	Lentiviral vector; truncated human CD2-T2A-2xStrep-tag II-Flag (C-terminal)

pHAGE-hΔCD2-T2A-BCL10 WT-FSS	C-terminal II-Flag-2xStrep tag, NotI/SalI (Schlauderer et al., 2018)
pHAGE-hΔCD2-T2A-BCL10 K17R-FSS	BCL10 with point mutation K17R; C-terminal II-Flag-2xStrep tag, NotI/SalI
pHAGE-hΔCD2-T2A-BCL10 K31R/K63R-FSS	BCL10 with two point mutations K31R and K63R; C-terminal II-Flag-2xStrep tag, NotI/SalI
pHAGE-hΔCD2-T2A-BCL10 K17R/K31R/K63R-FSS	BCL10 with three point mutations K17R C, K31R and K63R; C-terminal II-Flag-2xStrep tag, NotI/SalI
pHAGE-hΔCD2-T2A-BCL10 L104R-FSS	BCL10 with point mutation L104R; C-terminal II-Flag-2xStrep tag, NotI/SalI (Schlauderer et al., 2018)

6.11.2 Guide RNA and homology templates

Name	Sequence (5´-to-3´)
T6BM2 sgRNA	ATTTCATCAGTTGTCTCTAC (O'Neill et al., 2021)
T6BM2 ssODN HDR E/D	CCAGACAGGTGTCATTGCAGCCGGACTCCACACACATTCATTTCAAATTATCCCCCCCA CCACTACTGCCAGTTTGGTAGATCCAATGTGCCCGTGGACACGACCGACGAAATGCCATTCA GTTTTTCTGACAGGCTTATGATTTCTGAAAACTGACCTTCATGGTTTTGAAAATTAGAATAG TTACAGTAATCT

6.11.3 Genotyping primers

Name	Target	Sequence (5´-to-3´)
Malt1 TBM genotyping T6BM2	T6BM2 fwd general	ACGGATAAGAGTGGAGTGAT
	T6BM2 rev WT-specific	ATTTCATCAGTTGTCTCT
	T6BM2 rev Mut (E/A)-specific	ATTTCGTCGGTCGTCGCC
Malt1 TBM2 genotyping T6BM2	T6BM2 rev Mut (E/D)-specific	ATTTCGTCGGTCGTGTCC
Malt1 knockout genotyping	Malt1 flox del fwd	CTAGTCAGTCACCAGCTCAG
	Malt1 flox del rev	CTGGCTAACCAATCCTCAAAAC
	Malt1 flox rev	CAGTTCTCAATGCCAACGCAC
Malt1 IsoA genotyping	IsoA fwd general	TTAATGAATGATGATGATTTAAGGATG
	IsoA rev WT-specific	ACTCCAAAACCACATAACTCACA
	IsoA rev Mut-specific	CTCACTTGTTCTTCCTATGGT
Malt1 IsoB genotyping	IsoB fw	GTGAGTTATGTGGTTTTGGAGT
	IsoB rev	GACGACCTATTAGAGCTAGTATT

6.11.4 Sequencing primer

Name	Sequence (5´-to-3´)
T6BM2 fwd	GCATTTCCATTCCTCTCAG

6.11.5 Primer for qPCR and semi-qPCR

Name	Target	Sequence (5´-to-3´)
m*Malt1* IsoA qPCR	Malt1 ex5 fw	AAGTCCTATGCCTCACTACCAGTG
	Malt1 ex7/8 rev	GTTTAATTCATCTTCAGTGCACTCC
m*Malt1* IsoB qPCR	Malt1 ex5 fw	AAGTCCTATGCCTCACTACCAGTG
	Malt1 ex6/7 rev	GATGCCCCAAATTGTTTAATTCATCTATG
m*Hmbs qPCR*	Hmbs ex8/9 fw	GGAATTCAAGAGTATTCGGG
	Hmbs ex10 rev	CACAGCATACATGCATTCTTCTG
h*MALT1* IsoA qPCR	MALT1 ex6/6 fw	GAAGGTAGAAATCATCATAGGAAG
	MALT1 ex10 rev	GCTTTGAGCTTGGGGTGCTCC
h*MALT1* IsoB qPCR	MALT1 ex5	AAGCCCTATTCCTCACTACCAGTGG
	MALT1 ex6/8	GGATGACCAAGATTATTTAATTCATCTATG
h*RPII*	RPII fw	GCACCACGTCCAATGACAT
	RPII rev	GTGCGGCTGCTTCCATAA
Minigene	CD45 fw	GGGAGCTTGGTACCACGCGTCGACC
	CD45 rev	CAGCGCTTCCAGAAGGGCTCAGAGTGG
m+h*MALT1* IsoA+IsoB	MALT1 ex6 fw	ACCGAGACAGTCAAGATAGC
	MALT1 ex9/10 rev	GACTTTGTCCTTTGCCAAAGG
m+h*GAPDH*	GAPDH fw	ACCACAGTCCATGCCATCAC
	GAPDH rev	TCCACCACCCTGTTGCTGTA

6.11.6 siRNA

siRNA	Source
ON-TARGETplus Non-targeting pool (si-control)	Horizon Discovery, Cambridge, UK
ON-TARGETplus SMARTpool si-hnRNP U	Horizon Discovery, Cambridge, UK
ON-TARGETplus SMARTpool si-hnRNP L	Horizon Discovery, Cambridge, UK
ON-TARGETplus SMARTpool si-hnRNP LL	Horizon Discovery, Cambridge, UK

6.12 Antibodies

6.12.1 Cell stimulation antibodies

Name	Source
Mouse anti-human anti-CD3	BD Pharmigen, Frankfurt am Main
Mouse anti-human anti-CD28	BD Pharmigen, Frankfurt am Main
Rat anti-mouse IgG1	BD Pharmigen, Frankfurt am Main
Rat anti-mouse IgG2	BD Pharmigen, Frankfurt am Main
Hamster anti-mouse anti-CD3e	BD Pharmigen, Frankfurt am Main
Hamster anti-mouse anti-CD28	BD Pharmigen, Frankfurt am Main
Rabbit Anti-Syrian Hamster IgG (H+L)	Jackson ImmunoResearch, Cambridgeshire, UK

6.12.2 Flow Cytometry antibodies

Antibody	Dilution	Source	Identifier
Rat anti-mouse anti-CD16/32 [93]	1:200 up to 1:50	eBioscience, Frankfurt am Main	Cat#14-0161-85
Hamster anti-mouse anti-CD3-PECy7 [UCHT1]	1:300	eBioscience, Frankfurt am Main	Cat#25-0031-82

Rat anti-mouse anti-CD45R (B220)-PerCP-Cy5.5 [RA3-6B2]	1:200	Biolegend, San Diego, USA	Cat#103234
Rat anti-mouse anti-CD8a-FITC [53-6.7]	1:100	eBioscience, Frankfurt am Main	Cat#11-0081-85
Rat anti-mouse anti-CD8a-PE [53-6.7]	1:100	Biolegend, San Diego, USA	Cat#100707
Rat anti-mouse anti-CD4-PE [RM4-5]	1:300	eBioscience, Frankfurt am Main	Cat#12-0042-85
Rat anti-mouse anti-CD4-PerCP-Cy5.5 [RM4-5]	1:300	eBioscience, Frankfurt am Main	Cat#45-0042-82
Rat anti-mouse anti-CD44-PECy7 [IM7]	1:400	eBioscience, Frankfurt am Main	Cat#25-0441-82
Rat anti-mouse anti-CD44-FITC [IM7]	1:300	eBioscience, Frankfurt am Main	Cat#11-0441-81
Rat anti-mouse anti-CD62L-APC [MEL-14]	1:300	BD Pharmigen, Frankfurt am Main	Cat#553152
Rat anti-mouse anti-CD25-APC [PC61.5]	1:200	eBioscience, Frankfurt am Main	Cat#17-0251-82
Rat anti-mouse anti-CD86-FITC [GL-1]	1:100	eBioscience, Frankfurt am Main	Cat#11-0862-82
Hamster anti-mouse anti-CD69-APC [H1.2F3]	1:200	eBioscience, Frankfurt am Main	Cat#17-0691-8
Rat anti-mouse anti-Ox40-PECy7 [OX-86]	1:200	eBioscience, Frankfurt am Main	Cat#25-1341-80
Hamster anti-mouse anti-CD152 (CTLA-4)-PECy7 [UC10-4B9]	1:200	Biolegend, San Diego, USA	Cat#106313
Rat anti-mouse anti-CD19-APC [1D3]	1:200	Biomol, Hamburg	Cat#E-AB-F0986UE
Hamster anti-mouse anti-ICOS-FITC [C398.4A]	1:200	eBioscience, Frankfurt am Main	Cat#11-9949-82
Rat anti-mouse anti-IκBNS [4C1]	1:10	Core facility monoclonal antibodies HMGU, München	-
Rat anti-mouse anti-FoxP3-PE [FJK-16s]	1:100	eBioscience, Frankfurt am Main	Cat#12-5773-82
Hamster anti-mouse anti-CD279 (PD1)-FITC [J43]	1:300	eBioscience, Frankfurt am Main	Cat# 11-9985-85
Mouse anti-mouse/human anti-IκBα-PE [L35A5]	1:100	Cell Signaling Technology, Frankfurt	Cat#7523
Rat monoclonal anti-MALT1A [4A7]	1:10	Core facility monoclonal antibodies HMGU, München	-
Mouse anti-Rat IgG2c secondary FITC	1:100	Thermo Fisher Scientific, Waltham, USA	Cat#SA1-25270
Goat anti-rat IgG-AF647 [Poly4054]	1:200	Biolegend, San Diego, USA	Cat#405416
Mouse anti-human anti-CD2-APC [RPA-2.10]	1:400	Thermo Fisher Scientific, Waltham, USA	Cat#17-0029-41

6.12.3 Primary antibodies for Western blot and Co-IPs

Antibody	Dilution	Source	Identifier
Rabbit monoclonal anti-CARD11 [1D12]	1:1,000	Cell Signaling Technology, Frankfurt	Cat#4435
Mouse monoclonal anti-CYLD [E10]	1:1,000	Santa Cruz Biotechnology, Heidelberg	Cat#sc-74435
Mouse monoclonal anti-ubiquitin [P4D1]	1:1,000	Santa Cruz Biotechnology, Heidelberg	Cat#sc-8017
Rabbit monoclonal anti-M1-polyUb	1:1,000	Merck, Darmstadt	Cat#MABS19
Anti-linear ubiquitin [1E3]	1:1,000	Merck, Darmstadt	Cat# ZRB2114
Mouse monoclonal anti-IκBα [L35A5]	1:1,000	Cell Signaling Technology, Frankfurt	Cat#4814
Mouse monoclonal anti-phospho-IκBα (Ser32/36) [5A5]	1:1,000	Cell Signaling Technology, Frankfurt	Cat#9246
Mouse monoclonal anti-FLAG [M2]	1:10,000	Sigma-Aldrich, Taufkirchen	Cat#F3165
Mouse monoclonal anti-HOIP [# 875227]	1:5,000	R&D Systems, Minneapolis, USA	Cat#MAB8039
Rabbit polyclonal anti-SHARPIN	1:1,000	Proteintech, Manchester, UK	Cat#14626-1-AP
Rat monoclonal anti-HA [3F1]	1:10,000	Core facility monoclonal antibodies HMGU, München	-
Rat monoclonal anti-HA [12CA5]	1:1,000	Core facility monoclonal antibodies HMGU, München	-
Mouse monoclonal anti-HOIL-1 [H-1]	1:1,000	Santa Cruz Biotechnology, Heidelberg	Cat#sc-393754
Mouse monoclonal anti-Regnase-1/MCPIP1 [604421]	1:1,000	R&D Systems, Minneapolis, USA	Cat#MAB7875
Mouse monoclonal anti-ß-Actin [C-4]	1:4,000	Santa Cruz Biotechnology, Heidelberg	Cat#sc-47778
Mouse monoclonal anti-MALT1; mouse [D-1]	1:1,000	Santa Cruz Biotechnology, Heidelberg	Cat#sc-515389
Mouse monoclonal anti-human anti-MALT1; human [B-12]	1:1000	Santa Cruz Biotechnology, Heidelberg	Cat#sc-46677
Rat monoclonal anti-MALT1A [4A7]	1:10	Core facility monoclonal antibodies HMGU, München	-
Rabbit monoclonal anti-TRAF6 [EP591Y]	1:1,000	Abcam, Cambridge, UK	Cat#ab33915
Rabbit polyclonal anti-BCL10 [H-197]	1:1,000	Santa Cruz Biotechnology, Heidelberg	Cat#sc-5611
Rabbit monoclonal anti-BCL10 [EP606Y]	Co-IP 1ul	Abcam, Cambridge, UK	Cat#ab33905
Mouse monoclonal anti-hnRNP U [3G6]	1:1,000	Abcam, Cambridge, UK	Cat#ab10297
Mouse monoclonal anti-hnRNP L [4D11]	1:1,000	Abcam, Cambridge, UK	Cat#ab6106

Rabbit polyclonal anti-hnRNP LL	1:1,000	Cell Signaling Technology, Frankfurt	Cat#4783
Rat monoclonal anti-Roquin-1/2 [3F12-1-1-1]	1:10	Core facility monoclonal antibodies HMGU, München	-
Rabbit monoclonal anti-p65 [D14E12]	1:1,000	Cell Signaling Technology, Frankfurt	Cat#8242
Rabbit monoclonal anti-phospho-p65 (Ser536) [93H1]	1:1,000	Cell Signaling Technology, Frankfurt	Cat#3033
Rabbit polyclonal anti-ERK1/2	1:1,000	Calbiochem, San Diego, CA, USA	Cat# 442704
Rabbit polyclonal anti-phospho-ERK1/2 (Thr202/Tyr204)	1:1,000	Cell Signaling Technology, Frankfurt	Cat#9101
Rabbit polyclonal anti-JNK1/2	1:1,000	Cell Signaling Technology, Frankfurt	Cat#9252
Mouse monoclonal anti-phospho-JNK1/2 (Thr183/Tyr185) [G9]	1:1,000	Cell Signaling Technology, Frankfurt	Cat#9255
Rabbit monoclonal anti-N4BP-1; mouse [EPNCIR118]	1:1,000	Abcam, Cambridge, UK	Cat#ab133610
Rabbit polyclonal anti-N4BP-1; human	1:1,000	Cohesion Bioscience, London, UK	Cat# CPA2415

6.12.4 Secondary antibodies for Western blot

Antibody	Dilution	Source	Identifier
Donkey polyclonal anti-mouse IgG	1:5,000	Jackson ImmunoResearch, Cambridgeshire, UK	Cat#715-035-150
Donkey polyclonal anti-rabbit IgG	1:5,000	Jackson ImmunoResearch, Cambridgeshire, UK	Cat#711-035-152
Donkey polyclonal anti-rat IgG	1:5,000	Jackson ImmunoResearch, Cambridgeshire, UK	Cat#112-035-003
Maus anti-rat IgG2c	1:1,000	Core facility monoclonal antibodies HMGU, München	-

6.13 Software

Software	Source
Adobe Illustrator CS6 (version 16)	Adobe Systems, San José, USA
Adobe Photoshop CS2	Adobe Systems, San José, USA
CLC Main Workbench (version 7.0.3)	Qiagen, Hilden
Endnote X7.2	Clarivate Analytics, Philadelphia, USA
FlowJo (version 10)	FlowJo LLC, Ashland, USA
GraphPad Prism (version 8.0.2)	GraphPad, San Diego, USA
Microsoft Office 2010	Microsoft Corp., Redmond, USA

7 Methods

7.1 Mice

7.1.1 Generation of *Malt1* TBM2 mice

Design and generation of small guide RNA (sgRNA) for targeting *Malt1* T6BM2 was described previously (O'Neill et al., 2021). The short single stranded oligodeoxyribonucleotide (ssODNs) homology directed repair (HDR) template contains the patient-derived E-to-D point mutation in T6BM2, mutation of the PAM sequence to prevent multiple Cas9 cleavage, additional silent mutations and the artificial cleavage site for subsequent genotyping. sgRNA and HDR template sequences are listed in section 6.11.2. Active ribonucleoprotein complexes were delivered via electroporation. Briefly, guide RNA (200 ng/µl), HDR template (ssODN, 300 ng/µl), and Cas9 protein (200 ng/µl) were diluted in Opti-MEM buffer, incubated for 10 min at RT and 10 min at 37°C and electroporated into fertilized one-cell embryos. Zygotes were transferred into pseudopregnant CD-1 females and subsequent screening of F1 generation was performed via genomic sequencing. Heterozygous offspring mice were backcrossed and further intercrossed to obtain homozygous *Malt1*$^{TBM2/TBM2}$ mice.

7.1.2 Mouse genotyping PCR

For genotyping, the Phire Tissue Direct PCR Kit was used. Briefly, ear punches were incubated with 20 µl sample diluent and 0.5 µl DNA release reagent for 5 min at RT to extract DNA, followed by 2 min at 95°C to stop the reaction. Following protocol and cycler program were used for genotyping PCR:

Component	Amount
2x Phire direct PCR Master Mix	5 µl
forward primer (10 µM)	0.25 µl
reverse primer (10 µM)	0.25 µl
DNA	0.5 µl
water	4 µl
total	10 µl

Step	Temperature	Time	
Initial Melting	95 °C	180 sec	
Melting	95 °C	20 sec	32 cycles
Annealing	Tm primer	20 sec	
Extension	72	20 sec	
Final Extension	72	120 sec	

Amplified PCR products were analyzed on an Agarose gel (section 7.6.3). Genotyping primers are listed in section 6.11.3.

7.1.3 Blood analysis

Blood from the submandibular vein of mice was collected in eppis coated with 0.5 M EDTA (pH= 8.0) and containing 2 µl of 0.1 M EDTA. Blood and anticoagulant were gently mixed and additional 0.1 M EDTA was added to obtain a final concentration of 5 mM EDTA. For blood counts 30 µl EDTA whole blood was diluted with 180 µl Cellpack. The remaining blood was centrifuged (650 x g, 10 min, 4°C) and clear blood serum was transferred to a new eppi. For analysis of clinical parameters, 60 µl serum was added to 180 µl PBS. Blood analysis was performed at the Institute for Laboratory Medicine at the Klinikum Großhadern.

7.1.4 Analysis of cytokines and auto-antibodies

Cytokines and autoantibodies were measured from blood serum according to manufactures instructions. Blood was collected from the submandibular vein of mice and allowed to clot at RT. Blood was centrifuged at 14,000 x g for 10 min at 4 °C and clear blood serum was transferred and stored at -80 °C until measurement.

7.2 Cell culture methods

7.2.1 Storage of cell lines

For storage of suspension and adherent cell lines, $1x10^7$ cells were pelleted by centrifugation (350 x g, 5 min, RT) and resuspended in 1 ml freezing medium (RPMI/DMEM, 20% (v/v) FCS (fetal calf serum), 10% (v/v) DMSO ((dimethyl sulfoxide)). Cells were transferred to cryo vials and frozen in isopropanol-containing cryo-freezing containers at -80 °C overnight. For long-term storage, cell vials were kept into liquid nitrogen.

7.2.2 Cultivation of cell lines

Adherent cell lines (HEK293, HEK293T, HeLa, U2OS) were cultured in DMEM supplemented with 10 % FCS and 100 U/ml penicillin and 100 µg streptomycin until they reached 80% confluency. To split or seed cells, cell monolayer was washed with 1x PBS and detached with 0.5 – 2 ml 0.05% trypsin/EDTA solution. Trypsinization was stopped by adding fresh cell culture medium. Cells were diluted and seeded in appropriated cell culture flasks or dishes as needed.

Jurkat T cells were cultured in RPMI 1640 supplemented with 10 % FCS and 100 U/ml penicillin and 100 µg streptomycin at a density of 0.5 to $1.5x10^6$ cells/ml. All mammalian cell lines were maintained at 37°C in a humidified atmosphere at 5% CO2.

7.2.3 Isolation and cultivation of primary murine keratinocytes from neonatal skin

Isolation of keratinocytes was performed as described in (Au - Li et al., 2017). Pubs not older than 2 days of age were sacrificed by decapitation and bodies were rinsed in 80% ethanol. Limbs and tail were cut off and the skin was cut from the tail hole along the dorsal midline of the body to the opening of the neck. The whole skin was peeled off the body and over the leg stumps and rinsed in 15 ml sterile PBS (w/o Ca^{2+}) in a 10 cm dish. The skin was placed in a 2 ml eppi filled with ice cold dispase II digestion buffer (4 mg/ml dispase II in KC growth medium) and incubated overnight at 4°C, rotating. After 12 – 18 hours incubation, the skin was transferred into a fresh dish and washed once in PBS to remove dispase II. The skin was transferred to a new dish with the epidermal side down and the dermis side up by using two pairs of forceps. To separate dermis and epidermis, the dermis was slowly lifted up and away from the epidermis. The epidermis was transferred to a new dish, which contained 500 µl TrypLE Express enzyme, and floated on top of the solution with the basal layer downward. The skin was incubated in TripLE Express solution for 20 min at RT on a shaker with gentle agitation. Afterwards, 2 ml of KC growth medium were added and the epidermis was rubbed back and forth using forceps to release singe cells from the epidermal sheet. The cell suspension was collected and transferred to a 50 ml falcon. This procedure was repeated two more times and cell suspensions were combined. To break cell clumps, cell solution was pipetted up and down several times and passed through a 100 µm filter into a new 50 ml falcon. Cells were centrifuged (180 x g, 5 min, 4°C), resuspended in 1 ml cold KC growth medium, and placed on ice to avoid spontaneous differentiation. Finally, cells were seeded in 6-well-plates, precoated with attachment factor protein or gelatin, at a density of 0.5 – $1x10^6$ cells per well and cultured at 37°C. 24h after plating, medium was changed to remove unattached cells. Until cells reached desired confluency, medium was changed every two days.

7.2.4 Isolation of primary murine CD4+ T cells

Spleens were collected from mice and meshed in supplemented RPMI 1640 medium. Cells were resuspended with 1 ml 1x red blood cell (RBC) lysis solution for 5 min at RT to lyse erythrocytes. Reaction was stopped by adding 9 ml medium. CD4+ T cells were isolated by negative magnetic-activated cell sorting (MACS) selection using the murine CD4+ T cell isolation kit (Miltenyi Biotec) according to manufacturer´s instructions.

7.2.5 Isolation of primary human or murine PBMCs from blood

For isolation of primary human peripheral blood mononuclear cells (PBMCs), blood from donors was collected in lithium heparin monovettes. Blood was centrifuged (300 x g, 10 min, RT, no break) to separate plasma (upper layer), buffy coat (intermediate layer) and erythrocytes (lowest layer). The buffy coat layer containing leukocytes and platelets was collected (approx. 10-18 ml/50 ml blood)

and diluted with PBS up to a total volume of 35 ml. To isolate mononuclear cells (MNCs), diluted buffy coat was carefully layered onto 15 ml Lymphoprep density gradient medium and centrifuged (160 x g, 20 min, RT, no break). About 20 ml of the supernatant were removed and the sample was centrifuged again (350 x g, 20 min, RT, no break). Finally, the intermediate layer containing the MNCs was transferred and washed two times with PBMC buffer 1 (300 x g, 8 min, 4 °C). MNCs were resuspended in RPMI 1640 supplemented with 10% FCS, 100 U/ml penicillin, 100 µg streptomycin and 50 µM β-Mercatoethanol. All donors provided written informed consent.

For isolation of primary murine PBMCs, blood from mice was collected in EDTA coated eppis as described in section 7.1.3. Blood from several mice was pooled to have a total volume of 1 ml and diluted with 1 ml PBS (+2% FCS). Diluted blood was layered onto 1.5 ml Lymphoprep medium and centrifuged (800 x g, 20 min, RT, no break). The upper plasma layer was removed and MNCs were transferred and washed two times with PBS + 2% FCS (400 x g, 4 min, 4 °C).

7.3 Cell transfection and transduction

7.3.1 Transfection of Jurkat T cells by electroporation

Up to $8x10^6$ Jurkat T cells were resuspended in 400 µl old cell culture medium and mixed with up to 5 µg plasmid in a 4 mm electroporation cuvette. Cells were electroporated with Gene Pulser X System (220 V, 1000 µF, exponential program) and immediately transferred into pre-warmed medium. Cells were analyzed 24 – 48 hours after electroporation.

7.3.2 siRNA transfection of Jurkat T cells

For siRNA transfection, $5x10^5$ Jurkat T cells were seeded in 800 µl supplemented medium in a 12-well-plate. 50 – 200 µM siRNA were diluted in 100 µl Opti-MEM and mixed with 100 µl mastermix containing 99 µl Opti-MEM and 1 µl Atufect transfection reagent (1 µg/ml). After 30 min incubation at 37 °C, siRNA mixture was added dropwise to cells. After 6 hours, 1 ml of fresh pre-warmed medium was added and subsequent analysis was done 48 – 72 hours after transfection.

7.3.3 Calcium phosphate transfection of HEK293 cells

One the day prior to transfection, $2.5x10^6$ HEK293 cells were seeded in 9 ml medium in a 10-cm-dish. Up to 10 µg plasmid DNA were mixed with 450 µl sterile H_2O and 50 µl 2.5 M $CaCl_2$. DNA/$CaCl_2$ mixture was added dropwise to 500 µl sterile 2x HBS, while constantly vortexing and incubated for 20 min at RT to enable precipitate formation. Finally, DNA was added to cells and subsequent analysis was done on the following day.

For siRNA transfection, $5x10^4$ HEK293 cells were seeded in 3 ml medium in a 6-well-plate. On the following day, 50 µM siRNA were mixed with 45 µl sterile H_2O and 5 µl 2.5 M $CaCl_2$. Mixture was

added to 50 µl sterile 2x HBS. Medium was changed 6 – 9 hours after adding siRNA and knock down was analyzed 48 – 72 hours after transfection.

7.3.4 siRNA transfection of HeLa cells

For siRNA transfection of HeLa cells, $5x10^4$ cells were seeded in 3 ml medium in a 6-well-plate. 100 µM siRNA were diluted in 200 µl Opti-MEM and mixed with 200 µl mastermix containing 198 µl Opti-MEM and 2 µl Atufect (1 µg/ml). Following 30 min incubation at 37 °C, 1.6 ml supplemented DMEM was added to siRNA dilution. Medium was removed from HeLa cells and transfection mixture was added for 6 – 9 hours before subsequent medium change. Cells were analyzed 48 – 72 hours after transfection.

7.3.5 siRNA transfection of U2OS cells

$5x10^4$ U2OS cells were seeded in 3 ml medium in a 6-well-plate. 100 µM siRNA were diluted in 200 µl Opti-MEM and mixed with 200 µl transfection mixture consisting of 194 µl Opti-MEM and 6 µl Lipofectamine RNAiMAX. After 10 min incubation at RT, 1.6 ml supplemented DMEM was added, medium was removed from U2OS cells and exchanged with transfection mixture. After 6 – 9 hours, medium was changed and knock down was analyzed 48 – 72 hours after transfection.

7.3.6 Lentiviral transduction of Jurkat T cells

To generate stable BCL10 expressing cells, BCL10-deficient Jurkat NF-κB-EGFP reporter cells (generated by Thomas Seeholzer) were lentivirally transduced with pHAGE-hΔCD2-T2A-BCL10 constructs. Therefore, $2x10^6$ HEK293T cells were seeded in 8 ml supplemented DMEM in 10-cm-dishes. On the following day, the transfection mixture was prepared in 200 µl DMEM (without supplements) with 1.5 µg of the packaging vector psPAX2, 1 µg of the lentiviral envelope plasmid pMD2.G, 2 µg of the respective pHAGE-hΔCD2-T2A-BCL10 construct and 10 µl of X-tremeGENE HP DNA Transfection Reagent according to the manufacturer´s instructions. After 30 min incubation at RT, transfection mixture was added dropwise to the cells and incubated for 72 hours for virus production. Virus-containing supernatant was collected, sterile filtered (0.45 µM) and up to 1500 µl virus were added to $5x10^5$ Jurkat T cells in the presence of 8 µg/ml polybrene. 24 hours later, infected Jurkat T cells were washed three times with 5 ml PBS (350 x g, 4 min, RT) and resuspended in 1 ml supplemented RPMI. Cells were cultured and supplied with fresh medium as needed. One week after infection, transduction efficiency was validated by flow cytometry and anti-CD2 staining. Finally, BCL10 protein expression levels were analyzed by Western blot.

7.4 Cell stimulation

7.4.1 Stimulation of Jurkat T cells

To induce NF-κB signaling, Jurkat T cells were either stimulated with P/I ((Phorbol 12-myristate 13-acetate (PMA)/Ionomycin) or anti-CD3/CD28. PMA is a diacylglycerol (DAG) analogous and directly activates PKCθ downstream of the TCR complex, whereas Ionomycin induces Ca^{2+} release from the endoplasmatic reticulum into the cytosol. 200 ng/ml PMA and 300 ng/ml Ionomycin were added to Jurkat T cells in 2 ml old cell culture medium. For TCR stimulation, 1 µg/ml murine anti-human anti-CD3 (IgG1), 3 µg/ml murine anti-human anti-CD28 (IgG2a), and 3 µg/ml anti-mouse IgG1 and anti-mouse IgG2a antibodies each for crosslinking were added to 300 µl Jurkat T cell suspension. Cells were stimulated at 37°C for indicated time points.

7.4.2 Stimulation of murine splenocytes and CD4+ T cells

For stimulation of primary murine total splenocytes or purified CD4+ T cells, P/I was used as described in section 7.4.1. For anti-CD3/CD28 stimulation, a 12-well-plate was coated with 5 µg/ml rabbit anti-syrian hamster IgG in 600 µl PBS overnight at 4 °C. On the following day, 0.5 µg/ml hamster anti-mouse anti-CD3 antibody in 600 µl PBS was added for at least 1 h at RT. Finally, wells were washed two times with PBS to remove unbound anti-CD3 antibody and primary murine cells were added in 600 µl medium in the presence of 1.0 µg/ml soluble hamster anti-mouse anti-CD28 antibody. The plate was briefly centrifuged (350 x g, 1 min, RT) and incubated at 37 °C.

7.5 Flow cytometry

Cell populations were analyzed regarding their surface protein and/or intracellular protein expression or cytokine levels either on an Attune Acoustic Focusing Cytometer or on a FACSCanto II Flow Cytometer. Distinct lymphocyte populations were sorted using a BD FACS Aria III.

7.5.1 Staining of hΔCD2 in Jurkat T cells

To analyze cell surface expression of hΔCD2 in reconstituted BCL10-deficient Jurkat T cells, 200 µl cell suspension (density of approx. $1x10^6$ cells/ml) was transferred to an eppi and stained with anti-CD2-APC antibody (1:400) for 15 min at 4 °C in the dark. Cells were washed once with PBS, resuspended in 300 µl PBS and directly measured via flow cytometry.

7.5.2 Analysis of NF-κB-EGFP reporter Jurkat T cells

The lentiviral NF-κB-EGFP reporter contains six copies of the NF-κB/Rel-binding site of the immunoglobulin κ light chain enhancer (5´-ATCTGGGGATTCCCCA-3´) upstream of the conalbumin (cona) minimal promoter (Schmidt-Ullrich et al., 1996) and a hygromycin-EGFP-fusion gene (pHAGE-Igκ(6x)cona-HygEGFP). Lentiviral transduction of Jurkat T cells and subsequent stimulation ultimately

leads to NF-κB-dependent expression of EGFP (NF-κB-EGFP reporter cells). Stimulated cells were transferred to eppis, washed once with 500 µl PBS, resuspended in 300 µl PBS and EGFP expression was directly measured via flow cytometry. NF-κB-EGFP activation was quantified either by gating on the number of EGFP positive cells or by determining the Median Fluorescence Intensity (MFI).

7.5.3 Staining of cell surface marker in primary murine cells

Flow cytometry analysis of primary murine cells was performed with single-cell suspensions from murine spleen, lymph nodes or thymus. Organs were dissected and isolated cells were subjected to RBC lysis as described in section 7.2.4. For each staining, $1x10^6$ cells were transferred to wells of a 96-well, v-bottom-plate, washed twice with PBS (350 x g, 5 min, 4°C), and stained with eFluor780 live/dead cell permeable dye (1:1000 in PBS) for 30 min at 4 °C in the dark. Cells were washed once with FACS buffer and stained with anti-CD16/CD32 (Fc-block) for 20 min at RT to prevent unspecific antibody binding to Fc receptors. Afterwards, cells were stained with fluorescence-coupled antibodies in FACS buffer (dilutions are noted in section 6.12.2) for 20 min at RT, washed again with FACS buffer, resuspended in FACS buffer and directly measured via flow cytometry.

7.5.4 Intracellular FoxP3 staining

For intracellular FoxP3 staining or if cells were not measured on the same day, cells were fixed and permeabilized with the "FoxP3/transcription factor staining buffer set". Cells were washed once with permeabilization buffer and stained with anti-FoxP3 in permeabilization buffer for 20 min at RT. Finally, cells were washed once more with permeabilization buffer, resuspended in FACS buffer and measured via flow cytometry.

7.5.5 IκBNS and ICOS staining

For intracellular IκBNS and extracellular ICOS staining, $1x10^6$ primary murine splenocytes were used. Cells were added to a 96-well-plate and washed twice with PBS (350 x g, 5 min, 4°C). Cells were incubated with eFluor780 live/dead cell permeable dye (1:1000 in PBS, 30 min, 4°C) and washed once with PBS buffer. Next, cells were fixed in 2% PFA for 15 min at RT and permeabilized in saponin buffer for 15 min at RT. Cells were treated with Fc-block in saponin buffer for 15 min at 4°C. Afterwards, cells were stained with anti-IκBNS antibody in saponin buffer for 30 min at 4°C, washed once with saponin buffer, and stained with anti-rat IgG-AF647 secondary antibody in saponin buffer for 30 min at 4°C. Cells were washed twice with saponin buffer and the second wash was incubated for > 15 min at RT to wash out unbound antibodies. For surface stainings, cells were treated with anti-CD4, anti-CD8 and anti-ICOS in saponin buffer for 30 min at RT. Finally, samples were washed with saponin buffer, resuspended in FACS buffer and measured via flow cytometry.

7.5.6 Intracellular IκBa staining

To assess IκBα degradation via FACS staining, $1x10^6$ unstimulated, P/I- or CD3/28-stimulated primary murine splenocytes were collected and washed twice with FACS buffer (350 x g, 5 min, 4°C). Cells were stained with eFluor780 live/dead cell permeable dye (1:1000 in PBS, 30 min, 4°C), washed once with FACS buffer, and fixed in 2% PFA for 15 min at RT. Cells were either stored in FACS buffer at 4°C overnight or directly permeabilized in saponin buffer for 15 min at RT. Afterwards, cells were treated with Fc-block in saponin buffer for 20 min at RT, followed by intracellular anti-IκBα staining and simultaneous surface staining with anti-CD4 and anti-CD19 in saponin buffer for 30 min at 4°C. Cells were washed twice with saponin buffer and the second wash was incubated for > 15 min at RT to wash out unbound antibodies. Finally, samples were resuspended in FACS buffer and measured via flow cytometry.

7.5.7 Intracellular MALT1A staining

For intracellular MALT1A staining, $1x10^6$ primary murine splenocytes were collected, centrifuged (350 x g, 5 min, 4°C) and washed twice with PBS. Cells were stained with eFluor780 live/dead cell permeable dye (1:1000 in PBS, 30 min, 4°C), washed once with PBS buffer and fixed in 2% PFA for 15 min at RT. Cells were permeabilized in 70% ice-cold methanol for 20 min at 4°C. Cells were washed with FACS buffer and stored at 4°C or immediately treated with Fc-block in FACS buffer for 15 min at 4°C. Afterwards, cells were stained with anti-MALT1A 4A7 supernatant in FACS buffer for 30 min at 4°C, washed with FACS buffer and stained with anti-rat IgG2c secondary antibody in FACS buffer for 30 min at 4°C. Samples were washed twice with FACS buffer, including > 15 min incubation for the second wash, followed by cell surface staining. After a final wash, cells were resuspended in FACS buffer and measured via flow cytometry.

7.6 Molecular biology methods

7.6.1 Polymerase chain reaction (PCR)

Amplification of DNA sequences was performed using polymerase chain reaction (PCR). The following standard protocol and cycler program were used:

Component	Amount
DNA template	30 ng
forward primer (10 µM)	1.25 µl
reverse primer (10 µM)	1.25 µl
dNTPs (10mM)	1.25 µl
5x Herculase buffer	10 µl
DNA polymerase (Herculase II)	1 µl
H_2O	Ad 50 µl

Step	Temperature	Time	
Initial Melting	95 °C	4 min	
Melting	95 °C	1 min	29 cycles
Annealing	Tm primer – 5°C	1 min	
Extension	72°C	30 sec/kb	
Final Extension	72°C	10 min	

PCR products were analyzed for correct size on an agarose gel and purified (see section 7.6.3).

7.6.2 Site-directed mutagenesis

Mutants were generated by site-directed mutagenesis. In a first PCR (megaprimer PCR), a primer containing the desired mutation was used to generate a DNA fragment, which bears the mutation at one end and the flanking restriction site at the other end. In a second PCR, the purified megaprimer was used together with another primer containing a second restriction site, to generate the final DNA fragment. DNA fragments were analyzed on an agarose gel and purified (see section 7.6.3).

7.6.3 DNA restriction, agarose gel electrophoresis and DNA extraction

Amplified PCR products and plasmids were digested using restriction enzymes with the appropriate buffer. The digestion reaction was incubated at 37°C for 1 hour. 6x DNA loading buffer was added and samples were separated on an agarose gel, which was prepared by dissolving 1 - 2% (w/v) agarose in warm TAE or TBE buffer. To visualize DNA fragments, ethidium bromide was added. Samples and the 1 kb plus DNA ladder for size discrimination were loaded on the polymerized agarose gel and were run in TAE or TBE buffer at 80-120 V for approx. 40 min. DNA bands were visualized with UV light and were cut out. DNA was extracted from the gel using the "Nucleo-Spin Gel and PCR Clean-up" kit according to the manufacturer´s instructions.

7.6.4 Ligation

For ligation of digested PCR products and respective plasmids, either the T4 DNA ligase or the "Rapid DNA ligation Kit" were used according to the manufacturer´s instructions. Different molar ratios of vector to insert (1:2 to 1:5) were used depending on the relative sizes of PCR fragment and vector. The ligation reaction was incubated for 1 hour at RT and directly transformed into chemically competent *E. coli* cells.

7.6.5 Transformation of *E.coli*

For transformation *E. coli* Top10 or *E. coli* Stbl3 cells were used. Bacteria cells were mixed with the ligation samples and incubated for 20 min on ice. After the heat shock at 42°C for 45 s, samples were immediately incubated on ice for 2 min. Cells were supplemented with 250 µl S.O.C. medium and

incubated shaking for 1 hour at 37°C. Finally, cells were plated on LB agar plates with appropriate antibiotic and incubated at 37°C overnight.

7.6.6 Cultivation of *E.coli* and plasmid preparation

To isolate plasmid DNA from bacteria, pre-cultures were prepared by inoculating 5 ml LB medium containing appropriate antibiotic with a single *E. coli* colony and cultivated them in a shaker (180 rpm) over night at 37 °C. Plasmid DNA was isolated from 2 ml bacteria culture using the "NucleoSpin Plasmid Mini Kit" according to the manufacturer's instructions. For large-scale plasmid generation, the remaining pre-culture was added to 150 ml LB medium containing antibiotic and DNA isolation was performed with the "QIAGEN Plasmid Maxi Kit" according to the manufacturer's protocol.

7.6.7 DNA sequencing

All generated plasmids were sent to sequencing to Eurofins Genomics (Ebersberg) before they were used in further experiments.

7.6.8 RNA isolation

For extraction of RNA from cell lines, 0.5 – 3x 10^6 cells were used. Cells were centrifuged (350 x g, 5 min, 4°C) and washed with PBS. RNA was purified using either the "InviTrap Spin Universal RNA Mini Kit" or the "RNeasy Mini Kit" according to the manufacturer´s protocol.

For RNA isolation from primary murine or human cells, up to 1x10^7 cells were used. Cells were washed with PBS (350 x g, 5 min, 4°C), resuspended in 600 µl Trizol and briefly vortexed. After 5 min incubation at RT, cells were either frozen in -80°C or directly processed by adding 120 µl Roti-Phenol/Chloroform/Isoamylalcohol and shaking vigorously by hand for 15 s. Cells were incubated for 3 min at RT and centrifuged (13,000 rpm, 5 min, 4°C) to separate phases. The colorless upper aqueous phase was transferred to a fresh eppi and 80% ethanol was added (same amount as transferred RNA) and mixed by pipetting up and down. RNA was applied to "RNeasy mini columns" and further purified according to the manufacturer´s instructions. To elute RNA, 40 µl RNase-free H_2O was added and incubated for 2 min at RT, followed by 1 min centrifugation at RT. RNA was stored at -80°C.

7.6.9 cDNA synthesis

RNA levels were adjusted up to 1 µg and samples were reverse transcribed into cDNA using the "Verso cDNA Synthesis Kit" according to the manufacturer's instructions. Random hexamers were used for the synthesis. Generated cDNA was stored at -20°C.

7.6.10 Relative and absolute quantification of mRNA levels via real-time PCR (qPCR)

Quantitative real-time PCR (qPCR) was performed on a LightCycler 480 using "LightCycler 480 SYBR Green I Mastermix" and following standard protocol and cycler program:

Component	Amount
SYBR Green I Mastermix (2x)	5 µl
forward primer (20 µM)	0.5 µl
reverse primer (20 µM)	0.5 µl
cDNA	2.5 µl
water	1.5 µl
total	10 µl

Step	Temperature	Time	
Initial Melting	95 °C	10 min	
Melting	95 °C	10 sec	35 - 40 cycles
Annealing	60 °C	10 sec	
Extension	72	10 sec	
Melting Curve	65°C – 95°C		

To quantify target gene expression, either the ΔΔCp method (Pfaffl, 2001) for relative quantification or the standard-curve method for absolute quantification was used. Murine hydroxymethylbilane synthase (Hmbs) or human RNA polymerase II (RP2) were used as internal controls for normalization of relative mRNA levels. For absolute quantification of MALT1 isoforms, an internal standard curve with murine or human MALT1A and MALT1B plasmid DNA was included ranging from $3x10^{-2}$ to $3x10^{-7}$ ng DNA. Figure 7-1A shows example amplification curves of the titrated MALT1A standard and cDNA of *Malt1*$^{A/A}$, *Malt1*$^{B/B}$, *Malt1*$^{+/+}$, and H_2O control. The ct values of each standard dilution were plotted against the logarithm of their initial concentration (Figure 7-1B). The slope of each standard was used for calculating the concentration of samples. To determine actual mRNA transcript numbers following formula was used (Godornes et al., 2007) with $6.022\ x10^{23}$ (molecules) as Avogadro´s number, 660 Dalton (Da) being the average weight of a single base pair (bp) and 214 bp for MALT1A or 194 bp for MALT1B:

$$\text{Number of copies/mRNA} = \frac{Amount\ of\ mRNA\ (ng) \times 6.022\ x10^{23}}{Number\ of\ bp \times 1x10^{9} \times 660\ Da}$$

The calculated transcript numbers referred to the amount of mRNA/cDNA (ng) which was used in qPCR and were adjusted to 100 ng.

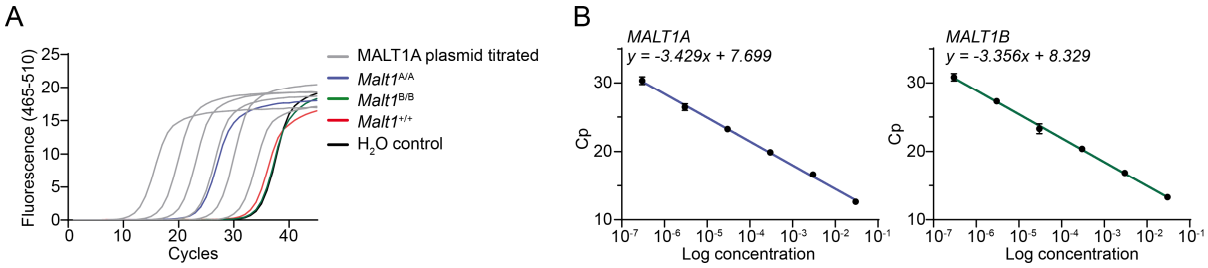

Figure 7-1: Absolute quantification of gene transcript numbers using the standard curve method.
A) Amplification curves of MALT1A standard ranging from $3x10^{-2}$ to $3x10^{-7}$ (light grey) and murine cDNA generated from *Malt1*$^{A/A}$ (blue), *Malt1*$^{B/B}$ (green), *Malt1*$^{+/+}$ (red) RNA and H_2O control (black).
B) Standard curves of MALT1A (left) and MALT1B (right) showing the cp values of different plasmid concentrations.

7.6.11 Semi-quantitative PCR (semi-qPCR)

For semi-quantitative PCR (semi-qPCR) Taq DNA polymerase and 10x Taq standard buffer were used according to the following protocol and cycler program:

Component	Amount
Template cDNA	Up to 50 ng
forward primer (10 µM)	1 µl
reverse primer (10 µM)	1 µl
dNTPs (10mM)	1 µl
10x Taq standard buffer	5 µl
Taq DNA polymerase	0.25 µl
H_2O	Ad 50 µl

Step	Temperature	Time	
Initial Melting	94 °C	10 min	
Melting	94 °C	20 s	28 – 35 cycles
Annealing	56°C	20 s	
Extension	65°C	20 s	
Final Extension	65°C	10 min	

PCR products were mixed with 6x DNA loading buffer and loaded on a 3% agarose gel (see section 7.6.3). DNA bands were visualized with UV light using a Geldocumentation system (Intas). In minigene assays, RP2 levels served as internal control and alternatively spliced products were quantified by densitometry using Adobe Photoshop. Percentage of exon7 inclusion was calculated relative to total PCR product.

7.6.12 Electrophoretic mobility shift assays

To analyze direct interaction of RBPs with RNA, electrophoretic mobility shift assays were performed by Dr. Alisha Jones (Institute of Structural Biology, Helmholtz Zentrum München) as described in Jones et al., 2021.

7.7 Biochemical and immunological methods

7.7.1 Preparation of whole cell lysates (WCL)

To analyze protein expression levels or downstream activation of NF-κB signaling $1x10^6$ – $5x10^6$ cells were harvested (350 x g, 5 min, 4°C), washed with ice-cold PBS and resuspended in 50 – 150 µl Co-IP lysis buffer supplemented with protease inhibitors. Lysis was performed on a shaker for 20 min at 4°C, followed by centrifugation (20,000 x g, 12 min, 4°C) to remove cell debris. Finally, cells were denatured by adding 4x SDS loading buffer and subsequent boiling for 5 min at 95°C. Lysates were analyzed by western blot after SDS-PAGE.

7.7.2 Co-immunoprecipitation (Co-IP) and Strep-Tactin pulldown (Strep-PD)

For immunoprecipitation (IP) of endogenous proteins or Strep-Tactin pulldown (Strep-PD) of stably expressed Strep-tagged proteins, $3x10^7$ – $5x10^7$ Jurkat T cells were lysed in 900 µl Co-IP buffer (20 min, 4°C, rotating). For IP of overexpressed proteins in HEK293 cells (section 7.3.3), cells were lysed in 500 µl Co-IP buffer on the day after transfection. Lysates were cleared by centrifugation (20,000 x g, 12 min, 4°C) and 30 µl of supernatant were collected as lysate controls. For IPs, the remaining supernatants were incubated with respective antibodies on a rotator overnight at 4°C. On the next day, 20 µl Protein G Sepharose beads (50% suspension) were added and incubated for another 1 - 2 hours at 4°C. Strep-tagged proteins were precipitated by using 30 µl Strep-Tactin Sepharose (1:1 suspension) at 4°C overnight. After incubation with Protein G Sepharose or Strep-Tactin Sepharose, beads were washed three times with 500 µl Co-IP buffer without protease inhibitors (2200 rpm, 3 min, 4°C). Finally, IPs or Strep-PDs were denatured by boiling in 25 µl 2x SDS sample buffer for 8 min. IPs/Strep-PDs and respective lysate controls were analyzed by western blot after SDS-PAGE.

7.7.3 Ubiquitination assay (denaturing IP or Strep-PD)

For detection of ubiquitinated endogenous or Strep-tagged BCL10, $5x10^7$ Jurkat T cells were harvested and washed twice with 1 ml ice-cold PBS. Cells were lysed in 450 µl Co-IP buffer (with protease inhibitors) containing 1% SDS at RT. Lysates were homogenized by passing 10x through a 20G syringe and 5x through a 26G syringe, followed by incubation (20 min, 4°C, rotating). Lysates were centrifuged (20,000 x g, 20 min, 4°C) and supernatants (ca. 420 µl) were transferred to ultracentrifugation tubes. After ultracentrifugation (45,000 rpm, 20 min, 4°C) lysates (ca. 400 µl) were transferred to 15 ml falcons and diluted with 4 ml Co-IP buffer without SDS (final SDS

concentration: 0.1 %). 30 µl of the diluted supernatants were collected for lysate controls. For BCL10-IP, 1 µl BCL10 antibody (EP606Y) was added overnight (4°C, rotating) and on the next day 20 µl Protein G Sepharose (50% suspension) for another 1 – 2 hours. For PD of Strep-tagged BCL10, 30 µl Strep-Tactin Sepharose (1:1 suspension) were added overnight (4°C, rotating). Beads were washed three times with 500 µl Co-IP buffer without protease inhibitors (2200 rpm, 3 min, 4°C; after the first wash, beads were transferred to 1.5 mL eppis) and buffer was completely removed via aspiration. Beads were mixed with 25 µl 2x SDS sample buffer and boiled for 8 min at 95°C. Denatured IPs/Strep-PDs and lysates were analyzed by western blot after SDS-PAGE.

7.7.4 Ubiquitin (Ub) chain cleavage assay

AMSH-LP and OTULIN were diluted in DUB dilution buffer to 2x final concentration. For *in vitro* ubiquitin (Ub) chain cleavage assays, 500 ng M1-linked tetra-ubiquitin (Ub_4) or K63-linked Ub_4 were added to 10 µl 1x DUB reaction buffer and incubated with 10 µl diluted AMSH-LP or OTULIN (final concentration: 100 nM) for 60 min at 30 °C. Afterwards, 20 µl 2x SDS sample buffer were added and mixture was boiled for 1 min at 95°C.

To analyze linkage specificity of BCL10 polyubiquitin chains, BCL10 was immunoprecipitated under denaturating conditions (see section 7.7.3) and beads were washed three times with 500 µl Co-IP buffer without protease inhibitors (2200 rpm, 3 min, 4°C). Buffer was completely removed by aspiration and beads were washed for another two times with 500 µl 1x DUB reaction buffer and again dry-sucked by aspiration. Finally, 15 µl 1x DUB reaction buffer and 15 µl diluted AMSH-LP or OTULIN (final concentration: 500 nM) were added and reaction was incubated for 60 min at 30°C. Beads were dry-sucked and IPs were denatured by boiling in 25 µl 2x SDS sample buffer for 5 min. *In vitro* cleavage assays and IPs were analyzed by western blot after SDS-PAGE.

7.7.5 SDS polyacrylamide gel electrophoresis (SDS-PAGE)

Proteins of cell lysates and IPs were separated by SDS polyacrylamide gel electrophoresis (SDS-PAGE). To estimate the molecular weight of the separated proteins, a prestained protein ladder was loaded next to the samples. Electrophoresis was performed in SDS Electrophoresis buffer at 90 – 110 V for approximately 2.5 hours. Proteins in the gel were transferred onto PVDF membranes by Western Blotting (see section 7.7.6).

7.7.6 Western blot (WB)

For immunodetection of proteins after SDS-PAGE, proteins were electrophoretically transferred onto PVDF membranes using a semi-dry Western Blot transfer system. PVDF membranes were activated in methanol and equilibrated in Blotting buffer together with Whatman filter papers. Membrane and

SDS gel were placed between soaked filter papers in the blotting device, and the transfer was performed for 110 min with a current of 70 mA per gel. After transfer, membranes were incubated for 1 hour in blocking solution (PBS-T with 5% milk) to avoid unspecific binding of antibodies. Blocked membranes were incubated overnight with primary antibodies (in PBS-T with 2.5% milk, see section 6.12.3), shaking at 4°C. On the following day, membranes were washed three times in PBS-T for 15 min to remove unbound primary antibodies. Membranes were incubated with Horseradish peroxidase (HRP)-coupled secondary antibodies (in PBS-T with 1.25% milk, see section 6.12.4) for 1 hour at RT and membranes were washed again with PBS-T. To visualize proteins, membranes were covered with enhanced chemiluminescence (ECL) substrate (1:20 in H_2O) which is converted by HRP. Oxidation of the substrate catalyzed by HRP and accompanied emission of light is detected by ECL films. For detection of several proteins on the same membrane, membranes were washed with PBS-T and incubated with stripping buffer for 30 min at RT to remove bound antibodies. After washing membranes several times with PBS-T for 10 min, membranes were blocked and incubated with specific primary and secondary antibodies as described previously.

7.8 Statistical analysis

7.8.1 Mouse experiments

Mouse experiments with 3 distinct groups were analyzed using One-way ANOVA with Brown-Forsythe and Welch ANOVA test (Figures 4-5 – 4-9, 4-11 – 4-12) or without (Figure 4-10). Statistical analysis for mouse experiments with 2 distinct groups were done using unpaired Student's t-test with Welch correction (Figures 4-3 and 4-27). For Figure 4-24C and D, two-way ANOVA with Tukey´s multiple comparisons test was used. Values represent the mean ± standard error of the mean (SEM) and statistical significance is indicated by p-values.

7.8.2 In vitro experiments

All experiments with suspension or adherent cells were performed at least three times unless otherwise indicated. Values represent the mean ± standard error of the mean (SEM). Experiments were analyzed by using unpaired Student's t-test. Statistical significance values are *$p < 0.05$, **$p < 0.01$, ***$p < 0.001$ and ****$p < 0.0001$.

8 Abbreviations

° C	degrees Celsius
aa	amino acid
AP-1	activator protein-1
APC	antigen presenting cell
APC	allophycocyanin
Asp	aspartic acid
BCL6	B cell chronic lymphocytic leukemia/lymphoma 6
BCL10	B cell chronic lymphocytic leukemia/lymphoma 10
BCR	B cell receptor
BENTA	B cell expansion with NF-κB and T cell anergy
BM	bone marrow
bp	base pair
BPS	branch point sequence
BSA	bovine serum albumin
Ca^{2+}	Calcium
CaMKII	Calmodulin kinase II
CARD	caspase-recruitment domain
CARMA1	CARD-containing MAGUK 1 (also known as CARD11)
CARD11	Caspase recruitment domain-containing protein 11
Cas9	CRISPR-associated protein-9
CASP10	caspase-10
CBM	CARD11-BCL10-MALT1
CC	coiled coil
CILK1	ciliogenesis associated kinase1
Co-IP	Co-immunoprecipitation
CRISPR	Clustered Regularly Interspaced Short Palindromic Repeats
C-terminus	Carboxyl-terminus
CTLA4	cytotoxic T-lymphocyte-associated protein 4
CYLD	cylindromatosis
CXCR5	C-X-C chemokine receptor type 5
DAG	diacylglycerol
DD	death domain
dKO	double knockout
DLBCL	diffuse large B cell lymphoma
DMEM	Dulbecco's Modified Eagle Medium
DMSO	dimethyl sulfoxide
DNA	deoxyribonucleic acid
dNTP	deoxyribonucleotide triphosphate
ds	double-stranded
dsRNA	double-stranded ribonucleic acid
DTT	dithiothreitol
DUB	deubiquitinase
ECL	enhanced chemiluminescence

EDTA	ethylenediaminetetraacetic acid
EGFP	enhanced green fluorescent protein
ER	endoplasmic reticulum
ERK 1/2	extracellular signal-regulated kinase ½
ESE	exonic splicing enhancer
ESS	exonic splicing silencer
EUCOMM	European Conditional Mouse Mutagenesis Program
FBS	fetal bovine serum
FCS	fetal calf serum
FITC	fluorescein isothiocyanate
FOXP3	forkhead box p3
GATA-3	GATA binding protein 3
Glu	glutamine
h	human
HEPES	2-[4-(2-Hydroxyethyl)-1-piperazino]-ethansulfonic acid
HIV-1	human immunodeficiency virus type-1
hnRNP	heterogeneous nuclear ribonucleoprotein
HOIL-1	heme-oxidized IRP2 ubiquitin ligase 1
HOIP	HOIL-1-interacting protein
HRP	horseradish peroxidase
HSPC	hematopoietic stem and progenitor cell
ICOS	inducible T cell co-stimulator
IFNγ	interferon γ (gamma)
Ig	immunoglobulin
IKK	IκB kinase
ILDR2	immunoglobulin-like domain containing receptor 2
IL-2	interleukin-2
Iono	ionomycin
IP_3	inositol 1,4,5-trisphosphate
IRF	interferon regulatory factors
ISE	intronic splicing enhancer
ISS	intronic splicing silencer
ITAM	immunoreceptor tyrosine-based activation motif
iTreg	induced regulatory T cell
IκB	inhibitor of κB
JNK	c-Jun N-terminal kinase
K	lysine
kb	kilo base
kDa	kilo Dalton
KH2PO4	potassium hydrogen phosphate
KO	knockout
LAT	linker for activation of T cells
LB	Luria-Bertani (medium)
LN	lymph node
LUBAC	linear ubiquitin chain assembly complex

MACS	magnetic-activated cell sorting
MAGUK	membrane associated guanylate kinase
MALT1	mucosa associated lymphoid tissue lymphoma translocation protein 1
MAPK	mitogen activated protein kinase
MEK	mitogen-activated protein kinase kinase
MFI	median fluorescence intensity
mg	milligram
MgCl2	magnesium chloride
MHC	major histocompatibility complex
min	minute
mL	milliliter
mRNA	messenger RNA
MZ	marginal zone
N4BP-1	NEDD4-binding protein 1
NaCl	sodium chloride
NaF	sodium fluoride
NEMO	NF-κB essential modulator
NFAT	nuclear factor of activated T cells
NF-κB	nuclear factor kappa B
NGS	next-generation sequencing
NIK	NF-κB-inducing-kinase
NK	natural killer
ng	nanogram
nm	nanometer
nt	nucleotide
N-terminus	amino-terminus
nTreg	natural regulatory T cell
P/S	penicillin/streptomycin
PBS	phosphate buffered saline
PBS-T	PBS-Tween 20
PCR	polymerase chain reaction
PDK-1	phosphoinositide-dependent kinase-1
PDZ	PSD-95/DLG/ZO1 homology
PE	phycoerythrin
PerCP	Peridinin-Chlorophyll-protein
PE-Cγ7	phycoerythrin-cyanine 7
PFA	paraformaldehyde
PI3K	phosphoinositide 3 kinase
PIP_2	phosphatidyl inositol 4,5-bisphosphate
PKC	protein kinase C
PLCγ	phospholipase C γ (gamma)
PM	paracaspase mutant
PMA	phorbol 12-myristate 13-acetate
Py-tract	poly-pyrimidine tract
RBP	RNA binding protein

RHD	Rel homology domain
RNA	ribonucleic acid
RORγt	RAR-related orphan receptor gamma t
rpm	rounds per minute
RRM	RNA recognition motif
RT	room temperature
RT-PCR	real-time PCR
s	second
SCF-βTrCP	Skp1-Cul1-F-box ligase containing the F-box protein βTrCP
SDS	Sodium dodecyl sulfate
SDS-PAGE	SDS polyacrylamide gel electrophoresis
SEM	standard error of the mean
SHARPIN	Shank-associated RH domain-interacting protein
sKO	single knockout
SLP-76	SH2-domain containing leukocyte protein of 76 kDa
snRNP	small nuclear ribonucleoprotein particle
SR	serine-/arginine-rich
SS	splice site
ssRNA	single-stranded ribonucleic acid
T6BM	TRAF6 binding motif
TAB	TAK1 binding protein
TAD	transactivation domain
TAE	Tris-acetate-EDTA
TAK	transforming growth factor beta activated kinase
TANK	TRAF family member associated NF-κB activator
TBM	TRAF6 binding mutant
TBMPM	TRAF6 binding mutant – paracaspase mutant
T-bet	T-box transcription factor
TCR	T cell receptor
Teff	T effector
Tfh	follicular T helper
TGF-β	transforming growth factor beta
Th	T helper
TEMED	Tetramethylethylenediamine
TLR	toll like receptor
Tm	melting temperature
TNF	tumor necrosis factor
TRAF	tumor-necrosis factor associated receptor-associated factor
Tconv	conventional T cell
Treg	regulatory T cell
Tris T	ris(hydroxymethyl)-aminomethan
U	Unit
Ubc13	Ubiquitin-conjugating enzyme E2 13
Uev1A	Ubiquitin-conjugating enzyme E2 variant 1A
UTR	untranslated region

mV	millivolt
WB	Western Blot
WT	wildtype
ZAP70	zeta-chain-associated protein 70 kDa
ZC3H12D	zinc finger CCCH domain-containing protein 12D
µg	microgram

9 References

Abbas, A. K., Lichtmann, A. H., & Pillai, S. (2021). *Cellular and Molecular Immunology* (Vol. 10). Elsevier: Jeremy Bowes.

Abd-Ellah, A., Voogdt, C., Krappmann, D., Möller, P., & Marienfeld, R. B. (2018). GSK3β modulates NF-κB activation and RelB degradation through site-specific phosphorylation of BCL10. *Sci Rep, 8*(1), 1352. doi: 10.1038/s41598-018-19822-z

Ammar, M., Bouchlaka-Souissi, C., Helms, C. A., Zaraa, I., Jordan, C. T., Anbunathan, H., . . . Bowcock, A. M. (2013). Genome-wide linkage scan for psoriasis susceptibility loci in multiplex Tunisian families. *Br J Dermatol, 168*(3), 583-587. doi: 10.1111/bjd.12050

Ammar, M., Jordan, C. T., Cao, L., Lim, E., Bouchlaka Souissi, C., Jrad, A., . . . Bowcock, A. M. (2016). CARD14 alterations in Tunisian patients with psoriasis and further characterization in European cohorts. *Br J Dermatol, 174*(2), 330-337. doi: 10.1111/bjd.14158

Au - Li, F., Au - Adase, C. A., & Au - Zhang, L.-j. (2017). Isolation and Culture of Primary Mouse Keratinocytes from Neonatal and Adult Mouse Skin. *JoVE*(125), e56027. doi: doi:10.3791/56027

Baens, M., Bonsignore, L., Somers, R., Vanderheydt, C., Weeks, S. D., Gunnarsson, J., . . . Marynen, P. (2014). MALT1 Auto-Proteolysis Is Essential for NF-κB-Dependent Gene Transcription in Activated Lymphocytes. *PLoS One, 9*(8), e103774. doi: 10.1371/journal.pone.0103774

Baens, M., Stirparo, R., Lampi, Y., Verbeke, D., Vandepoel, R., Cools, J., . . . Bornschein, S. (2018). Malt1 self-cleavage is critical for regulatory T cell homeostasis and anti-tumor immunity in mice. *Eur J Immunol, 48*(10), 1728-1738. doi: 10.1002/eji.201847597

Bedsaul, J. R., Carter, N. M., Deibel, K. E., Hutcherson, S. M., Jones, T. A., Wang, Z., . . . Pomerantz, J. L. (2018). Mechanisms of Regulated and Dysregulated CARD11 Signaling in Adaptive Immunity and Disease. *Front Immunol, 9*. doi: 10.3389/fimmu.2018.02105

Bell, P. A., Scheuermann, S., Renner, F., Pan, C. L., Lu, H. Y., Turvey, S. E., . . . Overall, C. M. (2022). Integrating knowledge of protein sequence with protein function for the prediction and validation of new MALT1 substrates. *Comput Struct Biotechnol J, 20*, 4717-4732. doi: 10.1016/j.csbj.2022.08.021

Boisson, B., Laplantine, E., Dobbs, K., Cobat, A., Tarantino, N., Hazen, M., . . . Notarangelo, L. D. (2015). Human HOIP and LUBAC deficiency underlies autoinflammation, immunodeficiency, amylopectinosis, and lymphangiectasia. *The Journal of experimental medicine, 212*(6), 939-951. doi: 10.1084/jem.20141130

Boisson, B., Laplantine, E., Prando, C., Giliani, S., Israelsson, E., Xu, Z., . . . Picard, C. (2012). Immunodeficiency, autoinflammation and amylopectinosis in humans with inherited HOIL-1 and LUBAC deficiency. *Nat Immunol, 13*(12), 1178-1186. doi: 10.1038/ni.2457

Bornancin, F., Renner, F., Touil, R., Sic, H., Kolb, Y., Touil-Allaoui, I., . . . Calzascia, T. (2015). Deficiency of MALT1 Paracaspase Activity Results in Unbalanced Regulatory and Effector T and B Cell Responses Leading to Multiorgan Inflammation. *The Journal of Immunology, 194*(8), 3723-3734. doi: 10.4049/jimmunol.1402254

Brüstle, A., Brenner, D., Knobbe-Thomsen, C. B., Cox, M., Lang, P. A., Lang, K. S., & Mak, T. W. (2017). MALT1 is an intrinsic regulator of regulatory T cells. *Cell Death & Differentiation, 24*(7), 1214-1223. doi: 10.1038/cdd.2015.104

Brüstle, A., Brenner, D., Knobbe, C. B., Lang, P. A., Virtanen, C., Hershenfield, B. M., . . . Mak, T. W. (2012). The NF-κB regulator MALT1 determines the encephalitogenic potential of Th17 cells. *J Clin Invest, 122*(12), 4698-4709. doi: 10.1172/jci63528

Busch, A., & Hertel, K. J. (2012). Evolution of SR protein and hnRNP splicing regulatory factors. *Wiley Interdiscip Rev RNA, 3*(1), 1-12. doi: 10.1002/wrna.100

Chaplin, D. D. (2010). Overview of the immune response. *J Allergy Clin Immunol, 125*(2 Suppl 2), S3-23. doi: 10.1016/j.jaci.2009.12.980

Chau, V., Tobias, J. W., Bachmair, A., Marriott, D., Ecker, D. J., Gonda, D. K., & Varshavsky, A. (1989). A multiubiquitin chain is confined to specific lysine in a targeted short-lived protein. *Science, 243*(4898), 1576-1583. doi: 10.1126/science.2538923

Chen, Z., Hagler, J., Palombella, V. J., Melandri, F., Scherer, D., Ballard, D., & Maniatis, T. (1995). Signal-induced site-specific phosphorylation targets I kappa B alpha to the ubiquitin-proteasome pathway. *Genes Dev, 9*(13), 1586-1597. doi: 10.1101/gad.9.13.1586

Chen, Z. J., Parent, L., & Maniatis, T. (1996). Site-specific phosphorylation of IkappaBalpha by a novel ubiquitination-dependent protein kinase activity. *Cell, 84*(6), 853-862. doi: 10.1016/s0092-8674(00)81064-8

Chen, Z. J., & Sun, L. J. (2009). Nonproteolytic functions of ubiquitin in cell signaling. *Mol Cell, 33*(3), 275-286. doi: 10.1016/j.molcel.2009.01.014

Chu, C., Zhang, Q. C., da Rocha, S. T., Flynn, R. A., Bharadwaj, M., Calabrese, J. M., . . . Chang, H. Y. (2015). Systematic discovery of Xist RNA binding proteins. *Cell, 161*(2), 404-416. doi: 10.1016/j.cell.2015.03.025

Cohen, P., & Strickson, S. (2017). The role of hybrid ubiquitin chains in the MyD88 and other innate immune signalling pathways. *Cell Death & Differentiation, 24*(7), 1153-1159. doi: 10.1038/cdd.2017.17

Coornaert, B., Baens, M., Heyninck, K., Bekaert, T., Haegman, M., Staal, J., . . . Beyaert, R. (2008). T cell antigen receptor stimulation induces MALT1 paracaspase-mediated cleavage of the NF-kappaB inhibitor A20. *Nat Immunol, 9*(3), 263-271. doi: 10.1038/ni1561

Crowe, S. O., Rana, A. S. J. B., Deol, K. K., Ge, Y., & Strieter, E. R. (2017). Ubiquitin Chain Enrichment Middle-Down Mass Spectrometry Enables Characterization of Branched Ubiquitin Chains in Cellulo. *Analytical Chemistry, 89*(8), 4428-4434. doi: 10.1021/acs.analchem.6b03675

Dainichi, T., Matsumoto, R., Mostafa, A., & Kabashima, K. (2019). Immune Control by TRAF6-Mediated Pathways of Epithelial Cells in the EIME (Epithelial Immune Microenvironment). *Front Immunol, 10*. doi: 10.3389/fimmu.2019.01107

Daniel, P.-H., Marta, L. M., & Gunnar, D. (2020). Branching and Mixing: New Signals of the Ubiquitin Signaling System. In Z. Xianquan (Ed.), *Ubiquitin* (pp. Ch. 1). Rijeka: IntechOpen.

David, L., Li, Y., Ma, J., Garner, E., Zhang, X., & Wu, H. (2018). Assembly mechanism of the CARMA1-BCL10-MALT1-TRAF6 signalosome. *Proceedings of the National Academy of Sciences, 115*(7), 1499-1504. doi: doi:10.1073/pnas.1721967115

Demeyer, A., Skordos, I., Driege, Y., Kreike, M., Hochepied, T., Baens, M., . . . Beyaert, R. (2019). MALT1 Proteolytic Activity Suppresses Autoimmunity in a T Cell Intrinsic Manner. *Front Immunol, 10*, 1898. doi: 10.3389/fimmu.2019.01898

Deng, L., Wang, C., Spencer, E., Yang, L., Braun, A., You, J., . . . Chen, Z. J. (2000). Activation of the IkappaB kinase complex by TRAF6 requires a dimeric ubiquitin-conjugating enzyme complex and a unique polyubiquitin chain. *Cell, 103*(2), 351-361. doi: 10.1016/s0092-8674(00)00126-4

Dierlamm, J., Stefanova, M., Michaux, L., Lincke, E., Leberecht, P., & Hossfeld, D. K. (1999). Unusual clinical course and acquisition of del(11)(q23) in second lymphatic blastic phase of a Ph-positive chronic myeloid leukemia. *Cancer Genet Cytogenet, 113*(1), 85-89. doi: 10.1016/s0165-4608(98)00282-9

Dubois, S. M., Alexia, C., Wu, Y., Leclair, H. M., Leveau, C., Schol, E., . . . Bidère, N. (2014). A catalytic-independent role for the LUBAC in NF-κB activation upon antigen receptor engagement and in lymphoma cells. *Blood, 123*(14), 2199-2203. doi: 10.1182/blood-2013-05-504019

Düwel, M., Welteke, V., Oeckinghaus, A., Baens, M., Kloo, B., Ferch, U., . . . Krappmann, D. (2009). A20 negatively regulates T cell receptor signaling to NF-kappaB by cleaving Malt1 ubiquitin chains. *J Immunol, 182*(12), 7718-7728. doi: 10.4049/jimmunol.0803313

Egawa, T., Albrecht, B., Favier, B., Sunshine, M. J., Mirchandani, K., O'Brien, W., . . . Littman, D. R. (2003). Requirement for CARMA1 in antigen receptor-induced NF-kappa B activation and lymphocyte proliferation. *Curr Biol, 13*(14), 1252-1258. doi: 10.1016/s0960-9822(03)00491-3

Elton, L., Carpentier, I., Staal, J., Driege, Y., Haegman, M., & Beyaert, R. (2016). MALT1 cleaves the E3 ubiquitin ligase HOIL-1 in activated T cells, generating a dominant negative inhibitor of LUBAC-induced NF-κB signaling. *Febs j, 283*(3), 403-412. doi: 10.1111/febs.13597

Emmerich, C. H., Ordureau, A., Strickson, S., Arthur, J. S., Pedrioli, P. G., Komander, D., & Cohen, P. (2013). Activation of the canonical IKK complex by K63/M1-linked hybrid ubiquitin chains. *Proc Natl Acad Sci U S A, 110*(38), 15247-15252. doi: 10.1073/pnas.1314715110

Essig, K., Hu, D., Guimaraes, J. C., Alterauge, D., Edelmann, S., Raj, T., . . . Heissmeyer, V. (2017). Roquin Suppresses the PI3K-mTOR Signaling Pathway to Inhibit T Helper Cell Differentiation and Conversion of Treg to Tfr Cells. *Immunity, 47*(6), 1067-1082.e1012. doi: 10.1016/j.immuni.2017.11.008

Fu, X.-D., & Ares, M. (2014). Context-dependent control of alternative splicing by RNA-binding proteins. *Nature Reviews Genetics, 15*(10), 689-701. doi: 10.1038/nrg3778

Fujita, H., Rahighi, S., Akita, M., Kato, R., Sasaki, Y., Wakatsuki, S., & Iwai, K. (2014). Mechanism underlying IκB kinase activation mediated by the linear ubiquitin chain assembly complex. *Mol Cell Biol, 34*(7), 1322-1335. doi: 10.1128/mcb.01538-13

Gavali, S., Liu, J., Li, X., & Paolino, M. (2021). Ubiquitination in T-Cell Activation and Checkpoint Inhibition: New Avenues for Targeted Cancer Immunotherapy. *International Journal of Molecular Sciences, 22*(19), 10800.

Gehring, T., Seeholzer, T., & Krappmann, D. (2018). BCL10 - Bridging CARDs to Immune Activation. *Front Immunol, 9*, 1539. doi: 10.3389/fimmu.2018.01539

Gerberick, G. F., Cruse, L. W., Miller, C. M., Sikorski, E. E., & Ridder, G. M. (1997). Selective modulation of T cell memory markers CD62L and CD44 on murine draining lymph node cells following allergen and irritant treatment. *Toxicol Appl Pharmacol, 146*(1), 1-10. doi: 10.1006/taap.1997.8218

Gerlach, B., Cordier, S. M., Schmukle, A. C., Emmerich, C. H., Rieser, E., Haas, T. L., . . . Walczak, H. (2011). Linear ubiquitination prevents inflammation and regulates immune signalling. *Nature, 471*(7340), 591-596. doi: 10.1038/nature09816

Gewies, A., Gorka, O., Bergmann, H., Pechloff, K., Petermann, F., Jeltsch, K. M., . . . Ruland, J. (2014). Uncoupling Malt1 threshold function from paracaspase activity results in destructive autoimmune inflammation. *Cell Rep, 9*(4), 1292-1305. doi: 10.1016/j.celrep.2014.10.044

Ginster, S., Bardet, M., Unterreiner, A., Malinverni, C., Renner, F., Lam, S., . . . Bornancin, F. (2017). Two Antagonistic MALT1 Auto-Cleavage Mechanisms Reveal a Role for TRAF6 to Unleash MALT1 Activation. *PLoS One, 12*(1), e0169026. doi: 10.1371/journal.pone.0169026

Godornes, C., Leader, B. T., Molini, B. J., Centurion-Lara, A., & Lukehart, S. A. (2007). Quantitation of rabbit cytokine mRNA by real-time RT-PCR. *Cytokine, 38*(1), 1-7. doi: 10.1016/j.cyto.2007.04.002

Golubovskaya, V., & Wu, L. (2016). Different Subsets of T Cells, Memory, Effector Functions, and CAR-T Immunotherapy. *Cancers (Basel), 8*(3). doi: 10.3390/cancers8030036

Gorham, J. D., Güler, M. L., Steen, R. G., Mackey, A. J., Daly, M. J., Frederick, K., . . . Murphy, K. M. (1996). Genetic mapping of a murine locus controlling development of T helper 1/T helper 2 type responses. *Proceedings of the National Academy of Sciences, 93*(22), 12467-12472. doi: doi:10.1073/pnas.93.22.12467

Ha, H., Han, D., & Choi, Y. (2009). TRAF-mediated TNFR-family signaling. *Curr Protoc Immunol, Chapter 11*, Unit11.19D. doi: 10.1002/0471142735.im1109ds87

Hachmann, J., Snipas, S. J., van Raam, B. J., Cancino, E. M., Houlihan, E. J., Poreba, M., . . . Salvesen, G. S. (2012). Mechanism and specificity of the human paracaspase MALT1. *Biochem J, 443*(1), 287-295. doi: 10.1042/bj20120035

Hailfinger, S., Nogai, H., Pelzer, C., Jaworski, M., Cabalzar, K., Charton, J. E., . . . Thome, M. (2011). Malt1-dependent RelB cleavage promotes canonical NF-kappaB activation in lymphocytes and lymphoma cell lines. *Proc Natl Acad Sci U S A, 108*(35), 14596-14601. doi: 10.1073/pnas.1105020108

Hasegawa, Y., Brockdorff, N., Kawano, S., Tsutui, K., Tsutui, K., & Nakagawa, S. (2010). The matrix protein hnRNP U is required for chromosomal localization of Xist RNA. *Dev Cell, 19*(3), 469-476. doi: 10.1016/j.devcel.2010.08.006

Hayden, M. S., & Ghosh, S. (2012). NF-κB, the first quarter-century: remarkable progress and outstanding questions. *Genes Dev, 26*(3), 203-234. doi: 10.1101/gad.183434.111

Haynes, B. F., Telen, M. J., Hale, L. P., & Denning, S. M. (1989). CD44--a molecule involved in leukocyte adherence and T-cell activation. *Immunol Today, 10*(12), 423-428. doi: 10.1016/0167-5699(89)90040-6

House, A. E., & Lynch, K. W. (2006). An exonic splicing silencer represses spliceosome assembly after ATP-dependent exon recognition. *Nat Struct Mol Biol, 13*(10), 937-944. doi: 10.1038/nsmb1149

Howes, A., O'Sullivan, P. A., Breyer, F., Ghose, A., Cao, L., Krappmann, D., . . . Ley, S. C. (2016). Psoriasis mutations disrupt CARD14 autoinhibition promoting BCL10-MALT1-dependent NF-κB activation. *Biochem J, 473*(12), 1759-1768. doi: 10.1042/bcj20160270

Hu, S., Alcivar, A., Qu, L., Tang, J., & Yang, X. (2006a). CIAP2 inhibits anigen receptor signaling by targeting Bcl10 for degredation. *Cell Cycle, 5*(13), 1438-1442. doi: 10.4161/cc.5.13.2866

Hu, S., Du, M. Q., Park, S. M., Alcivar, A., Qu, L., Gupta, S., . . . Yang, X. (2006b). cIAP2 is a ubiquitin protein ligase for BCL10 and is dysregulated in mucosa-associated lymphoid tissue lymphomas. *J Clin Invest, 116*(1), 174-181. doi: 10.1172/jci25641

Hui, J., Hung, L.-H., Heiner, M., Schreiner, S., Neumüller, N., Reither, G., . . . Bindereif, A. (2005). Intronic CA-repeat and CA-rich elements: a new class of regulators of mammalian alternative splicing. *Embo j, 24*(11), 1988-1998. doi: https://doi.org/10.1038/sj.emboj.7600677

Hulpiau, P., Driege, Y., Staal, J., & Beyaert, R. (2016). MALT1 is not alone after all: identification of novel paracaspases. *Cell Mol Life Sci, 73*(5), 1103-1116. doi: 10.1007/s00018-015-2041-9

Ikeda, F., Deribe, Y. L., Skånland, S. S., Stieglitz, B., Grabbe, C., Franz-Wachtel, M., . . . Dikic, I. (2011). SHARPIN forms a linear ubiquitin ligase complex regulating NF-κB activity and apoptosis. *Nature, 471*(7340), 637-641. doi: 10.1038/nature09814

Israël, L., Bardet, M., Huppertz, A., Mercado, N., Ginster, S., Unterreiner, A., . . . Bornancin, F. (2018). A CARD10-Dependent Tonic Signalosome Activates MALT1 Paracaspase and Regulates IL-17/TNF-α–Driven Keratinocyte Inflammation. *Journal of Investigative Dermatology, 138*(9), 2075-2079. doi: https://doi.org/10.1016/j.jid.2018.03.1503

Ivanov, II, McKenzie, B. S., Zhou, L., Tadokoro, C. E., Lepelley, A., Lafaille, J. J., . . . Littman, D. R. (2006). The orphan nuclear receptor RORgammat directs the differentiation program of proinflammatory IL-17+ T helper cells. *Cell, 126*(6), 1121-1133. doi: 10.1016/j.cell.2006.07.035

Jattani, R. P., Tritapoe, J. M., & Pomerantz, J. L. (2016). Intramolecular Interactions and Regulation of Cofactor Binding by the Four Repressive Elements in the Caspase Recruitment Domain-containing Protein 11 (CARD11) Inhibitory Domain. *J Biol Chem, 291*(16), 8338-8348. doi: 10.1074/jbc.M116.717322

Jaworski, M., Marsland, B. J., Gehrig, J., Held, W., Favre, S., Luther, S. A., . . . Thome, M. (2014). Malt1 protease inactivation efficiently dampens immune responses but causes spontaneous autoimmunity. *Embo j, 33*(23), 2765-2781. doi: 10.15252/embj.201488987

Jeltsch, K. M., Hu, D., Brenner, S., Zöller, J., Heinz, G. A., Nagel, D., . . . Heissmeyer, V. (2014). Cleavage of roquin and regnase-1 by the paracaspase MALT1 releases their cooperatively repressed targets to promote T(H)17 differentiation. *Nat Immunol, 15*(11), 1079-1089. doi: 10.1038/ni.3008

Jones, A. N., Graß, C., Meininger, I., Geerlof, A., Klostermann, M., Zarnack, K., . . . Sattler, M. (2022). Modulation of pre-mRNA structure by hnRNP proteins regulates alternative splicing of MALT1. *Science Advances, 8*(31), eabp9153. doi: doi:10.1126/sciadv.abp9153

Jordan, C. T., Cao, L., Roberson, E. D., Pierson, K. C., Yang, C. F., Joyce, C. E., . . . Bowcock, A. M. (2012a). PSORS2 is due to mutations in CARD14. *Am J Hum Genet, 90*(5), 784-795. doi: 10.1016/j.ajhg.2012.03.012

Jordan, Catherine T., Cao, L., Roberson, Elisha D. O., Duan, S., Helms, Cynthia A., Nair, Rajan P., . . . Bowcock, Anne M. (2012b). Rare and Common Variants in CARD14, Encoding an Epidermal Regulator of NF-kappaB, in Psoriasis. *The American Journal of Human Genetics, 90*(5), 796-808. doi: https://doi.org/10.1016/j.ajhg.2012.03.013

Kanarek, N., & Ben-Neriah, Y. (2012). Regulation of NF-κB by ubiquitination and degradation of the IκBs. *Immunol Rev, 246*(1), 77-94. doi: 10.1111/j.1600-065X.2012.01098.x

Keusekotten, K., Elliott, P. R., Glockner, L., Fiil, B. K., Damgaard, R. B., Kulathu, Y., . . . Komander, D. (2013). OTULIN antagonizes LUBAC signaling by specifically hydrolyzing Met1-linked polyubiquitin. *Cell, 153*(6), 1312-1326. doi: 10.1016/j.cell.2013.05.014

Kiledjian, M., & Dreyfuss, G. (1992). Primary structure and binding activity of the hnRNP U protein: binding RNA through RGG box. *Embo j, 11*(7), 2655-2664. doi: 10.1002/j.1460-2075.1992.tb05331.x

Kim, W., Bennett, E. J., Huttlin, E. L., Guo, A., Li, J., Possemato, A., . . . Gygi, S. P. (2011). Systematic and quantitative assessment of the ubiquitin-modified proteome. *Mol Cell, 44*(2), 325-340. doi: 10.1016/j.molcel.2011.08.025

King, C. G., Kobayashi, T., Cejas, P. J., Kim, T., Yoon, K., Kim, G. K., . . . Choi, Y. (2006). TRAF6 is a T cell-intrinsic negative regulator required for the maintenance of immune homeostasis. *Nat Med, 12*(9), 1088-1092. doi: 10.1038/nm1449

Kirisako, T., Kamei, K., Murata, S., Kato, M., Fukumoto, H., Kanie, M., . . . Iwai, K. (2006). A ubiquitin ligase complex assembles linear polyubiquitin chains. *Embo j, 25*(20), 4877-4887. doi: 10.1038/sj.emboj.7601360

Klein, T., Fung, S.-Y., Renner, F., Blank, M. A., Dufour, A., Kang, S., . . . Overall, C. M. (2015). The paracaspase MALT1 cleaves HOIL1 reducing linear ubiquitination by LUBAC to dampen lymphocyte NF-κB signalling. *Nat Commun, 6*(1), 8777. doi: 10.1038/ncomms9777

Komander, D., & Rape, M. (2012). The ubiquitin code. *Annu Rev Biochem, 81*, 203-229. doi: 10.1146/annurev-biochem-060310-170328

Komander, D., Reyes-Turcu, F., Licchesi, J. D. F., Odenwaelder, P., Wilkinson, K. D., & Barford, D. (2009). Molecular discrimination of structurally equivalent Lys 63-linked and linear polyubiquitin chains. *EMBO Rep, 10*(5), 466-473. doi: https://doi.org/10.1038/embor.2009.55

Koseki, T., Inohara, N., Chen, S., Carrio, R., Merino, J., Hottiger, M. O., . . . Núñez, G. (1999). CIPER, a novel NF kappaB-activating protein containing a caspase recruitment domain with homology to Herpesvirus-2 protein E10. *J Biol Chem, 274*(15), 9955-9961. doi: 10.1074/jbc.274.15.9955

Kurgyis, Z., Vornholz, L., Pechloff, K., Kemény, L. V., Wartewig, T., Muschaweckh, A., . . . Ruland, J. (2021). Keratinocyte-intrinsic BCL10/MALT1 activity initiates and amplifies psoriasiform skin inflammation. *Sci Immunol, 6*(65), eabi4425. doi: 10.1126/sciimmunol.abi4425

Kutukculer, N., Seeholzer, T., O'Neill, T. J., Graß, C., Aykut, A., Karaca, N. E., . . . Krappmann, D. (2021). Human immune disorder associated with homozygous hypomorphic mutation affecting MALT1B splice variant. *J Allergy Clin Immunol, 147*(2), 775-778.e778. doi: 10.1016/j.jaci.2020.07.034

Kutzner, K., Woods, S., Karayel, O., Gehring, T., Yin, H., Flatley, A., . . . Krappmann, D. (2022). Phosphorylation of serine-893 in CARD11 suppresses the formation and activity of the CARD11-BCL10-MALT1 complex in T and B cells. *Sci Signal, 15*(723), eabk3083. doi: 10.1126/scisignal.abk3083

Lee, Y., & Rio, D. C. (2015). Mechanisms and Regulation of Alternative Pre-mRNA Splicing. *Annu Rev Biochem, 84*, 291-323. doi: 10.1146/annurev-biochem-060614-034316

Lee, Y. J., Wang, Q., & Rio, D. C. (2018). Coordinate regulation of alternative pre-mRNA splicing events by the human RNA chaperone proteins hnRNPA1 and DDX5. *Genes Dev, 32*(15-16), 1060-1074. doi: 10.1101/gad.316034.118

Li, S., Yang, X., Shao, J., & Shen, Y. (2012). Structural insights into the assembly of CARMA1 and BCL10. *PLoS One, 7*(8), e42775. doi: 10.1371/journal.pone.0042775

Lin, C. L., Taggart, A. J., & Fairbrother, W. G. (2016). RNA structure in splicing: An evolutionary perspective. *RNA Biol, 13*(9), 766-771. doi: 10.1080/15476286.2016.1208893

Liu, X., Nurieva, R. I., & Dong, C. (2013). Transcriptional regulation of follicular T-helper (Tfh) cells. *Immunol Rev, 252*(1), 139-145. doi: https://doi.org/10.1111/imr.12040

Lobry, C., Lopez, T., Israël, A., & Weil, R. (2007). Negative feedback loop in T cell activation through IκB kinase-induced phosphorylation and degradation of Bcl10. *Proceedings of the National Academy of Sciences, 104*(3), 908-913. doi: doi:10.1073/pnas.0606982104

Lork, M., Staal, J., & Beyaert, R. (2019). Ubiquitination and phosphorylation of the CARD11-BCL10-MALT1 signalosome in T cells. *Cell Immunol, 340*, 103877. doi: 10.1016/j.cellimm.2018.11.001

Lowes, M. A., Suárez-Fariñas, M., & Krueger, J. G. (2014). Immunology of Psoriasis. *Annu Rev Immunol, 32*(1), 227-255. doi: 10.1146/annurev-immunol-032713-120225

Lu, H. Y., Bauman, B. M., Arjunaraja, S., Dorjbal, B., Milner, J. D., Snow, A. L., & Turvey, S. E. (2018). The CBM-opathies-A Rapidly Expanding Spectrum of Human Inborn Errors of Immunity Caused by Mutations in the CARD11-BCL10-MALT1 Complex. *Front Immunol, 9*, 2078. doi: 10.3389/fimmu.2018.02078

Martinez-Contreras, R., Fisette, J. F., Nasim, F. U., Madden, R., Cordeau, M., & Chabot, B. (2006). Intronic binding sites for hnRNP A/B and hnRNP F/H proteins stimulate pre-mRNA splicing. *PLoS Biol, 4*(2), e21. doi: 10.1371/journal.pbio.0040021

Martinez, N. M., & Lynch, K. W. (2013). Control of alternative splicing in immune responses: many regulators, many predictions, much still to learn. *Immunol Rev, 253*(1), 216-236. doi: 10.1111/imr.12047

Matsumoto, R., Wang, D., Blonska, M., Li, H., Kobayashi, M., Pappu, B., . . . Lin, X. (2005). Phosphorylation of CARMA1 plays a critical role in T Cell receptor-mediated NF-kappaB activation. *Immunity, 23*(6), 575-585. doi: 10.1016/j.immuni.2005.10.007

Matsushita, K., Takeuchi, O., Standley, D. M., Kumagai, Y., Kawagoe, T., Miyake, T., . . . Akira, S. (2009). Zc3h12a is an RNase essential for controlling immune responses by regulating mRNA decay. *Nature, 458*(7242), 1185-1190. doi: 10.1038/nature07924

McCully, R. R., & Pomerantz, J. L. (2008). The protein kinase C-responsive inhibitory domain of CARD11 functions in NF-kappaB activation to regulate the association of multiple signaling cofactors that differentially depend on Bcl10 and MALT1 for association. *Mol Cell Biol, 28*(18), 5668-5686. doi: 10.1128/mcb.00418-08

McManus, C. J., & Graveley, B. R. (2011). RNA structure and the mechanisms of alternative splicing. *Curr Opin Genet Dev, 21*(4), 373-379. doi: 10.1016/j.gde.2011.04.001

Meininger, I., Griesbach, R. A., Hu, D., Gehring, T., Seeholzer, T., Bertossi, A., . . . Krappmann, D. (2016). Alternative splicing of MALT1 controls signalling and activation of CD4(+) T cells. *Nat Commun, 7*, 11292. doi: 10.1038/ncomms11292

Meininger, I., & Krappmann, D. (2016). Lymphocyte signaling and activation by the CARMA1-BCL10-MALT1 signalosome. *Biol Chem, 397*(12), 1315-1333. doi: 10.1515/hsz-2016-0216

Mellett, M., Meier, B., Mohanan, D., Schairer, R., Cheng, P., Satoh, T. K., . . . French, L. E. (2018). CARD14 Gain-of-Function Mutation Alone Is Sufficient to Drive IL-23/IL-17-Mediated Psoriasiform Skin Inflammation In Vivo. *J Invest Dermatol, 138*(9), 2010-2023. doi: 10.1016/j.jid.2018.03.1525

Mino, T., Murakawa, Y., Fukao, A., Vandenbon, A., Wessels, H. H., Ori, D., . . . Takeuchi, O. (2015). Regnase-1 and Roquin Regulate a Common Element in Inflammatory mRNAs by Spatiotemporally Distinct Mechanisms. *Cell, 161*(5), 1058-1073. doi: 10.1016/j.cell.2015.04.029

Motta-Mena, L. B., Heyd, F., & Lynch, K. W. (2010). Context-dependent regulatory mechanism of the splicing factor hnRNP L. *Mol Cell, 37*(2), 223-234. doi: 10.1016/j.molcel.2009.12.027

Nilsen, T. W., & Graveley, B. R. (2010). Expansion of the eukaryotic proteome by alternative splicing. *Nature, 463*(7280), 457-463. doi: 10.1038/nature08909

Noels, H., van Loo, G., Hagens, S., Broeckx, V., Beyaert, R., Marynen, P., & Baens, M. (2007). A Novel TRAF6 binding site in MALT1 defines distinct mechanisms of NF-kappaB activation by API2middle dotMALT1 fusions. *J Biol Chem, 282*(14), 10180-10189. doi: 10.1074/jbc.M611038200

O'Neill, T. J., Seeholzer, T., Gewies, A., Gehring, T., Giesert, F., Hamp, I., . . . Krappmann, D. (2021). TRAF6 prevents fatal inflammation by homeostatic suppression of MALT1 protease. *Sci Immunol, 6*(65), eabh2095. doi: 10.1126/sciimmunol.abh2095

Oberdoerffer, S., Moita, L. F., Neems, D., Freitas, R. P., Hacohen, N., & Rao, A. (2008). Regulation of CD45 alternative splicing by heterogeneous ribonucleoprotein, hnRNPLL. *Science, 321*(5889), 686-691. doi: 10.1126/science.1157610

Oeckinghaus, A., & Ghosh, S. (2009). The NF-kappaB family of transcription factors and its regulation. *Cold Spring Harb Perspect Biol, 1*(4), a000034. doi: 10.1101/cshperspect.a000034

Oeckinghaus, A., Wegener, E., Welteke, V., Ferch, U., Arslan, S. C., Ruland, J., . . . Krappmann, D. (2007). Malt1 ubiquitination triggers NF-kappaB signaling upon T-cell activation. *Embo j, 26*(22), 4634-4645. doi: 10.1038/sj.emboj.7601897

Oikawa, D., Hatanaka, N., Suzuki, T., & Tokunaga, F. (2020). Cellular and Mathematical Analyses of LUBAC Involvement in T Cell Receptor-Mediated NF-κB Activation Pathway. *Front Immunol, 11*. doi: 10.3389/fimmu.2020.601926

Oruganti, S. R., Edin, S., Grundström, C., & Grundström, T. (2011). CaMKII targets Bcl10 in T-cell receptor induced activation of NF-κB. *Mol Immunol, 48*(12-13), 1448-1460. doi: 10.1016/j.molimm.2011.03.020

Parkin, J., & Cohen, B. (2001). An overview of the immune system. *Lancet, 357*(9270), 1777-1789. doi: 10.1016/s0140-6736(00)04904-7

Paul, S., Kashyap, A. K., Jia, W., He, Y. W., & Schaefer, B. C. (2012). Selective autophagy of the adaptor protein Bcl10 modulates T cell receptor activation of NF-κB. *Immunity, 36*(6), 947-958. doi: 10.1016/j.immuni.2012.04.008

Paul, S., & Schaefer, B. C. (2013). A new look at T cell receptor signaling to nuclear factor-κB. *Trends Immunol, 34*(6), 269-281. doi: 10.1016/j.it.2013.02.002

Pelzer, C., Cabalzar, K., Wolf, A., Gonzalez, M., Lenz, G., & Thome, M. (2013). The protease activity of the paracaspase MALT1 is controlled by monoubiquitination. *Nat Immunol, 14*(4), 337-345. doi: 10.1038/ni.2540

Pfaffl, M. W. (2001). A new mathematical model for relative quantification in real-time RT-PCR. *Nucleic Acids Res, 29*(9), e45. doi: 10.1093/nar/29.9.e45

Pohl, C., & Dikic, I. (2019). Cellular quality control by the ubiquitin-proteasome system and autophagy. *Science, 366*(6467), 818-822. doi: doi:10.1126/science.aax3769

Qiao, Q., Yang, C., Zheng, C., Fontán, L., David, L., Yu, X., . . . Wu, H. (2013). Structural architecture of the CARMA1/Bcl10/MALT1 signalosome: nucleation-induced filamentous assembly. *Mol Cell, 51*(6), 766-779. doi: 10.1016/j.molcel.2013.08.032

Rebeaud, F., Hailfinger, S., Posevitz-Fejfar, A., Tapernoux, M., Moser, R., Rueda, D., . . . Thome, M. (2008). The proteolytic activity of the paracaspase MALT1 is key in T cell activation. *Nat Immunol, 9*(3), 272-281. doi: 10.1038/ni1568

Reiley, W. W., Jin, W., Lee, A. J., Wright, A., Wu, X., Tewalt, E. F., . . . Sun, S. C. (2007). Deubiquitinating enzyme CYLD negatively regulates the ubiquitin-dependent kinase Tak1 and prevents abnormal T cell responses. *The Journal of experimental medicine, 204*(6), 1475-1485. doi: 10.1084/jem.20062694

Rivkin, E., Almeida, S. M., Ceccarelli, D. F., Juang, Y. C., MacLean, T. A., Srikumar, T., . . . Cordes, S. P. (2013). The linear ubiquitin-specific deubiquitinase gumby regulates angiogenesis. *Nature, 498*(7454), 318-324. doi: 10.1038/nature12296

Rosebeck, S., Lim, M. S., Elenitoba-Johnson, K. S., McAllister-Lucas, L. M., & Lucas, P. C. (2016). API2-MALT1 oncoprotein promotes lymphomagenesis via unique program of substrate ubiquitination and proteolysis. *World J Biol Chem, 7*(1), 128-137. doi: 10.4331/wjbc.v7.i1.128

Rosenbaum, M., Gewies, A., Pechloff, K., Heuser, C., Engleitner, T., Gehring, T., . . . Ruland, J. (2019). Bcl10-controlled Malt1 paracaspase activity is key for the immune suppressive function of regulatory T cells. *Nat Commun, 10*(1), 2352. doi: 10.1038/s41467-019-10203-2

Rosenbaum, M., Schnalzger, T., Engleitner, T., Weiß, C., Mishra, R., Mibus, C., . . . Ruland, J. (2022). MALT1 protease function in regulatory T cells induces MYC activity to promote mitochondrial function and cellular expansion. *Eur J Immunol, 52*(1), 85-95. doi: 10.1002/eji.202149355

Rossbach, O., Hung, L. H., Schreiner, S., Grishina, I., Heiner, M., Hui, J., & Bindereif, A. (2009). Auto- and cross-regulation of the hnRNP L proteins by alternative splicing. *Mol Cell Biol, 29*(6), 1442-1451. doi: 10.1128/mcb.01689-08

Ruefli-Brasse, A. A., French, D. M., & Dixit, V. M. (2003). Regulation of NF-kappaB-dependent lymphocyte activation and development by paracaspase. *Science, 302*(5650), 1581-1584. doi: 10.1126/science.1090769

Ruland, J., Duncan, G. S., Elia, A., del Barco Barrantes, I., Nguyen, L., Plyte, S., . . . Mak, T. W. (2001). Bcl10 is a positive regulator of antigen receptor-induced activation of NF-kappaB and neural tube closure. *Cell, 104*(1), 33-42. doi: 10.1016/s0092-8674(01)00189-1

Ruland, J., Duncan, G. S., Wakeham, A., & Mak, T. W. (2003). Differential requirement for Malt1 in T and B cell antigen receptor signaling. *Immunity, 19*(5), 749-758. doi: 10.1016/s1074-7613(03)00293-0

Ruland, J., & Hartjes, L. (2019). CARD-BCL-10-MALT1 signalling in protective and pathological immunity. *Nat Rev Immunol, 19*(2), 118-134. doi: 10.1038/s41577-018-0087-2

Sakaguchi, S., Yamaguchi, T., Nomura, T., & Ono, M. (2008). Regulatory T Cells and Immune Tolerance. *Cell, 133*(5), 775-787. doi: https://doi.org/10.1016/j.cell.2008.05.009

Satpathy, S., Wagner, S. A., Beli, P., Gupta, R., Kristiansen, T. A., Malinova, D., . . . Choudhary, C. (2015). Systems-wide analysis of BCR signalosomes and downstream phosphorylation and ubiquitylation. *Mol Syst Biol, 11*(6), 810. doi: 10.15252/msb.20145880

Scharschmidt, E., Wegener, E., Heissmeyer, V., Rao, A., & Krappmann, D. (2004). Degradation of Bcl10 induced by T-cell activation negatively regulates NF-kappa B signaling. *Mol Cell Biol, 24*(9), 3860-3873. doi: 10.1128/mcb.24.9.3860-3873.2004

Schlauderer, F., Seeholzer, T., Desfosses, A., Gehring, T., Strauss, M., Hopfner, K. P., . . . Lammens, K. (2018). Molecular architecture and regulation of BCL10-MALT1 filaments. *Nat Commun, 9*(1), 4041. doi: 10.1038/s41467-018-06573-8

Schmidt-Ullrich, R., Mémet, S., Lilienbaum, A., Feuillard, J., Raphaël, M., & Israël, A. (1996). NF-kappaB activity in transgenic mice: developmental regulation and tissue specificity. *Development, 122*(7), 2117-2128.

Schmitz, M. L., & Krappmann, D. (2006). Controlling NF-kappaB activation in T cells by costimulatory receptors. *Cell Death Differ, 13*(5), 834-842. doi: 10.1038/sj.cdd.4401845

Schulze-Luehrmann, J., & Ghosh, S. (2006). Antigen-receptor signaling to nuclear factor kappa B. *Immunity, 25*(5), 701-715. doi: 10.1016/j.immuni.2006.10.010

Scott, D. C., & Schulman, B. A. (2019). Chapter Two - Dual-color pulse-chase ubiquitination assays to simultaneously monitor substrate priming and extension. In M. Hochstrasser (Ed.), *Methods in Enzymology* (Vol. 618, pp. 29-48): Academic Press.

Shambharkar, P. B., Blonska, M., Pappu, B. P., Li, H., You, Y., Sakurai, H., . . . Lin, X. (2007). Phosphorylation and ubiquitination of the IkappaB kinase complex by two distinct signaling pathways. *Embo j, 26*(7), 1794-1805. doi: 10.1038/sj.emboj.7601622

Shankarling, G., & Lynch, K. W. (2013). Minimal functional domains of paralogues hnRNP L and hnRNP LL exhibit mechanistic differences in exonic splicing repression. *Biochem J, 453*(2), 271-279. doi: 10.1042/bj20130432

Shi, J. H., & Sun, S. C. (2018). Tumor Necrosis Factor Receptor-Associated Factor Regulation of Nuclear Factor κB and Mitogen-Activated Protein Kinase Pathways. *Front Immunol, 9*, 1849. doi: 10.3389/fimmu.2018.01849

Shimizu, S., Fujita, H., Sasaki, Y., Tsuruyama, T., Fukuda, K., & Iwai, K. (2016). Differential Involvement of the Npl4 Zinc Finger Domains of SHARPIN and HOIL-1L in Linear Ubiquitin

Chain Assembly Complex-Mediated Cell Death Protection. *Mol Cell Biol, 36*(10), 1569-1583. doi: 10.1128/mcb.01049-15

Smith-Garvin, J. E., Koretzky, G. A., & Jordan, M. S. (2009). T cell activation. *Annu Rev Immunol, 27*, 591-619. doi: 10.1146/annurev.immunol.021908.132706

Smith, S. A., Ray, D., Cook, K. B., Mallory, M. J., Hughes, T. R., & Lynch, K. W. (2013). Paralogs hnRNP L and hnRNP LL exhibit overlapping but distinct RNA binding constraints. *PLoS One, 8*(11), e80701. doi: 10.1371/journal.pone.0080701

Snyder, N. A., & Silva, G. M. (2021). Deubiquitinating enzymes (DUBs): Regulation, homeostasis, and oxidative stress response. *J Biol Chem, 297*(3), 101077. doi: 10.1016/j.jbc.2021.101077

Sommer, K., Guo, B., Pomerantz, J. L., Bandaranayake, A. D., Moreno-García, M. E., Ovechkina, Y. L., & Rawlings, D. J. (2005). Phosphorylation of the CARMA1 linker controls NF-kappaB activation. *Immunity, 23*(6), 561-574. doi: 10.1016/j.immuni.2005.09.014

Staal, J., Driege, Y., Bekaert, T., Demeyer, A., Muyllaert, D., Van Damme, P., . . . Beyaert, R. (2011). T-cell receptor-induced JNK activation requires proteolytic inactivation of CYLD by MALT1. *Embo j, 30*(9), 1742-1752. doi: https://doi.org/10.1038/emboj.2011.85

Sun, L., Deng, L., Ea, C. K., Xia, Z. P., & Chen, Z. J. (2004). The TRAF6 ubiquitin ligase and TAK1 kinase mediate IKK activation by BCL10 and MALT1 in T lymphocytes. *Mol Cell, 14*(3), 289-301. doi: 10.1016/s1097-2765(04)00236-9

Sun, S. C. (2010). CYLD: a tumor suppressor deubiquitinase regulating NF-kappaB activation and diverse biological processes. *Cell Death Differ, 17*(1), 25-34. doi: 10.1038/cdd.2009.43

Szabo, S. J., Kim, S. T., Costa, G. L., Zhang, X., Fathman, C. G., & Glimcher, L. H. (2000). A novel transcription factor, T-bet, directs Th1 lineage commitment. *Cell, 100*(6), 655-669. doi: 10.1016/s0092-8674(00)80702-3

Tange, T. O., Damgaard, C. K., Guth, S., Valcárcel, J., & Kjems, J. (2001). The hnRNP A1 protein regulates HIV-1 tat splicing via a novel intron silencer element. *Embo j, 20*(20), 5748-5758. doi: 10.1093/emboj/20.20.5748

Taylor, K., & Sobczak, K. (2020). Intrinsic Regulatory Role of RNA Structural Arrangement in Alternative Splicing Control. *International Journal of Molecular Sciences, 21*(14), 5161.

Tokunaga, F., Nakagawa, T., Nakahara, M., Saeki, Y., Taniguchi, M., Sakata, S.-i., . . . Iwai, K. (2011). SHARPIN is a component of the NF-κB-activating linear ubiquitin chain assembly complex. *Nature, 471*(7340), 633-636. doi: 10.1038/nature09815

Topp, J. D., Jackson, J., Melton, A. A., & Lynch, K. W. (2008). A cell-based screen for splicing regulators identifies hnRNP LL as a distinct signal-induced repressor of CD45 variable exon 4. *Rna, 14*(10), 2038-2049. doi: 10.1261/rna.1212008

Uehata, T., Iwasaki, H., Vandenbon, A., Matsushita, K., Hernandez-Cuellar, E., Kuniyoshi, K., . . . Akira, S. (2013). Malt1-induced cleavage of regnase-1 in CD4(+) helper T cells regulates immune activation. *Cell, 153*(5), 1036-1049. doi: 10.1016/j.cell.2013.04.034

Uren, A. G., O'Rourke, K., Aravind, L. A., Pisabarro, M. T., Seshagiri, S., Koonin, E. V., & Dixit, V. M. (2000). Identification of paracaspases and metacaspases: two ancient families of caspase-like proteins, one of which plays a key role in MALT lymphoma. *Mol Cell, 6*(4), 961-967. doi: 10.1016/s1097-2765(00)00094-0

Valkevich, E. M., Sanchez, N. A., Ge, Y., & Strieter, E. R. (2014). Middle-down mass spectrometry enables characterization of branched ubiquitin chains. *Biochemistry, 53*(30), 4979-4989. doi: 10.1021/bi5006305

Van Nuffel, E., Schmitt, A., Afonina, I. S., Schulze-Osthoff, K., Beyaert, R., & Hailfinger, S. (2017). CARD14-Mediated Activation of Paracaspase MALT1 in Keratinocytes: Implications for Psoriasis. *Journal of Investigative Dermatology, 137*(3), 569-575. doi: https://doi.org/10.1016/j.jid.2016.09.031

Vignali, D. A., Collison, L. W., & Workman, C. J. (2008). How regulatory T cells work. *Nat Rev Immunol, 8*(7), 523-532. doi: 10.1038/nri2343

Vinuesa, C. G., Cook, M. C., Angelucci, C., Athanasopoulos, V., Rui, L., Hill, K. M., . . . Goodnow, C. C. (2005). A RING-type ubiquitin ligase family member required to repress follicular helper T cells and autoimmunity. *Nature, 435*(7041), 452-458. doi: 10.1038/nature03555

Vogel, K. U., Edelmann, S. L., Jeltsch, K. M., Bertossi, A., Heger, K., Heinz, G. A., . . . Heissmeyer, V. (2013). Roquin paralogs 1 and 2 redundantly repress the Icos and Ox40 costimulator mRNAs and control follicular helper T cell differentiation. *Immunity, 38*(4), 655-668. doi: 10.1016/j.immuni.2012.12.004

Vyas, J. M., Van der Veen, A. G., & Ploegh, H. L. (2008). The known unknowns of antigen processing and presentation. *Nat Rev Immunol, 8*(8), 607-618. doi: 10.1038/nri2368

Wagner, S. A., Beli, P., Weinert, B. T., Nielsen, M. L., Cox, J., Mann, M., & Choudhary, C. (2011). A proteome-wide, quantitative survey of in vivo ubiquitylation sites reveals widespread regulatory roles. *Mol Cell Proteomics, 10*(10), M111.013284. doi: 10.1074/mcp.M111.013284

Wahl, M. C., Will, C. L., & Lührmann, R. (2009). The spliceosome: design principles of a dynamic RNP machine. *Cell, 136*(4), 701-718. doi: 10.1016/j.cell.2009.02.009

Wang, Y.-S., Wu, K.-P., Jiang, H.-K., Kurkute, P., & Chen, R.-H. (2020). Branched Ubiquitination: Detection Methods, Biological Functions and Chemical Synthesis. *Molecules, 25*(21), 5200.

Warf, M. B., & Berglund, J. A. (2010). Role of RNA structure in regulating pre-mRNA splicing. *Trends Biochem Sci, 35*(3), 169-178. doi: 10.1016/j.tibs.2009.10.004

Warrington, R., Watson, W., Kim, H. L., & Antonetti, F. R. (2011). An introduction to immunology and immunopathology. *Allergy, Asthma & Clinical Immunology, 7*(1), S1. doi: 10.1186/1710-1492-7-S1-S1

Wegener, E., Oeckinghaus, A., Papadopoulou, N., Lavitas, L., Schmidt-Supprian, M., Ferch, U., . . . Krappmann, D. (2006). Essential role for IkappaB kinase beta in remodeling Carma1-Bcl10-Malt1 complexes upon T cell activation. *Mol Cell, 23*(1), 13-23. doi: 10.1016/j.molcel.2006.05.027

Wertz, I. E., Newton, K., Seshasayee, D., Kusam, S., Lam, C., Zhang, J., . . . Dixit, V. M. (2015). Phosphorylation and linear ubiquitin direct A20 inhibition of inflammation. *Nature, 528*(7582), 370-375. doi: 10.1038/nature16165

Wiesmann, C., Leder, L., Blank, J., Bernardi, A., Melkko, S., Decock, A., . . . Renatus, M. (2012). Structural determinants of MALT1 protease activity. *J Mol Biol, 419*(1-2), 4-21. doi: 10.1016/j.jmb.2012.02.018

Willis, T. G., Jadayel, D. M., Du, M. Q., Peng, H., Perry, A. R., Abdul-Rauf, M., . . . Dyer, M. J. (1999). Bcl10 is involved in t(1;14)(p22;q32) of MALT B cell lymphoma and mutated in multiple tumor types. *Cell, 96*(1), 35-45. doi: 10.1016/s0092-8674(00)80957-5

Wu, C. J., & Ashwell, J. D. (2008). NEMO recognition of ubiquitinated Bcl10 is required for T cell receptor-mediated NF-kappaB activation. *Proc Natl Acad Sci U S A, 105*(8), 3023-3028. doi: 10.1073/pnas.0712313105

Wu, Z., Jia, X., de la Cruz, L., Su, X. C., Marzolf, B., Troisch, P., . . . Hoyne, G. F. (2008). Memory T cell RNA rearrangement programmed by heterogeneous nuclear ribonucleoprotein hnRNPLL. *Immunity, 29*(6), 863-875. doi: 10.1016/j.immuni.2008.11.004

Xue, L., Morris, S. W., Orihuela, C., Tuomanen, E., Cui, X., Wen, R., & Wang, D. (2003). Defective development and function of Bcl10-deficient follicular, marginal zone and B1 B cells. *Nat Immunol, 4*(9), 857-865. doi: 10.1038/ni963

Yagi, J., Arimura, Y., Takatori, H., Nakajima, H., Iwamoto, I., & Uchiyama, T. (2006). Genetic background influences Th cell differentiation by controlling the capacity for IL-2-induced IL-4 production by naive CD4+ T cells. *International Immunology, 18*(12), 1681-1690. doi: 10.1093/intimm/dxl102

Yamasoba, D., Sato, K., Ichinose, T., Imamura, T., Koepke, L., Joas, S., . . . Takeuchi, O. (2019). N4BP1 restricts HIV-1 and its inactivation by MALT1 promotes viral reactivation. *Nature Microbiology, 4*(9), 1532-1544. doi: 10.1038/s41564-019-0460-3

Yang, Y., Schmitz, R., Mitala, J., Whiting, A., Xiao, W., Ceribelli, M., . . . Staudt, L. M. (2014). Essential role of the linear ubiquitin chain assembly complex in lymphoma revealed by rare germline polymorphisms. *Cancer Discov, 4*(4), 480-493. doi: 10.1158/2159-8290.cd-13-0915

Yang, Y. K., Yang, C., Chan, W., Wang, Z., Deibel, K. E., & Pomerantz, J. L. (2016). Molecular Determinants of Scaffold-induced Linear Ubiquitinylation of B Cell Lymphoma/Leukemia 10 (Bcl10) during T Cell Receptor and Oncogenic Caspase Recruitment Domain-containing Protein 11 (CARD11) Signaling. *J Biol Chem, 291*(50), 25921-25936. doi: 10.1074/jbc.M116.754028

Ye, H., Arron, J. R., Lamothe, B., Cirilli, M., Kobayashi, T., Shevde, N. K., . . . Wu, H. (2002). Distinct molecular mechanism for initiating TRAF6 signalling. *Nature, 418*(6896), 443-447. doi: 10.1038/nature00888

Ye, J., Beetz, N., O'Keeffe, S., Tapia, J. C., Macpherson, L., Chen, W. V., . . . Maniatis, T. (2015). hnRNP U protein is required for normal pre-mRNA splicing and postnatal heart development and function. *Proceedings of the National Academy of Sciences, 112*(23), E3020-E3029. doi: doi:10.1073/pnas.1508461112

Yoshida, H., Jono, H., Kai, H., & Li, J. D. (2005). The tumor suppressor cylindromatosis (CYLD) acts as a negative regulator for toll-like receptor 2 signaling via negative cross-talk with TRAF6 AND TRAF7. *J Biol Chem, 280*(49), 41111-41121. doi: 10.1074/jbc.M509526200

Yu, D., Tan, A. H., Hu, X., Athanasopoulos, V., Simpson, N., Silva, D. G., . . . Vinuesa, C. G. (2007). Roquin represses autoimmunity by limiting inducible T-cell co-stimulator messenger RNA. *Nature, 450*(7167), 299-303. doi: 10.1038/nature06253

Yu, J. W., Jeffrey, P. D., Ha, J. Y., Yang, X., & Shi, Y. (2011). Crystal structure of the mucosa-associated lymphoid tissue lymphoma translocation 1 (MALT1) paracaspase region. *Proceedings of the National Academy of Sciences, 108*(52), 21004-21009. doi: doi:10.1073/pnas.1111708108

Zhang, W., Zeng, F., Liu, Y., Zhao, Y., Lv, H., Niu, L., . . . Li, X. (2013). Crystal structures and RNA-binding properties of the RNA recognition motifs of heterogeneous nuclear ribonucleoprotein L: insights into its roles in alternative splicing regulation. *J Biol Chem, 288*(31), 22636-22649. doi: 10.1074/jbc.M113.463901

Zheng, W., & Flavell, R. A. (1997). The transcription factor GATA-3 is necessary and sufficient for Th2 cytokine gene expression in CD4 T cells. *Cell, 89*(4), 587-596. doi: 10.1016/s0092-8674(00)80240-8

Zhu, J., Mayeda, A., & Krainer, A. R. (2001). Exon Identity Established through Differential Antagonism between Exonic Splicing Silencer-Bound hnRNP A1 and Enhancer-Bound SR Proteins. *Mol Cell, 8*(6), 1351-1361. doi: https://doi.org/10.1016/S1097-2765(01)00409-9

Zinngrebe, J., Montinaro, A., Peltzer, N., & Walczak, H. (2014). Ubiquitin in the immune system. *EMBO Rep, 15*(1), 28-45. doi: 10.1002/embr.201338025

Zotti, T., Polvere, I., Voccola, S., Vito, P., & Stilo, R. (2018). CARD14/CARMA2 Signaling and its Role in Inflammatory Skin Disorders. *Front Immunol, 9*. doi: 10.3389/fimmu.2018.02167

10 Appendix

10.1 Publications

Di Pilato, M., Gao, Y., Sun, Y., Fu, A., **Grass, C.**, Seeholzer, T., Feederle, R., Mazo, I., Kazer, S.W., Litchfield, K., von Andrian, U. H., Mempel, T. R., Jenkins, R. W., Krappmann, D., Keller, P. (2023) Translational studies using the MALT1 inhibitor (S)-Mepazine to induce Treg fragility and potentiate immune checkpoint therapy in cancer. *J Immunother Precis Oncol.*, 6(2):61-73. doi: 10.36401/JIPO-22-18.

*Jones, A. N., **Graß, C.**, Meininger, I., Geerlof, A., Klostermann, M., Zarnack, K., Krappmann, D., & Sattler, M. (2022). Modulation of pre-mRNA structure by hnRNP proteins regulates alternative splicing of *MALT1*. *Science Advances*, 8(31), eabp9153. doi: 10.1126/sciadv.abp9153

Kutzner, K., Woods, S., Karayel, O., Gehring, T., Yin, H., Flatley, A., **Graß, C.**, Wimberger, N., Tofaute, M. J., Seeholzer, T., Feederle, R., Mann, M., & Krappmann, D. (2022). Phosphorylation of serine-893 in CARD11 suppresses the formation and activity of the CARD11-BCL10-MALT1 complex in T and B cells. *Sci Signal*, 15(723), eabk3083. doi: 10.1126/scisignal.abk3083

O'Neill, T. J., Seeholzer, T., Gewies, A., Gehring, T., Giesert, F., Hamp, I., **Graß, C.**, Schmidt, H., Kriegsmann, K., Tofaute, M. J., Demski, K., Poth, T., Rosenbaum, M., Schnalzger, T., Ruland, J., Göttlicher, M., Kriegsmann, M., Naumann, R., Heissmeyer, V., Plettenburg, O., Wurst, W., & Krappmann, D. (2021). TRAF6 prevents fatal inflammation by homeostatic suppression of MALT1 protease. *Sci Immunol, 6*(65), eabh2095. doi: 10.1126/sciimmunol.abh2095

Gewies, A., **Graß, C.**, & Krappmann, D. (2021). Methods to Study CARD11-BCL10-MALT1 Dependent Canonical NF-κB Activation in Jurkat T Cells. *Methods Mol Biol, 2366*, 125-143. doi: 10.1007/978-1-0716-1669-7_8

Kutukculer, N., Seeholzer, T., O'Neill, T. J., **Graß, C.**, Aykut, A., Karaca, N. E., Durmaz, A., Cogulu, O., Aksu, G., Gehring, T., Gewies, A., & Krappmann, D. (2021). Human immune disorder associated with homozygous hypomorphic mutation affecting MALT1B splice variant. *J Allergy Clin Immunol, 147*(2), 775-778.e778. doi: 10.1016/j.jaci.2020.07.034

Gehring, T., Erdmann, T., Rahm, M., **Graß, C.**, Flatley, A., O'Neill, T. J., Woods, S., Meininger, I., Karayel, O., Kutzner, K., Grau, M., Shinohara, H., Lammens, K., Feederle, R., Hauck, S. M., Lenz, G., & Krappmann, D. (2019). MALT1 Phosphorylation Controls Activation of T Lymphocytes and Survival of ABC-DLBCL Tumor Cells. *Cell Rep, 29(4),* 873-888.e810. doi: 10.1016/j.celrep.2019.09.040

* Parts of this thesis are published here.

10.2 Acknowledgments

First, I would like to express my gratitude to my supervisor Daniel Krappmann for his constant support and advice, and for guiding me through my projects.

I also want to thank the members of my thesis committee for the time and effort they put into reviewing my thesis: Prof. Dr. Christof Osman, Prof. Dr. Heinrich Jung, Prof. Dr. Laura Busse, Prof. Dr. Pascal Falter-Braun, and PD Dr. Serena Schwenkert.

Many thanks go to the members of my HELENA thesis advisory committee, Prof. Dr. Heinrich Leonhardt and Prof. Dr. Marc Schmidt-Supprian.

Further, I want to thank our collaboration partners Alisha Jones, Arie Geerlof, Michael Sattler, Florian Giesert, and Katja Lammens for contributing to this work.

I thank our Animal Welfare Officer Dr. Sibylle Sabrautzki and the HMGU animal caretakers.

I am very thankful to the present and former members of the Krappmann lab for their help, support and motivation: Andreas, Anna, Aurelia, Bahareh, Franzi, Hongli, Katrin, Kerstin, Kristina, Marie, Nicole, Simone, Thomas, Tom, and Torben. Special thanks go to Tom, the best teacher and supporter, and my lab hubby Thomas, who was the best companion I could have wished for during this thesis.

I also would like to thank my friends, especially my Würzburg friends, who continuously reminded me what´s important in life.

I am so deeply grateful to my family. My sister, Verena, who is the reason I started this long journey, and my parents, who guided me with lots of love, support and encouragement through my studies and thesis. And finally, Marcel, without your love, support and endurance on good days and bad, this thesis would not have been possible. Thank you so much!

Für meinen Opi.